Dissecting PINK1/parkin Mitophagy Dynamics

Dissertation

der Mathematisch-Naturwissenschaftlichen Fakultät
der Eberhard Karls Universität Tübingen
zur Erlangung des Grades eines
Doktors der Naturwissenschaften
(Dr. rer. nat.)

vorgelegt von
Anna Lechado I Terradas
aus Flaçà/Spanien

Tübingen
2022

Gedruckt mit Genehmigung der Mathematisch-Naturwissenschaftlichen Fakultät der Eberhard Karls Universität Tübingen.

Tag der mündlichen Qualifikation:	14.06.2023
Dekan:	Prof. Dr. Thilo Stehle
1. Berichterstatter/-in:	Prof. Dr. Jennifer Ewald
2. Berichterstatter/-in:	Prof. Dr. Philipp Kahle

"The position that being is permanent, timeless, and unchangeable substance and the opposite of becoming (…) makes sense only on the basis of the idealistic notion that a thought is the ultimate reality. But when we start out with the reality of human being existing, loving, hating, suffering, then there is no being that is not at the same time becoming and changing. **Living structures can be only if they become; they can exist only if they change. Change and growth are inherent qualities of the life process.**"

Erich Fromm, *To have or to be* (1976)

Contents

1. Summary 1

2. Introduction 4

2.1. Mitochondria 5

2.1.1. Mitochondrial structure and dynamics 5

2.1.2. Mitochondrial functions: more than the powerhouse of the cell 7

2.2. Cellular degradation pathways 9

2.2.1. Ubiquitin conjugating system and the UPS 9

2.2.2. Autophagic degradation 12

2.3. Mitophagy 15

2.3.1. Mitophagy induction *in vitro* 15

2.3.2. Ubiquitin-mediated mitophagy 16

a) PINK1/Parkin mitophagy 16

b) Antagonizing PINK1/parkin mitophagy: role of DUBs 20

c) Other E3 ligases 21

2.3.3. Ubiquitin-independent mitophagy 22

2.3.4. Mitophagy in Parkinson's disease 23

2.4. Aims of the study 24

3. Materials and methods 25

3.1. Reagents 25

3.2. Buffers and solutions 27

3.3. Molecular biology 27

3.3.1. RNA extraction and RT-PCR 27

3.3.2. Molecular cloning 28

3.3.3. Transformation of electrocompetent bacteria 29

3.3.4. Amplification and sequencing of plasmid DNA 30

3.4. Cell culture 31

3.4.1. Generation of stable parkin HeLa cell lines 31

3.4.2. Maintenance of cells 31

3.4.3. Transient transfections and treatments 32

3.4.4. RNAi of TAX1BP1 33

3.5. Protein biochemistry 33

3.5.1. Protein extracts for proteomic analysis 33

3.5.2. Cell lysates for Western blot 33
3.5.3. Mitochondria purification 34
3.5.4. Pulldown of 6HIS-tagged proteins 34
3.5.5. Western blot analysis 35
3.5.6. immunofluorescence 35
3.5.7. Transmission electron microscopy 37
3.6. Cell profiler-based image analysis 38
3.6.1. Mitochondria morphology upon mitophagy induction 38
3.6.2. Ubiquitination of mitochondrial aggregates 38
3.6.3. EGFP-LC3B recognition of TOM20 and SSBP1 material 39
3.6.4. Mitophagy in pentaKO cells expressing WT, K549R and ΔCC3-TAX1BP1 40
3.7. Statistical analysis 40

4. Results 42

4.1. Generation of WT- or C431A-parkin HeLa stable cell lines 42
4.2. Proteomic analysis reveals sequential sub-organelle turnover of mitochondria 43
4.2.1. Validation of mitochondrial sub-compartment degradation 45
4.2.2. Differential mitochondrial sub-compartment degradation under endogenous parkin expression 50
4.3. Mitochondrial sub-compartments are ubiquitinated in a sequential manner 52
4.4. Autophagy-link confirmation of parkin-dependent mitochondrial turnover 56
4.4.1. Sequential involvement of the autophagy machinery 57
4.4.2. Sequential involvement of the lysosomal machinery 60
4.4.3. Mitochondria engulfed by autophagosomes show OMM damages 62
4.5. Parkin is not enriched in inner- mitochondrial aggregates 63
4.6. Active parkin is ubiquitinated after mitophagy induction 66
4.7. Early proteasomal degradation is needed for mitophagy progression 67
4.8. Identification of proteasome-dependent OMM proteins turnover after short mitochondrial depolarization 71
4.9. Delayed inhibition of the proteasome impairs complete mitochondrial turnover 74
4.10. Identification of potential proteasome-dependent inner- mitochondrial proteins .. 76
4.11. Phospho-proteome and ubiquitylome analysis reveals a potential link between phosphorylation and ubiquitintion on VDAC1/2 78
4.12. Dephosphorylation of S115 enhances total VDAC2 ubiquitination 80
4.13. VDAC2-S115 dephosphorylation enhances K27-linked ubiquitination at K120 83
4.14. Proteomic ubiquitylome screen reveals TAX1BP1 ubiquitination to take place upon PINK1/parkin induction 86

4.15. Ubiquitination of TAX1BP1 takes place after the early proteasomal degradation ... 87

4.16. TAX1BP1 translocates to mitochondria upon mitochondrial depolarization 89

4.17. TAX1BP1 engages with LAMP1 as well as TOM20- and SSBP1-puncta 91

4.18. Ubiquitinated TAX1BP1 is present in mitochondria upon depolarization 93

4.19. TAX1BP1 knock-down does not impair overall mitophagy in WT-parkin HeLa cells 95

4.20. Over-expression of TAX1BP1 enhances mitophagy in WT-parklin HeLa cells..... 95

4.21. Influence of TAX1BP1 on PINK1/parkin mitophagy progression in a knock-out autophagy adaptor HeLa cell line..... 97

4.21.1. Over-expression of wild-type TAX1BP1 rescues defective mitophagy 98

4.21.2. Changes in mitochondrial turnover under K549R- and ΔCC3-TAX1BP1 expression 102

4.21.3. Changes in K549R- and ΔCC3-TAX1BP1 translocation 105

5. Discussion 110

5.1. Can PINK1/parkin degradation occur in a piecemeal manner? 110

5.1.1. Evidence for PINK1/parkin mitophagy..... 110

5.1.2. Differential degradation of mitochondrial proteins 111

5.1.3. Are later stages of PINK1/parkin mitophagy characterized by the formation of mitoplasts? 113

5.1.4. Autophagic targeting of ubiquitinated mitochondria and mitochondrial sub-compartments 114

5.2. Is parkin accountable for ubiquitination of all mitochondrial material? 120

5.3. Influence of the proteasome at early stages of PINK1/parkin mitophagy 122

5.3.1. Is proteasomal degradation a pre-requisite for mitophagy progression? 122

5.3.2. Does UPS degradation influence the turnover of distinct OMM proteins? 123

5.4. Influence of the proteasome at late stages of PINK1/parkin mitophagy 125

5.5. TAX1BP1 involvement in PINK1/parkin mitophagy 126

5.5.1. Defining TAX1BP1 role in the process: non-essential autophagy adaptor? 126

5.5.2. Trying to understand the behavior of ubiquitin-dead TAX1BP1 mutants 127

5.6. An example of PTM crosstalk in mitophagy: VDAC1/2..... 129

5.7. An updated model of PINK1/parkin mitophagy..... 132

5.8. Wholesale or piecemeal PINK1/parkin mitophagy? 136

5.9. Outlook 137

6. References 142

7. Appendix..... 157

7.1. Abbreviations 157
7.2. List of Figures 159
7.3. List of Tables 161

Acknowledgements 162

Publications 163

Collaborations 164

1.Summary

Mitochondria homeostasis is crucial for cellular integrity. Several quality control mechanisms can revert mitochondrial damage. However, in situations of acute and irreversible mitochondrial stress, specific pathways are activated to promote the selective degradation of mitochondria: mitophagy. One of the pathways regulating this process is orchestrated by the mitochondrial serine/threonine kinase PINK1 and the E3 ubiquitin ligase parkin. Importantly, while the early mechanisms leading to PINK1/parkin mitophagy activation and progression have been well characterized and are known to involve phosphorylation and ubiquitination post-translational modifications (PTMs), the later steps of the pathway that culminate in complete mitochondrial elimination remained understudied. In addition, the possibility that cross-talk events between phosphorylation and ubiquitination occur during the pathway was unexplored. Thus, the main objectives of this work are: to first gain a better knowledge of the overall pathway dynamics, especially focusing on the later stages and secondly, to explore the role of individual PTMs and their potential cross-talk during parkin-dependent mitophagy.

This study demonstrates that CCCP-induced parkin-dependent mitochondrial degradation does not occur at once but involves the consecutive ubiquitination and autophagic targeting of distinct mitochondrial sub-compartments. In addition, while early stages of PINK1/parkin mitophagy involve proteasomal degradation of several outer mitochondrial membrane (OMM) proteins, this step could be confirmed as a pre-requisite for mitophagy progression. Importantly, at later stages of PINK1/parkin mitophagy, a second proteasomal-dependent step was found to complete the degradation of inner mitochondrial structures. The E3 ligase parkin was ubiquitinated and degraded during mitophagy before pathway culmination. In addition, this study evidences an existing cross-talk between phosphorylation and ubiquitination of the parkin substrate VDAC2; phosphorylation of S115 negatively influences VDAC2 ubiquitination and impairs its parkin-dependent turnover. In addition, this work highlights the involvement of TAX1BP1 as a secondary autophagy receptor involved in PINK1/parkin mitophagy and raises the question of how ubiquitination of the autophagy receptor could modulate its function.

Overall, this study sheds some light on the dynamics of PINK1/parkin mitophagy and proposes an updated model of the pathway. The findings described in this work may serve as a resource of knowledge for the design of future studies in the context of mitophagy in PD or in other pathophysiological scenarios where defects in mitochondrial quality control are at the limelight of disease pathophysiology.

Zusammenfassung

Die Homöostase der Mitochondrien ist entscheidend für zelluläre Integrität. Mehrere Qualitätskontrollmechanismen können mitochondriale Schäden rückgängig machen. In Situationen akuten und irreversiblen mitochondrialen Stresses werden jedoch spezifische Prozesse aktiviert, um den selektiven Abbau von geschädigten Mitochondrien zu fördern, a.a Mitophagie. Eine Form von Mitophagie wird von der mitochondrialen Serin/Threonin-Kinase PINK1 und der E3-Ubiquitin-Ligase Parkin orchestriert. Während die frühen Mechanismen, die zur PINK1/Parkin-Mitophagie-Aktivierung und -Progression führen, gut charakterisiert sind und bekanntlich post-translationale Modifikationen (PTMs) wie Phosphorylierung und Ubiquitinierung beinhalten, sind die späteren Schritte den Prozessen, die in der vollständigen Beseitigung der Mitochondrien kulminieren, noch nicht ausreichend untersucht worden. Darüber hinaus wurde die Möglichkeit nicht untersucht, dass es während dieses Prozesses zu Überschneidungen zwischen Phosphorylierung und Ubiquitinierung kommt. Die Hauptziele dieser Arbeit sind daher: erstens eine bessere Kenntnis der Gesamtdynamik des Weges zu erlangen, wobei der Schwerpunkt auf den späteren Phasen liegt, und zweitens die Rolle einzelner PTMs und deren potenzielles Cross-Talk während der Parkin-abhängigen Mitophagie zu untersuchen.

Diese Studie zeigt, dass der CCCP-induzierte Parkin-abhängige mitochondriale Abbau nicht auf einmal erfolgt, sondern die aufeinanderfolgende Ubiquitinierung und autophagische Ausrichtung verschiedener mitochondrialer Subkompartimente beinhaltet. Darüber hinaus konnte bestätigt werden, dass frühe Stadien der PINK1/Parkin-Mitophagie den proteasomalen Abbau mehrerer üßerer mitochondrial Membranproteine beinhalten, was eine Voraussetzung für das Fortschreiten der Mitophagie darstellt. Wichtig ist, dass in späteren Stadien der PINK1/Parkin-Mitophagie ein zweiter Proteasom-abhängiger Schritt gefunden wurde, der den Abbau innerer mitochondrialer Strukturen abschließt. Die E3-Ligase Parkin wurde während der Mitophagie ubiquitiniert und abgebaut, bevor der Weg seinen Höhepunkt erreichte. Darüber hinaus belegt diese Studie eine Wechselwirkung zwischen Phosphorylierung und Ubiquitinierung des Parkin-Substrats VDAC2; die Phosphorylierung von S115 wirkt sich negativ auf die Ubiquitinierung von VDAC2 aus und beeinträchtigt dessen Parkin-abhängigen Umsatz. Darüber hinaus unterstreicht diese Arbeit die Beteiligung von TAX1BP1 als sekundärer Autophagie-Rezeptor, der an der PINK1/Parkin-Mitophagie beteiligt ist, und wirft die Frage auf, wie die Ubiquitinierung des Autophagie-Rezeptors seine Funktion modulieren könnte.

Insgesamt wirft diese Studie ein Licht auf die Dynamik der PINK1/Parkin-Mitophagie und schlägt ein aktualisiertes Modell des Prozesses vor. Die in dieser Arbeit beschriebenen Ergebnisse können als Wissensquelle für die Gestaltung zukünftiger Studien im Zusammenhang mit der Mitophagie bei Morbus Parkinson oder in anderen pathophysiologischen Szenarien dienen, in denen Defekte in der mitochondrialen Qualitätskontrolle im Mittelpunkt der Pathophysiologie stehen.

2. Introduction

Intracellular structures resembling mitochondria were first identified by the swiss anatomist and histologist Albert von Kölliker (1). However, it was not until forty years later that the anatomy professor Richard Altmann was the first one to name them as "bioblasts" and recognized them as elementary living units having metabolic and genetic autonomy (2). While Altmann's perspective drew much skepticism during the early years, further investigations during the first half of the 20th century recognized mitochondria to possess particular enzymes involved in aerobic phosphorylation (3), providing the first links of the organelle with cellular bioenergetics. It was not until the second half of the 20th century when the genetic origin of the key identified enzymes was revealed: starting with the discovery of mitochondrial DNA (mtDNA) in 1963 and its further sequencing studies in the early 1980s (3,4). Mitochondria functions were first restricted to cellular bioenergetics until in the early 1990s, when first evidences of the organelle being involved in other signaling pathways appeared. In the present day, current research continues enhancing their role in multiple biological processes ranging from regulation of cell death and stem cell differentiation to regulation of the immune response and autophagy (5).

The multiple cellular functions in which mitochondria are involved argue for a central role of the organelle in cellular homeostasis and thus enhance the importance of mitochondrial quality control systems. Indeed, alterations in mitochondrial function can be minimized by the activation of mitochondria quality control mechanisms (e.g: mitochondrial biogenesis, dynamics and autophagic removal). However, if defects in any of the repairing mechanisms exist, the mitochondrial quality control system can be seriously compromised and lead to a progressive accumulation of defective mitochondria (6,7). One of the mechanisms leading to the selective removal of defective mitochondria (mitophagy) involves the mitochondrial serine/threonine kinase PINK1 and the ubiquitin E3 ligase parkin, mutations of both proteins being linked with early-onset Parkinson's disease (PD) (8–10). In addition to neurodegeneration, defective mitophagy has been recently implicated in other pathologies such as metabolic-related disorders, myocardial and vascular atrophies and liver diseases (11). Further enhancing the role of mitophagy in cellular homeostasis and placing its focus of research as an essential resource for the understanding of its multiple complexity layers.

2.1. Mitochondria

2.1.1. Mitochondrial structure and dynamics

The multifaceted involvement of mitochondria in cellular homeostasis can be parallelly linked to their dynamic nature in shape. In fact, the nomenclature chosen by Carl Benda to describe these organelles comes from the two Greek terms *mitos* (thread) and *chondros* (grains), already indicative of two distinct morphological structures mitochondria can adapt (12). Indeed, while mitochondria are present in almost all eukaryotic cell types, their shape can be modulated depending on the cellular demands, being mitochondria either engaged in large networks or found as isolated organelles. Interestingly, mitochondrial duality in shape is analogous to their compartmentalized structure, as they are formed by two lipid membranes characterized to have distinct lipid composition and function: the outer mitochondrial membrane (OMM) and the inner mitochondrial membrane (IMM). The IMM delimits the inner parts of the mitochondria into the intermembrane space (IMS) and matrix, where the most of the metabolic reactions take place. The OMM, in contrast, separates the organelle from the cytosolic environment (5,13) (Figure 2.1).

The OMM is a permeable membrane that allows the trespassing of anions and small molecules through diverse anion channels and porins (e.g: voltage-dependent anion channel, VDAC), has a comparable lipid composition as extracellular lipid membranes and is a platform involved in many cellular signaling pathways (14). The IMM, however, possesses a very characteristic architecture that allows the expansion of inner mitochondrial surface by the formation of invaginations inside the organelle (cristae), where the enzymes responsible for oxidative phosphorylation (OXPHOS) reaction are located (5) (Figure 2.1). Contrary to the OMM, the IMM lipid composition is similar to bacterial plasma membranes and only allows the transfer of protons, O_2, CO_2 and H_2O. This selectivity allows the formation of an electrochemical gradient between the IMS and the matrix and is crucial for ATP production (15,16).

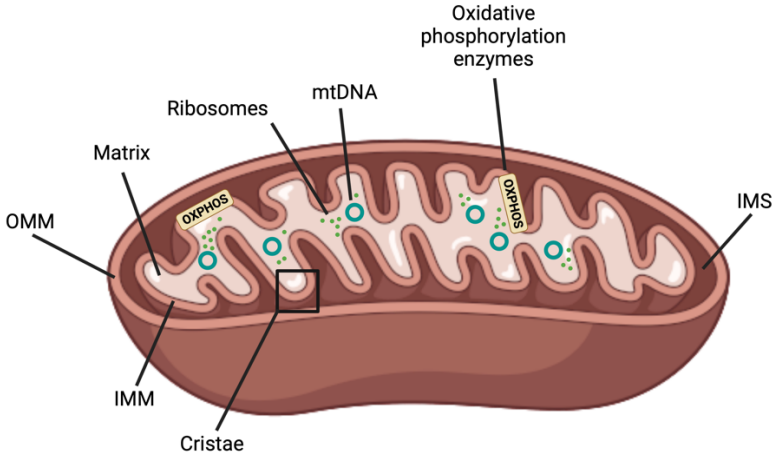


Figure 2.1: Sub-organelle organization of mitochondria. Two lipid bilayers are responsible for mitochondria compartmentalization. The outer mitochondrial membrane (OMM) separates the organelle from the cytosol and the inner mitochondrial membrane delimits the intermembrane space (IMS) from the matrix. Characteristic of IMM structure are its invaginations, termed cristae, where the enzymes responsible for oxidative phosphorylation and ATP production (OXPHOS) are located. Mitochondrial DNA (mtDNA) and ribosomes are also located in the matrix. Adapted from "Mitochondria 3D" by BioRender.com (2022). Retrieved from https://app.biorender.com/biorender-icons.

Mitochondrial shape duality confers the dynamic nature of mitochondria and is regulated via fission and fusion events that allow the fragmentation or coupling to the mitochondrial network. In addition, mitochondria are also mobile organelles which rely on microtubule filaments for their transport, being for example crucial at nerve fibers and neuronal synapses. Mitochondrial dynamics are tightly regulated and modulated in response to particular cellular needs. For example, mitochondria fragmentation is crucial for mitochondrial transport and cell cycle and is upregulated upon mitochondrial stress conditions, allowing localized fragmentation of the mitochondrial network to minimize damage of the whole network (6,17). On the other hand, mitochondrial fusion allows the exchange of mtDNA, metabolites and proteins between mitochondrial populations and is mostly associated to cell survival mechanisms (18) (Figure 2.2).

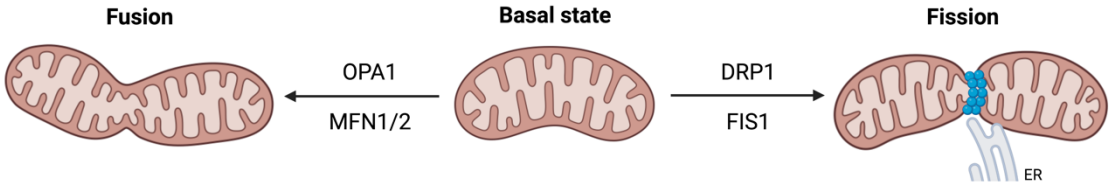


Figure 2.2: Mitochondrial dynamics. Homeostasis of the mitochondrial network is regulated via fusion and fission events. Fusion is mediated by MFN1/2 and OPA1 while fission is dependent on FIS1, DRP1 and involves ER-engulfing on mitochondria constricted membranes. Created with Biorender.

The molecular mechanisms allowing the regulation of mitochondrial dynamics occur at mitochondria sites in contact with the endoplasmic reticulum (ER) and require the involvement of myotubules and cytosolic, OMM and IMM proteins. Mitochondrial fission requires the translocation of dynamin-related protein 1 (DRP1) to mitochondria where it forms a complex with several other OMM proteins including the fission-1 homologue (FIS1), further allowing

DRP1 oligomerization and subsequent OMM and IMM constriction (19). DRP1-mediated mitochondrial fission additionally involves ER-mitochondrial wrapping and actin polymerization at the ER-mitochondria association sites (5,20–23). Mitochondrial fission allows the isolation of mitochondria from the whole network and thus facilitates the transport of mitochondria to higher energy demand localizations within the same cell. This is especially crucial in highly polarized cell types (e.g: neurons), where mitochondrial transport is mediated via the interaction of a Rho-like GTPases Miro1/2, the adaptor protein TRAK1/2 and motor proteins coupled to the microtubule network (18).

In contrast, regulation of mitochondrial fusion is mediated at the OMM and IMM level and it involves proteins belonging to the dynamin-like GTPase family: the OMM located proteins mitofusins (MFN1/2) and the IMM protein OPA1. Similar as DPR1, MFN1 relies on its GTP-dependent dimerization, which allows MFN1 to act as a tether between OMM fusing mitochondria (24). On the other hand, OPA1 is in charge of mediating OMM-IMM fusion via a complex mechanism that still raises questions up to this day. One of the plausible models involves the formation of OMM pores through direct OPA1-MFN1 interaction, OPA1 assembly at IMM sites and a tight equilibrium between the full length and processed OPA1 isoforms (L-OPA1 and S-OPA1), being L-OPA1 suggested to directly interact with the IMM lipid cardiolipin (CL) and promote membrane interaction stabilization (25,26). In addition to its involvement in mitochondrial fusion, OPA1 cooperates with the multiprotein complex mitochondrial contact site and cristae organizing system (MICOS) to regulate cristae architecture (27,28).

2.1.2. Mitochondria functions: more than the powerhouse of the cell

Mitochondria are key players in cellular bioenergetics as they are the main responsible for cellular ATP production. Through repeated oxidation of cellular metabolites, they generate an increased amount of reduced NADH and $FADH_2$ in the matrix. The reduced forms of NADH and $FADH_2$ allow the entry of electrons into the electron transport chain (ETC), which results in the formation of a proton gradient across the IMS, eventually allowing the generation of ATP. More specifically, electrons from NADH and $FADH_2$ are transferred to complex I and II and further transferred onto ubiquinone (Q). During this process, a net release of four protons to the IMS is mediated by complex I. Reduced ubiquinone (QH_2) relays the electrons to complex III (cytochrome c reductase) which further mediates the transfer of one electron at a time to cytochrome c. This results in the total transfer of four protons to the IMS for the transfer of two electrons from QH_2 to cytochrome c. Further, cytochrome c mediates the transport of electrons

to complex IV (cytochrome c oxidase, COX), where oxygen acts as the final electron acceptor which terminates in the production of H_2O in the matrix and the transport of two more protons to the IMS. The accumulation of a proton gradient at the IMS generates a mitochondrial membrane potential (ΔΨ) which further allows the conversion of ADP to ATP via the reflux of the protons back to the matrix through complex V (ATP synthase) (Figure 2.3) (16). Importantly, the ETC is susceptible to superoxide formation as electrons can dissipate from this transport process at several steps of the chain. Antioxidant mechanisms mediate the conversion of superoxide molecules to H_2O_2 in the IMS and matrix, counteracting the formation of reactive oxygen species (ROS). However, if the antioxidant system is compromised in any way, increased ROS production can endanger mitochondrial function and have further implications on disease pathogenesis (6,29).

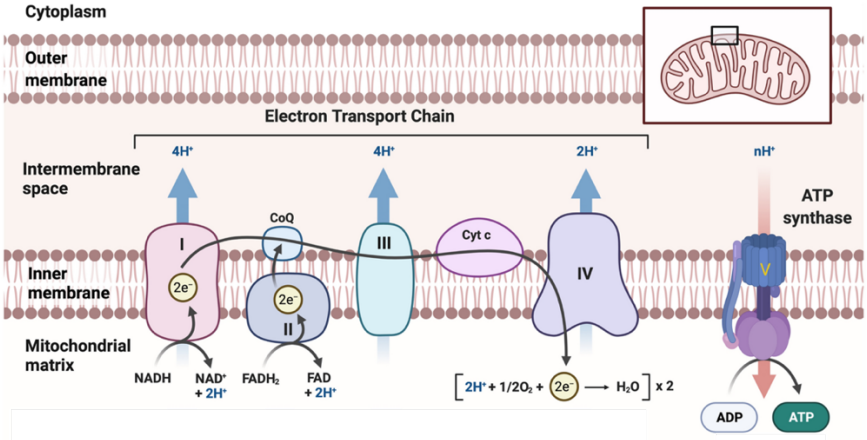


Figure 2.3: Oxidative phosphorylation and ATP production of mitochondria. Oxidative phosphorylation relies on the transfer of electrons from NADH and $FADH_2$ coming from the metabolic oxidative reactions occurring inside the matrix (e.g: Krebs cycle). Electrons are transferred from complex I to complex IV to the final electron acceptor oxygen (O_2), reducing it to water. During this process, protons are transferred from the matrix to the IMS, generating a proton gradient that drives the formation of ATP, mediated by complex V (ATP synthase). Adapted from Wu *et al.* 2022 (30).

Mitochondria link to cellular homeostasis goes beyond their implication in cellular bioenergetics, as they are also involved in apoptosis induction. The first links of mitochondria with cell death regulation date from the mid 1970s, when an increase in mitochondria permeability was observed upon calcium-induced stress (31,32). This particular increase in mitochondria permeability is due to the formation of the mitochondrial permeability transition pore (mPTP) and was later characterized as the point of no return in the activation of apoptosis pathway. Interestingly, the molecular components of the mPTP were not exactly clear from the beginning and several models have been proposed throughout the years (14,33). The current proposed model of mPTP architecture involves the Bcl-2 family members Bax and Bak, which undergo oligomerization at the OMM upon apoptotic-induced stress. Their oligomerization promotes the release of inner mitochondrial apoptotic signals like cytochrome c or SMAC/DIABLO that finally

trigger the classical caspase-mediated cell death cascade (34). Interestingly, Bax and Bak are not the only OMM proteins that can mediate the induction of OMM permeability. Indeed, one of the first models of mPTP formation included VDAC as the main architecture component of the pore as VDAC1 oligomerization can induce apoptosis. Thus, it has been suggested that multiple pathways and mechanisms can coexist to allow the release of cytochrome c (35,36). In addition to promote cytochrome c release, VDAC has been shown to interact with both pro- and anti-apoptotic Bcl-2 family members, thus indicating VDAC as potential regulators of cellular fate (37–42).

Additionally, mitochondria have been recently linked with inflammatory response activation (pyroptosis). This process can occur via the release of mtDNA at the cytosol, where it acts as a danger-associated molecular pattern that promotes the oligomerization of the inflammasome and activates macrophages and T cells. On the other hand, mtDNA release can be additionally mediated extracellularly by T lymphocytes, inducing antiviral responses or acting as a trap for larger pathogens (43).

2.2. Cellular degradation pathways

Cellular homeostasis is subject to the global cellular equilibrium between anabolism and catabolism processes inside the cell. Two of the main pathways involved in the degradation of cellular components are the ubiquitin proteasome system (UPS) and the autophagy degradation pathway. While both systems rely on ubiquitin signaling for eventual degradation of missfolded proteins or organelles, the molecular mechanisms that eventually drive substrate degradation differs between the two systems. The UPS regulates the degradation of missfolded proteins while autophagy degradation pathway is involved in the degradation of protein aggregates, cellular organelles and invading pathogens. Importantly, defects in any of the systems can lead to pathological implications (44,45).

2.2.1. Ubiquitin conjugating system and the UPS

Protein ubiquitination is a process regulated by three distinct enzymes: ubiquitin activators (E1), ubiquitin conjugators (E2) and ubiquitin ligases (E3). Frist, ubiquitin activators allow the activation of cytosolic ubiquitin by ATP hydrolysis and bind to ubiquitin through a thioester linkage. Activated ubiquitin is transferred to the active site of an E2 enzyme, allowing ubiquitin

E3 ligases to transfer activated ubiquitin to lysine residues of protein substrates (46), for example triggering ubiquitinated proteins for UPS-dependent degradation (Figure 2.4).

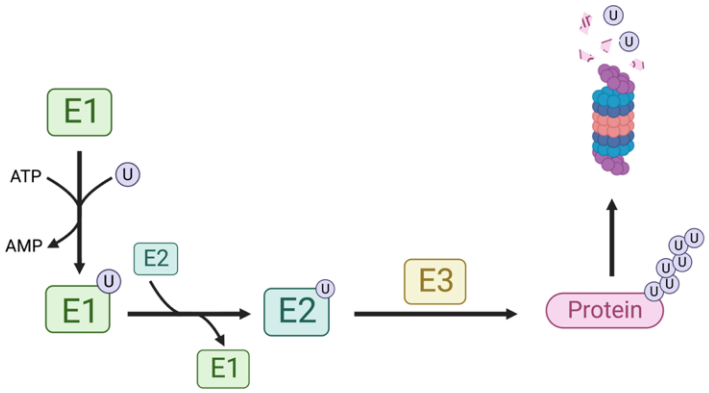


Figure 2.4: Ubiquitin conjugating system and UPS-mediated degradation. Cytosolic ubiquitin (U) is activated by a ubiquitin activating enzyme (E1) in a process that relies on ATP hydrolysis. Then, active ubiquitin is transferred from an E1 to a ubiquitin conjugating enzyme (E2). Subsequently, a ubiquitin ligase (E3) will mediate the final transfer of ubiquitin molecule to a designated protein. Repeated rounds of ubiquitination may lead to the formation of a poly-ubiquitin chain on the substrate, which will be recognized by the 19S proteasome and further internalized into the 20S core for subsequent degradation. Created with Biorender.

The UPS is a cytosolic protease complex comprised of a proteolytic core (20S proteasome) and a regulatory cap (19S proteasome). Protein degradation via the UPS is an ATP-dependent mechanism that relies on the ubiquitination of targeted proteins. Ubiquitinated proteins are recognized by the 19S unit which promotes protein unfolding in order to facilitate the entrance of the target protein to the 20S lumen (47). Further, polypeptides inside the 20S core unit are subject to cleavage (48). Importantly, during parkin-dependent mitophagy, the UPS mediates the degradation of specific OMM proteins involved in mitochondrial dynamics (e.g: MFN1) (49–51).

The ubiquitin sequence contains seven lysine residues (K6, K11, K27, K29, K33, K48 and K63) and a starting methionine (M1) to which ubiquitin itself can be linked (Figure 2.5). When repeated rounds of ubiquitin transfer occur, involving either the coupling of ubiquitin to a lysine or a methionine residue of ubiquitin itself, homomeric ubiquitin chains are formed. However, if different lysines are involved in the process, this can result in the formation of mixed or branched chains (heteromeric). In addition to ubiquitin chains, single ubiquitin molecules (mono-ubiquitination) or repeated addition of ubiquitin molecules (multiple mono-ubiquitination) can also be added to substrates (Figure 2.5). Furthermore, ubiquitin chains can also be post-translationally modified via phosphorylation or acetylation, providing another layer of complexity on ubiquitin chain assembly (52). Different ubiquitin chain topologies can trigger protein degradation or be part of signaling cascades. Ubiquitin chain decoding is mediated by the specific interaction of ubiquitin binding domains (UBD) which are known to be diverse in

affinity of chain recognition type (53–55). Additionally, specific chain-linkage types can also trigger the action of specific de-ubiquitinating enzymes (DUBs), counteracting ubiquitin chain synthesis and thus being one of the important regulators of the ubiquitin conjugating system (56).

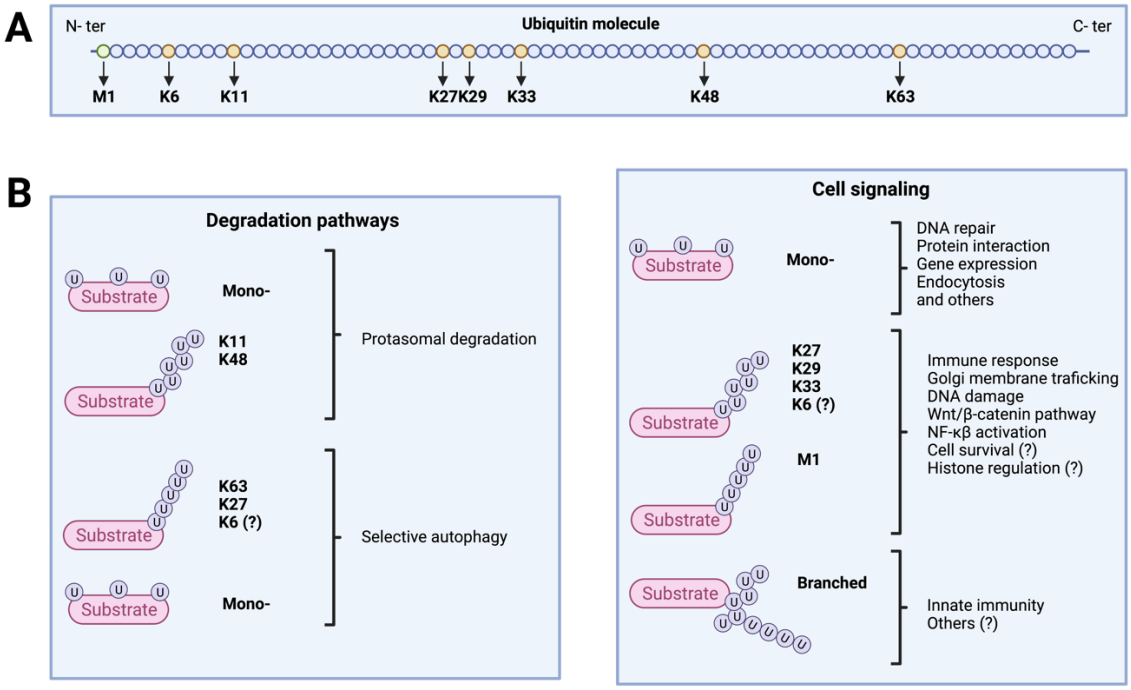


Figure 2.5: Cellular consequences of distinct ubiquitin chain-linkages. (A) Schematic representation of a ubiquitin molecule. Highlighted are the residues which can undergo ubiquitination. **(B)** Cellular responses of the distinct ubiquitin chain-linkages, either triggering degradation or signaling pathways. Created with Biorender.

Given the distinct layers of regulation in the formation of ubiquitin chains and how they might be modulated and decoded, there is an extensive agreement in the idea of an existing ubiquitin code (52,57,58). Indeed, extensive proteomics research together with the development of new tools allowing the recognition of single and branched ubiquitin chains types on substrates, has improved the understanding on the multiple pathways that the distinct ubiquitin chain topologies can be involved in (54,59). For example, K48-linked ubiquitin chains, heterotypic K11-linked chains and mono-ubiquitination target ubiquitinated proteins for proteasomal degradation, while ubiquitin chains with K27-, K63-linkage chains and mono-ubiquitination have been implicated with the selective removal of cellular organelles or pathogens (53,60–62). Similarly, K6-linked chains have been linked to selective autophagic removal of mitochondria (63,64), however it remains unclear if they are specifically recognized by any autophagy receptors or if they might be involved in additional cellular functions (53). Specific chain types can also trigger distinct signaling pathways. For example, homotypic K11- chains have been implicated in the regulation of cell cycle, K33-linked chains are associated with T-cell response

and post-Golgi trafficking, and K27-linked chains are linked with DNA damage and innate immunity (53). On the other hand, K63, K48 and K29- chain types have also been involved in Wnt/beta-catenin signaling, an essential pathway regulating embryonic development (65), while M1-linked chains are known key players in inflammatory immune response controlling the transcription of NF-kB transcription factor (53,58) (Figure 2.5). Interestingly, DUBs can also act upon specific ubiquitin chains. For example, K6-linked chains are targeted by USP30 and USP8 in the context of selective mitochondria elimination (66–68), while K11-linked chains are specifically targeted by the DUB Cezanne, involved in the regulation of cell cycle via modulation of transcription factor activation (53).

2.2.2. Autophagic degradation

The term *"autophagy"* comes from the Greek terminology of *auto* (self) and *phagein* (to eat) and was first suggested by Christian de Duve more than fifty years ago, when he identified some sort of highly hydrolytic granules in liver tissue samples (69,70), now widely known as lysosomes. For many years, the functional relevance and mechanisms of the process were unknown, until in 1993 a genetic screen in yeast revealed the importance of several autophagy-related proteins (ATGs) to be essential for the delivery of autophagic cargo to lysosomes (vacuole in yeast) (71). From this point on, research in the field of autophagy increased exponentially, allowing for a better understanding of the process. Today, autophagy is considered an essential catabolic process conserved in high eukaryotes that allows the recycling of cellular nutrients.

Importantly, the mechanisms leading to autophagy degradation have been generally associated with a non-selective degradation process. However, in the later years, research has evidenced that selective forms of autophagy are key for cellular homeostasis and rely on cargo-specific recognition, mediated by autophagy receptors (e.g: p62 sequestosome-1 [p62/SQSTM], or optineurin). Autophagy receptors interact with (i) ubiquitinated proteins through their UBD and with (ii) autophagosomes via their LC3-interacting region (LIR) motifs (44). Selective forms of autophagy include the degradation of (i) cellular organelles like mitochondria (mitophagy), lysosomes (lysophagy), endoplasmic reticulum (reticulophagy) and peroxisomes (pexophagy), (ii) degradation of invading pathogens (xenophagy) and (iii) degradation of protein aggregates (aggrephagy) (72). Increasing research in the field has led to the identification of multiple autophagy receptors involved in different types of selective autophagy; those are summarized in Table 2.1.

Table 2.1: Autophagy receptors involved in mammalian selective autophagy.

Type of selective autophagy	Selected cargo	Autophagy receptors	References
Mitophagy	Mitochondria	*Ubiquitin-dependent:* p62/SQSTM, OPTN, TAX1BP1, NDP52, NBR1	(62,73–75)
		Ubiquitin-independent: PHB2, FUNC1, AMBRA1, FKBP8, BNIP3, BCL2L13, NIX, CL, Ceramide	(76–84)
Lysophagy	Lysosomes	p62/SQSTM, TAX1BP1, TRIM16	(85–87)
Xenophagy	Pathogens	p62/SQSTM, OPTN, TAX1BP1, NDP52, NBR1	(88–91)
Aggrephagy	Aggregates	p62/SQSTM, OPTN, TAX1BP1, NBR1, TOLLIP	(92–96)

Given that the mechanisms triggering the early steps of both selective and general autophagy are similar and that this work is focused on a selective type of autophagy degradation, only the general mechanisms involved in mammalian selective autophagy will be introduced. Initial steps of the process require the formation of an isolation membrane -phagophore- which will further be elongated and eventually engulf the selected cargo (autophagosome). Further, the engulfed material will be degraded by lysosomal hydrolases after the fusion of an autophagosome with a lysosomes (autophagolysosome) (44,97) (Figure 2.6A).

The regulatory mechanisms leading to phagophore formation can be activated via several cellular stressors, either promoting general or selective autophagy. For example, nutrient deprivation may induce general autophagy while cargo-selective stress induction (e.g: ROS increase, drug-mediated membrane rupture) can induce selective autophagy (e.g: mitophagy or lysophagy, respectively) (85,97,98). Upon induction, cellular stress is sensed by the two main regulators of the autophagic pathway: the kinase mammalian target of rapamycin (mTOR) and AMP-activated protein kinase (AMPK). Under conditions of cellular homeostasis, mTOR complex I interacts with the uncoordinated protein 51-like kinase 1 (ULK1), impeding AMPK-mediated activation of ULK1 via phosphorylation. However, under autophagy inducing conditions, mTOR dissociates from ULK1, allowing AMPK1 to activate ULK1 via phosphorylation (99). ULK1 activation allows the formation of ULK1 complex, formed by ATG13, ATG101 and the focal adhesion kinase-interacting protein of 200 kDa (FIP200). Active ULK1 complex translocates to ER-associated isolation membrane sites, where it interacts with ATG14L, one of the members of the PI3K-II complex, responsible of phosphatidylinositol 3-phosphate (PI3P) production at the localized ER regions (omegasome). Further, the binding of the WD40 repeat protein interacting with phoinositides WIPI2 (WIPI2) allows for omegasome maturation to phagophores (100) (Figure 2.6B).

Phagophore elongation requires the action of two conjugation systems: ATG12 and ATG8, both dependent on the E1 ubiquitin ligase ATG7 which allows the interaction of ATG12 with ATG5 and the processing of pre-ATG8 proteins to further allow their lipidation (101). The conjugated system ATG5-ATG12 interacts with WIPI2 and ATG16L1 to allow the coupling of phosphatidylethanolamine (PE) to processed ATG8 proteins, normally divided into two sub-families (LC3s and GABARAPs) (102). Importantly, the lipidation of LC3 and GABARAPS is not only required for autophagosome elongation but also for autophagy receptor recognition and subsequent cargo-delivery to lysosomes (101) (Figure 2.6B).

Later steps of maturation involve the sealing and closure of the autophagosome. Autophagosome sealing is mediated via ULK1 complex and ATG9, which allow the delivery of additional membrane material at the phagophore. On the other hand, autophagosome closure is mediated via the recruitment of the machineries responsible for autophagosome-lysosome fusion (SNARE and HOPS complexes) and lysosomal delivery (kinesin motor) (44) (Figure 2.6B).

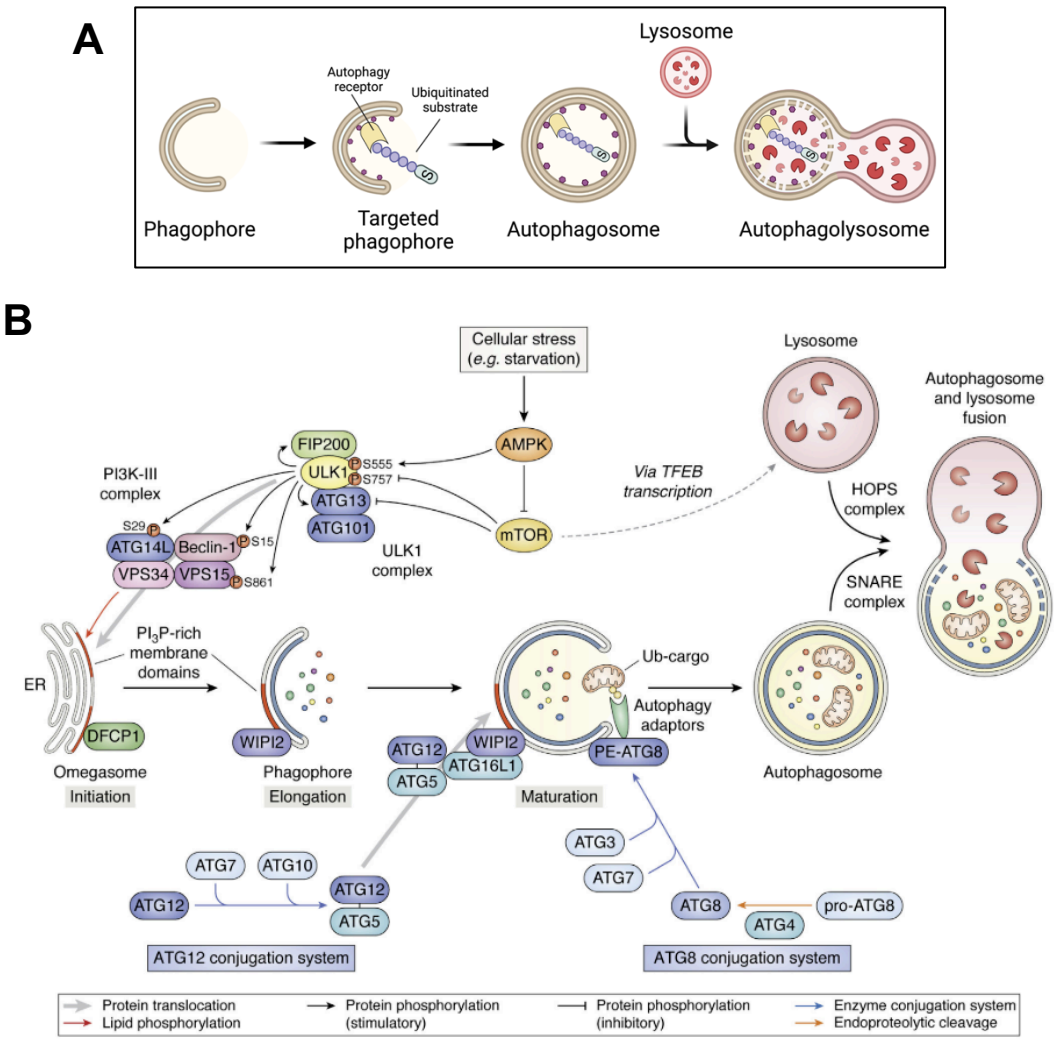


Figure 2.6: Selective autophagic degradation pathway. (A) Autophagic degradation relies on the formation of initial phagophores which are later targeted to ubiquitinated cargo via the interaction of autophagic receptors. Ubiquitinated cargo is recognized by autophagic receptors through their UBD domain. Parallelly, the LIR domain of

the autophagy receptors interacts with lapidated forms of LC3 or GABARAPs, coupling the building phagophore with the targeted cargo. Autophagic cargo is finally engulfed by a sealed phagophore (autophagosome) which will later fuse with a lysosome, further promoting cargo degradation. Created with Biorender. **(B)** Cellular stress is sensed by the main autophagy regulators (AMPK and mTOR). Upon activation, AMPK phosphorylates ULK1 which activates its kinase activity and phosphorylates members of the ULK1 and PI3K-III complex. This promotes the translocation of the PI3K-III complex to the endoplasmic reticulum (ER), where phosphatidylinositol-3-phosphate (PI3P) production is activated. Membrane ER domains rich in PI3P are recognized by WIP2 and DFCP1, promoting phagophore formation. At this point, the ATG12 and AT8 conjugating systems, responsible for phagophore elongation and maturation are activated; the ATG12 system mediates the conjugation of lapidated ATG8 into building membranes, promoting phagophore elongation. Autophagy receptors (here as; adaptors) can bind to lipidated ATG8 proteins, allowing selective autophagic removal of ubiquitinated cargo. Upon autophagosome sealing and closure, HOPS and SNARE complexes mediate membrane-membrane fusion events allowing fusion of lysosomes with the autophagosomes, leading to complete degradation of autophagic cargo. Adapted from Lechado et al. 2021

Importantly, dysregulations in the molecular mechanisms leading to any of the steps during phagophore formation, cargo recognition or lysosomal fusion and delivery have been implicated in multiple diseases like cancer, neurodegenerative diseases, immune diseases and aging (44).

2.3. Mitophagy

Mitophagy is the mechanism by which faulty mitochondria are selectively degraded through autophagy. This degradation relies on the recognition of damaged mitochondria by autophagy receptors and it can be either mediated in a ubiquitin-dependent or independent manner. Ubiquitin-mediated mitophagy relies on autophagy receptors which are able to recognize ubiquitin chains on specific mitochondrial proteins via their UBD. Additionally, they are able to directly link the mitochondrial cargo to building autophagosomes through their LIR motifs (59). On the other hand, ubiquitin-independent mitophagy relies on autophagy receptors lacking an UBD but capable of interacting with LC3 or GABARAP proteins via their LIR motifs. In addition to receptor mediated autophagic targeting, the recognition of damaged mitochondria can also occur via lipid-mediated targeting, involving phospholipids like CL or ceramide (103).

2.3.1. Mitophagy induction in vitro

Mitochondria homeostasis strongly depends on the proper balance of the mitochondrial ΔΨ and ROS production. Under experimental conditions, it is quite convenient to compromise mitochondrial health via the induction of increased ROS generation and/or the collapse of the mitochondrial ΔΨ (104). For instance, the collapse of the mitochondrial ΔΨ can be rapidly induced by the use of proton ionophores like m-chlorophenyl hydrazone (CCCP). Proton ionophores are strong mitochondrial uncouplers able to attach and transport protons, thereby disrupting the proton gradient and indirectly blocking ATP production. In addition,

mitochondrial toxins which directly target specific complexes of the ETC can also induce similar mitochondrial damage. Two of the most common mitochondrial toxins are oligomycin A and antimycin A. Antimycin A (AA) directly inhibits complex III and promotes a high increase in ROS production while limitedly disrupting the mitochondrial ΔΨ. On the other hand, oligomycin A blocks the ATP synthase complex and directly disrupts the mitochondrial ΔΨ in a milder way as CCCP (105). Due to their complementary effects in OXPHOS inhibition, treatment combinations of both toxins are of common use. Other toxins like MPTP can specifically inhibit complex I and induce PD-like phenotypes in humans (106).

In contrast, other strategies relying on the over-expression of mitochondrial-targeted photosensitizers allow for a more localized mitochondrial damage without the need of compromising the whole mitochondrial network. For example, Killer Red (mt-KR) is an encoded photosensitizer which, upon expression, can be irradiated using green light (540-580 nm). When its expression is targeted to mitochondria, this allows for a notable increase in ROS production on the targeted region, eventually promoting subsequent parkin-dependent mitochondria elimination (107,108).

2.3.2. Ubiquitin mediated mitophagy

There are several types of ubiquitin mediated mitophagy, according to the ubiquitin E3 ligase involved in the process. One of the most studied types of ubiquitin mediated mitophagy is the one depending on the RING-between-RING (RBR) E3 ubiquitin ligase parkin and PTEN-induced kinase 1 (PINK1), commonly known as PINK1/parkin dependent mitophagy. In addition, de-ubiquitination enzymes (DUBs) capable of antagonizing parkin-dependent ubiquitination of OMM proteins, additional E3 ligases and ubiquitin-independent autophagy receptors have also been reported to be involved in PINK1/parkin-dependent elimination of mitochondria (51).

a) PINK1/parkin mitophagy

Under healthy conditions, the PINK1 kinase is imported to the matrix via its N-terminal mitochondrial targeting sequence (MTS). There, the mitochondrial processing protease cleaves the MTS of PINK1 and further allows the IMM presenilin-associated rhomboid-like protease (PARL) to remove the membrane-anchoring segment of PINK1 (109,110). This last processing mechanism promotes PINK1 re-translocation to the cytosol, where it is rapidly degraded by the UPS (111). However, if mitochondria homeostasis is disrupted, either by direct inhibition of the

OXPHOS complexes or by a direct increase in ROS levels, the mitochondrial ΔΨ is compromised, leading to an accumulation of PINK1 at the OMM and subsequent activation of PINK1/parkin mitophagy (112,113). PINK1/parkin mitophagy is a dynamic pathway that can be separated in three distinct phases: (i) initiation, (ii) progression and (iii) autophagic targeting. (Figure 2.7).

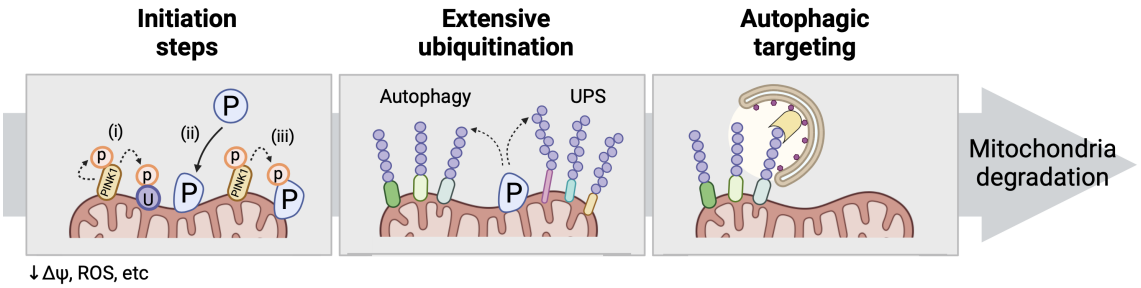


Figure 2.7: Dynamics of PINK1/parkin mitophagy. Initiation steps of PINK1/parkin mitophagy include PINK1 accumulation at the OMM, subsequent activation of PINK1 via autophosphorylation and PINK1-mediated phosphorylation of pre-existing ubiquitin (pUb) molecules at the OMM. This later step drives parkin translocation to the OMM where its interaction with pUb and direct PINK1-phosphorylation mediate a drastic conformational change of the E3 ligase. Upon activation, parkin mediates the conjugation of ubiquitin chains on OMM substrates which may lead to UPS-mediated degradation or trigger the coupling of autophagy receptors. Autophagy receptor recognition of ubiquitinated mitochondria can couple mitochondrial cargo to building autophagosomes, eventually promoting the degradation of mitochondria. Created with Biorender.

Pathway initiation involves the activation the kinase activity of PINK1 and parkin translocation to the OMM in a PINK1-dependent manner. While the mechanisms leading to PINK1 insertion at the OMM upon depolarization are not yet fully elucidated (114), PINK1 accumulation promotes its autophosphorylation leading to the activation of its kinase activity (115). At this point, PINK1-dependent phosphorylation events induce the translocation of parkin to the mitochondria, promoting the activation of the E3 ligase via a substantial conformational change in the organization of its domains (see Figure 2.8).

As a ring-between-ring E3 ubiquitin ligase, parkin contains five distinct domains; an N-terminal ubiquitin-like domain (UBL), the first ring domain (RING0), a central RING1 domain responsible for the interaction with an E2 enzyme, an in-between ring domain (IBR), a repressive region (REP) and a C-terminal RING2 domain in which the catalytic cysteine residue is found (C431) (116). For parkin to reach an active state, three inhibitory domain-domain interactions need to be released: two interactions blocking the RING1 domain and one interaction blocking the RING0 domain. The interaction site of the E2 enzyme is blocked (i) by the REP region and (ii) by the UBL domain and the catalytic domain is blocked (iii) by the RING0 domain (117–120) (Figure 2.8). Importantly, the domain re-organization of the parkin occurs in a PINK1-dependent manner: interaction of PINK1-dependent phosphorylation of ubiquitin at S65 and direct phosphorylation of the UBL domain by PINK1 (Figure 2.8). First, the interaction of RING1 with phosphorylated

ubiquitin at S65 (pS65-ubiquitin) allows the release of the RING1-UBL interaction (120–123). As a consequence of UBL release, PINK1 is able to phosphorylate S65 of parkin and promotes the phosphorylated domain to be in close proximity to the regions RING0 and RING1 (124,125). Further, the RING2 domain is released from its interaction with the RING0, simultaneously allowing the exposure of (i) the catalytic site of parkin and (ii) the interaction of RING1 with a loaded E2 enzyme. Such individual domain re-organizations ultimately promote a global conformational change in parkin that allows the activation of its E3 ligase activity. Additionally, it has been reported that after PINK1-mediated activation of parkin, the E3 ligase also ubiquitinates its own UBL domain at residues K27 and K48 (125–128) (Figure 2.8). However, the overall implications of parkin self-autoubiquitination remain poorly understood.

Fully active parkin and further PINK1-dependent phosphorylation of ubiquitin molecules at the OMM mediate pathway progression, which is characterized by extensive parkin-dependent ubiquitination of mitochondrial proteins. Active parkin recognizes pS65-ubiquitin on OMM substrates and mediates the binding of additional ubiquitin molecules on OMM substrates targeted with pre-existing pS65-ubiquitin. In turn, PINK1 recognizes the newly added ubiquitin molecules and phosphorylates ubiquitin at S65, overall generating an amplification of the signal and allowing the formation of pS65-ubiquitin chains on multiple OMM substrates (64,129,130). Overall, parkin is known to ubiquitinate several OMM proteins (e.g.: mitofusins and VDACs), with recent proteomic studies identifying parkin-dependent ubiquitination of inner mitochondrial proteins as well (68,126,131,132). Interestingly, it is suggested that parkin has evolved to have spatial selectivity instead of substrate-selectivity, given that artificially targeted exogenous proteins can also be ubiquitinated by parkin under depolarizing conditions (133). Based on this, the lack of substrate selectivity would allow for a rapid and efficient targeting of defective mitochondria.

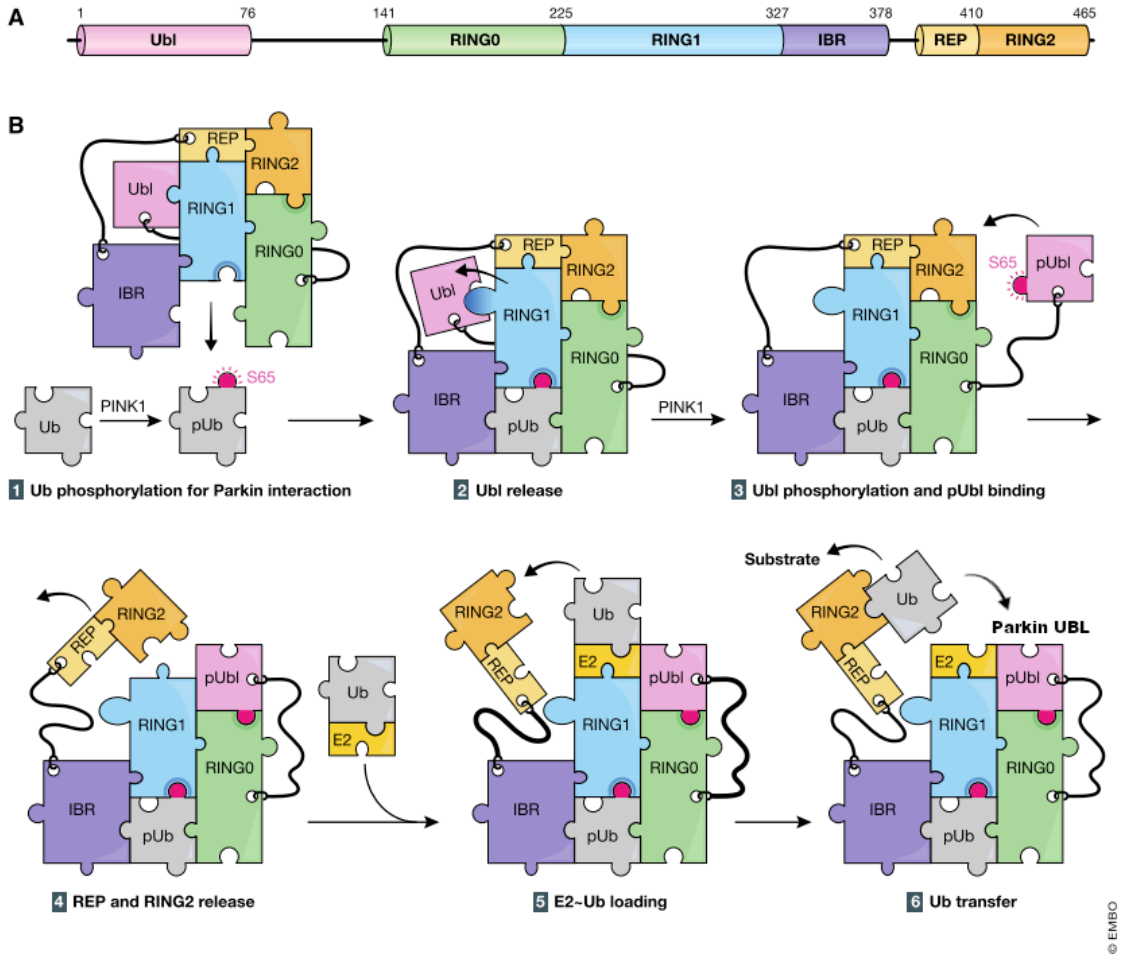


Figure 2.8: Structural organization of active parkin. (A) Schematic representation of parkin domains, including: ubiquitin-like domain (UBL), ring domains (RING0 and RING1), an in-between ring domain (IBR), a repressive region (REP) and the catalytic RING2 domain. **(B)** Parkin activation relies on the interaction with phosphorylated ubiquitin (pUb) and PINK1-dependent phosphorylation of S65 at the UBL domain of parkin. Interaction of parkin with pUb allows for the release of the UBL domain which is later phosphorylated by PINK1 at S65 (steps 1-3). Phosphorylated UBL domain (pUBL) further interacts with RING0, allowing the release of RING2 and the REP motive and subsequent interaction with a loaded E2 enzyme (steps 4-5). Finally, the catalytic site of parkin mediates the transfer of active ubiquitin to protein substrates and its own UBL domain (step 6). Adapted from Onishi *et al.* 2020 (116).

Importantly, while parkin is able to build several ubiquitin-linked chains, recent studies have indicated that the most abundant linkage-chain types on mitochondria upon parkin-dependent mitophagy involve K48- and K63-linked chain topologies (131,134). In addition, proteasome inhibition experiments have indicated that parkin-dependent ubiquitination triggers the degradation of specific OMM substrates and that UPS is involved in the degradation of OMM proteins (49,135,136). This suggests that while some parkin-dependent substrates targeted with K48-ubiquitin chains will be degraded by the UPS system, K63-linked ubiquitinated OMM proteins will likely be targeted by autophagy receptors (Figure 2.7). Indeed, *in vitro* studies have reported an increased affinity of OPTN and p62/SQSTM for K63-linked ubiquitin chains, in comparison to K48-linked chains (64,73). However, it remains to be elucidated if distinct autophagy receptors have distinct affinities for specific ubiquitin chain-linkages (59). Overall,

extended parkin-dependent ubiquitination of OMM proteins leads to the recognition of ubiquitinated mitochondria by autophagy receptors such as OPTN, NDP52, p62/SQSTM, TAX1BP1 and NBR1 (62,73–75) (Table 2.1). Importantly, autophagy receptors are subject to post-translational modifications (PTMs) that can modulate their activation. For example, OPTN and p62/SQSTM can undergo phosphorylation close to its UBD region, enhancing its binding affinity to ubiquitin chains (61,73). This process is known to be mediated by the serine/threonine kinase TBK1 (TBK1), also known to phosphorylate TAX1BP1 and NDP52 (61). However, it remains to be clarified how TBK1- dependent phosphorylation may regulate individual binding affinity of these later autophagy receptors.

Upon autophagy receptor binding to ubiquitinated mitochondria, the mitochondrial cargo becomes linked with building autophagosomes. This further allows the engulfment of mitochondrial material into autophagosomes. In later stages, complete autophagosomes will fuse with lysosomes generating autophagolysosomes that allow for complete degradation of mitochondrial material. The current model of PINK1/parkin mitophagy portrays that extended parkin-dependent ubiquitination of OMM proteins allows for the recognition of autophagy receptors, allowing for the engulfment of the whole organelle in a process termed wholesale mitophagy (44,59,116) (Figure 2.6A).

b) Antagonizing PINK1/parkin mitophagy: role of DUBs

Parkin-mediated mitophagy can be negatively influenced by the action of DUBs, which specifically mediate the removal of ubiquitin molecules. In the context of PINK1/parkin mitophagy, this modulation can occur at different levels: by influencing (i) parkin-dependent ubiquitination of OMM proteins, (ii) direct parkin ubiquitination of itself and/or (iii) by modulating components of the autophagy machinery.

Both USP30 and USP15 are known to counteracts parkin-dependent ubiquitination and have been reported to rescue PINK1/parkin defective phenotypes in Drosophila and PD-patient fibroblasts. Interestingly, USP30 seems to have certain affinity for the removal of K6-linked chains but its de-ubiquitinating activity diminishes if the K6-ubiquitin chains are phosphorylated (67,137). Similar than USP30 -though in a milder manner-, the mitochondrial USP35 DUB has been reported to also influence mitophagy. While the knock-down of USP35 enhances general parkin-dependent mitophagy under CCCP-induced mitochondrial stress conditions, USP35 shuttles from the mitochondria to the cytosol after depolarization induction (138), perhaps

suggesting that cytosolic translocation of the DUB may mediate the regulation of autophagy modulators or effectors as it has been shown for other DUBs. For example, USP33 has also been reported to interact with the RAS-like GTPase RALB, which upon USP33-mediated de-ubiquitination promotes autophagy induction (139). Similarly, nuclear USP36 has been reported to influence the expression of ATG14L/beclin-1 in the context of parkin-dependent mitophagy (140).

Another mechanism by which parkin-dependent ubiquitination can be indirectly compromised is through direct modulation of parkin autoubiquitination. For example, the mitochondrial DUB USP33 has been recently reported to remove K63-linked chains from parkin upon mitochondria depolarization, impairing parkin translocation to mitochondria (141). The DUB USP8 is also known to directly interact with parkin self-ubiquitination, specifically removing K6-linked chains from parkin UBL. However, contrary to USP33, the removal of K6-ubiquitin chains from parkin allows parkin translocation to mitochondria and promotes parkin-dependent mitophagy (66).

c) Other E3 ligases

Since the identification of parkin as an important E3 ligase involved in the selective removal of mitochondria, ubiquitin-dependent mitophagy has been a focus of research which has led to the identification of other E3 ligases capable of ubiquitinating mitochondria and inducing mitophagy in a similar manner as parkin. While some E3 ligases translocate to mitochondria under conditions of mitochondrial stress (e.g: HUWE1, AHRIH1), others are already localized on mitochondria (e.g: MARCH5 or MUL1).

The mitochondrial E3 ligase MARCH5/MITOL has been recently proposed to be implicated in PINK1/parkin mitophagy via two distinct mechanisms. First, Koyano and colleagues suggested the E3 ligase to form an ubiquitin mono-layer on mitochondria, which would set a lower threshold for PINK1-dependent ubiquitin phosphorylation and subsequent activation of the amplification loop of PINK1/parkin signaling (133). Interestingly, recent proteomic studies have observed a pre-existing amount of mono ubiquitin on healthy mitochondria, both under WT and S65A-parkin conditions, perhaps indicative of mitochondrial E3 ligases being involved in basal mitochondria ubiquitination (68). On the other hand, MARCH5/MITOL has also been indicated to mediate UPS-dependent parkin turnover by direct ubiquitination of parkin at K220 (142).

Mitochondria-induced stress conditions also can trigger the activation of the mitochondrial ubiquitin ligase MUL1 (MUL1). Interestingly, MUL1-dependent ubiquitination can rescue defective mitophagy phenotype in *in vivo* models lacking PINK1 or parkin (143). Given that MUL1 is able to directly ubiquitinate the parkin substrate MFN2 and promote its proteasomal degradation, it has been recently suggested that the MUL1-MFN2 may play a role in mitochondria morphology in situations of mitochondrial-induced stress with impaired PINK1/parkin mitophagy (144). Similarly, E3 ligases that rely in close proximity to mitochondria could mediate parkin-independent mitochondrial ubiquitination. For instance, the ubiquitin ligase GP78 (also known as AMFR) localizes at ER-mitochondria contact sites and is known to induce mitophagy by recruiting LC3 to ER-mitochondrial contact sites. In addition of promoting ubiquitin-dependent turnover of MFN in cells lacking parkin expression (145). GP78 has also been recently reported to be involved in a dual organelle turnover mechanism involving initial formation of severely OMM-damaged mitochondria (mitoplasts) and subsequent autophagic degradation of both E3 ligase and mitoplasts under mitochondria depolarizing conditions (146). Interestingly, in healthy mitochondria, GP78 has been recently suggested to be involved in UPS-dependent PINK1 degradation by directly interacting and ubiquitinating the kinase in cooperation with other members of the ER-associated degradation pathway (147).

Other E3 ubiquitin ligases that are known to translocate to mitochondria upon stress-induced conditions are HUWE1 and ARIH1. HUWE1 is able to promote mitophagy in a PINK1/parkin-independent manner by directly ubiquitinating MFN and subsequently promoting autophagic degradation of mitochondria via ubiquitin-independent autophagy receptors (148) (Table 4.2). On the other hand, the E3 ligase ARIH1 relies on PINK1-phosphorylation to promote parkin-independent mitophagy (149).

2.3.3. Ubiquitin-independent mitophagy

Mitochondrial cargo can additionally be linked with the autophagic machinery via the direct interaction of ubiquitin-independent autophagy receptors which are able to interact with LC3 or GABARAP proteins through their LIR domain (44) (Table 2.1). While most of the identified ubiquitin-independent autophagy receptors possess a transmembrane domain that allows their mitochondria localization, their interaction with ATG proteins is not intrinsic but is activated upon hypoxia or mitochondrial uncoupling (51,103). Particularly, the autophagy receptor FKBP8, prohibitin-2 and the phospholipid CL have been recently shown to be implicated in PINK1/parkin dependent mitophagy. The autophagy receptor FKBP8 is intrinsically expressed at the OMM and

it is considered to have anti-apoptotic functions as it has been reported to interact with Bcl-2 and Bcl-XL and promote mitophagy via the interaction of LC3A (83,103,150). In addition, FKBP8 has been recently implicated with MITOL/MARCH5 translocation to the ER during parkin-dependent mitophagy (142).

Similarly, the IMM protein prohibitin-2 (PHB2) has been shown to interact with LC3B in the context of parkin-dependent mitophagy (76). Mitochondrial PHB2 forms a complex with prohibitin-1 (PBH1). Interestingly, PHB1/2 expression is not exclusive of mitochondria as they are also located in the nucleus and cytosol, where they mediate multiple functions. In mitochondria, PHB1/2 complexes regulate mitochondrial architecture and have chaperone functions, being involved in the import of newly synthesized inner mitochondrial proteins (e.g: OPA1 and complex I) (151,152).

In addition to mitochondrial proteins, mitochondrial lipids can also link mitochondrial cargo to building autophagosomes (44,103). For example, upon mitochondrial stress-induced conditions, the IMM lipid CL can translocate to OMM via the phospholipid scramblase 3. There, it is able to directly interact with LC3B and further promote mitochondria elimination (153). Additionally, CL-LC3B interaction has been also reported to occur under basal conditions (154), perhaps indicative of a potential implication of CL at early stages of the autophagic pathway.

2.3.4. Mitophagy in Parkinson's disease

Parkinson's disease (PD) is the second most common neurodegenerative disease and is clinically characterized by motor defects including muscle rigidity, tremors, unstable posture and bradykinesia (inability to start movements). Pathophysiological hallmarks of PD are a dramatic loss of dopaminergic neurons in the substantia nigra (SN) and the formation of Lewy bodies in the remaining neurons. Although the exact molecular mechanisms underlaying PD pathogenesis remain unclear to date, extensive research has highlighted the importance of mitochondrial homeostasis in PD patients, being oxidative stress one of the suggested causes of mitochondrial disfunction (10). In addition, dopaminergic neurons have been suggested to be particularly susceptible to mitochondrial functionality due to their increased energy demand and dopamine metabolism, both potentially contributing to increased levels of ROS in this neuronal sub-population (155,156). Importantly, mutations in PINK1 and parkin are linked with early-onset hereditary forms of PD (8,9). PD-associated mutations in both PINK1 and parkin compromise mitochondria elimination in cell-based models (62,112,113,157) and expression of mutant forms

of both PINK1 and parkin in *Drosophila* lead to PD-associated motor phenotypes (158,159). Thus, while the mechanisms leading to PD pathogenesis likely involve multiple pathways, it is possible that the combination of accumulated defective mitochondria and their compromised autophagic elimination could contribute to the selective loss of dopaminergic neurons.

2.4. Aims of the study

Since the establishment of a relationship between PD pathogenesis and mutations in PINK1 and parkin, extensive research has proven how the two proteins are able to mediate the specific removal of compromised mitochondria and how PD-related mutations of both proteins can compromise this pathway. Proteomic studies have also provided extensive evidence of the influence of PTMs during the pathway, identifying ubiquitination as one of the hallmarks for PINK1/parkin progression and phosphorylation as an essential PTM for pathway initiation. However, while the molecular mechanisms of the pathway initiation and progression are almost fully characterized, later stages of the pathway remained understudied. In addition, the possibility that the PTMs involved in this pathway could influence one-another in a regulatory manner, remains unexplored.

Therefore, the main objectives of this work were at first exploratory and relayed on proteomic analysis of PTM dynamics, aiming to identify: (i) novel mediators of mitophagy (e.g: parkin substrates or autophagy regulators) and (ii) particular phosphorylation and/or ubiquitination regulatory events. Later, the focus was additionally placed on the validation of a piecemeal mitophagy model and the involvement of the proteasome system at initial and later stages of PINK1/parkin mitophagy.

Overall, this work tries to deepen the knowledge of PINK1/parkin dependent mitophagy dynamics, with a particular focus on the later steps of the pathway leading to complete mitochondria elimination.

3. Materials and methods

3.1. Reagents

All chemicals used in this study were of analytical grade and are listed below.

Table 3.1: List of chemicals used in this study

Reagent	Manufacturer
1,4-Dithiothreitol (DTT)	Carl Roth GmbH (Karslruhe, DE)
2-propanol	Merck KGaA (Darmstadt, DE)
40% Acrylamid/Bis-Acrylamid solution 19:1	Bio-Rad
Accutase	Sigma
Adenosine-triphosphate (ATP)	Biomol
Agar	Becton Dickinson
Agarose	Invitrogen
Ammonium persulfate (APS)	Sigma
Ampicillin (Sodium Salt)	Sigma
Ascorbic acid	Sigma
B12	Gibco
BigDye Terminator v.3.1 kit	Applied Biosystems
Bovine Serum Albumin (BSA)	Roth
Bradford reagent Kit	Bio-Rad
CCCP	Sigma
CHIR 99021	Axon Medchem
Collagen I	Cohesion
Cultrex	Gibco
Dimethyl sulfoxide (DMSO)	Sigma
DMEM/HAM's F12	Merck
DNA ladder mix	Thermo Fischer
dNTPs (dATP, dCTP, dGTP, dTTP)	Fermentas
Dulbecco's modified Eagle Medium (DMEM) high glucose	Sigma
Ex Taq DNA polymerase	Takara
Fetal bovine serum (FBS)	Merk
Fluorescent mounting medium	Dako
FuGene6	Promega
G418	Merck
Glutaraldehyde 25%, aqueous solution	Electron Microscopy Sciences
GoTaq Polymerase Kit	Promega
Hiperfect	Qiagen
Hoechst 33342	Molecular Probes
Hybond-P polyvinyllidene difluoride (PVDF) membrane	Millipore
Imidazole	Merck
Immobilon Western HRP substrate	Millipore
L-glutamine	Sigma
Lysotracker	Invitrogen
Matrigel	Corning
MG132	Sigma
Midori green	Sigma
N,N,N',N'-Tetraacetylethylenediamine (TEMED)	Merck
N2	Gibco

Table 3.1: (continued)

Neurobasal media	Gibco
Ni-NTA beads	Qiagen
Non-fat dried milk powder	AppliChem
Nonident P-40 (NP-40)	Sigma
Normal goat serum (NGS)	Sigma
NuPage MES/MOPS SDS Running buffer 20x	Invitrogen
OptiMEM	Invitrogen
Paraformaldehyde 20%, aqueous solution	Electron Microscopy Sciences
Pen/Strep	Millipore
Penicillin sulphate 100x	Biochrom
poly-D-lysin	Sigma
Poly-D-lysine (PDL)	Sigma
Protease inhibitors (complete)	Roche
Protein standard (Dual colour)	Bio-Rad
Puromorphamine	Calbiochem
Puromycin	InvivoGen
QIAfilter plasmid Maxi/MidiPrep Kit	Qiagen
QIAquick gel extraction kit	Qiagen
QIAquick PCR Purification Kit	Qiagen
Restriction enzymes	Thermo Fischer
RNeasy RNA extraction Kit	Qiagen
Shrimp alkaline phosphatase (SAP)	Roche
Sodium azide (NaN3)	Sigma
Sodium dodecyl sulphate (SDS)	Sigma
Sodium pyrophosphate (NaPPi)	Sigma
Subcellular fractionation kit for cultured cells	Thermofischer
T4 Ligase	Thermo Fischer
Transcriptor High Fidelity cDNA Synthesis Kit	Sigma
Triton-X-100	AppliChem
Trypsin	Sigma
Tryptone/Peptone	Roth
Tween-20	Merck
Urea	Roth
Western Blocking Reagent	Roche
Y-27632 (Apo-I)	Seleckchem
β-Mercaptoethanol	Roth

3.2. Buffers and solutions

Table 3.2: List of buffers and solutions used in this study

Solution	Composition
6x Laemmli buffer	325 mM Tris, 9 % SDS, 50 % glycerol, 9 % ß-mercaptoethanol, 0.03 % bromophenol blue at pH 7 in H_2O
8 M urea buffer	10 mM Tris, 100 mM NaH_2PO_4, 8 M urea, 10 mM Imidazole at pH 8.0 in H_2O
8 M urea wash buffer	10 mM Tris, 100 mM NaH_2PO_4, 8 M urea, 20 mM Imidazole at pH 6.3 in H_2O
LB medium	1 % tryptone, 0.5 % yeast extract, 0.5 % NaCl in H_2O
LB agar	1.2% agar in LB medium
Minipreparation buffer I	25 mM Tris, 10 mM EDTA, 100 µg/ml RNAse A, 0.9% Glucose in H_2O
Minipreparation buffer II	200 mM NaOH, 1 % SDS in H_2O
Minipreparation buffer III	3 M Potassium acetate, 11.5% acetic acid at pH 5.0 in H_2O
Mitochondria buffer (MB)	210 mM mannitol, 70 mM sucrose, 10 mM HEPES, 1 mM EDTA at pH 7.5 in H_2O
NuPAGE Transfer buffer (20x)	25 mM Bicine, 25 mM Bis-Tris, 1 mM EDTA at pH 7.2 in H_2O
Phosphate buffered saline (PBS)	2.2 mM KH_2PO_4, 7.8 mM Na_2HPO_4, 150 mM NaCl at pH 7.4 in H_2O
Primary antibody solution	5 % Western Blocking Reagent, 0.02 % NaN_3 in TBS
SDS-PAGE running buffer	25 mM Tris, 192 mM glycine in H_2O
SDS-PAGE separating gel buffer	1.5 M Tris, 0.4 % SDS at pH 8.8 in H_2O
SDS-PAGE stacking gel buffer	0.5 M Tris, 0.4 % SDS at pH 7 in H_2O
Secondary antibody solution	5 % non-fat milk powder in TBS-T
Sucrose 1,2 M	1.2 M sucrose, 10 M HEPES, 1 mM EDTA, 0.1 % BSA at pH 7.5 in H_2O
Sucrose 1,6 M	1.6 M sucrose, 10 M HEPES, 1 mM EDTA, 0.1 % BSA at pH 7.5 in H_2O
TEM fixation buffer	0.1 M HEPES, 4 mM $CaCl_2$, pH 7.2
Tris buffered saline (TBS)	50 mM Tris, 150 mM NaCl at pH 7.4 in H_2O
TBS-T	0.1% Tween-20 in TBS
Transfer buffer	25 mM Tris, 192 mM glycine, 20 % Methanol in H_2O
Western blot blocking solution	5 % non-fat milk powder in TBST

3.3. Molecular biology

3.3.1. RNA extraction and RT-PCR

For the generation of pCMV-6xHIS-VDAC2 constructs, VDAC2 cDNA was obtained from mRNA of HeLa WT-parkin expressing cells. Starting from a confluent 6-well plate of WT-parkin HeLa cells, cell material was lysed in 100µL of RNAeasy lysis buffer and purification of RNA was performed following manufacturer's instructions (Qiagen). Upon obtention of clean RNA, 600ng of RNA were used as a template for reverse transcription PCR (RT-PCR) reaction using a Transcription High Fidelity cDNA Synthesis Kit (Roche). The product of the RT-PCR was used for a second PCR in order to add restriction enzyme sites to the VDAC2 insert (see Table 3.4).

3.3.2. Molecular cloning

All plasmids used in this study contained N-terminal tags and are listed in Table 3.3. Plasmids encoding wild-type ubiquitin and LC3-II were previously generated by Sven Geisler and are characterized in the literature (160,161). For the generation of pcDNA3.1(-)-3xFlag-parkin construct, WT- or C431A-parkin was amplified from EGFP-parkin construct and sub-cloned in pCMV-3xFlag vector using EcoRI and NotI restriction enzymes. Finally, 3xFlag-parkin WT and C431A was later sub-cloned into a pcDNA3.1(-) vector. For the generation of VDAC2 constructs, cDNA obtained from RT-PCR was used as a template (see previous chapter). Plasmids encoding TAX1BP1 WT, K549R and ΔCC3 were amplified from commercial vectors obtained from Origene (WT TAX1BP1, Cat. Num: RC208233) or eZyvec on demand (K549R and ΔCC3, Quote: D2022-10) and further sub-cloned into a pCMV-6xHIS to ensure equal expression conditions. All cloning PCRs were performed using an ExTaq polymerase (Takara) and specific primers containing restriction sites for subsequent enzyme digestion (shown in Table 3.4). For site-directed mutagenesis, a two-step process was followed. First, two PCR reactions were performed; one from the 5' end to the point-mutation site and the second from the point-mutation site to the 3' end. Primers annealing at both ends of the template contained restriction sites for the desired enzymes and primers annealing at point-mutation sites introduced the desired nucleotide base substitutions (see Table 3.4). The second step of the process consisted on a third PCR reaction using only 5' and 3' primers and the products of both previous PCRs as a template, allowing the amplification of the full DNA product with the desired point-mutations and the restriction enzyme sites at both 5' and 3' ends. Amplified DNA products were separated on 0.5-2% agarose gels, visualized by midori-green DNA staining and UV light. The bands of the amplified DNA products were cut and purified with a Gel Extraction Kit (Qiagen) following manufacturer's instructions. Afterwards, both DNA insert as well as the desired backbone plasmids were digested with restriction enzymes (Thermo). The backbone was dephosphorylated to avoid recirculation of the plasmid using Shrimp Alkaline Phosphatase (SAP) for 1h at 37°C. Ligation reactions were performed following a 5:1 ratio (insert:backbone) and were incubated overnight at 4°C.

Table 3.3: List of constructs used in this study. Constructs were kindly provided by Sven Geisler (SG) or generated during this work (AL). Amp: Ampicillin, Kan: Kanamycin.

Consctruct	pCMV-6xHIS	pcDNAa3.1(-)-3xFlag	pEGFP-C1	Reference
Parkin				AL
WT		♦	♦	
C431A		♦	♦	
VDAC2				AL
WT	♦			
S115A, S115D, K120R, S115A/K120R, S115D/K120R	♦			
TAX1BP1				AL
WT	♦			
K549R, ΔCC3	♦			
Ubiquitin				SG
WT	♦			
LC3B				SG
LC3-II			♦	
Antibiotic resistance	Amp.	Kan.	Amp.	

Table 3.4: List of mutagenesis and cloning primers used in this study.

Primer	**Sequence** (5' – 3')
EcoRI Parkin FL fw	GGGAATTCCCATGATAGTGTTTGTCAGGTTCAACTCCAGC
Parkin NotI rev	CCGCGGCCGCCTACACGTCGAACCAGTGGTCCC
EcoRI VDAC2 fw	GGAAGAATTCCCGCGACCCACGGACAGAC
VDAC2 SalI rev	ATACGTCGACAGTTAAGCCTCCAACTCCAGGG
VDAC2 S115D rev	TTCCTGTGTTTGGATCGAAGGTAGTATCAAATGTCAG
VDAC2 S115A rev	CCTGTGTTTGGTGCGAAGGTAGTATCAAATGTC
VDAC2 S115A fw	GACATTTGATACTACCTTCGCACCAAACACAGG
VDAC2 S115D fw	GACATTTGATACTACCTTCGATCCAAACACAGG
VDAC2 K120R fw	CACAGGACGGAAAAGTGGTAAAATC
VDAC2 K120R rev	GATTTTACCACTTTTCCGTCCTGTG
Bsp120I 6HIS-TAX1BP1 fw	CAATCAGGGCCCCACATGCATCATCAC
TAX1BP1 SalI rev	CTAAGGTCGACCCCTAGTCAAAATTTAG

3.3.3. Transformation of electrocompetent bacteria

Electrocompetent bacteria were transformed with ligation products (2-5µl) via electroporation using a Micropulser electroporation device (Bio-Rad). Bacteria were incubated at 37°C and 350rpm for 1h and later plated on agar plates with the corresponding antibiotic resistance encoded in the transformed plasmids. Plates were incubated overnight at 37°C. Afterwards, bacterial colonies were screened for positively transformed via colony PCR. Here, individual colonies were picked and dissolved in water and specific primers annealing with the backbone and insert were used for the identification of positive colonies. The amplified fragments were separated on 0.5-2% agarose gels to verify the correct insert size.

3.3.4. Amplification and sequencing of plasmid DNA

The positive bacterial colonies were inoculated in 4ml of LB containing the corresponding antibiotic resistance (see table 3.3) and were incubated overnight with shaking at 37°C. Afterwards, bacteria were pelleted at 10000rpm for 1min at RT and were lysed using 150μl of minipreparation buffer I-III, mixing by inverting before the addition of each buffer. Bacterial lysates were pelleted at 13000rpm for 10min at RT and supernatants were transferred to a new vessel. To precipitate plasmid DNA, 1ml of ethanol was added, samples were centrifuged at 13000rpm for 10min at RT and supernatant was discarded. Pelleted DNA was washed with 1ml of 70% ethanol and centrifuged at 13000rpm for 10min at RT. DNA pellets were resuspended with 50μl of RNAase-free water and their concentration was measured at 260nm using a Nanodrop 2000/2000c (Thermofisher). All constructs were sequenced using a BigDye Terminator Kit (Applied Biosystems) and an ABI 31000 Genetic Analyser (Applied Biosystems). Upon completion of sequencing reaction, sequences were analyzed using Benchling web services (www.benchling.com). All primers used for sequencing can be found on Table 3.5. Positive colonies not containing non-desired mutations were inoculated in 50ml LB media containing the required antibiotics and incubated overnight with shaking at 37°C. Afterwards, plasmid DNA was extracted using a Midi- or Maxiprep QIAfilter Kit (Qiagen) according to manufacturer instructions and was resuspended in 100-500μl of RNAse-free water. DNA plasmid concentrations were measured using Nanodrop 2000/2000c.

Table 3.5: List of sequencing primers used in this study

Primer	Sequence (5' – 3')
pCMV seq for	GATCCGGTACTAGAGGAACTGA
pCMV seq rev	GCAATAGCATCACAAATTTCAC
Seq_T7 fw	TAATACGACTCACTATAGGG
Seq BGH rev	TAGAAGGCACAGTCGAGG
Parkin Int1 fw	GCAGGAAGGACTCACCACCAGC
Parkin Int2 fw	GGCTGTGGAGCGGGGCTGCTGCC
VDAC2 Int1 fw	CCAATGTGTATTCCTCCATCAT
VDAC2 Int2 rev	CTGCAAAGTTATTCCTTGTCAG
TAX1BP1 Int1 fw	CCATGTCATCTTTCAAAATGTGGCCAAGA
TAX1BP1 Int2 fw	ACCATGAAAGAAAAAGAAGAACTGT
TAX1BP1 Int3 fw	GGTCCAGACTTTAAAAAATATAGAT
TAX1BP1 Int4 fw	TCCGTCTTCAGATGGCTG
TAX1BP1 Int5 rev	ATATTGCAGAACTGGTTGTGCAT
TAX1BP1 Int6 rev	TAGAACATTCTGATCAAAATGGGTCT

3.4. Cell culture:

3.4.1. Generation of stable parkin HeLa cell lines

Parental HeLa cells were transfected with linearized WT or C431A 3xFlag-parkin construct (BglII enyzme). After 24h of transfection, cells were further selected with 1.2mg/ml G418 (Merck) for 13 days. Upon selection, cells were seeded at a very low confluency in order to allow further expansion of individual monoclonal colonies. Monoclonal colonies of WT- and C431A-parkin were screened for optimal comparable parkin protein levels and percentage of positive cell population.

3.4.2. Maintenance of cells

Cells were grown at 37°C and 5% CO_2 in Dulbecco's modified eagle medium (DMEM) or DMEM/HAM's F12 as specified in Table 3.7. HeLa and HEK293 cells were split every 3-4 days, diluting them 1:10 to a new culturing flask with new fresh media. For subsequent experiments, all HeLa cells were detached with trypsin and seeded in plates and/or poly-D-lysin (PDL) pre-coated coverslips. HEK293 cells were mechanically detached and seeded in PDL and collagen I pre-coated coverslips. wtNPCs were cultivated with Matrigel (Corning) or Cultrex (Gibco) and their media was changed every 3-4 days. For subsequent experiments, wtNPCs were detached using Accutase (Sigma) and seeded in Matrigel or Cultrex pre-coated plates with fresh media containing 10µM Apo-I. For immunofluorescence experiments, wtNPC were cultured in PDL and collagen I pre-coated coverslips. WT-parkin HeLa cells were sub-cultured up to a maximum of 28 passages and were further replaced with newly thawed cells. HeLa and HEK293 cells were frozen in FBS with 10% DMSO while wtNPC were frozen in NPC media (see table 3.8) supplemented with 10% DMSO and 10µM Apo-I.

Table 3.7: List of cell lines used in this study. ATCC: American Type Culture Collection

Cell line	Cell type	Organism	Culture media	Reference
HeLa	Cervical cancer cells	Human	10 % FBS in DMEM	ATCC
HeLa WT-parkin	Cervical cancer cells stably expressing WT parkin	Human	10 % FBS in DMEM	This study
HeLa C431A-parkin	Cervical cancer cells stably expressing C431A parkin	Human	10 % FBS in DMEM	This study
HeLa PentaKO	Cervical cancer cells where the autophagy adaptors NBR1, p62/SQSTM, OPTN, NDP52, TAX1BP1 where knocked-out	Human	10 % FBS in DMEM	(75)
HEK293	Human embryonic kidney cells	Human	10 % FBS in DMEM	Invitrogen
wtNPC K7.1	Neural progenitor cells derived from healthy controls	Human	50 % Neurobasal in DMEM Ham's F12, 2mM L-glutamine, 100 µl/ml Pen/Strep, 500 µl 100X N2, 500 µl 50X B27, 2 µM CHIR, 200 M ascorbic acid, 0.5 µM purmorphamine	(162)
wtNPC LS	Neural progenitor cells from healthy controls	Human	50 % Neurobasal in DMEM Ham's F12, 2mM L-glutamine, 100 µl/ml Pen/Strep, 500 µl 100X N2, 500 µl 50X B27, 2 µM CHIR, 200 M ascorbic acid, 0.5 µM purmorphamine	(163)

3.4.3. Transient transfections and treatments

WT-parkin and PentaKO cells were seeded and let grow up to a 50% of confluence before transfection. DNA plasmids were transfected using FuGene6 (Promega) transfection reagent according to manufacturer's instructions. Briefly, DNA plasmids were mixed with FuGene6 at a 3:1 ratio and diluted with OptiMEM media. Transfection reactions were incubated at RT for 20min and were dropwise spread on cultured cells. Treatments were applied accordingly after 24h of transfection.

To achieve mitochondrial depolarization, HeLa and HEK293 cells were treated with 10µM carbonyl cyanide m-chlorophenylhydrazone (CCCP) while wtNPC cells were treated with 100µM Antimycin A supplemented with 10µM Apo-I (Seleckchem). Delayed proteasomal inhibition was achieved with 10µM MG132 treatment. For pre-UPS inhibition experiments, 20µM MG132 was added half an hour before mitochondrial depolarization treatment. Upon addition of CCCP, MG132 concentration was diluted to half (10µM). Proteasomal inhibition was maintained in combination with CCCP up until the end of the treatment.

3.4.4. RNAi of TAX1BP1

Knock down was achieved with transient transfection of small interference RNA (siRNA) specific for TAX1BP1. Transfection was performed using the transfection reagent Hiperfect according to manufacturer´s instructions. Briefly, cells were seeded in 6-well plates until they reached a confluence of 80%. For three consecutive days, siRNA mixture containing 5nM of siRNA, 12μL of Hiperfect in 400μl of OptiMEM were dropwise spread to cultured cells. The media was changed 6h after silencing induction each day. After the last media change, cells were treated with CCCP for the indicated time-points. Sequences of the specific siRNA used in this work are listed in Table 3.8.

Table 3.8: Specific sequences of siRNA used for TAX1BP1 knock-down experiments.

siRNA	Cat. Num.	Target sequence
Hs_TAX1BP1_7	SI02781268	CAGATCAATCAGCTAATAATA
Hs_TAX1BP1_9	SI03036124	AAGGGTCTTACTGAAGTAACA

3.5. Protein biochemistry

3.5.1. Protein extracts for proteomic analysis

Cells were seeded in big petri disges (Ø: 150mm) and treated with CCCP for the indicated time-points. After treatment, cells were washed with PBS, recovered with 1ml of PBS in a new vessel and further pelleted at 2188g and 4°C for 5min. Cell pellets were frozen at -80°C until subsequent fractionation steps performed by Katharina Zittlau. Sub-cellular fractionation was achieved using the subcellular fractionation kit for cultured cells (Thermo Fischer Scientific) according to manufacturer's instructions. Fractions containing mitochondrial material were pooled to ensure lack of nuclear contaminants and were used for subsequent proteome, phosphoproteome and ubiquitylome analysis as described previously (132). Alternatively, whole cell lysate fractions in urea buffer were given to Katharina Zittlau for subsequent proteomic analysis (experiments from chapters 4.6-8).

3.5.2. Cell lysates for Western blot

Upon end of treatment, cells were washed with 10ml PBS 1X. Later, cells were harvested and recovered with 1ml of PBS 1X. Further, cells were centrifuged for 1min at 10000rpm. For a starting material of a confluent 10cm dish, cell pellets were resuspended with 100μl of urea lysis buffer. Cell lysates were passed through a 23G gauge needle for at least 5 times and they were further centrifuged for 15min at 18000rpm. Protein quantification was performed using

Bradford assay kit (Bio-rad). Total proteins were diluted in 6X Laemmli and urea buffer to a final equal protein concentration across samples. Finally, samples were boiled for 10min at 95°C for subsequent Western blot analysis.

3.5.3. Mitochondria purification

Cells were washed with PBS, further recovered with 1ml PBS in a new vessel and pelleted for 10min at 600g and 4°C. Pellets were resuspended with mitochondrial buffer (2ml MB for 10^8 cells). Cell lysis was performed at 4°C using a glass homogenizer with three series of 30 mechanical stokes. After the first lysing series, cell material was pelleted (600g for 10min at 4°C) and 1ml of supernatant was recovered in a new vessel (F1). The remaining supernatant was used to resuspend the pelleted cell material and two new series of mechanical lysing were performed with an in-between step of centrifugation (600g for 10min at 4°C). Supernatants were pooled together and correspond to F1. The remaining pellet was resuspended with 800µl of MB buffer and was centrifuged at 7000g and 4°C for 10min. Supernatant was recovered as F2. Crude mitochondria pellets were resuspended with 250µl of MB buffer and layered on a discontinuous sucrose gradient (6ml of 1.2 M over 5ml of 1.6 M) on ultra-clear tubes (14 x 89mm, Beckmann). Loaded sucrose gradients were centrifuged at 96000g with acceleration and deceleration parameters set on 3 for 2h at 4°C using a Beckman ultracentrifuged equipped with a SW40Ti rotor. After centrifugation, sucrose buffer was removed from the top with a 20G syringe until reaching bands of interest: on the top sucrose layer the band corresponding to non-enriched mitochondria fraction (non-Mito) was collected and at the interface of the two layers the band corresponding to enriched mitochondria (Mito) was collected. After collection, sucrose was diluted with four volumes of MB. Non-Mito and Mito fractions were centrifuged at 13000g for 10min at 4°C and pellets were resuspended in urea buffer. Equal protein amounts of each fraction were subjected to Western blot analysis.

3.5.4. Pulldown of 6HIS-tagges proteins

Cell lysates were obtained as described previously (see section 3.5.2) using urea buffer at pH 8.0. A minimum of 300µg of total protein was incubated with Ni-NTA agarose in a spinning wheel overnight at 4°C. Incubation reactions contained 300µg of total protein and 30µl of Ni-NTA beads and were diluted in 1ml of urea pulldown buffer containing 10µM imidazole to prevent unspecific binding of the beads. After incubation, beads were centrifuged at 4°C for 1min at 10000rpm and further washed three times with urea wash buffer containing 20µM of imidazole. Washing incubation steps were performed in a spinning wheel at RT for 5min with in-between

centrifugation steps of 1min at 10000rpm. After the third washing step, samples were centrifuged for 1min at 10000rpm to recover remaining washing buffer and a Hamilton needle was used to completely remove all urea washing buffer. Further, 50µl of 2X Laemmli buffer was added to the beads. Finally, proteins were eluted by boiling samples for 15min at 95°C with shaking at 1200rpm. Samples were centrifuged one last time at 10000rpm for 1min to precipitate the beads and supernatant was recovered in a new vessel. For further Western blot analysis of pulldown samples, 10µl of total eluate was used.

3.5.5. Western blot analysis

Proteins were separated in 7.5, 10 or 15% self-casted SDS-polyacrylamide gels, pre-casted 4-12% Bis-Tris NuPAGE (Invitrogen) or 4-20% Bis-Tris Tru-PAGE gels (Sigma). Self-casted gels were run for initial 30min at 100V and later at 140V while pre-cast gels were run at 100V. Proteins were transferred to Hybond-P polyvinyllidene difluoride (PVDF) membranes for 2h at 100V and 4°C. Membranes were blocked with 5% non-fat dried milk or 5% BSA for 1h at RT. Afterwards, membranes were further incubated with primary antibodies overnight at 4°C and later incubated for 1h at RT with the corresponding HPR-conjugated secondary antibodies. Proteins were visualized with Immobilon Western chemiluminescent HRP substrate and Ultracruz x-ray films (Santa Cruz). Membranes were washed three times for 5min with TBS-T after each incubation step. Primary and secondary antibodies used in Western blot (WB) are listed in tables 3.9-3.10.

3.5.6. Immunofluorescence

All primary and secondary antibodies used for immunofluorescence (IF) are listed in tables 3.9-3.10. Cells were seeded on pre-coated coverslips (Ø: 12mm) and treated with CCCP at the indicated time-points. After treatment, cell media was removed and cells were washed with 1X PBS. Afterwards, cells were fixed with 4% PFA for 20min at RT. Fixed cells were washed three times with 1X PBS and were further permeabilized with 1% Triton-X for 5min at RT. After three washing steps with 1X PBS, blocking was achieved with 10% of FBS in PBS for 1h at RT. Primary antibodies were diluted in 5% FBS and incubated for 2h at RT. After three washing steps, secondary antibodies diluted in 10% FBS were incubated for 1h at RT. After two additional washing steps, nuclei were stained with Hoechst 33342 (2ug/ml/PBS) and coverslips were washed again. Coverslips were finally mounted on microscopy slides with fluorescent mounting media (Dako). Imaging was performed using an AxioImager microscope equipped with ApoTome

imaging system (Carl Zeiss). Images were processed using ZEN 2.3 lite software (Carl Zeiss) and ImageJ. For endogenous detection of LC3B, normal goat serum was used instead of FBS.

Staining of lysotracker in fixed cells was achieved by adding 500nM of LysoTracker-RED (Invitrogen) to cultured cells 30min before fixation. Further, media was replaced with ice-cold DMEM for 10min and cultured cells were gently washed with 1X PBS at 4ºC. Afterwards, cells were normally fixed with 4% PFA as described previously. Lysotracker was imaged on the 568 nm channel and mitochondrial material was stained with Alexa fluor 350 and further imaged on the Hoechst channel as previously described.

For the quantification of transfected VDAC2 experiments, a minimum number of total cells or transfected cells were manually counted as described below. Analysis of mitochondrial morphology under no treatment conditions was assessed in a minimum of 100 cells per transfection condition and were further classified in elongated, aggregated or degraded mitochondria. Quantification of residual VDAC2 positive cells after 14h of mitochondrial depolarization was assessed by monitoring at least 500 total cells per transfection condition. Further, the number of cells still expressing VDAC2 at that time-point in relation to the total cell number was computed as a percentage. Mitochondrial morphology analysis at later stages of mitophagy only in VDAC2-positive transfected cells was performed by analyzing at least 100 cells per transfection condition and a final percentage relative to the total transfected cell number was computed. Here, mitochondria morphology was simply classified between mitochondrial puncta or aggregates.

Table 3.9: **List of primary antibodies used in this work and the concentrations used.** WB: Western blot; IF: immunofluorescence.

Antibody	Company	Cat. Num	Species	WB	IF
B-Actin	Sigma Aldrich	A5441	Mouse	1:5000	-
Calnexin	Proteintech	66903	Mouse	-	1:1000
Calnexin	Enzo Life Sciences	ADI-SPA-860	Rabbit	1:1000	-
COX4	Cell Signaling	4850	Rabbit	1:6000	1:1000
CS	GeneTex	GTX110624	Rabbit	1:6000	1:1000
HIS	Invitrogen	clone H.8	Mouse	1:10000	1:1000
LAMP1	Hybridoma Iowa biobank	Clone H4A3	Mouse	-	1:500
LC3B	GeneTex	GT3612	Mouse	1:1000	1:250
Mfn1	Abnova	H00055669-M04	Mouse	1:1000	1:1000
p62/SQSTM	BD Biosciences	610832	Mouse	1:1000	1:500
Parkin	Cell Signaling	4211S	Mouse	1:10000	1:1000
Parkin	Cell signaling	2132	Rabbit	-	1:1000
Phosphorylated ubiquitin (S65)	Cell signaling	52802	Rabbit	1:1000	-
PINK1	Cell signaling	6946	Rabbit	1:1000	-

Table 3.9: (continued)

SSBP1	R&D Systems	AF6588	Sheep	1:500	1:1000
TAX1BP1	Novus Biologicals	NBP1-86662	Rabbit	1:1000; 1:10000	1:500
TOM20	Santa Cruz	sc-11415	Mouse	-	1:1000
TOM20	Proteintech	11802-1-AP	Rabbit	1:6000	1:1000
TOM70	ProteinTech	14528-1-AP	Rabbit	1:1000	1:1000
Total ubiquitin (FK2 clone)	Enzo Life Sciences	BML-PW88100100	Mouse	-	1:1000
Total ubiquitin (Ubi-1 clone)	Millipore	MAB1510	Mouse	1:10000; 1:1000	-
Ubiquitin (K27-linkage)	Abcam	ab181537	Rabbit	1:10000	-
Ubiquitin (K48-linkage)	Millipore	05-1307	Rabbit	1:10000	-
Ubiquitin (K63-linkage)	Millipore	05-1308	Rabbit	-	1:1000
VDAC	Millipore	AB10527	Rabbit	1:30000	-
VDAC2	Proteintech	11663-1-AP	Rabbit	1:1000	1:500
Vinculin	Sigma Aldrich	V9131	Mouse	1:6000	-

Table 3.10: **List of secondary antibodies used in this work.** WB: Western blot; IF: immunofluorescence.

Antibody	Company	Cat. Num.	Species	WB	IF
anti-mouse HRP	Amersham Pharmacia	115-035-003	Goat	1:10000	
anti-rabbit HRP	Amersham Pharmacia	111-035-003	Goat	1:10000	
anti-sheep HRP	Amersham Pharmacia	718-035-147	Goat	1:10000	
anti-sheep Alexa Fluor 647	Invitrogen	A-21448	Donkey		1:1000
anti-mouse Alexa Fluor 488	Invitrogen	A-21202	Donkey		1:1000
anti-rabbit Alexa Fluor 488	Invitrogen	A-21206	Donkey		1:1000
anti-mouse Alexa Fluor 568	Invitrogen	A-10037	Donkey		1:1000
anti-rabbit Alexa Fluor 568	Invitroge	A-10042	Donkey		1:1000
anti-rabbit Alexa Fluor 350	Invitrogen	A-11046	Goat		1:1000
anti-mouse Alexa Fluor 350	Invitrogen	A-10045	Goat		1:1000

3.5.7. Transmission electron microscopy

WT-parkin HeLa cells were seeded on poly-D-lysin pre-coated squared coverslips (22 x 22mm) and treated with CCCP for the indicated time-points. After treatment, cells were pre-fixed under growing conditions with cell medium supplemented with 2.5% glutaraldehyde and 4% paraformaldehyde with adjusted pH of 7.2 for 20min. After that, cells were fixed with TEM fixation buffer supplemented with 2.5% glutaraldehyde and 4% paraformaldehyde with adjusted pH of 7.2 for 1h at RT first and then for 3h at 4ºC with the fixative buffer being replaced a few times. Finally, cells were shipped to Prof. Dr. Stefan Geimer (University of Bayreuth) where additional fixation, sample embedding, slicing and imaging steps were performed.

3.6. Cell profiler-based image analysis

For semi-quantitative image analysis, CellProfiler (4.2.1 version) software was used. In all analysis, individual cells were recognized with the nuclear staining. Further, a cytoplasm area of 60-100 pixels (px) apart from the nucleus was established. Nuclei were not considered as part of the cytoplasm. All mitochondria material was related to each individual cell cytoplasm to obtain single-cell values. All quantification analyses rely on pooled single cell values from at least three independent experiments with the exception of the analysis of ubiquitination of mitochondrial aggregates (see below). Mean colocalization coefficient image values obtained in CellProfiler analysis can be obtained upon request.

3.6.1. Mitochondria morphology upon mitophagy induction

Mitochondria material was recognized using the mitochondrial markers TOM20, COX4 and SSBP1 in three different analyses due to differences in staining pattern and background. For the identification of mitochondrial morphology, mitochondria were identified as primary objects when in between a range of 6-500px. Further, mitochondrial objects were merged to account for mitochondrial network condensation when the distance between the initial primary objects was $\leq$2px apart. Merged mitochondrial objects with an area of 300-500px were considered aggregates while mitochondrial material of an area $<$300px were considered puncta.

3.6.2. Ubiquitination of mitochondrial aggregates

Mitochondrial material was recognized with COX4 and SSBP1 markers. For the analysis of COX4 aggregates, all COX4 objects within a range of 15-40px were identified as primary objects. Ubiquitin objects were identified using the FK2 antibody (n=2, discontinued product). Ubiquitin objects within a range of 6-50px were considered as primary ubiquitin objects. Both COX4 and ubiquitin primary objects were merged as a single object if the individual objects were in contact (distance of 0px). For the analysis of the 14h time-point, an intensity threshold in ubiquitin staining was applied due to strong background: only pixel intensities between the range of 0.12-1px were considered.

For the analysis of SSBP1 aggregates after 4h of CCCP, all SSBP1 objects within a range of 6-100px were identified as primary objects and merged as a single object if they were less than 3px apart. After identification, only SSBP1 aggregates >100px were considered for further overlap analysis. For the time-point of 14h CCCP, a threshold on SSBP1 pixel intensity was

applied, only considering pixels with an intensity range of 0.15-1. Further, SSBP1 objects of the size range of or 15-40px were identified and only SSBP1 objects >10px with a maximum intensity of 0.6 were considered for further analysis. Finally, SSBP1 individual objects that were in contact with each other were merged. Ubiquitin objects within a range of 6-50px were considered as primary ubiquitin objects, only that for the time-point of 14h CCCP, ubiquitin objects <10px were not taken into account.

To quantify the ubiquitin area co-localizing with both COX4 and SSBP1 aggregates, merged ubiquitin objects were masked with merged mitochondrial objects and the overlapping area was computed by the software. Further, the total mitochondrial area was computed by multiplying the individual number of COX4 or SSBP1 objects by their mean merged pixel area. Finally, the percentage of total mitochondrial area overlapping with ubiquitin was calculated.

For the classification of COX4 aggregates (positive or negative for ubiquitin), the same CellProfiler analyzing considerations as described previously were applied except that, to avoid the presence of false positive COX4 aggregates, only mitochondrial merged material >300px was considered.

3.6.3. EGFP-LC3B recognition of TOM20 and SSBP1 material

For quantification of positive mitochondrial material (aggregates and puncta) with EGFP-LC3B, only the time-point of 8h CCCP was considered. LC3B objects of 4-500px size were identified and only positively transfected cells were considered for further analysis. Identification of SSBP1 material was performed as follows: objects of 4-50px size were identified and merged as a single object if they were less than 5px apart. The merged SSBP1 objects with a ≥500px area were considered aggregates and smaller SSBP1 merged objects were considered puncta. Identification of TOM20 material was performed as follows: objects of 6-50px size were taken into account. Because TOM20 material engages into dots prior than SSBP1, all TOM20 material that was not overlapping with SSBP1 aggregates was considered as TOM20 puncta. Those were further classified according to their co-localization with SSBP1 in TOM20-SSBP1 or TOM20 (single) dots using a mask; if ≥40% of the TOM20 dot area was overlapping with SSBP1, the TOM20 dots were considered positive for SSBP1. Further, in order to determine positive or negative colocalization of mitochondrial puncta and aggregates with LC3B objects, mitochondrial material was masked with LC3B objects and for previously identified (a) TOM20 dots, (b) TOM20-SSBP1 dots and (c) SSBP1 clumps. TOM20 single dots and TOM20-SSBP1 dots with ≥50% overlap fraction of LC3B were considered LC3B-positive. SSBP1 clumps with ≥1% overlap fraction with LC3B objects were considered LC3B-positive.

3.6.4. Mitophagy in pentaKO cells expressing WT, K549R- and ΔCC3- TAX1BP1

First, individual parkin and TAX1BP1 objects of 6-40 and 3-40px of size, respectively, were identified. Further, parkin and TAX1BP1 objects were merged per cytoplasm/individual cells and only positive cells for both markers were considered. Mitochondrial SSBP1 objects of 4-500px size were identified and further merged if the individual objects were in close contact (distance between objects = 0px). Mitochondrial pixel area was computed by the software and further converted to desired units. All transfection conditions were taken into account for this analysis.

For the analysis of TAX1BP1 translocation on SSBP1 material, only cells with a mean TAX1BP1 intensity of ≥10aiu (arbitrary intensity units) were taken into account. Next, total SSBP1 area was masked with TAX1BP1 or parkin merged objects and the area of overlapping region was computed by the software. Of the total TAX1BP1 identified in a cell, the percentage of TAX1BP1 overlapping on SSBP1 material was calculated (% TAX1BP1 overlapping) and the same was performed for parkin (% parkin overlapping). Finally, the percentage of the total mitochondrial area overlapped by TAX1BP1 or parkin was calculated (% SSBP1 overlapped). The analysis was only performed for WT and TAX1BP1 mutant transfection conditions.

3.7. Statistical analysis

All experiments were performed at least three times with exception of ubiquitin staining of mitochondrial aggregates (n=2). For Western blot quantification, protein band area was measured using ImageJ software. Protein band intensities were normalized to actin in all whole cell lysate samples. For mitochondrial purification experiments, protein bands were normalized to their fraction control as follows: CM and Mito fractions were normalized to TOM20 and the Non-Mito fraction was normalized to LAMP1. Quantification of total and specific linkage ubiquitin species in VDAC2 pulldown experiments was performed as follows: ubiquitin smear intensities were first normalized to empty control and then further normalized to the corresponding VDAC2 pulldown signal for each VDAC2 transfected construct.

Statistical analysis of Western blot and CellProfiler-based quantifications was performed using Graph Pad prism 9 software. Statistical comparisons between more than two conditions were analyzed using one-way ANOVA. Significance between groups was established using Dunnett's test when comparing to a single control condition or Tukey's test when multiple comparisons were made. Fishers LSD test was used to establish significance between tested conditions (indicated in figure) when one-way ANOVA test indicated overall significant differences in the data set but further Tukey's test did not show any significant differences between groups. Statistical comparisons between two conditions were made using unpaired t-

tests. Overall significance was established when p-value<0.05; significant levels are indicated with asterisks following: ****: p<0.0001, ***: p<0.0005, **: p<0.005, *: p<0.05.

For the statistical analysis of quantitative proteomics related to proteasomal influence at early and later stages of mitophagy (chapter 4.8 and 4.9), Perseus software (version 1.6.15.0) was used (164). MitoCarta 3.0 was used as data base for mitochondrial sub-compartment protein classification (165). Only proteins present in at least two replicates were considered for downstream analysis. Identification of significantly regulated proteins between treatments was performed by using a one-sample t-test with p-value of either ≤0.1 or ≤0.05, for proteins with a fold change (Log_2 t-test difference) of >1.3. All other statistical analysis of proteome and ubiquitylome changes of protein clusters were performed by Katharina Zittlau and are described in Zittlau *et al.* 2022

4. Results

4.1. Generation of WT- or C431A-parkin HeLa stable cell lines

For the identification of novel parkin-dependent ubiquitination events under a defined parkin-dependent ubiquitination background, HeLa cells -which lack the expression of endogenous parkin (166) (Figure 4.1A)- were initially transfected with cDNAs encoding the catalytically active wild-type (WT) parkin or ligase-dead parkin (C431A). Next, cell clones with comparable parkin-expression levels were selected and further maintained to obtain stably parkin-expressing HeLa cell lines (see chapter 3.4.1). Ligase-dead parkin (C431A) is unactive and mitophagy deficient due to its inability to accept ubiquitin molecules at its active center (118,125,167). Successful mitophagy was induced in cells expressing WT-parkin. There are several ways to induce PINK1/parkin-mitophagy (105) (see section 2.3.1); throughout this study, mitophagy was induced through acute mitochondria depolarization using CCCP.

Generation of stable WT- and C431A-parkin expressing HeLa cells was achieved by transfection of N-terminally triple flag-tagged WT- or C431A-parkin expression constructs and further antibiotic selection for 13 days (140). Subsequently, WT- and C431A-parkin protein levels were screened by means of Western blot analysis to eventually chose the final WT- or C431A-parkin clones with comparable parkin-expressing levels (Figure 4.1A). Next, to control for successful and defective mitophagy phenotypes, mitochondria morphology as well as relative mitochondria protein levels were assessed upon CCCP-induced mitophagy in both WT- and C431A-parkin HeLa cells (Figure 4.1B-C).

As expected, initial mitochondrial fragmentation was observed after short times of mitochondrial depolarization which led to complete mitochondrial removal if extended up to 18h in WT-parkin cells only (Figure 4.1B). Consistently, parkin translocation was observed in WT-parkin expressing conditions while C431A-parkin remained cytosolic even after extended depolarization times (Figure 4.1B). Additionally, a strong increase in phosphorylated ubiquitin at S65 (pS65-Ubi) and successful degradation of specific mitochondrial substrates (VDAC and TOM20) was seen in WT-parkin cells only, while only a mild increase in pS65-Ubi and no mitochondria protein degradation was observed in C431A-parkin HeLa (Figure 4.1C). These data confirmed the expected phenotypes of successful and defective mitophagy in WT- and C431A-parkin expressing HeLa cells, respectively.

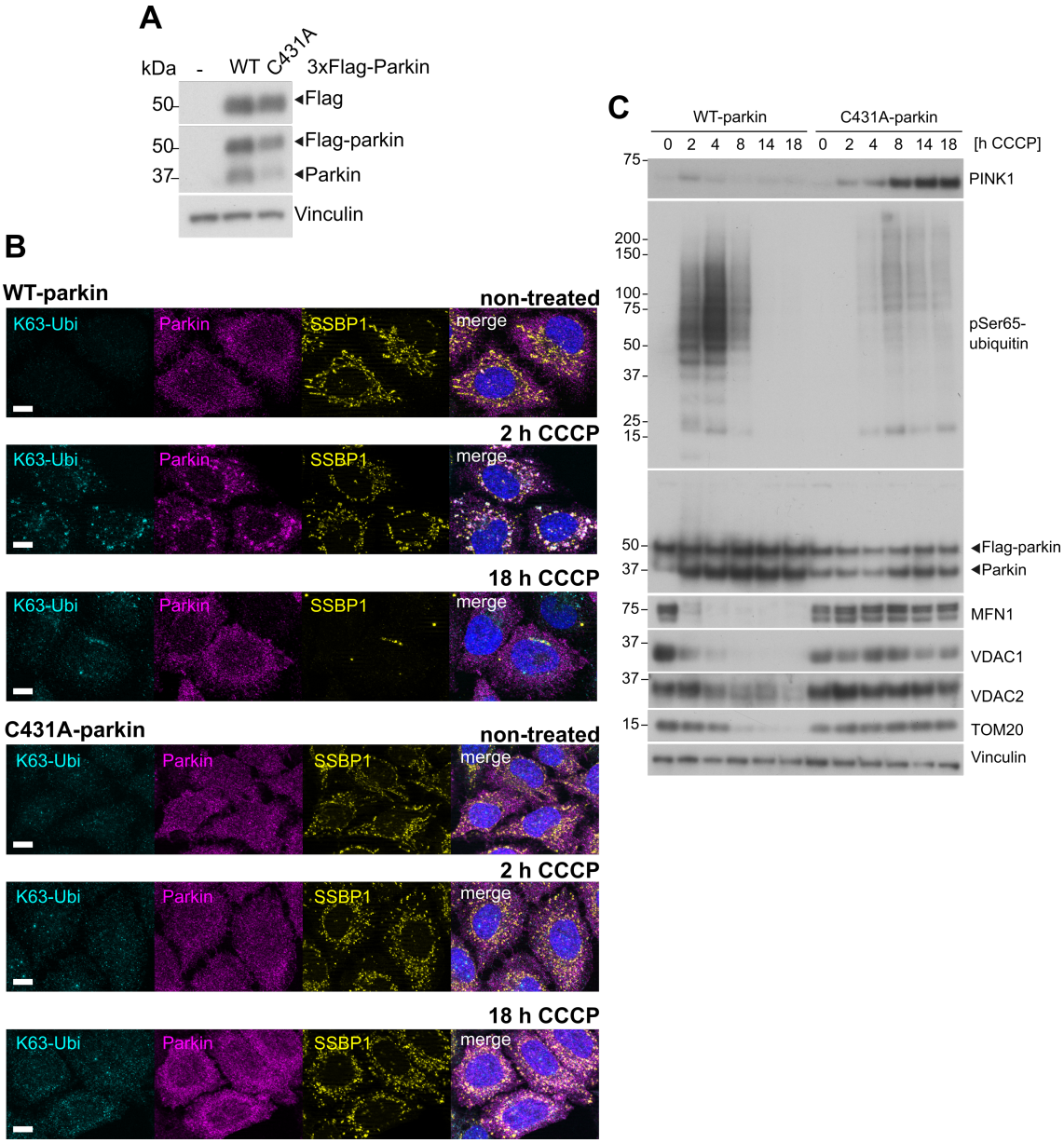


Figure 4.1: General mitophagy on stable WT- and C431A-parkin HeLa cells. (A) Parental HeLa (-) and selected HeLa cell clones stably expressing WT- and C431A-parkin, respectively. **(B)** Representative images showing mitochondria (yellow), parkin (magenta) and K63-linked ubiquitin chains (cyan) at basal levels (non-treated) or after the indicated treatment time-points on WT- and C431A-parkin expressing cells. Scale bars = 10 µm. **(C)** Mitophagy time-course in WT- and C431A-parkin cells after CCCP treatment at the indicated time-points. Data published in (132).

4.2. Proteomic analysis reveals sequential sub-organelle turnover of mitochondria

After having confirmed deficient or successful mitophagy phenotypes on the generated stable cell lines, mitophagy time-course experiments were performed to further analyze proteomic, ubiquitination and phosphorylation changes in an exploratory manner. Briefly, CCCP-dependent mitochondrial depolarization was induced at specific time points (2, 6, 12 and 18 h) in WT- and C431A-parkin expressing cells. After fractionation of whole cell lysate samples, mitochondria-containing fractions were pooled together for mass spectrometry analysis. Different labelling

methods were used for assessing whole proteome, 44econdar-proteome or ubiquitylome changes. For the identification of regulated phosphorylations, phosphorylated peptides were enriched and further labelled with triple dimethyl combinations in two separate sets for each parkin-expressing cell line (Table 4.1). For ubiquitylome analysis, ubiquitinated peptides were enriched and labelled with a single set of 10-plex tandem mass tag (10-plex TMT) (Table 4.1). These experiments were performed in collaboration with Prof. Dr. Boris Macek and the doctoral fellow M. Sc. Katharina Zittlau (Proteomic Center Tübingen, PCT). Briefly, cell culture, treatment and cell harvesting were performed by the author and cell pellets were given to Katharina Zittlau for further sub-cellular fractionation and further proteomic sample processing and analysis (described in 125).

Table 4.1: Phosphoproteome and ubiquitylome labeling schemes for each treatment conditions and parkin-expressing HeLa cell line. Three-plex di-methyl isotopes are indicated as follows; H: high, M: medium, L: low. 10-plex TMT isotopes are indicated with numbers 1-10. Data set numbering correspond to supplementary tables S1-3 described in Zittlau *et al.* 2022.

Phosphoproteome

Dimethyl labelling	H_1	M_1	L_1	L_2	M_2	H_2
CCCP treatment (h)	0	2	6	0	12	18
WT-parkin	Data set WT #1			Data set WT #2		
C431A-parkin	Data set C431A #1			Data set C431A #2		

Ubiquitylome and proteome

10-plex TMT isotopes	1	2	3	4	5	6	7	8	9	10
CCCP treatment (h)	0	2	6	12	18	0	2	6	12	18
Parkin (WT or C431A)	Data set WT					Data set C431A				

At a total proteomic level, hierarchal clustering of downregulated proteins appearing in WT-parkin HeLa cells only, allowed for the identification of 14 different protein clusters. Of those, only clusters containing mitochondrial proteins were taken into account and were linked to the corresponding sub-compartment, according to MitoCarta3.0 database (Figure 4.2) (132). Strikingly, differences in turnover kinetics for each mitochondrial sub-compartment were observed and seemed to be time-dependent (Figure 4.2).

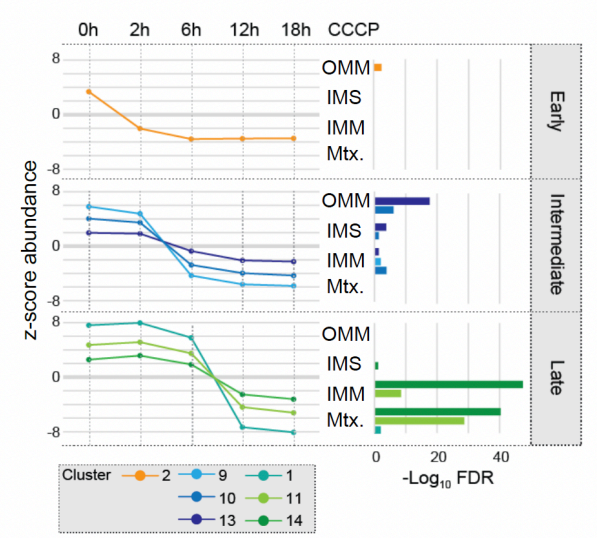


Figure 4.2: Proteomic analysis of mitochondrial sub-compartment turnover kinetics. Average z-score abundance of each cluster at the indicated treatment time-points. Over representation analysis combined with half-maximum of z-score abundance allows for classification of clusters according to their turnover kinetics into early (OMM), intermediate (OMM/IMS/IMM) and late (IMM/matrix). Author: Katharina Zittlau. Data published in (132).

4.2.1. Validation of mitochondrial sub-compartment degradation

At the start of this study, the general understanding of PINK1/parkin-dependent mitochondrial turnover mostly accounted for mitochondria being degraded as a single organelle (44,59,168–170), with few studies reporting parkin-dependent mitochondrial sub-organelle turnover differences and piecemeal mitophagy (98,135,171,172). For this reason, validation of the observed differences in mitochondrial sub-compartment degradation upon proteomic-analysis was needed. To simplify sub-organelle turnover analysis, different mitochondrial sub-compartment marker proteins were chosen: MFN1, TOM70, VDAC and TOM20 (OMM); COX4 (IMM) and CS and SSBP1 (matrix). Note that most of the markers were chosen based on antibody availability and performance rather than relative proteomic abundance in WT-parkin HeLa cells.

To assess individual protein turnover, protein levels at several time-points of mitochondrial depolarization were analyzed by means of Western blot quantification (Figure 4.3). Similar to what was observed in proteomic experiments, clear turnover kinetic differences were observed between OMM and inner mitochondrial (IMM and matrix) proteins, the turnover rate of the later ones being generally slower than OMM proteins (Figure 4.3A-B). As expected, no mitochondrial degradation was observed in C431A-parkin HeLa (Figure 4.3A).

Interestingly, clear differences on the degradation of OMM proteins were observed already after short mitochondrial depolarization (Figure 4.3A-C). While VDAC1 and TOM20 did not yet reach significant degradation levels, TOM70 and MFN1 were significantly degraded and had half-lives

of ≈1h and ≈2h, respectively (Figure 4.3B-C). On the other hand, VDAC1 and TOM20 degradation was not significant until 4h of CCCP treatment (Figure 4.3C and D), showing approximate half-lives of ≈3h and ≈4h, respectively (Figure 4.3B). Surprisingly, turnover kinetics of all inner-mitochondrial markers (IMM and matrix) were overall slower than OMM proteins (Figure 4.3A-B). For example, COX4 showed comparable turnover kinetics to TOM20 with 50% and 75% degradation ratios after 4h and 8h of CCCP, respectively (Figure 4.3D-E). On the other hand, matrix protein turnover was not prominent until 8h of mitochondrial depolarization, being significantly slower than IMM and OMM protein turnover (Figure 4.3D-E). Interestingly, different turnover rates were observed for CS and SSBP1, SSBP1 turnover was slower than CS after 8h of CCCP treatment but reached comparable degradation levels after 14h of treatment (Figure 4.3E). As expected, all markers were significantly degraded after extended mitochondria depolarization (18h of CCCP) (Figure 4.3F).

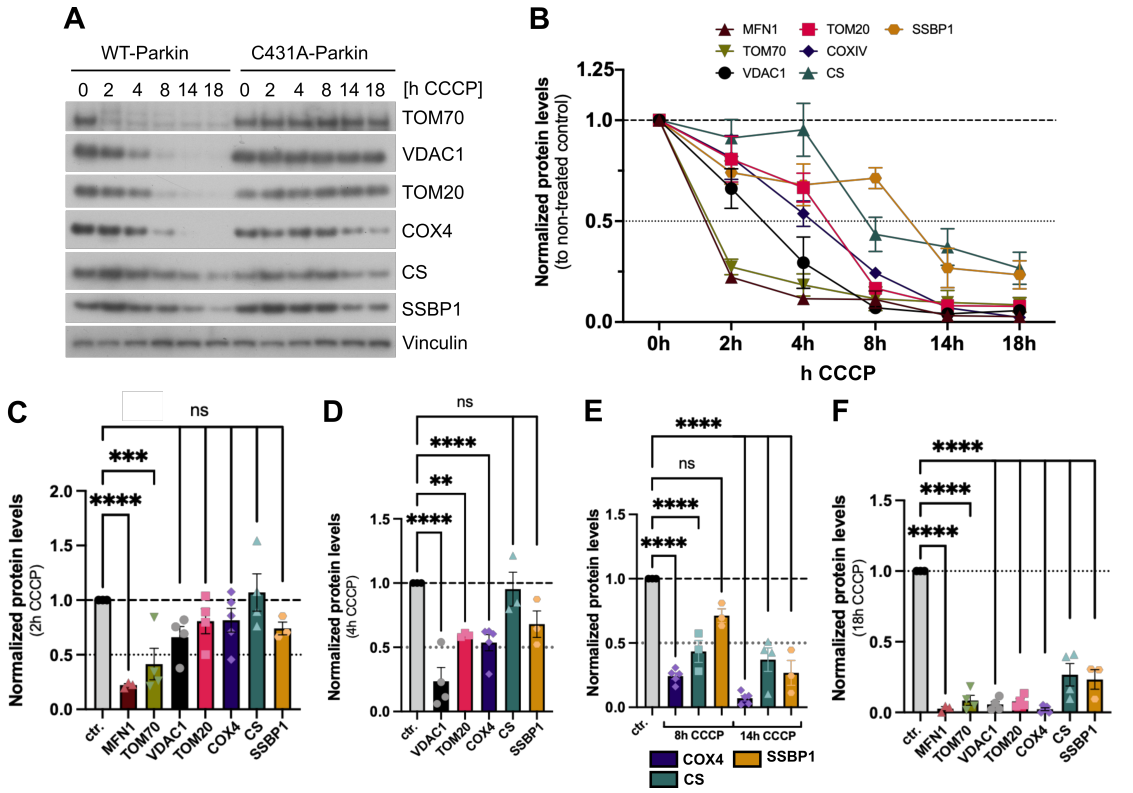


Figure 4.3: Western blot analysis of mitochondrial sub-compartment turnover kinetics. (A) Mitophagy curve of WT- and C431A-parkin cell lines showing protein levels of the indicated markers for each sub-compartment at the indicated CCCP treatment time-points. **(B-F)** Average protein levels normalized to basal protein levels for each marker in WT-parkin cells (B) over the course of mitophagy or (C-F) at the indicated time-points showing individual protein turnover significance compared to non-treated conditions (ctr.). Data published in (132,173).

Next, to further characterize sub-organelle turnover kinetics, mitochondria morphology was qualitatively assessed by means of fluorescence microscopy (Figure 4.4). Consistently, while mitochondria were elongated under basal conditions (Figure 4.4A-B, panel i), fragmentation of mitochondria was evident after 4h of depolarization (Figure 4.4A-B, panel ii and iii). In accordance with previous experiments, mitochondrial depolarization induced differential

degradation of OMM proteins, being MFN1 and TOM70 completely degraded after 4h of CCCP while TOM20 was still present in the form of mitochondrial aggregates (Figure 4.5A and B, panel ii). Notably, fine differences on mitophagy kinetics were observed on individual cells, showing higher levels of MFN1 and TOM70 than the majority of the cell population (Figure 4.4A and B, panel iii).

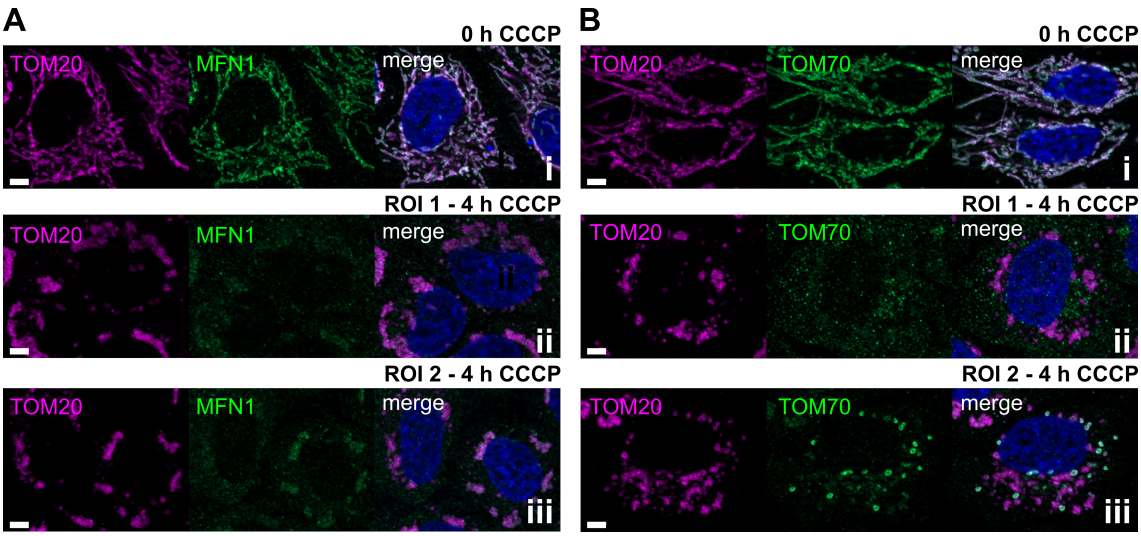


Figure 4.4: Turnover of MFN1 and TOM70 is upstream of TOM20 degradation. (A-B) Representative images of TOM20 (magenta) and **(A)** MFN1 or **(B)** TOM70 under no stress conditions or after CCCP treatment. ROI 1 represents the average cell population. ROI 2 represents < 50% of cells showing slower mitophagy kinetics. Scale bars = 5 µm. Data published in (173).

Similar to TOM20 behavior, VDAC2 was also engaged in mitochondrial aggregates after mitochondrial depolarization. However, its signal was not as prominent as TOM20 (Figure 4.5A), probably due to increased degradation kinetics as seen previously for VDAC1 (Figure 4.3D). At that stage, mitochondrial aggregates were positive for both TOM20 and SSBP1 (Figure 4.5B, panel i) and some puncta-like structures positive for TOM20 and disengaged from inner mitochondrial aggregates were detected (Figure 4.5B, panel ii). Interestingly, upon longer mitochondrial depolarization treatments, most of TOM20 material was engaged in puncta while inner mitochondrial proteins were found in mitochondrial aggregates (Figure 4.5B, panel iii-iv). On the other hand, while COX4 was engaged in mitochondrial aggregates and puncta, SSBP1 remained on mitochondrial aggregates after 4-8h of CCCP treatment (Figure 4.5C, panel ii-iv). Interestingly, different morphological profiles were observed for CS and SSBP1 after extended depolarization treatment (Figure 4.5D): while SSBP1 was engaged in relatively big aggregates, CS-puncta were observed after 8h of mitochondrial depolarization (Figure 4.5C, panel ii-v). After 14h of depolarization, the IMM protein COX4 was mostly reduced to puncta while the matrix proteins SSBP1 and CS remained in mitochondrial aggregates. After extended depolarization (18h CCCP) SSBP1- and CS-aggregates seemed to be disrupted and SSBP1- and CS-only puncta were observed (Figure 4.5C, panel vi-vii).

Next, to conclude the validation, morphological behavior of TOM20, COX4 and SSBP1 after short or extended mitochondrial depolarization was assessed by means of CellProfiler image-based analysis (Figure 4.5E-H). Briefly, mitochondrial profiles were filtered by pixel size and categorized as puncta or aggregates (see section 3.6). After extended mitochondria depolarization, TOM20-aggregates were completely reduced while COX4-aggregates were only reduced to half in comparison to an earlier time-point (Figure 4.5E-F). Notably, SSBP1-positive aggregates did not decrease after extended depolarization (Figure 4.5E-F). Intriguingly, the number of initial TOM20-aggregates was lower than COX4- or SSBP1-aggregates under the same depolarization conditions (Figure 4.5E-F). On the other hand, while TOM20-puncta were already observed after 4h of CCCP treatment and slightly decreased after longer depolarization (Figure 4.5G), COX4-puncta increased with extended depolarization (Figure 4.5G). Similar to SSBP1-aggregates, number and size of SSBP1-puncta did not show any differences with longer treatment (Figure 4.5G). However, COX4-puncta size slightly increased after longer depolarization while size of TOM20-puncta was significantly reduced (Figure 4.5H).

Taken together, these data confirm the observed sub-organelle turnover differences initially observed in proteomics analysis.

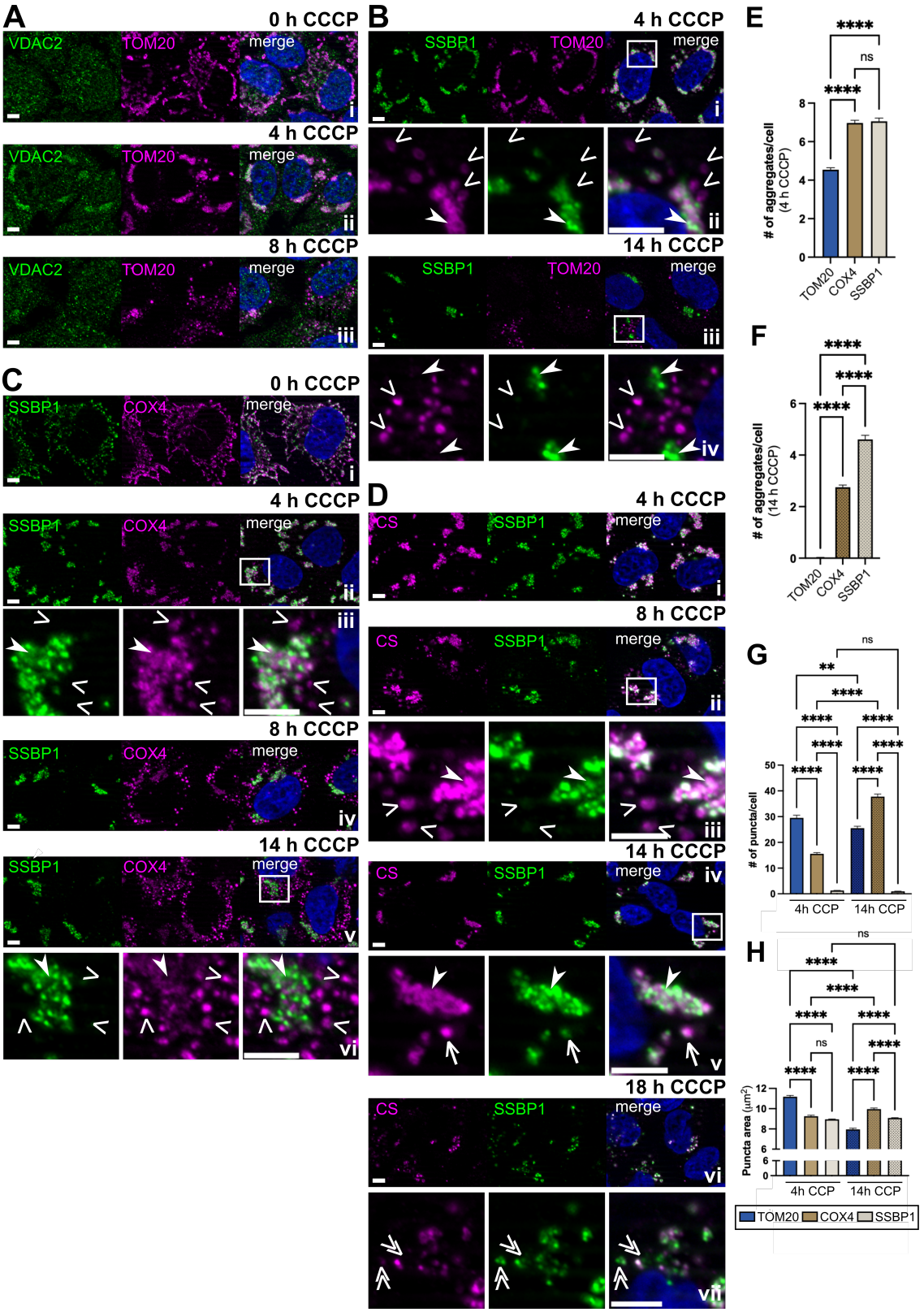


Figure 4.5: Morphological differences of OMM and inner- mitochondrial markers upon mitochondrial turnover. (A) Representative images of TOM20 (magenta) and VDAC2 (green) under no stress conditions or after CCCP treatment. **(B-D)** Distinct morphologies of SSBP1 (green) with (B) TOM20, (C) COX4 and (D) CS (all magenta) at the indicated time-points of CCCP treatment. Open arrowheads indicate SSBP1-free material. Closed arrow heads indicate mitochondrial aggregates positive for green and magenta markers. Arrows indicate CS-SSBP1-positive puncta. Double arrowheads indicate SSBP1 material free of CS. Scale bars = 5 µm. Data published in (173).

4.2.2. Differential mitochondrial sub-compartment degradation under endogenous parkin expression

In order to extend the previous findings to endogenous parkin-expressing conditions, mitophagy was induced in cell lines expressing endogenous parkin and the morphology of outer and inner mitochondrial markers was assessed by means of qualitative immunofluorescence. For these experiments, CCCP-induced or antimycin A-induced mitophagy was performed in HEK293 as well as neural precursor cells (NPCs). Extended depolarization treatments were needed in order to see morphological changes or mitochondrial degradation, probably due lower parkin-expression levels in comparison to WT-parkin HeLa cells (Figure 4.6)

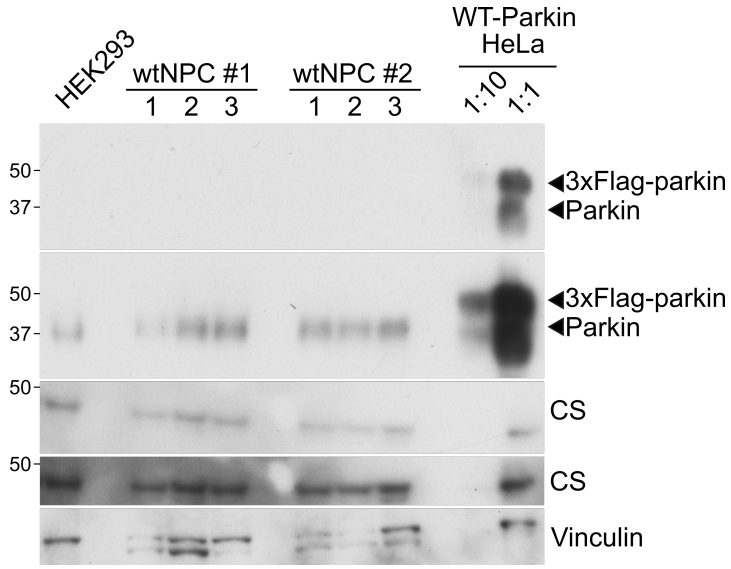


Figure 4.6: Relative parkin expression levels in HEK293, wild-type NPC (wtNPC) and WT-parkin HeLa cell lines. Whole cell lysates were used for all samples. 5 μg of total protein were loaded except for WT-parkin HeLa (1:10) where 0.5 μg of total protein was used. For both wtNPC cell lines, samples of three independent replicates are shown (numbers 1-3).

Mitochondria of HEK293 cells were elongated under basal conditions (Figure 4.7A-B, panels i) but showed signs of degradation after extended CCCP treatment (Figure 4.7A-B, panels ii). On the other hand, while CCCP-induced depolarization in HEK293 cells promoted mitochondrial fragmentation, the observed mitochondrial aggregates were not as prominent as the ones observed in WT-parkin HeLa cells and mostly contained outer and inner- mitochondrial markers (Figure 4.7A-B, panels ii). Nevertheless, the presence of TOM20-positive puncta which were not engaged with CS- or COX4-aggregates could be observed (Figures 4.7A-B, panels iii and 4.7B, panel iv).

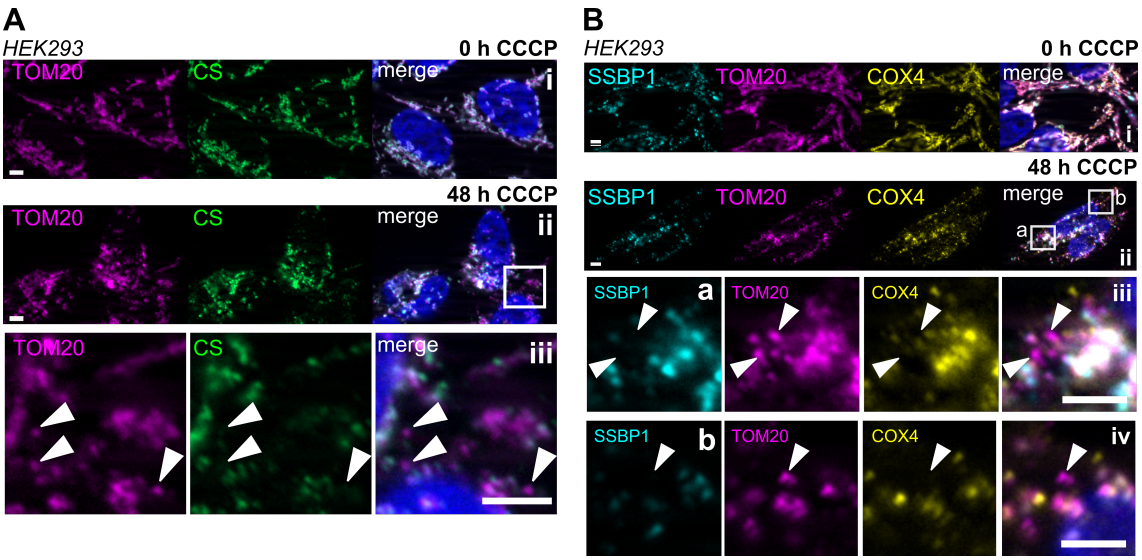


Figure 4.7: CCCP-induced mitophagy in HEK293 cell line. (A-B) Representative immunofluorescence images showing (A) TOM20 (magenta) and CS (green) or (B) SSBP1 (cyan), COX4 (yellow) and TOM20 (magenta) at the indicated CCCP treatment time-points. Arrowheads indicate TOM20-positive puncta negative for CS material. Scale bars = 5 µm. Data published in (173).

Additionally, given the importance of parkin-dependent mitophagy in neurodegenerative diseases, mitochondrial morphology upon induction of parkin-dependent mitophagy was assessed in two wild-type NPC lines (Figure 4.8). Similar as observed in HEK293, extended mitochondria depolarization induced global mitochondrial degradation but mitochondrial aggregates were not as prominent as in WT-parkin HeLa cells (Figure 4.8A-B, panels ii and iv). In addition, similarly as in HEK293 cells, TOM20-positive puncta disengaged from CS material were detected (Figure 4.8A-B, panels iii and iv).

Together, these data suggest that mitochondrial sub-compartment degradation can also take place under endogenous parkin-expressing conditions. In addition, it is noteworthy that parkin-dependent mitophagy kinetics in all endogenously expressing parkin cell lines was considerably slower than in WT-parkin HeLa, indicating that parkin over-expression levels can influence PINK1/parkin mitophagy dynamics.

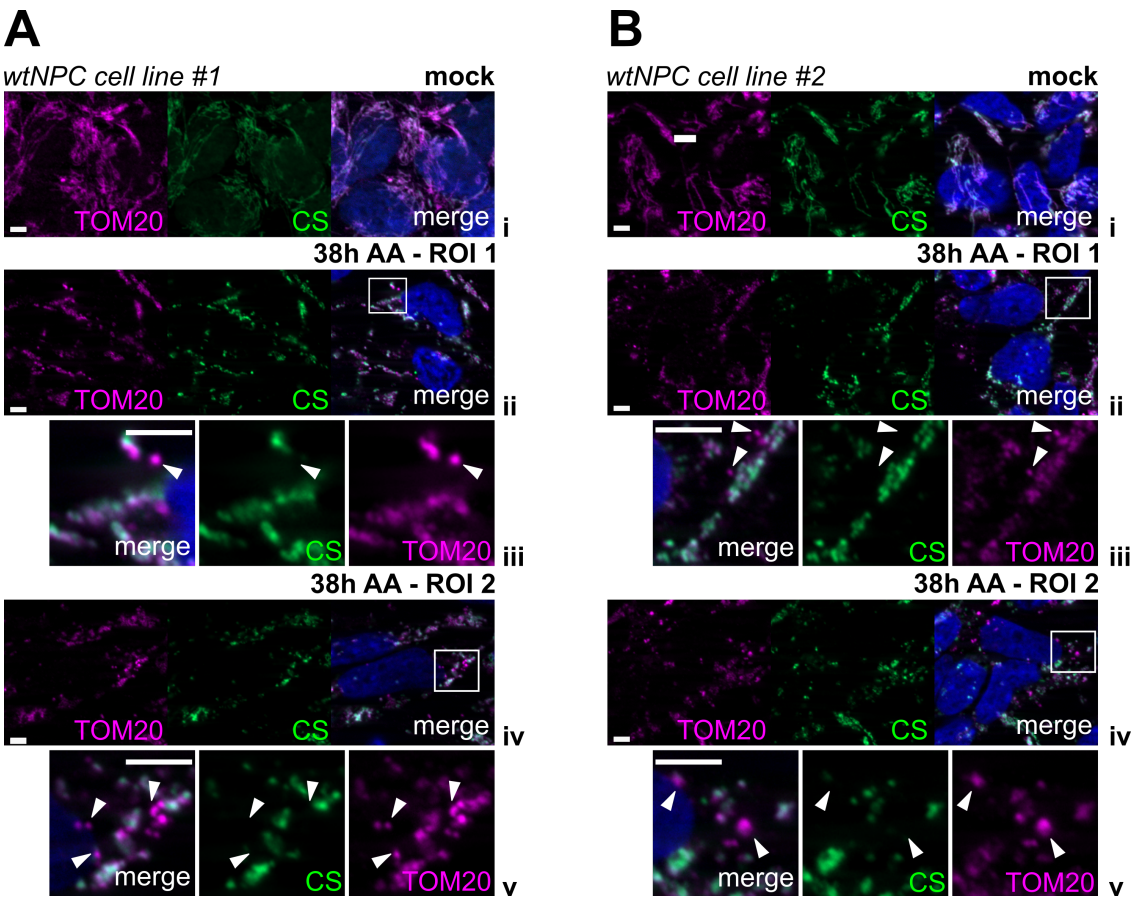


Figure 4.8: Induced mitophagy in wild-type NPC cell lines. (A-B) Representative immunofluorescence images showing TOM20 (magenta) and CS (green) for both wtNPC cell lines (A) #1 and (B) #2. Arrowheads indicate TOM20-positive puncta negative for CS material. Scale bars = 5 µm. Data published in (173).

4.3. Mitochondrial sub-compartments are ubiquitinated in a sequential parkin-dependent manner

PINK1/parkin mitochondrial turnover is ruled by parkin-dependent ubiquitination on mitochondrial proteins (131,134,174,175). Interestingly, ubiquitination levels of WT-parkin HeLa cells did not reach a plateau state after extended CCCP-treatment but were rather dynamic, being transiently upregulated (4h CCCP) and later reduced after extended depolarization (14-18h CCCP) (Figure 4.1C). Additionally, mitochondrial sub-organelle turnover also followed dynamic kinetics (Figure 4.2-5). Thus, to gain a better insight on parkin-dependent ubiquitination dynamics in our cell model, mass-spectrometry analysis on the overall ubiquitination events was performed by Katharina Zittlau (see chapter 4.2). Briefly, hierarchical clustering analysis allowed for the identification of four different clusters containing parkin-dependent ubiquitinated proteins which could be related to separate mitochondrial sub-compartment (132). Surprisingly, not only OMM proteins were present in the identified clusters, but IMM and matrix proteins were also included (Figure 4.9A). Ubiquitination events on significantly downregulated OMM, IMM and matrix proteins in WT-parkin cells are summarized on Table 4.2.

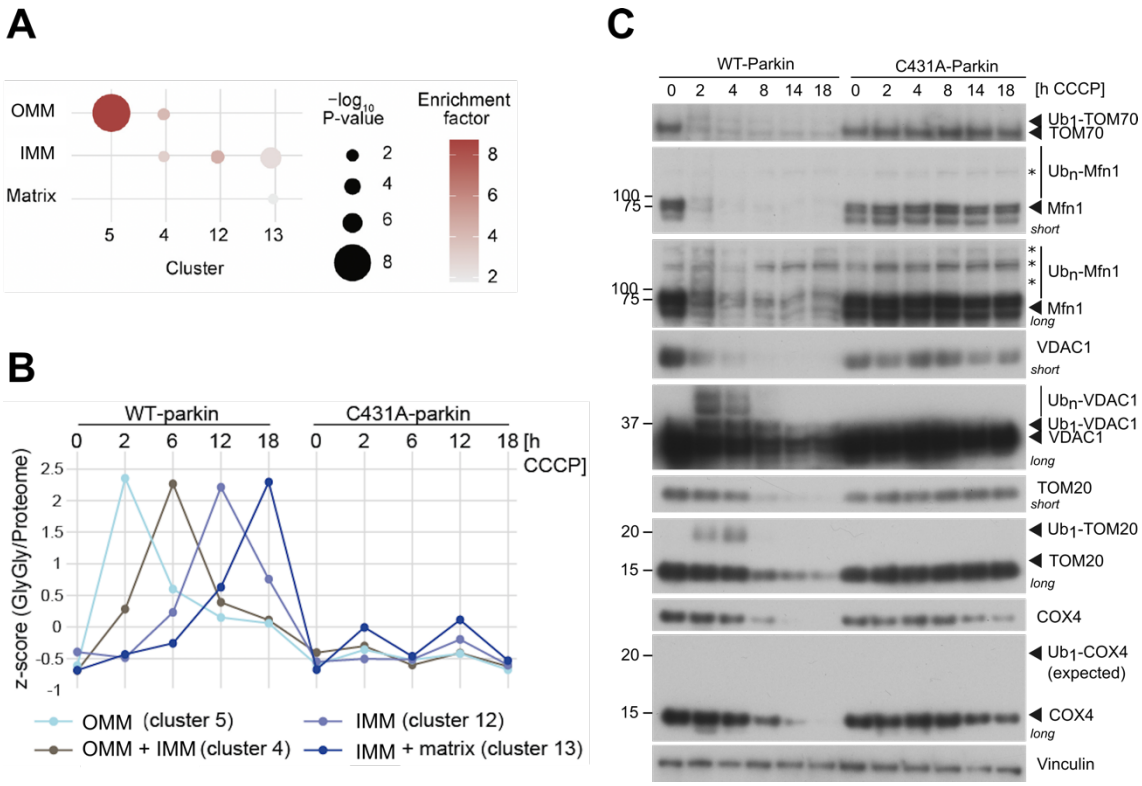


Figure 4.9: Mitochondrial sub-compartment ubiquitination kinetics. (A) Mitochondrial sub-compartment composition of the identified ubiquitylome clusters showing parkin-dependent and CCCP treatment response. Author: Katharina Zittlau. (B) Ubiquitin kinetic profiles of previously identified clusters in WT- and C431A-parkin cells at the indicated CCCP-treatment time-points. Author: Katharina Zittlau. **(C)** Mitophagy time-course in WT- and C431A-parkin expressing cells showing ubiquitination profiles of specific OMM markers. Data published in (132).

Interestingly, while global OMM ubiquitination peaked after 2h of CCCP treatment, maximum levels of IMM and matrix ubiquitination were achieved after 6h or 18h of mitochondrial depolarization, respectively (Figure 4.9B). Importantly, the differences on protein-specific mitochondrial degradation dynamics observed previously (Figure 4.3-5) could be related to OMM-specific ubiquitination events (Figure 4.9C). More specifically, while VDAC1 was highly ubiquitinated after 2h of mitochondrial depolarization, MFN1 and TOM70 ubiquitination were barely detectable at that stage, probably due to increased protein degradation, as evidenced by Western blot quantification analysis (Figure 4.3B-F). On the other hand, while TOM20 ubiquitination was already detectable after 2h of depolarization, it reached maximum levels after 4h of CCCP treatment (Figure 4.9C).

Table 4.2: List of ubiquitination sites on OMM, IMM and matrix proteins. Only proteins belonging to significantly downregulated proteome clusters are shown, except for VDAC2. Cluster number corresponds to ubiquitylome (Ub) cluster. Mitochondria localization according to MitoCarta 3.0. Complete ubiquitylome data set can be found on https://msviewer.ucsf.edu/prospector/cgi-bin/msform.cgi?form=msviewer with accession key: *suxnuntnwt*. OMM: outer mitochondrial membrane; IMS: inner mitochondrial space; IMM: inner mitochondrial membrane. Data published in (132).

	Gene name	Protein name	Lysine position	Cluster Ub
OMM	CISD1	MitoNEET	51, 55, 68, 79, 104	5
	CPT1A	Carnitine palmitoyltransferase 1ª	180	5
	FIS1	Mitochondrial fission 1 protein	25	5
	FKBP8	Peptidyl-prolyl cis-trans isomerase FKBP8	271	5
	MTARC1	Mitochondrial amidoxime reducing component 1	295	5
	MTARC2	Mitochondrial amidoxime reducing component 2	59	5
	MFN1	Mitofusin-1	395, 396, 399, 416	5
	RHOT2	Mitochondrial Rho GTPase 2	409	5
	RMDN3	Regulator of microtubule dynamics protein 3	305	13
	TOMM40	Mitochondrial import receptor subunit TOM40 homolog	351	13
	TOMM70	Mitochondrial import receptor subunit TOM70	168, 170, 178, 359, 536, 570	5
	VDAC1	Voltage-dependent anion-selective channel protein 1	20, 53, 109	13
	VDAC2	Voltage-dependent anion-selective channel protein 2	31, 64, 120	13
	VDAC3	Voltage-dependent anion-selective channel protein 3	109	13
IMS/IMM	AIFM1	Apoptosis-inducing factor 1	105, 195	13
	ATAD3B	ATPase family AAA domain-containing protein 3B	117, 198, 214	12
	ATP5A1	ATP synthase subunit alpha	167, 531, 539	13
	ATP5I	ATP synthase subunit e	49, 50, 69	13
	ATP5B	ATP synthase subunit beta	124, 198	13
	CYC1	Cytochrome c1	50	13
	HTRA2	Serine protease HTRA2	237	13
	NDUFA8	ADH dehydrogenase [ubiquinone] 1 alpha subcomplex subunit 8	54	13
	PHB1	Prohibitin 1	4, 83, 202	13
	PHB2	Prohibitin 2	6, 89, 216, 262, 296	13
	PTGES2	Prostaglandin E synthase 2	141, 269	4
	SLC25A11	Mitochondrial 2-oxoglutarate/malate carrier protein	15, 46	13
	SLC25A24	Calcium-binding mitochondrial carrier protein ScaMC-1	96, 285, 477	13
	TIMM8B	Mitochondrial import inner membrane translocase subunit Tim8 B	80	4
	TIMM9	Mitochondrial import inner membrane translocase subunit Tim9	12	12
	TIMM13	Mitochondrial import inner membrane translocase subunit Tim13	16	4
	UQCRFS1	Cytochrome b-c1 complex subunit Rieske	163	13
Matrix	HSPD1	60 kDa heat shock protein	87, 191, 206, 300	13
	THNSL1	Threonine synthase-like 1	44	13

Unfortunately, despite the detection of ubiquitinated inner mitochondrial proteins in MS/MS analysis, ubiquitination of inner- mitochondrial proteins could not be confirmed by means of Western blot analysis (Figure 4.9C). To try to overcome this issue, total ubiquitination of inner-mitochondrial proteins was assessed by means of qualitative immunofluorescence. There, ubiquitination of inner- mitochondrial material -either represented by COX4 or SSBP1- could be detected after 8-14h of CCCP treatment (Figures 4.10A, panels iv-vi and 4.10B, panels iii-vi). Interestingly, some TOM20-puncta were positive for total ubiquitin after 4h and 8h of CCCP treatment (Figure 4.10A, panels iii, v-vi) while COX4-puncta were mostly positive for total ubiquitin after 8h and 14h (Figure 4.10B, panels ii, iv and vi).

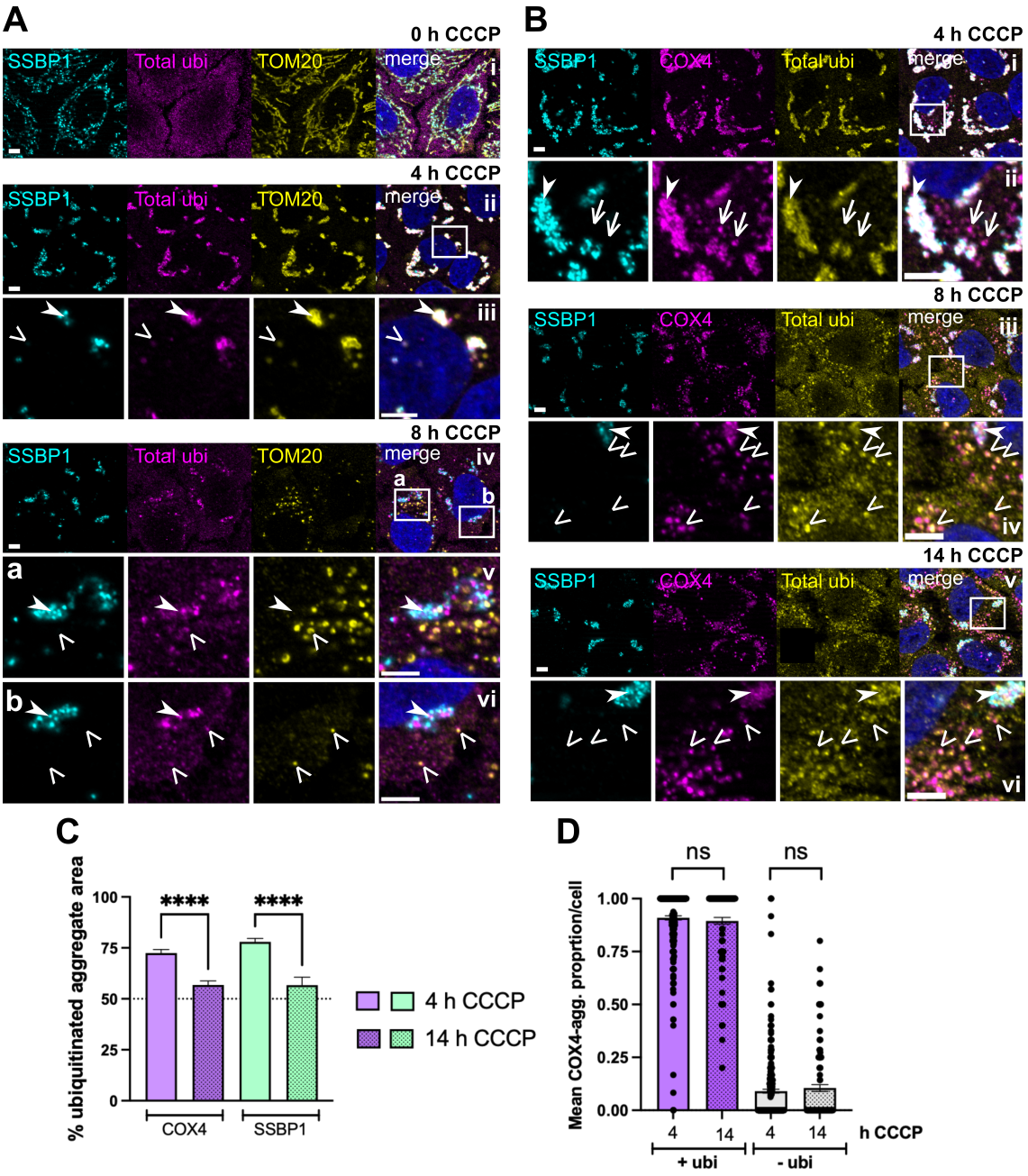


Figure 4.10: Fragmented mitochondria and inner- mitochondrial aggregates are ubiquitinated upon mitochondrial depolarization. (A) Fragmented mitochondria represented by TOM20 (yellow) as well as SSBP1-aggregates (cyan) are

positive for total ubiquitin (magenta). Open arrowheads indicate TOM20-puncta positive for total ubiquitin. Closed arrowheads indicate fragmented mitochondria (at 4h CCCP) or SSBP1-aggregates (at 8h CCCP) positive for total ubiquitin. **(B)** Fragmented mitochondria (at 4h CCCP) and inner- mitochondrial aggregates positive for COX4 are ubiquitinated (magenta). Arrows indicate COX4-puncta negative for total ubiquitin. Open arrowheads indicate COX-puncta positive for total ubiquitin. Closed arrowheads indicate fragmented mitochondria (at 4h CCCP) or inner mitochondrial aggregates (at 8h CCCP) positive for total ubiquitin. Scale bars = 5 µm. **(C)** Percentage of inner-mitochondrial total area covered by ubiquitin after the indicated treatments. **(D)** Mean proportion of COX4-aggregates positive or negative for total ubiquitin. Agg.: aggregate. Data published in (132).

Next, in order to better characterize late ubiquitination of inner- mitochondrial aggregates, CellProfiler image-based analysis was performed to assess total ubiquitin co-localization on mitochondrial aggregates after short and extended depolarization treatment (Figure 4.10C and D). For this analysis, areas of mitochondrial aggregates positive for total ubiquitin were computed and related to total mitochondrial area per cell, giving a percentage of mitochondrial aggregate area covered by ubiquitin. Upon quantification, a 25 % reduction on the percentage of ubiquitinated mitochondrial aggregate area was observed after extended CCCP treatment for both COX4- and SSBP1-aggregates (Figure 4.10C). However, most of COX4-aggregates were positive for ubiquitin after long depolarization treatment (Figure 4.10D). Unfortunately, due to an increased background of total ubiquitin immunostaining after extended CCCP treatment (Figure 4.10A-B), CellProfiler-based analysis of TOM20- and COX4-puncta ubiquitin co-localization was not performed.

Taken together, these data indicate a potential relationship between the sequential sub-organelle degradation dynamics and their ubiquitination status during the course of mitophagy, being late stages of mitophagy characterized by ubiquitinated inner mitochondrial aggregates. Interestingly, while most of inner- mitochondrial aggregates appear ubiquitinated at later stages of mitophagy, a significant reduction on ubiquitin coverage was detected.

4.4. Autophagy-link confirmation of parkin-dependent mitochondrial turnover

Characterization of mitochondria sub-organelle turnover dynamics revealed different OMM, IMM and matrix morphologies after intermediate and late stages of PINK1/parkin mitophagy, suggesting the involvement of distinct degradation pathways for OMM and inner mitochondrial substrates. On the other hand, previous data in this study also suggested a potential link between the turnover dynamics of mitochondrial sub-compartments and their ubiquitination kinetics, perhaps indicating common grounds for protein turnover pathways. Because one of the hallmarks of mitophagy is the autophagic targeting of ubiquitinated mitochondrial material, the

involvement of autophagy receptors and autophagosomes on mitochondrial cargo was further characterized.

4.4.1. Sequential involvement of the autophagy machinery

As it has previously been reported, parkin promotes autophagy receptor recognition of mitochondrial ubiquitinated proteins during mitophagy (59). However, upon mass-spectrometry analysis of total proteome in WT-parkin HeLa cells, only the autophagy receptor p62/SQSTM and TAX1BP1/3 were detected (Table 4.3). In addition, while few reports involved TAX1BP1 in parkin-dependent mitophagy at the beginning of this study (59,176), several studies linked p62/SQSTM with mitochondrial turnover (62,177,178). For these reasons, p62/SQSTM was used as a reference autophagy receptor throughout this study and TAX1BP1 involvement was further characterized (see chapters 4.16-18).

Table 4.3: List of autophagy adaptors detected in LC-MS/MS analysis upon mitophagy induction in WT-parkin HeLa. Classification of all five known autophagy adaptors according to their identification in mass-spectrometry screens of total proteme (T), ubiquitylome (Ub) and phosphoproteome (P). Identified ubiquitinated or phosphorylated residues are indicated. n= 1 or 2 indicates the number of replicates where the modified residue was found.

Autophagy adaptor	Detected in MS/MS screen			Ubiquitinated residues	Phosphorylated residues
	T	Ub	P		
Optineurin	no	-	-	-	-
NDP52	no	-	-	-	-
NBR1	no	-	-	-	-
SQSTM	yes	yes	yes	K13 (n=1) and K435 (n=2)	- n=2 T221, S233, T269, S272, S275, S276, S277, S284, S361 and S366 - n=1 S266, S284, S332, S342, S355, and S365
TAX1BP1	yes	yes	yes	K439, K549 and K571 (all n=1)	S344 (n=1)

First, the implication of p62/SQSTM in WT-parkin HeLa mitophagy was assessed (Figure 4.11A). While p62/SQSTM localization was cytosolic under basal conditions (Figure 4.11A, panel i), mitochondrial translocation of the autophagy receptor was observed after 4h of mitochondrial depolarization (Figure 4.11A, panel ii). Importantly, inner mitochondrial aggregates as well as TOM20 puncta were also positive for this autophagy receptor after extended depolarization treatment (Figure 4.11A, panels iii).

Given that autophagy receptors are known to interact with LC3B through their LIR domain (44), LC3B recruitment on fragmented mitochondria as well as inner mitochondrial aggregates was

investigated (Figure 4.11B-G). Upon 8h of mitochondria depolarization, endogenous LC3B-puncta which partially co-localized with TOM20 puncta were observed (Figure 4.11B, zoom panels a-c). However, LC3B-puncta were not highly enriched at the overlapping TOM20 puncta regions (Figure 4.11B, zoom panels a-c), making it difficult to conclude the involvement of the autophagosome marker on TOM20 material. On the other hand, no LC3B recruitment was observed neither on TOM20-positive or TOM20-negative mitochondrial aggregates (Figure 4.11B, zoom panels a-b). Thus, to enhance LC3B signal-to-noise ratio, WT-parkin expressing cells were transfected with EGFP-LC3B (Figure 4.11C) and single-cell analysis of mitochondrial puncta and aggregates co-localizing with EGFP-LC3B puncta was performed with CellProfiler (Figure 4.11D-G). After 8h of mitochondria depolarization, brighter LC3B-puncta were observed, indicating a true enrichment of LC3B in puncta-like structures (Figure 4.11C). In addition, similarly as for endogenous LC3B, some overlap of EGFP-LC3B-structures with TOM20-puncta and SSBP1-aggregates was observed (Figure 4.11C). TOM20-puncta were either completely (closed arrowheads) or partially overlapped (arrows) with EGFP-LC3B structures, possibly indicating different stages of autophagy-dependent TOM20 turnover. In addition, a significant lower number of TOM20-puncta free of LC3B were observed (open arrowheads) (Figure 4.11C, zoom panel a and Figure 4.11D). Moreover, no differences in size were observed for TOM20-puncta co-localizing with or free of LC3B (Figure 4.11D), suggesting that TOM20 free-LC3B puncta could be simply TOM20 puncta not yet targeted by autophagosomes at that stage of the pathway. Additionally, EGFP-LC3B puncta were also engaged with SSBP1-aggregates (Figure 4.11F). However, the number of LC3B structures involved in their recognition was limited and focalized in particular regions (Figure 4.11C, zoom panel c), possibly indicating reduced autophagosome formation at the vicinity of inner- mitochondrial aggregates at this stage of the pathway. Interestingly, LC3B-positive SSBP1-aggregates showed bigger sizes than LC3B-negative SSBP1-aggregates (Figure 4.11G), suggesting the involvement of autophagosomes for SSBP1-aggregate degradation. Moreover, in some cells with faster mitophagy kinetics (Figure 4.11C, panel ii), SSBP1-puncta both positive and negative for LC3B were observed (Figure 4.11C, zoom panels c-d). While SSBP1-LC3B-positive puncta were mostly seen at peripheral cytoplasmic regions (Figure 4.11C, zoom panel d), SSBP1-LC3B-negative puncta were found in close proximity of remaining TOM20-puncta, possibly indicating different mitophagy stages at the mitochondrial network (Figure 4.11C, zoom panel d).

Overall, these data indicate that degradation of OMM material as well as inner- mitochondrial aggregates relies on autophagy adaptor recognition and further autophagosome engulfment of outer- and inner- mitochondrial cargo.

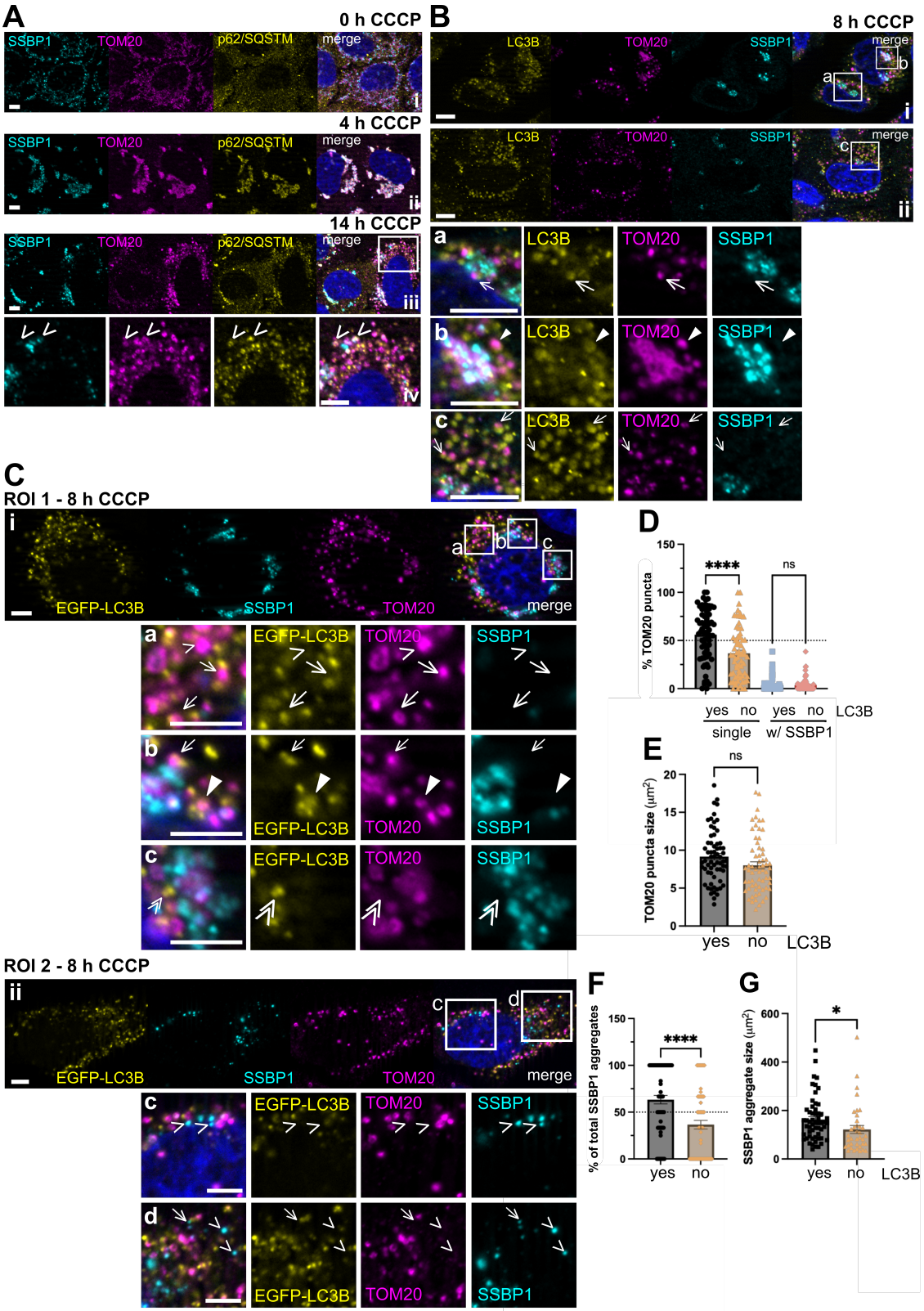


Figure 4.11: p62/SQSTM and LC3B engagement on mitochondrial cargo after mitochondrial depolarization. (A) p62/SQSTM (yellow) is recruited to fragmented mitochondria (magenta and cyan) as well as inner- mitochondrial material (cyan) at the indicated CCCP treatment time-points. **(B-C)** (B) Endogenous LC3B (yellow) or (C) EGFP-LC3B (yellow) engaged with TOM20 material (magenta) after 8h of mitochondrial depolarization. In (B) two ROIs are chosen (i-ii) to account for all identified TOM20- and LC3B-structures. In (C), ROI 1 accounts for the majority of cell population while ROI 2 represents 10% of WT-parkin HeLa cell population. Arrows indicate mitochondrial material partially co-localizing with LC3B. Open arrows indicate mitochondrial material free of LC3B. Closed arrows indicate TOM20-puncta completely overlapped by LC3B. Double open arrowheads indicate LC3B puncta on SSBP1-aggregates. **(D-G)**

CellProfiler-based quantification of **(D)** single and SSBP1-positive (w/ SSBP1) TOM20-puncta, **©** area of single TOM20-puncta, **(F)** percentage of total SSSBP1-aggregate classified for positive (yes) or negative (no) EGFP-LC3B recognition and **(G)** area of SSBP1-aggregates classified for positive (yes) or negative (no) LC3B co-localization. Scale bars = 5 µm. Data published in (173).

4.4.2. Sequential involvement of the lysosomal machinery

Following LC3B engagement on mitochondrial cargo, mature autophagosomes are fused with lysosomes for complete cargo turnover (44,179). Hence, to confirm if there were any temporal differences on the delivery of mitochondrial sub-compartment material to lysosomes, the involvement of total and active lysosomes on mitochondrial sub-compartment material was assessed. For the identification of total lysosomes, the lysosomal associate marker protein 1 (LAMP1) was used while Lysotracker-RED -a fluorescent marker that is widely used to monitor lysosome acidification (104,180)- was used to monitor active lysosomes.

LAMP1 puncta were found in close apposition with TOM20 puncta after early depolarization (4h CCCP) while they co-localized with both TOM20 and COX4 puncta after intermediate CCCP treatment (8h CCCP) (Figure 4.12A-B). Intriguingly, remaining COX4-positive or SSBP1-aggregates did not co-localized with LAMP1 neither after intermediate (8h CCCP) or extended (14h CCCP) depolarization treatment (Figure 4.12B-C). Similar results were obtained when analyzing active lysosome co-localization with mitochondrial cargo (Figure 4.13). While TOM20 and COX4 puncta clearly co-localized with the active lysotracker marker after 8h of CCCP treatment, no co-localization was observed for TOM20-, COX4- or CS-aggregates at any time-point of the pathway (Figure 4.13A-B).

Overall, temporal differences in the engagement of mitochondrial sub-compartment marker with total lysosomes were observed. Thus, these results indicate that OMM and IMM proteins are delivered to the lysosomal machinery after early (4h CCCP) or intermediate (8h CCCP) depolarization treatment. Respectively, SSBP1-aggregates are not directly targeted to lysosomes, suggesting either delayed degradation and/or intermediate additional steps for the complete turnover of inner mitochondrial aggregates.

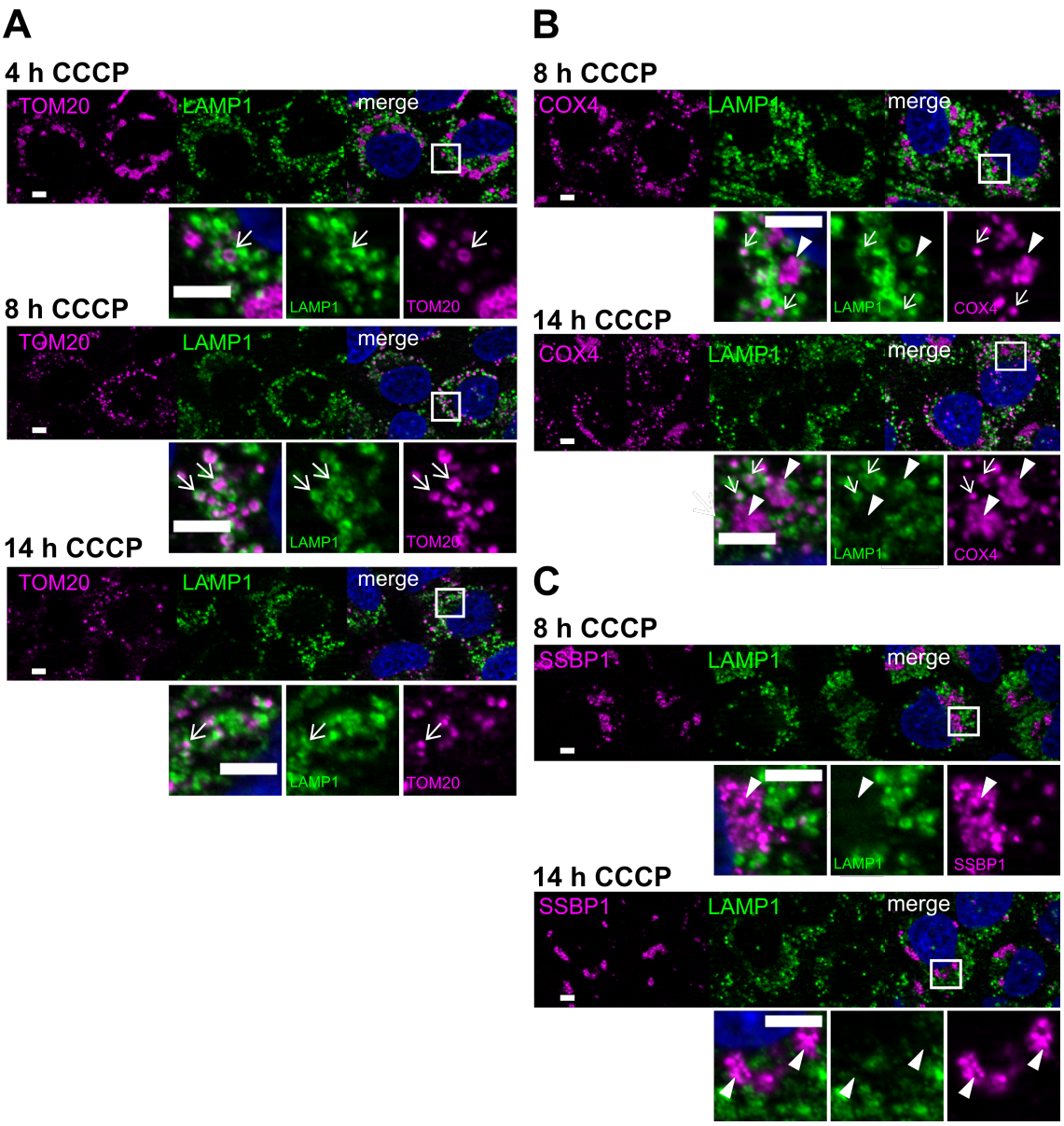


Figure 4.12: Mitochondrial sub-compartment cargo is differentially engaged with LAMP1. (A-C) Representative images showing LAMP1 (green) together with (A) TOM20, (B) COX4 or (C) SSBP1 (magenta) at different stages of mitophagy as indicated. Scale bars = 5 µm. Data published in (173).

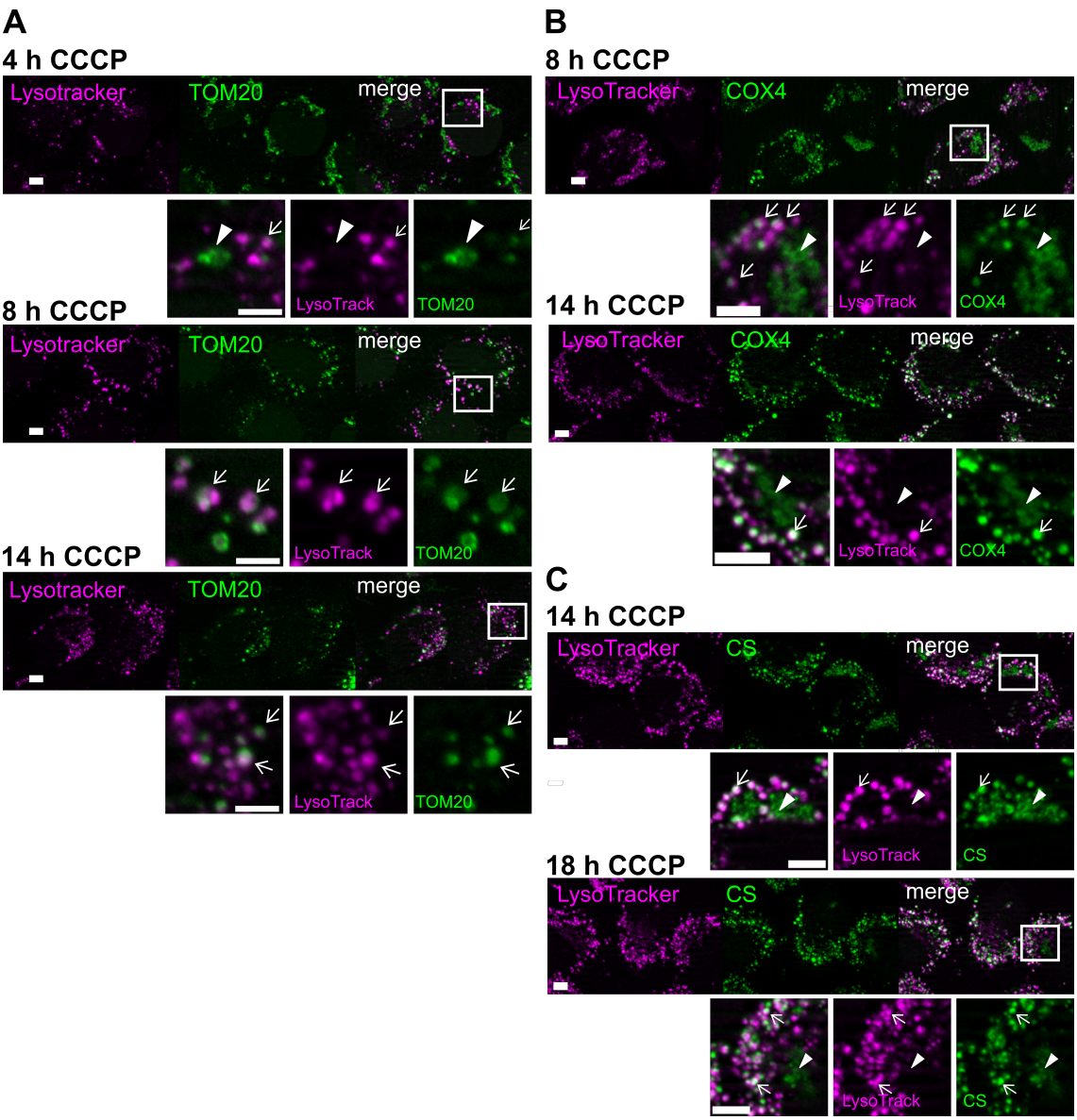


Figure 4.13: Mitochondrial sub-compartment cargo is differentially engaged with active lysosomes. (A-B) Active lysosomes represented with Lysotracker-RED (magenta) together with (A) TOM20 or (B) COX4 (green) at different stages of CCCP-induced mitophagy as indicated. Scale bars = 5 µm. Data published in (173).

4.4.3. Mitochondria engulfed by autophagosomes show OMM damages

As previously shown, late stages of PINK1/parkin-dependent mitophagy in WT-parkin HeLa were characterized by the presence of ubiquitinated inner mitochondrial aggregates devoid of TOM20 (Figures 4.5 and 4.10-11). In addition, inner mitochondrial aggregates were not directly targeted by autophagosomes (Figure 4.11) nor active lysosomes (Figures 4.13). Thus, to gain a better resolution on the nature of inner mitochondrial aggregates and additionally validate autophagy-dependent mitochondrial turnover in our cell model, transmission electron microscopy (TEM) imaging was performed in collaboration with Dr. Stefan Geimer and Dr. Benedikt Westermann (University Bayreuth) (Figure 4.14).

Under no depolarizing conditions, WT-parkin HeLa cells showed elongated mitochondria (Figure 4.14A). However, upon 8h of CCCP treatment, mitochondrial aggregates (zoomed region) as well as autophagosomes engulfing mitochondria (arrowhead) could be observed (Figure 4.14B), confirming autophagy-dependent mitochondrial turnover in WT-parkin HeLa cells.

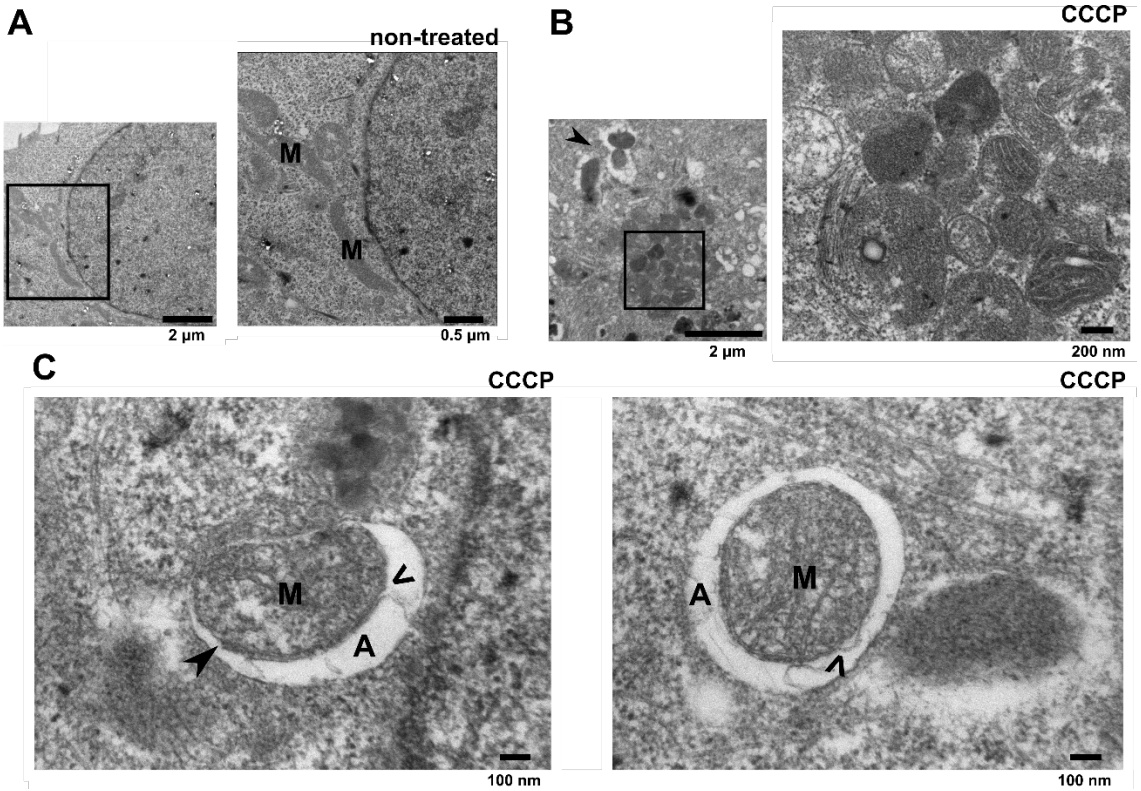


Figure 4.14: Transmission electron microscopy images of mitochondria in WT-parkin HeLa cells. (A-B) Examples of (A) basal elongated mitochondria or (B) mitochondrial aggregates appearing after 8h of CCCP treatment (right zoom panel) and mitochondria being engulfed by autophagosomes (closed arrowhead). **(C)** Examples of engulfed mitochondria with damaged OMM after 4h of CCCP treatment. Events of OMM rupture are indicated with open arrowheads. Closed arrowheads indicate situations where OMM finishes abruptly. M: mitochondria, A: autophagosome. Images obtained by Stefan Geimer (University of Bayreuth). Data published in (173).

Unfortunately, given the difficulty to interpret abnormalities on OMM ultrastructure of mitochondria that are not surrounded by an additional membrane (i.e: autophagosomes), elucidating the exact nature of inner mitochondrial aggregates was not possible using regular TEM imaging. However, examples of engulfed mitochondria with damaged OMM after 4h of CCCP treatment were observed (Figure 4.14C), indicating that OMM rupture might occur at intermediate stages of PINK1/parkin-dependent mitophagy in WT-parkin HeLa.

4.5. Parkin is not enriched on inner mitochondrial aggregates

Mass-spectrometry analysis of the total ubiquitination events occurring upon induction of PINK1/parkin mitophagy revealed extended ubiquitination of OMM proteins after short

depolarization times (Table 4.2 and Figure 4.9C). Importantly, most of the ubiquitination's observed only took place in WT-parkin HeLa, strongly indicating parkin as the E3 ligase responsible for those events. Similarly, ubiquitination events on IMM and matrix proteins were also detected after late depolarization times in WT-parkin HeLa cells only (Figure 4.9B and 4.10A-B), also suggesting direct parkin involvement on later stages of mitophagy. Thus, in order to confirm if parkin is responsible for IMM and matrix ubiquitination, parkin localization was assessed by means of fluorescence microscopy (Figure 4.15A-C).

As previously seen, parkin localized at the cytosol under basal conditions but translocated to mitochondria upon early mitochondrial depolarization (2h CCCP) (Figure 4.15A, panels © and ii), being highly enriched on fragmented mitochondria after 2-4h of CCCP treatment (Figure 4.15A, panel ii-iii). However, when most of TOM20 was reduced to puncta and SSBP1-aggregates were left behind (8h CCCP), parkin was not enriched on the remaining mitochondrial aggregates (Figures 4.15A, panel iv and 4.15B, zoom panel a) but was rather engaged in puncta-like structures, sometimes co-localizing with TOM20 (Figure 4.15B, zoom panel a). After extended time-points of depolarization, the majority of parkin was found at the cytosol and was not enriched on the remaining SSBP1-aggregates (Figure 4.15B, zoom panel b). However, some enriched parkin regions that did not co-localize with mitochondrial material were sporadically observed (Figure 4.15A, panel v). In addition, to check if the lack of parkin enrichment in SSBP1-aggregates could be also extrapolated to IMM material, combined immunostainings with COX4 and parkin were performed (Figure 4.15C). Similar to what was observed for parkin on SSBP1-aggregates, COX4-aggregates were not positive for parkin. On the contrary, parkin was enriched on COX4-puncta similarly as what was observed for TOM20 material (Figure 4.15C, zoom panels a-b).

To further understand parkin behavior at later stages of PINK1/parkin-mitophagy, relative protein levels over the time-course of mitophagy were monitored by means of Western blot (Figure 4.15D). Additionally, mass-spectrometry analysis of the total proteome upon CCCP-induced mitophagy in WT-parkin HeLa cells was analyzed (see chapter 4.2) (Figure 4.15E). Upon Western blot analysis, an upregulation of parkin protein levels was observed upon early depolarization treatment in WT-parkin cells only (Figure 4.15D-E). Of note, remaining parkin protein levels after extended CCCP treatment (8-18h) were variable, being downregulated or kept at basal levels (Figure 4.15D-E). These differences could be due to a reduction of parkin expressing cells after increased cell culture maintenance (i.e: high cell passage) of WT-parkin cells (data not shown, observational). Additionally, strong WT-parkin ubiquitination was

observed after early depolarization treatment while C431A-parkin ubiquitination took place at intermediate time-points of the pathway (Figure 4.15D). Both WT- and C431A-parkin were eventually ubiquitinated after extended mitochondrial depolarization treatment.

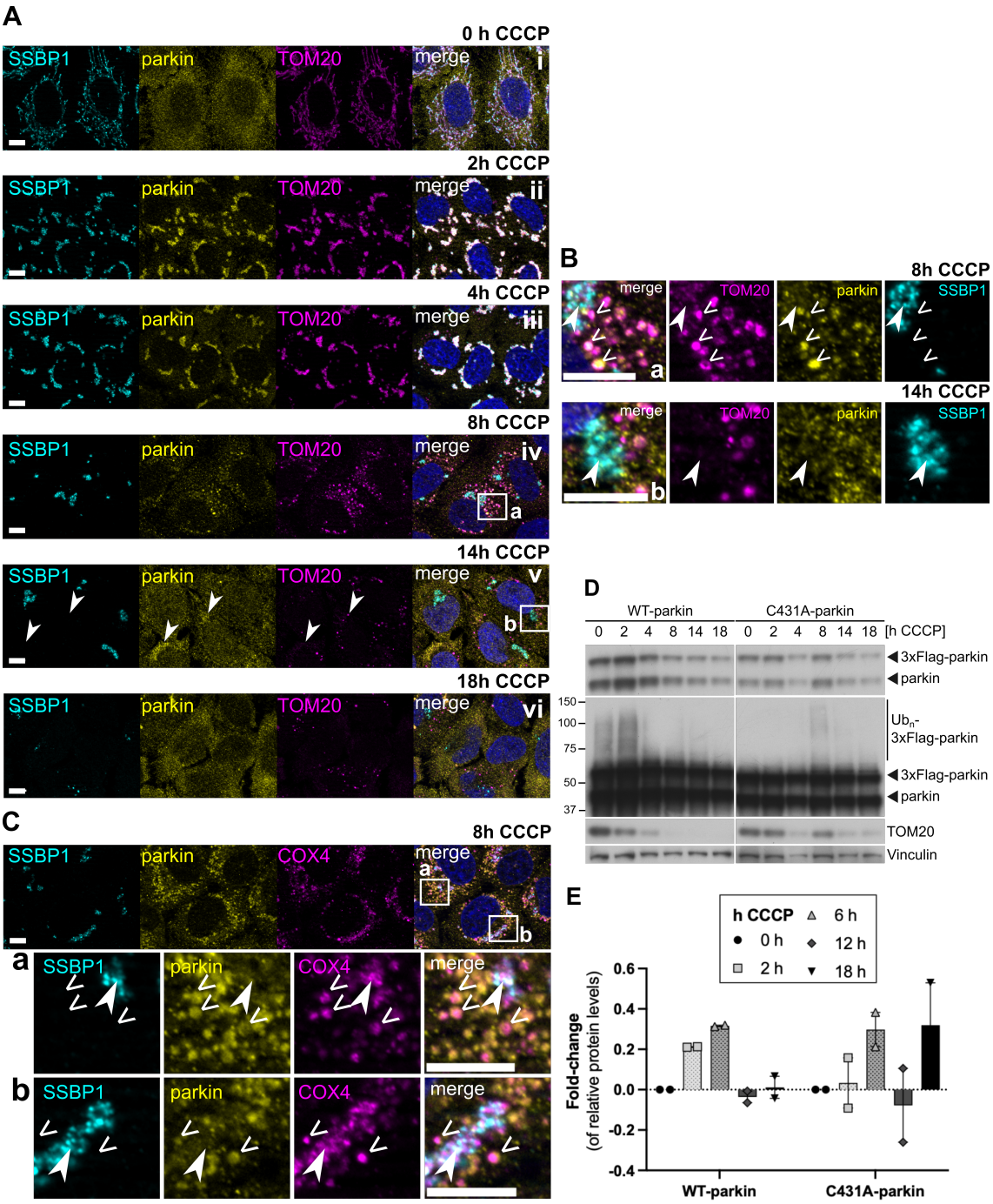


Figure 4.15: Parkin sub-cellular localization and expression levels over the course of mitophagy. (A-C) Immunostaining images showing (A-B) TOM20 (magenta) or © COX4 together with SSBP1 (cyan) and parkin (yellow). Panels in (B) are zoomed regions of the indicated time-points in (A). Thick arrowheads in (A) indicate parkin enriched regions free of mitochondrial material. In (B-C), thick arrowheads indicate SSBP1-aggregates free of parkin and open arrowheads indicate mitochondrial puncta positive for parkin. Scale bars = 5 μm. **(D)** Parkin levels on WT- or C431A-parkin HeLa upon mitochondrial depolarization time-course. **©** Parkin levels detected in total proteome analysis at several CCCP treatment time-points. Fold-change was obtained after normalization of relative protein to non-treated conditions (0h CCCP). Bars: mean ± SEM. Data from two biological replicates from (132).

Taken together, these data suggest the E3 ligase parkin to be potentially degraded along with OMM sub-compartment material. These opens the window to potential other E3-ligases being responsible for the ubiquitination of IMM and matrix substrates during late stages of mitophagy.

4.6. Active parkin is ubiquitinated after mitophagy induction

Global parkin ubiquitination levels were enhanced in both WT- parkin after short mitochondrial depolarization treatment (2 h CCCP) (Figure 4.15D). While most ubiquitination events occurring during mitophagy trigger the degradation of ubiquitinated cargo, it seems unlikely that parkin ubiquitination would promote its turnover at such an early stage of PINK1/parkin-dependent mitophagy. However, to discard this hypothesis, proteasome degradation was inhibited with MG132 prior to mitochondrial depolarization and parkin ubiquitination was monitored (Figure 4.16). Consistently, extended depolarization treatment alone induced a decrease on parkin protein levels (Figure 4.16A). However, when UPS was inhibited, parkin levels remained slightly unchanged and an increase in parkin ubiquitination was observed after extended treatment (8-18 h) (Figure 4.16A). These data might initially suggest that parkin is targeted by the proteasome at later stages of the pathway, however, given that early inhibition of UPS blocks mitophagy progression (see chapter 4.7), we cannot conclude a direct proteasome-dependent parkin degradation, at least during successful turnover of mitochondrial proteins.

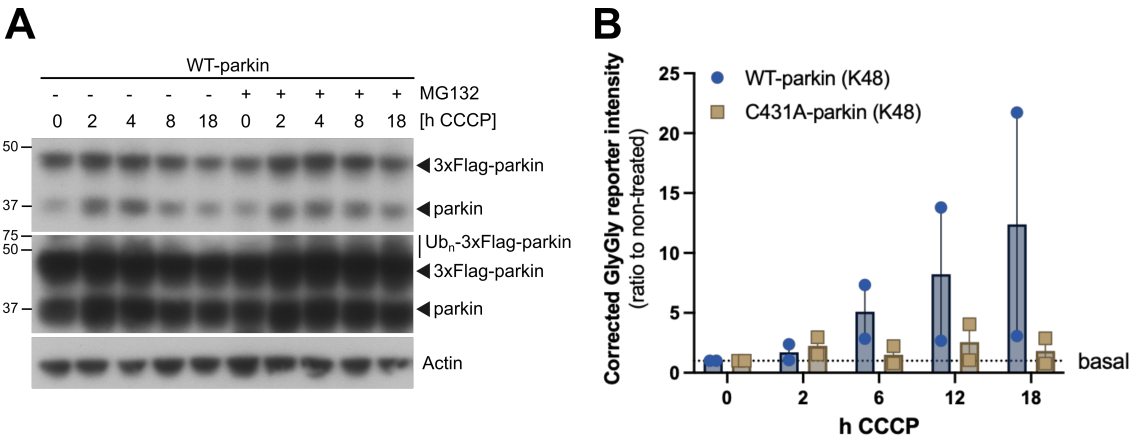


Figure 4.16: Parkin ubiquitination during mitophagy. (A) Parkin ubiquitination is enhanced under proteasome inhibition and extended mitochondria depolarization conditions (6-18h CCCP). **(B)** Normalized K48-parkin ubiquitination levels occurring after mitochondria depolarization conditions only. Data were normalized to ubiquitination levels under non-treated conditions (0h CCCP). Bars: mean ± SEM. Each data point is the mean average of a single biological replicate.

To gain more information on parkin ubiquitination occurring during successful mitochondrial turnover, specific parkin ubiquitination sites found after mass-spectrometry analysis of total ubiquitination events were analyzed as described previously (see chapter 4.2) (Table 4.4).

Table 4.4: List of ubiquitination sites found on Parkin. Complete ubiquitylome data set can be found on https://msviewer.ucsf.edu/prospector/cgi-bin/msform.cgi?form=msviewer with accession key: suxnuntnwt.

Position	*Parkin domain*	WT and/or C431A	*Identified in replicate*
K48	UBL	Both	R1, R2
K408	IBR – RING2	Both	R1

Both WT- and C431A-parkin were ubiquitinated on lysine residues K48 and K408. While K48 is found at the UBL domain, K408 is localized between RING2 and the IBR region of parkin. K408 ubiquitination was identified in one replicate and seemed to follow the same upregulation dynamics in both WT- and C431A-parkin (data not shown) (132). On the other hand, even though ubiquitination profiles varied among replicates, K48- ubiquitination of WT-parkin seemed to follow a regulated tendency in WT-parkin in comparison to C431A-parkin, being upregulated between 6-18h CCCP (Figure 4.16B). On the other hand, no differences in K48-parkin ubiqutination of WT- or C431A-parkin were observed after early depolarization treatment (2h CCCP) (Figure 4.16B).

Overall, WT-parkin was not enriched in inner mitochondrial aggregates (Figure 4.15A-C) and at this stage, a decrease in parkin protein levels together with an increase in K48-parkin ubiquitination were observed (Figure 4.16). Taken together, these data may indicate that WT-parkin is degraded at later stages of mitophagy, perhaps being influenced by the proteasome. Future validation studies involving parkin pulldown and subsequent analysis of ubiquitinated species might help clarify the ubiquitination status of parkin and its potential proteasome-dependent degradation at later stages of the pathway.

4.7. Early proteasomal degradation is needed for mitophagy progression

As it has been demonstrated in previous studies, the UPS is involved in the degradation of specific OMM proteins like MFN1 or DRP1, happening shortly after the induction of PINK1/parkin mitophagy (49,50,181). Thus, in order to confirm previous results and gain more insight into the relevance of proteome-dependent mitochondrial degradation, proteasome inhibition combined with mitochondrial depolarization treatment experiments were performed (Figure 4.17). For this purpose, the proteasomal inhibitor MG132 was administered before or after inducing mitochondrial depolarization with the uncoupler CCCP.

When WT-parkin cells were pre-treated with MG132 followed by regular mitochondrial depolarization, an accumulation of ubiquitinated MFN1 as well as total MFN1 was detected

(Figure 4.17A). In addition, while overall degradation of VDAC1 and TOM20 was impaired, their ubiquitination patterns were different from the ones observed under non proteasome inhibitory conditions, showing mono-ubiquitination events for VDAC1 and highly reduced ubiquitination of TOM20 (Figure 4.17A). Furthermore, an impairment on the overall degradation of COX4 and CS was also observed under UPS inhibitory conditions (Figure 4.17A). To confirm inhibition of mitochondria degradation under these conditions, mitochondrial morphology was assessed in WT-parkin HeLa cells as well as HEK293 (Figures 4.17B and 4.18). Upon UPS inhibition combined with mitochondria depolarization for 18h, mitochondria aggregated perinuclearly and no separation of OMM and inner mitochondrial material was observed in both WT-parkin and HEK293 cells (Figures 4.17B and 4.18).

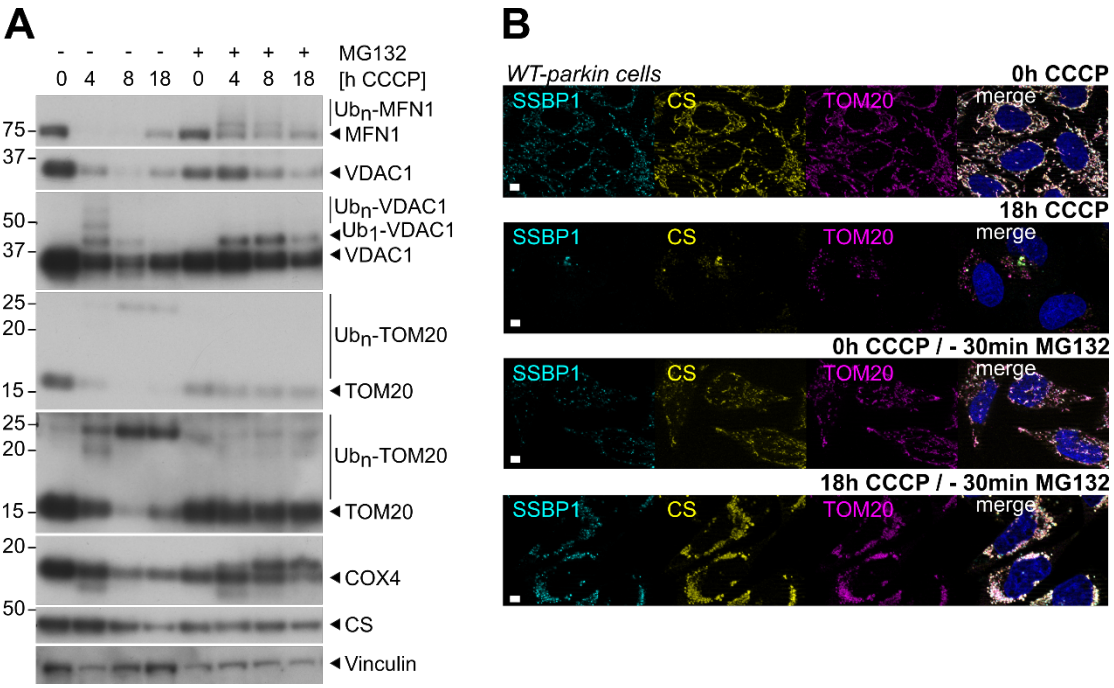


Figure 4.17: Mitophagy impairment upon pre-proteasomal inhibition in WT-parkin HeLa. (A) WT-parkin HeLa cells were treated with CCCP alone or in combination with MG132 (pre-treatment, -30min). Representative Western blots are shown for the indicated mitochondrial proteins. **(B)** Immunofluorescence images showing mitochondrial morphology after CCCP treatment alone or in combination with MG132. Scale bars = 5 μm. Data published in (173).

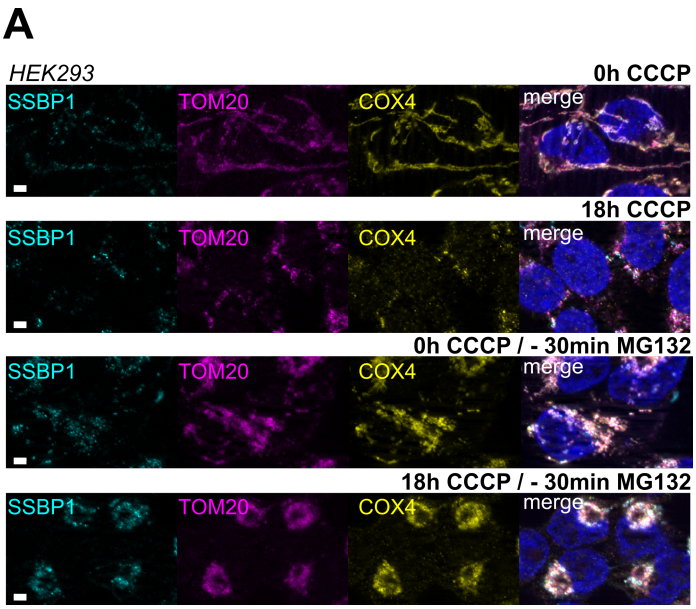


Figure 4.18: Mitophagy impairment upon pre-proteasomal inhibition in HEK293. (A) HEK293 were treated with CCCP alone or in combination with MG132 (pre-treatment, -30min). Representative immunofluorescence images showing mitochondrial morphology after CCCP treatment alone or in combination with MG132. Scale bars = 5 µm. Data published in (173).

In order to gain more insight on the nature of the late mitochondrial aggregates observed after pre-UPS and extended CCCP treatment, localization of parkin as well as ubiquitin species was assessed (Figure 4.19). All mitochondrial aggregates observed in WT-parkin HeLa cells upon extended UPS inhibition were positive for parkin (Figure 4.19A). In addition, pS65-ubiquitin levels were highly increased upon extended UPS inhibition combined with CCCP treatment (Figure 4.19B), suggesting the engagement of active parkin on mitochondrial aggregates after long combined CCCP and MG132 treatments in WT-parkin HeLa. Unfortunately, parkin levels in HEK293 cells were not detectable (data not shown) and parkin localization could not be assessed for this cell line.

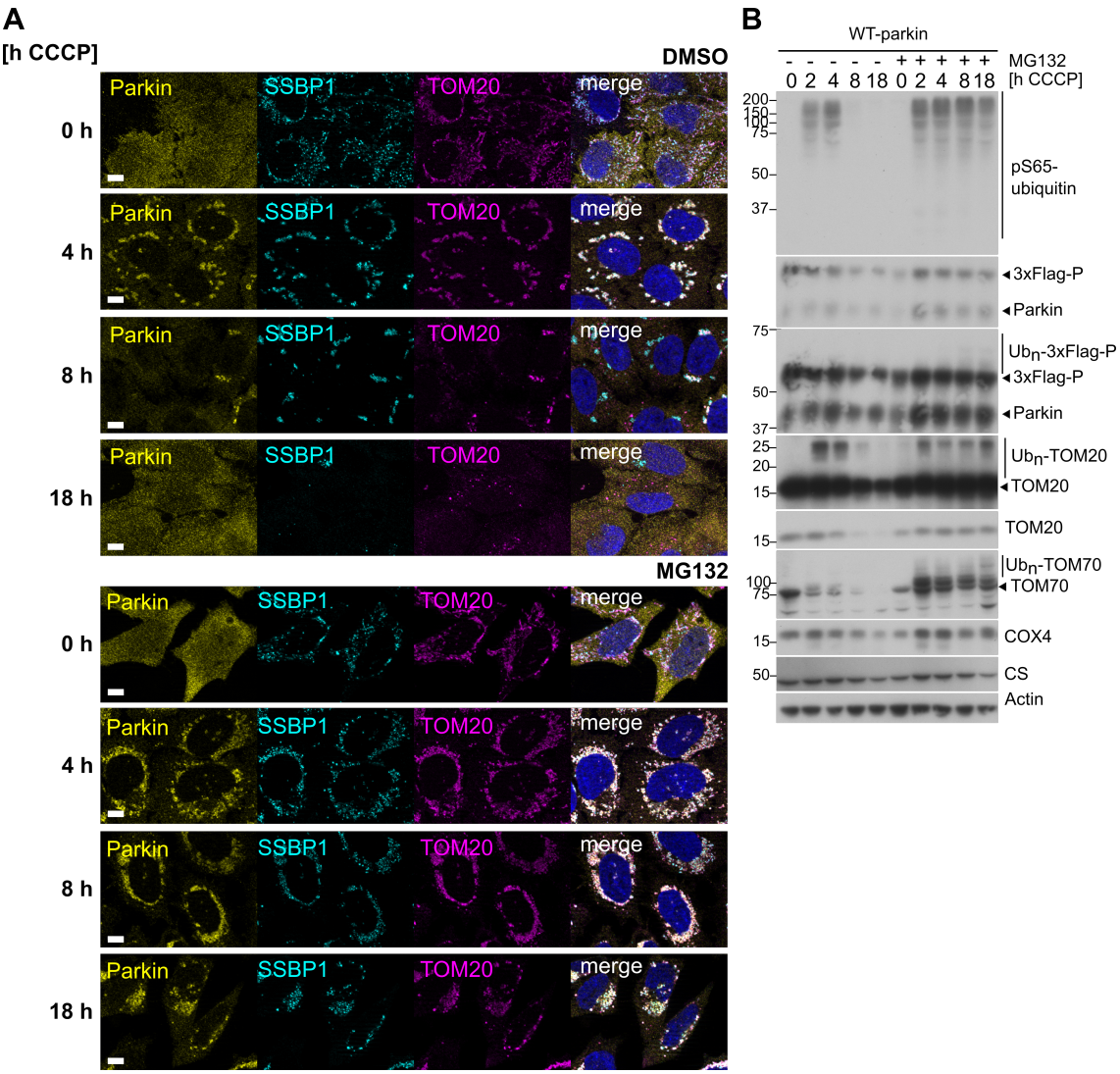


Figure 4.19: Parkin remains on mitochondria upon pre-proteasomal inhibition. (A) Representative immunofluorescence images showing parkin (yellow) localization upon CCCP treatment with or without previous UPS inhibition with MG132**.** Scale bars = 5 µm. **(B)** Accumulation of pS65-ubiquitin and parkin on mitochondria upon pre-UPS inhibition.

As previously seen, proteasomal inhibition not only had an impact on the overall mitochondrial degradation, but also influenced ubiquitination of specific OMM proteins (Figure 4.17A). In order to confirm this finding, WT-parkin cells were transfected with 6HIS-ubiquitin to further allow pulldown of ubiquitinated proteins under UPS inhibitory conditions or simple mitochondrial depolarization. Two replicates were taken into account for this experiment. In agreement with previous studies, regular mitochondrial depolarization induced the ubiquitination of MFN1 as well as TOM70 after short times of mitochondrial depolarization, while ubiquitinated TOM70 and MFN1 accumulated after pre-UPS inhibition (Figure 4.20) (160). Additionally, a reduction of TOM20 and VDAC1 ubiquitination was observed upon UPS inhibition combined with mitochondrial depolarization treatment in whole cell lysate samples (Figure 4.20), as observed in previous experiments (Figure 4.17A and 4.19B). Upon Ni-NTA pulldown, it was possible to

purify ubiquitinated MFN1 after combined UPS inhibition and CCCP treatment (Figure 4.20, right panel, lanes 8-9, 11-12). On the other hand, Ni-NTA pulldown revealed a reduction of VDAC1 ubiquitination under proteasome inhibitory conditions when compared to depolarizing conditions only (Figure 4.20, right panel, lanes 9 and 12). However, while this reduction was observed in both pulldown experiments, the time-points in which the ubiquitinated VDAC1 species were accumulated under depolarizing conditions were not identical between the two replicates.

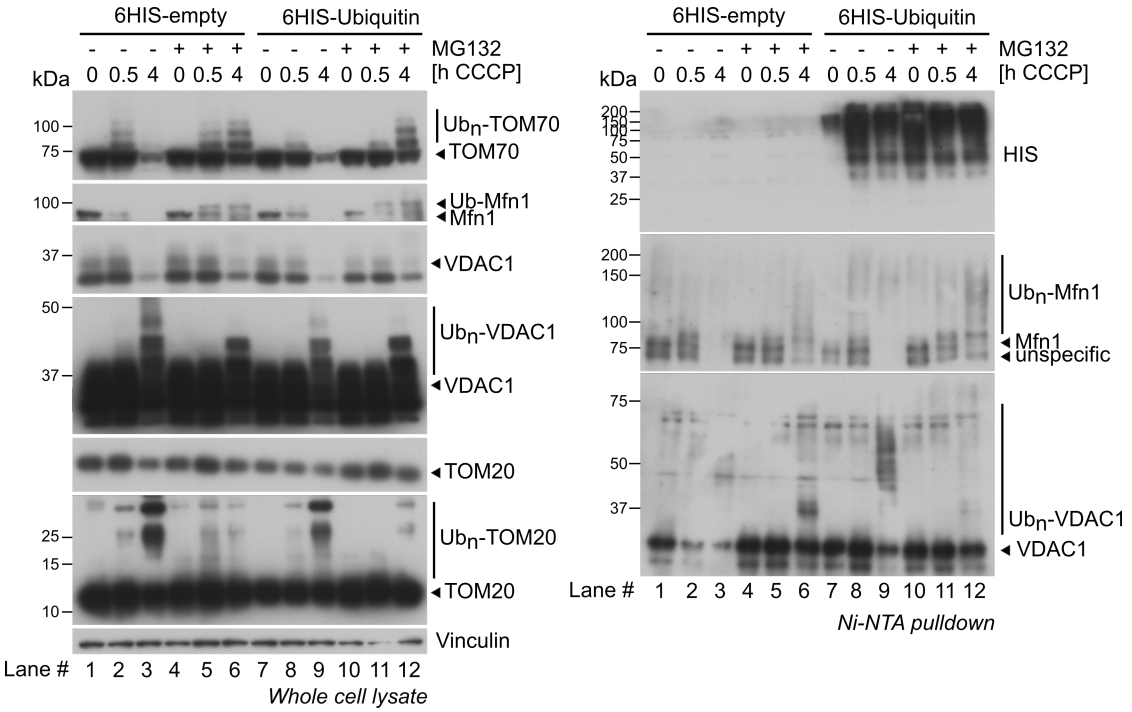


Figure 4.20: Reduction of VDAC and TOM20 ubiquitination after pre-UPS inhibition. (A) WT-parkin cells were transfected with 6HIS-ubiquitin and treated with CCCP alone or in combination with MG132 (pre-treatment, -30min). Whole cell lyates (left) were subjected to Ni-NTA pulldown (right) to purify ubiquitinated proteins in both conditions. A decrease on VDAC1 ubiquitination upon pre-UPS treatment compromised ubiquitinated-VDAC1 pulldown (right). N=2, experimental replicates.

These data are in agreement with other studies and confirm that an initial activation of UPS is necessary for further mitophagy progression (135,136). In addition, differences in VDAC1 and TOM20 ubiquitination upon early UPS inhibition suggest those two mitochondrial proteins to not be solely targeted by the UPS for their complete turnover.

4.8. Identification of proteasome-dependent OMM proteins turnover after short mitochondrial depolarization

Similar to what was observed for mitochondrial sub-organelle protein degradation, differences on OMM protein turnover kinetics were observed in this work: MFN1 and TOM70 were rapidly

degraded in comparison to VDAC1 and TOM20 (see chapter 4.2). In addition, under conditions of early proteasome inhibition, the ubiquitination status of MFN1 and TOM70 was highly increased in comparison to VDAC1 (Figure 4.17, 4.19 and 4.20). Thus, to confirm differential UPS-targeting of OMM proteins, early and delayed proteasome inhibition experiments were subjected to mass-spectrometry analysis. Here, four different conditions were assessed: (a) intermediate mitochondrial depolarization alone (8h CCCP), (b) intermediate CCCP treatment combined with pre-UPS inhibition (-0.5h MG132 + 8h CCCP), (c) CCCP treatment combined with delayed UPS inhibition (+2h MG132 + 8h CCCP) and (d) no mitochondrial depolarization (Figure 4.21A). Next, di-methyl labelled comparisons were performed between: (i) delayed UPS inhibition to CCCP treatment only (set pink: H/L), (ii) pre-UPS inhibition over CCCP treatment only (set pink: M/L), (iii) CCCP treatment only to non-treated conditions (set blue: M/L) and (iv) delayed UPS inhibition compared to pre-UPS inhibition, both combined with CCCP treatment (set pink: H/M) (Figure 4.21A). In this and in chapter 4.10, experimental treatments and initial sample processing were carried out by the master student Sandra Schepers as part of her master thesis, while further sample processing for LC/MS-MS measurement was performed by Katharina Zittlau. Proteomic analysis was performed by Katharina Zittlau with the exception of comparison (iv). Authorship of data is indicated in figure legends 72ecndary72a.

Consistently with previous data, induction of mitochondrial depolarization for 8h caused a significant degradation of OMM, IMS and IMM proteins (Figure 4.21B). However, under conditions of MG132 pre-treatment, degradation of all these mitochondrial sub-compartments was impaired (Figure 4.21C). Matrix proteins which are generally degraded at >8h CCCP were not much affected after 8h of CCCP treatment (Figure 4.21B-C). Next, to identify potential UPS-targeted OMM substrates, delayed MG132 inhibition was compared to MG132 pre-inhibition, both under mitochondrial depolarizing conditions (8h CCCP) (Figure 4.21D). Known OMM substrates of the proteasome like MFN1, TOM70 and MIRO2 (RHOT2) were affected by a delayed proteasome inhibition, all of them showing negative fold-change values and significant Log2 t-test p-values ($p<0.05$ or 0.1) (Figure 4.21D). Interestingly, MFN1, TOM70 and MIRO2 were equally influenced by delayed UPS inhibition: while MFN1 seemed to be strongly affected by proteasomal degradation, the influence of proteasomal degradation at t<2h for both TOM70 and MIRO2 seemed to be milder, showing lower significance (TOM70 and MIRO2) and fold change (MIRO2) values compared to MFN1. Interestingly, other OMM proteins like TOM20, or VDAC2/3 were below the established significance level (fold change>1.3), suggesting a much lower (if any) influence by the proteasome after t<2h CCCP (Figure 4.21D).

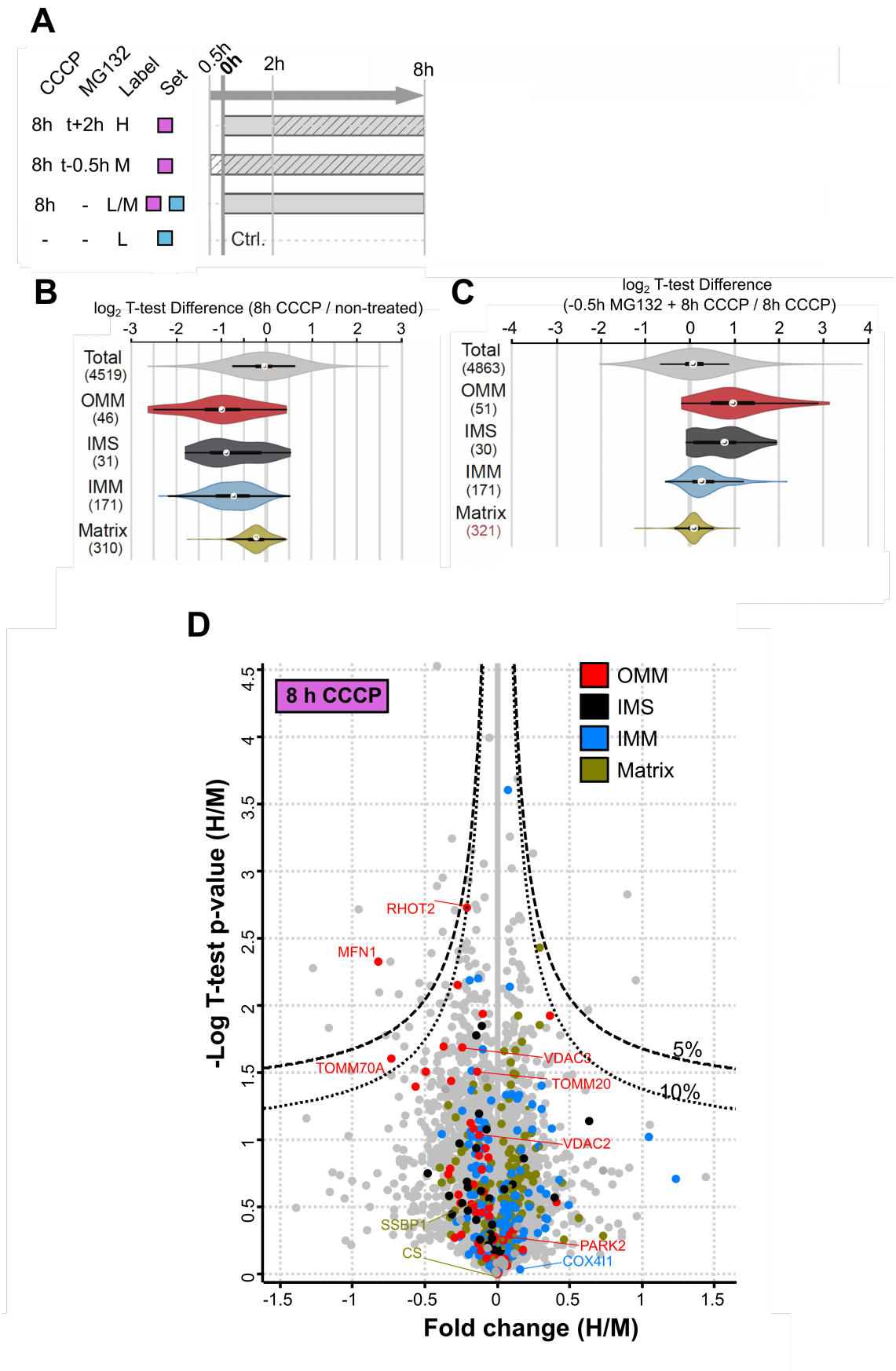


Figure 4.21: Proteomic analysis of the influence of UPS on OMM protein degradation. **(A)** Experimental design and dimethyl labelling scheme used. Treatment starting point is defined as "t". Solid grey: CCCP treatment. Dashed lines: MG132 treatment. **(B-C)** Violin plots showing (B) mitochondrial sub-compartment degradation after 8h of CCCP treatment alone normalized to non-treated conditions (set blue: M/L) or (C) mitochondrial sub-compartment protein

accumulation after 8h of CCCP treatment and pre-UPS inhibition normalized to CCCP treatment alone (set pink: M/L). Log_2 of t-test difference values are shown for each sub-compartment. **(D)** Volcano plot showing mitochondrial degradation happening after delayed proteasomal inhibition (t+2h) compared to pre-UPS inhibition (t-0.5h) combined with intermediate depolarization in both cases (8h CCCP) (set pink: H/M). Dashed curves lines indicate threshold of significance when $p \leq 0.05$ (5%) or $p \leq 0.1$ (10%) for proteins with a fold change>1.3. Mitochondrial sub-compartment classification according to MitoCarta3.0. Author: Katharina Zittlau. (Panels A-C).

4.9. Delayed inhibition of the proteasome impairs complete mitochondrial turnover

As previously seen, late stages of PINK1/parkin mitophagy induced the formation of SSBP1-aggregates devoid of TOM20. In addition, a limited LC3B recognition together with a lack of co-localization of lysosomal markers was observed (see chapter 4.2 and 4.4). Overall, these data suggested intermediate steps for the degradation of inner- mitochondrial aggregates. Hence, similarly to what occurs at early stages of mitophagy, we hypothesized that the UPS could be involved in the degradation of inner- mitochondrial aggregates. For this purpose, delayed proteasome inhibition experiments were performed. Here, mitochondrial depolarization was induced for a total of 24h combined with MG132 treatment from 8h onwards, allowing the normal degradation of OMM substrates from 0-8h and inhibiting the UPS from 8-24h. These experiments were performed by the master student Sandra Schepers as part of her master thesis.

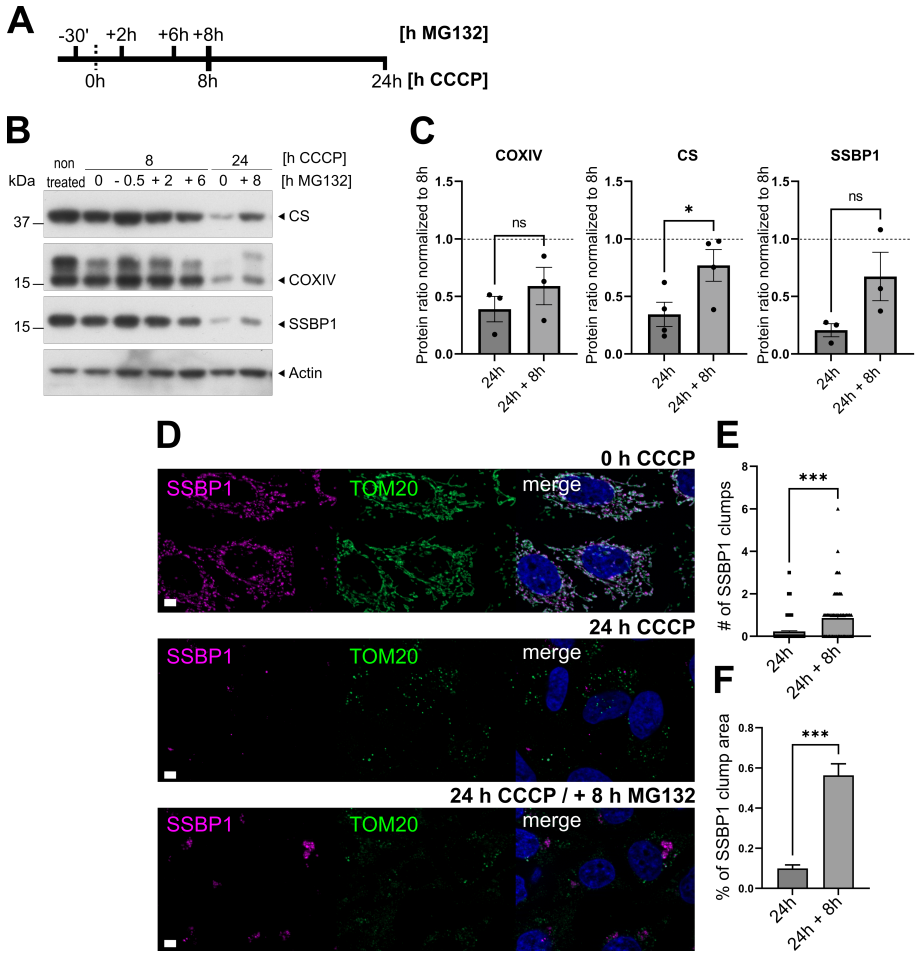


Figure 4.22: Turnover of inner- mitochondrial proteins is influenced by the UPS. (A) Experimental scheme of delayed UPS inhibition and extended depolarization treatment. **(B-C)** Influence of delayed MG132 on inner mitochondrial proteins. Western blot quantifications are shown in panel C. Bars: mean ± SEM. **(D-F)** Single cell analysis of immunofluorescence images showing SSBP1 (magenta) and TOM20 (green) after delayed UPS inhibition. (D) Representative immunofluorescence images are shown for CCCP treatment only or in combination with delayed UPS inhibition. Scale Bars = 5 µm. **(E-F)** Cell-Profiler based analysis of © number of SSBP1-aggregates and (F) SSBP1-aggregate area in relation to cell area are shown. Each data point represents a single cell value. Bars: mean ± SEM. Author: Sandra Schepers. Data published in (173).

Under delayed UPS inhibitory conditions, degradation of COX4, CS and SSBP1 was compromised in comparison to normal treatment conditions (Figure 4.22B-C). These results were confirmed by assessing mitochondrial morphology under the same treatment conditions, where an increase in SSBP1-aggregates number and size was observed upon delayed UPS inhibition (Figure 4.22D-F). Taken together, these data suggest the involvement of the UPS as an intermediate degradation pathway taking place at later stages of mitophagy.

4.10. Identification of potential proteasome-dependent inner- mitochondrial proteins

Next, to confirm UPS-dependent degradation of inner- mitochondrial proteins and identify potential late UPS targets, delayed UPS inhibited experiments seen in the previous chapter were extended to LC-MS/MS proteomic analysis. Here, three different conditions were assessed: (a) extended mitochondrial depolarization alone (24h CCCP), (b) extended CCCP treatment combined with delayed-UPS inhibition (+8h MG132 + 24h CCCP) or (c) no mitochondria depolarization. Next, di-methyl labelled comparisons were performed between (i) delayed UPS inhibition over CCCP treatment alone (set green: H/M) and (ii) extended CCCP treatment alone over non-treated conditions (set green: M/L) (Figure 4.23A).

Consistently with previous data, delayed UPS inhibition combined with extended CCCP treatment compromised the complete degradation of inner mitochondrial proteins (IMM and matrix) when compared to extended CCCP treatment conditions (Figure 4.23B). Interestingly, after performing statistical analysis on the significantly upregulated proteins (one sample t-test, $p<0.05$), many mitochondrial ribosome proteins (MRPL13, MRPL53, MRPL27, MRPL4, MRPL24, MRPL2) as well as isoleucine tRNA ligase (IARS2) and two subunits of complex I of the ECT (NDUB5/9) were upregulated upon delayed UPS inhibition (Figure 4.23C). Surprisingly, proteins residing at the OMM or IMM like metaxin-2 (MTX2) and the metallprotease YME1L1 were also upregulated upon delayed UPS inhibition and extended CCCP treatment (Table 4.5). Both MTX2 and YME1L1 are known to interact with proteins involved with mitochondrial architecture such as the MICOS complex or OPA1 (see chapter 5.4). In addition, the anti-apoptotic BCL-2 protein MCL1 was upregulated upon delayed UPS inhibition. Interestingly, MCL1 is known to promote cell survival when localized at the OMM. Overall, this suggests mitochondrial remodeling processes and activation of cell survival pathways to potentially occur during later stages of parkin-dependent mitophagy (>8h CCCP). Taken together, proteomics data are in agreement with previous experiments (Figure 4.22) and suggest a potential proteasomal-dependent step at later stages of mitophagy.

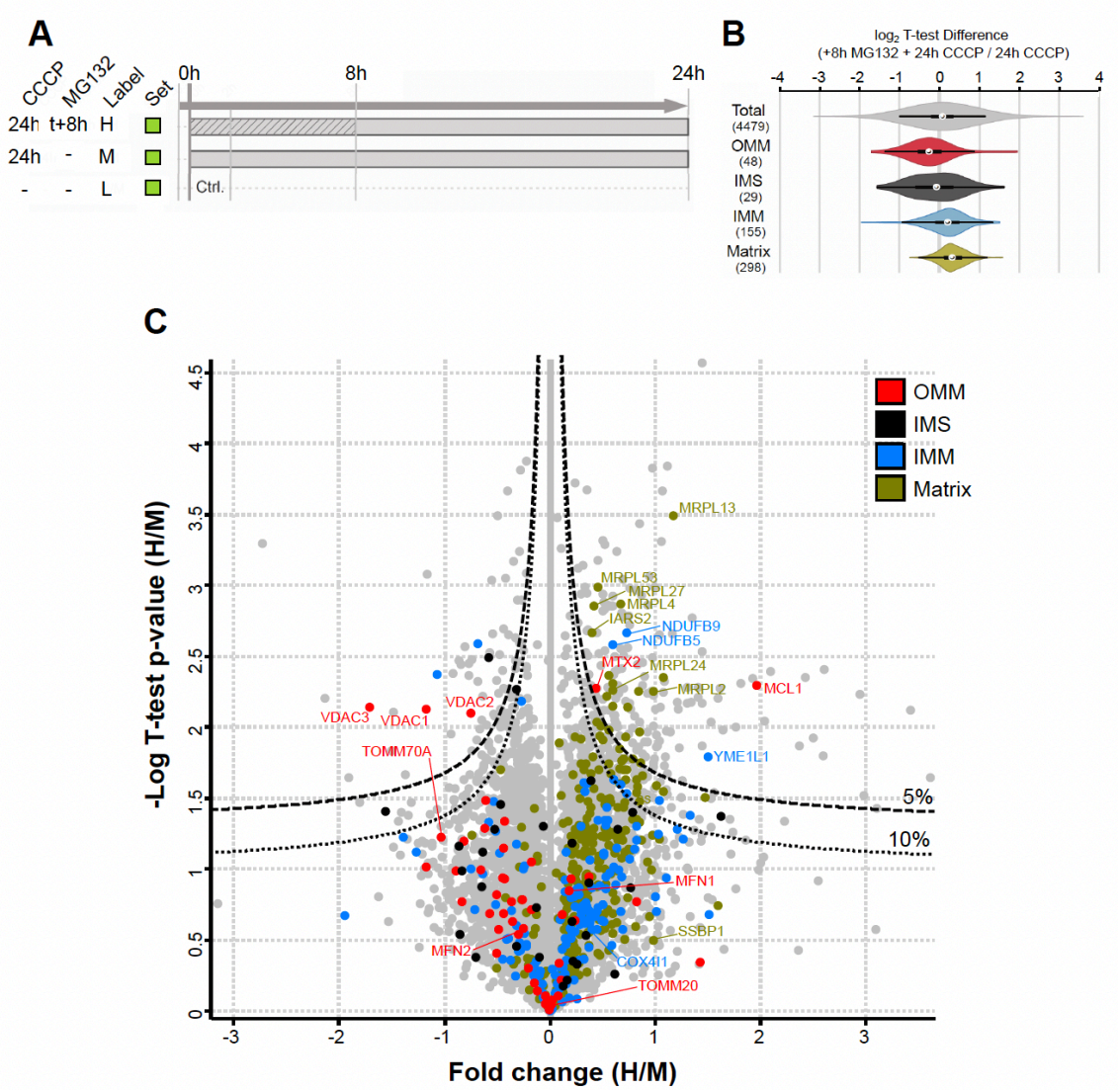


Figure 4.23: Proteomic analysis of the influence of UPS on inner- mitochondrial protein degradation. **(A)** Experimental design and dimethyl labelling scheme used. Treatment starting point is defined as "t". Solid grey: CCCP treatment. Dashed lines: MG132 treatment. **(B)** Violin plot showing mitochondrial sub-compartment degradation after delayed UPS treatment and extended CCCP treatment normalized to extended CCCP treatment conditions. Set green: H/M. Log_2 of t-test difference values are shown for each sub-compartment. **(C)** Volcano plot showing mitochondrial degradation impairment happening after delayed proteasomal inhibition and extended CCCP treatment (t+8h) compared to extended CCCP treatment (24h CCCP). Dashed curves lines indicate threshold of significance when $p \leq 0.05$ (5%) or $p \leq 0.1$ (10%) for proteins with a fold change≥ 1.3. Mitochondrial sub-compartment classification according to MitoCarta3.0. Author: Katharina Zittlau (panels A-B). Data published in (173).

Table 4.5: List of OMM, IMM and matrix proteins highly upregulated upon delayed UPS inhibition and extended CCCP treatment. Gene names of the interesting targets from Figure 4.23 are shown. If proteins were identified in the proteomics data-set from Zittlau *et al.* 2022, their corresponding proteasome cluster is indicated. N/A indicates protein was not identified.

OMM	***Function***	***Proteome cluster***
MCL1	Apoptosis regulation	N/A
MTX2	Mitochondrial morphology	Cluster 13
IMM		
NDUFB5/9	Electron transfer	N/A
YME1L1	Mitochondrial morphology	Cluster 11
Matrix		
MRPL2/4/13/27/53	Mitochondrial protein translation	N/A
IARS2	Aminoacid transfer to 78econdary78al tRNA	N/A

4.11. Phosphoproteome and ubiquitylome analysis reveals a potential link between phosphorylation and ubiquitintion on VDAC1/2

Early steps of PINK1/parkin mitophagy are strongly dependent on phosphorylation and ubiquitination events happening on several OMM substrates (51). Hence, we hypothesized that direct (de)phosphorylation of OMM proteins could influence parkin-dependent ubiquitination of specific OMM proteins. In order to answer to this question, we took advantage of the phosphoproteome and ubiquitylome data-set described at the beginning of this work (see chapter 4.2.1). Here, OMM proteins that were both ubiquitinated and phosphorylated in a range of 5-10 residues upon PINK1/parkin induction in WT-parkin HeLa cells were selected (Table 4.6).

Table 4.6: List of proteins that undergo phosphorylation and ubiquitination on close by residues upon PINK1/parkin mitophagy induction. Only proteins with modified residues in positions separated by 5-10 amino acid residues are shown.

Gene name	Phosphorylation	Ubiquitination	Ubiquitylome cluster
VDAC1	S104	K109	13
VDAC2	S115	K120	13
TIMM8A	S96	K86	N/A
Cytochrome c	S48	K54	N/A

Among our candidates, the VDAC1 and VDAC2 were considered interesting targets as they are both known to be direct parkin substrates (68,126). Upon CCCP-induced mitophagy in WT-parkin HeLa cells, residues corresponding to the third cytosolic loop of both VDAC1/2 were found to be phosphorylated and ubiquitinated; phosphorylation occurred on S104 or S115 of VDAC1 and VDAC2, respectively, while the identified ubiquitinated lysines were five amino acids upstream of the phosphorylation site in both cases (K109 and K120, respectively) (Table 4.6) (Figure

4.24A). For subsequent PTM dynamic analysis of VDAC1 and VDAC2, reporter phosphorylation or ubiquitination signals were normalized to proteomic levels and dynamics of both PTM were computed for both VDACs (Figure 4.2B-C). Phosphorylation of both S115 and S104 was identified in both parkin cell lines. Dephosphorylation of these serine residues only occurred in mitophagy competent WT-parkin cells but not in the parkin inactive (C431A) cell line (Figure 4.24A-B). Conversely, ubiquitination of the nearby lysine (K109 or K120) in both VDAC1 and VDAC2 was upregulated in WT-parkin cells only, while no changes in ubiquitination were seen in the C431A-parkin cell line.

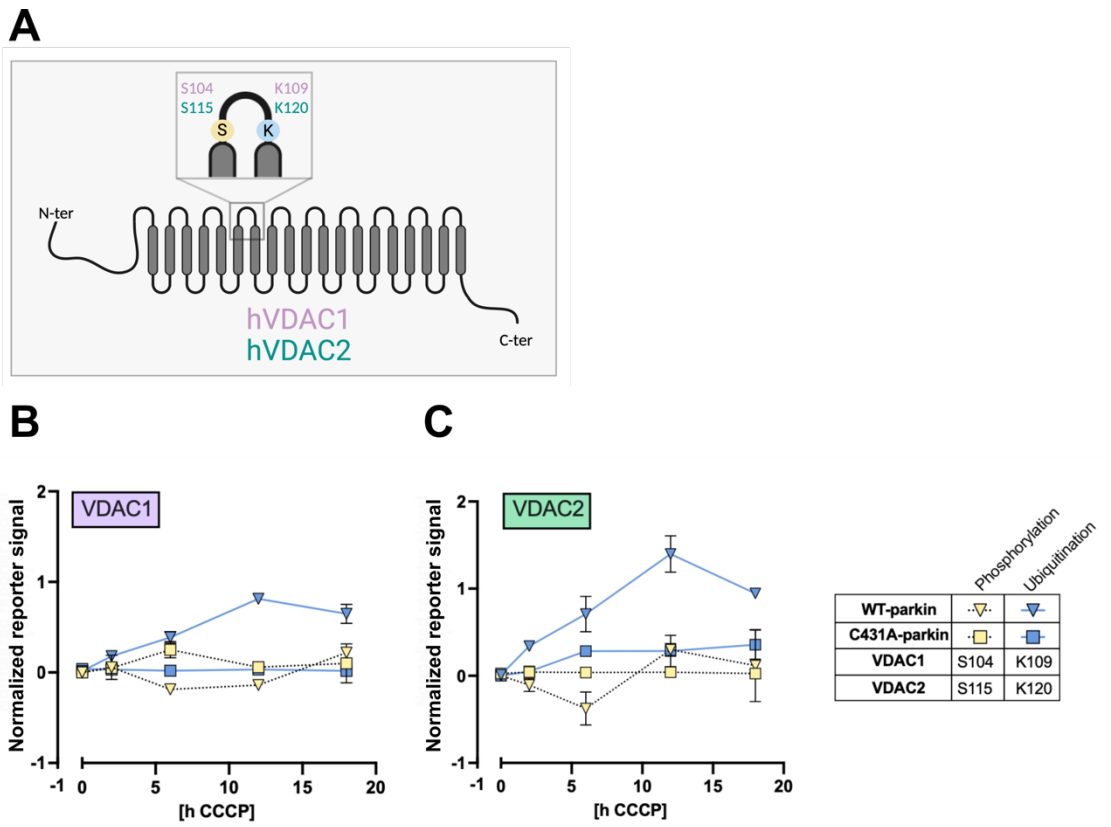


Figure 4.24: Phosphorylation and ubiquitin dynamics of VDAC1/2 over the course of mitophagy. (A-B) Relative reporter signals of ubiquitination (blue) or phosphorylation (yellow) of (A) VDAC1 and (B) VDAC2 found in WT- and C431A-parkin HeLa cells. Data normalized to proteomic abundance and non-treated treated conditions. . Data published in (132).

As both VDAC1 and VDAC2 seemed to be dephosphorylated in S104 and S115, respectively, followed by an increase in ubiquitination of K109 or K120 in the same cytosolic loop, we hypothesized that these de-phosphorylations events could regulate subsequent ubiquitination in the same cytosolic loop of the OMM protein. Validation experiments were designed for both VDAC proteins. Validation of VDAC1 S104 de-phosphorylation effects was inconclusive as only a mild impairment in the ubiquitination pattern of 79econdar-mimic VDAC1 (S104D) was observed

without having a significant impact on overall VDAC1 turnover (data not shown). For this reason, only VDAC2 validation experiments are shown here.

Phospho-dead and 80econdar-mimic mutants of VDAC2 with an N-terminal 6HIS-tag were generated. Serine substitutions to alanine or aspartic acid were used for mimicking a 80econdar-dead or 80econdar-mimic situation, respectively. Next, analysis of residual VDAC2 protein amounts as well as ubiquitination status of the protein was analyzed by means of Ni-NTA pulldown and subsequent Western blot analysis (see chapters 4.12-13).

4.12. Dephosphorylation of S115 enhances total VDAC2 ubiquitination

In a first attempt to analyze the impact of VDAC2 ubiquitination-dependent degradation upon mitochondria depolarization, 80econdar-dead or 80econdar-mimic VDAC2 levels were compared to WT-VDAC2 after mitochondrial depolarization treatment (Figure 4.25). While degradation of endogenous VDAC2 was almost complete after 4h of depolarization, a significant increase of the overexpressed WT- and S115D-VDAC2 compared to endogenous VDAC2 levels was observed, indicating successful over-expression of the generated constructs (Figure 4.25A-B). Surprisingly, S115D-VDAC2 was significantly increased in comparison to WT-VDAC2 after 4h of CCCP treatment (Figure 4.25A-B). In contrast, S115A-VDAC2 levels seemed to decrease when compared to WT-VDAC2 levels at the same time point (Figure 4.25A-B).

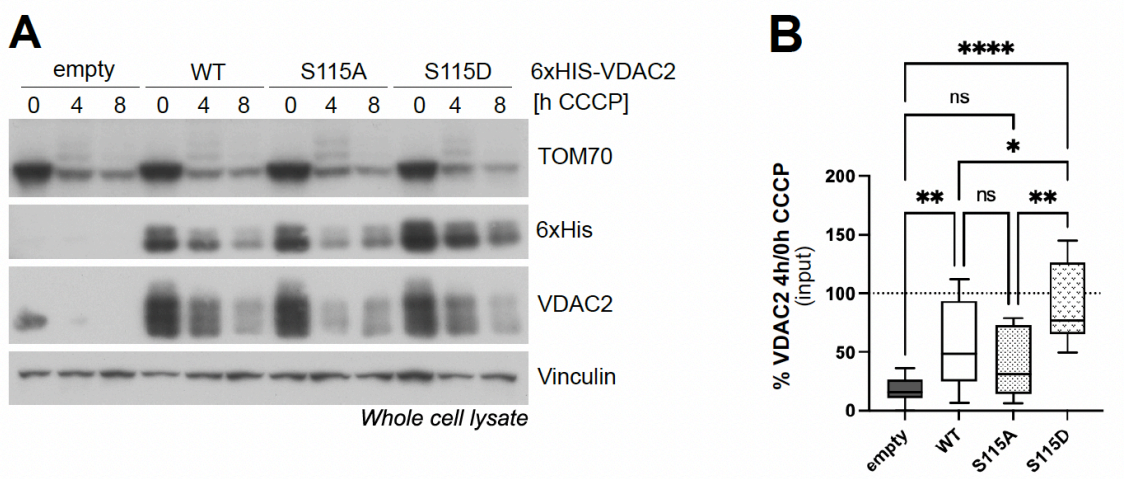


Figure 4.25: Influence of 80econdar-mimic S115 on total VDAC2 turnover. (A-B) Representative Western blots (A) and Western blot quantification (B) showing VDAC2 levels after transfection of WT-, S115A- or S115D-VDAC2 isoforms. Normalized whole cell lysate VDAC2 levels to non-treated conditions. . Data published in (132).

Similar to what was observed for total VDAC2 levels, pulldown analysis revealed increased levels of S115D-VDAC2 after 4h of mitochondrial depolarization (Figure 4.26A-B). In addition, even though differences of total ubiquitination of S115D-VDAC2 did not show to be significantly

different when compared to WT-VDAC2, a slight decrease in S115D-VDAC2 ubiquitination was observed (Figure 4.26A-C). On the other hand, a significant increase in total ubiquitination was observed for S115A-VDAC2 when compared to WT-VDAC2 (Figure 4.26A-C). Next, in order to identify if specific ubiquitin-chain linkages were responsible for the differences observed in total ubiquitination levels of the VDAC2 mutants, specific antibodies for K48- as well as K27-linked ubiquitin chains were used (Figure 4.26A-D). While K48-linked ubiquitin chains did not differ between any of the VDAC2 mutants, K27-linked ubiquitin chains seemed to differentially affect both VDAC2 mutants (Figure 4.26A-D). Indeed, when quantifying the specific K27-linked high molecular ubiquitin smears, increased levels of K27-linked ubiquitination for S115A-VDAC2 were observed while no apparent differences were found for S115D-VDAC2 (Figure 4.26D).

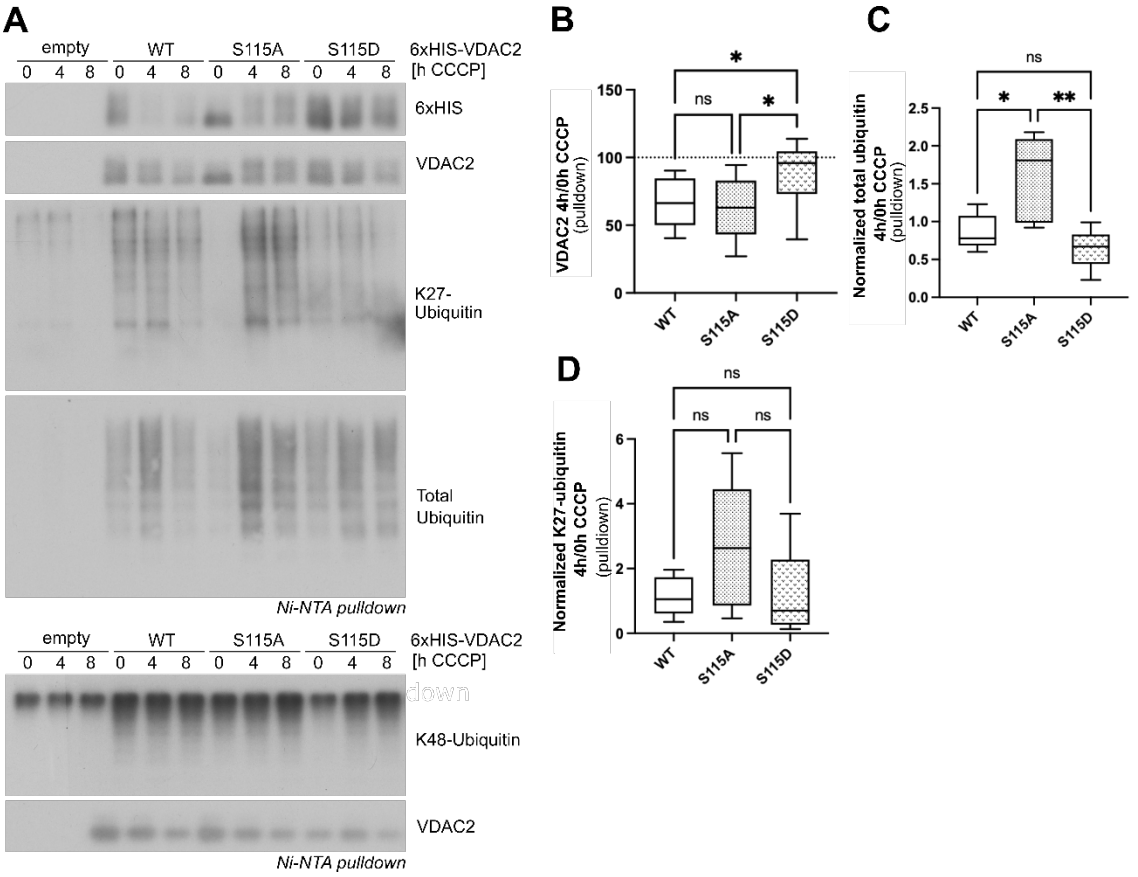


Figure 4.26: Influence of 81econdar-mimic S115 on 6HIS-VDAC2 turnover. (A-B) Representative Western blots of Ni-NTA pulldown (A) and Western blot quantifications (B) showing VDAC2 levels after transfection of WT-, S115A- or S115D-VDAC2 isoforms and mitochondrial depolarization. Normalized VDAC2 levels to non-treated conditions. **(C-D)** Quantification of (C) total ubiquitin or (D) K27-linked ubiquitin chains upon transfection of WT VDAC2 or mutants. Normalized ubiquitin levels to empty vector and further to VADC2 levels of the same blot. . Data published in (132).

Next, to confirm differences in S115A- and S115D-VDAC2 and assess if global mitophagy was affected upon S115A- and S115D-VDAC2 transfection, mitochondrial morphology was assessed by means of semi-quantitative immunofluorescence (Figure 4.27). Overall, overexpression of WT-, S115A- and S115D-VDAC2 mutants did not have any impact on basal mitochondrial

morphology when compared to control conditions (Figure 4.27A-B). Additionally, no apparent changes in overall mitochondrial fragmentation and turnover were observed amongst all VDAC2 isoforms after 4h or 14h of mitochondrial depolarization (Figure 4.27C-D). Semi-quantitative analysis of mitochondrial morphology of WT- or mutant-VDAC2 revealed no changes on the number of transfected cells with CS aggregates or puncta (Figure 4.27E), indicating that global mitophagy was not affected upon transfection of serine VDAC2 mutants in comparison to WT-VDAC2 (Figure 4.27D-E). However, the number of cells still overexpressing residual S115D-VDAC2 after extended depolarization (14h CCCP) was significantly greater than the percentage of positive cells expressing WT-VDAC2 (Figure 4.27F). These data suggest that phosphorylation of S115 may influence VDAC2 turnover in a ubiquitin-dependent manner. However, these subtle alterations did not affect mitophagy progression as a whole (Figure 4.27C-D).

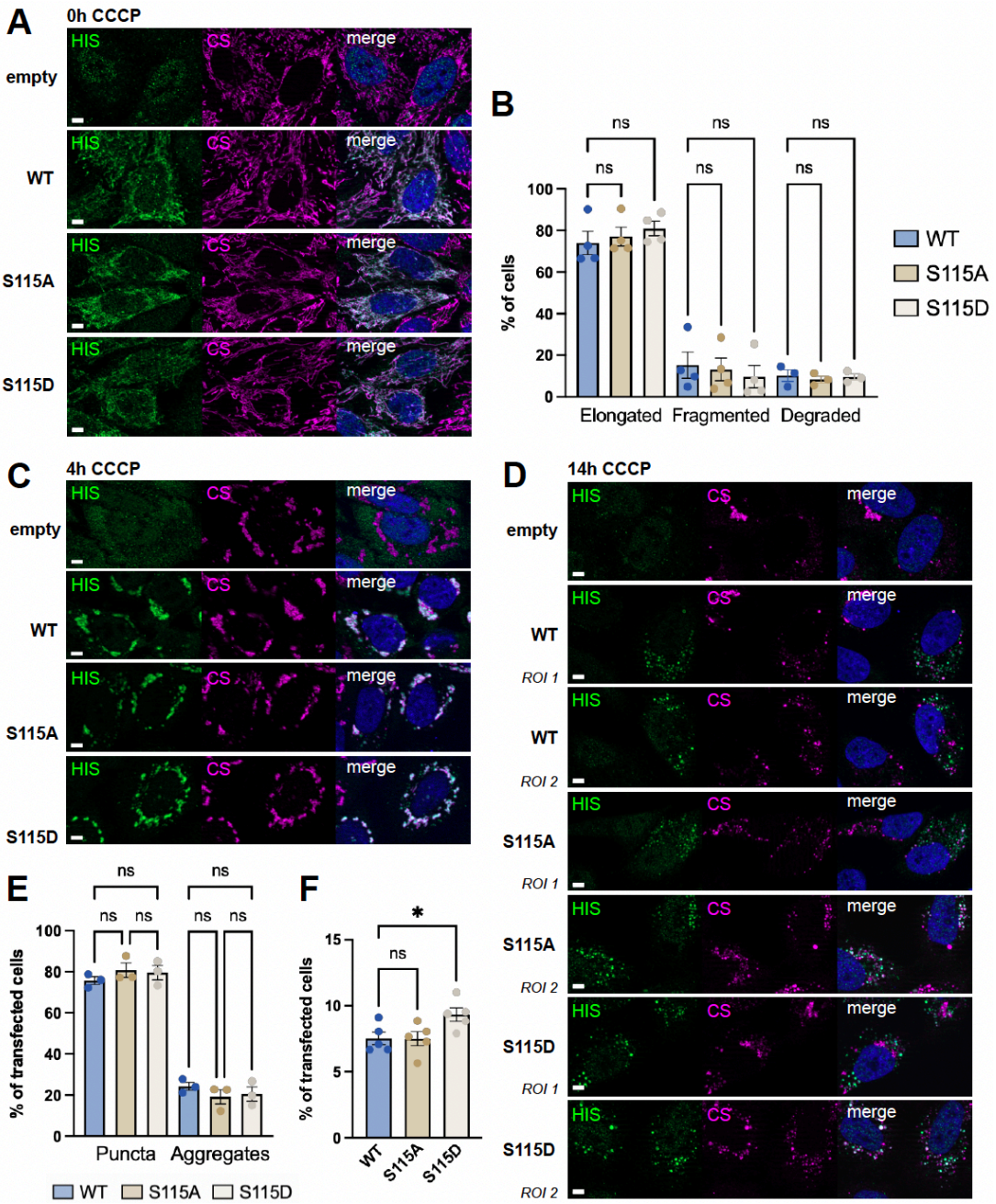


Figure 4.27: Mitochondrial morphology upon WT-, S115A- and S115D-VDAC2 transfection. (A) Representative immunofluorescence images showing transfected VDAC2 (green) and mitochondria represented by CS (magenta) under non-treated conditions. **(B)** Quantification of basal mitochondria morphology upon transfection of VDAC2 WT- and serine mutants under control conditions. **(C-D)** Representative immunofluorescence images showing transfected VDAC2 (green) and CS (magenta) upon (C) 4h or (D) 14h of CCCP treatment. In panel (C) two ROIs are shown to account for all mitochondria morphology profiles found. **(E-F)** Classification of positive VDAC2 remaining cells after 14h of CCCP for WT- and serine VDAC2 mutants showing CS-puncta or CS-aggregates. **(F)** Percentage of positive VDAC2 remaining cells after 14h of CCCP for WT- and serine VDAC2 mutants. Scale bars = 5 μm. Bars: mean ± SEM. Data published in (132).

4.13. VDAC2-S115 dephosphorylation enhances K27-linked ubiquitination at K120

In order to pin-point if the increase of S115A-VDAC2 ubiquitination requires the availability of K120, ubiquitin-dead (K120R) as well as double serine and lysine mutants (S115A-K120R and

S115D-K120R) were generated. Similarly, as performed in the previous chapter, the remaining amounts of VDAC2 mutants after 4h of mitochondrial depolarization were analyzed via Western blot analysis. In addition, due to a strong variability of the assay (Figure 4.25-26), the experiment was also repeated for the single serine mutants analyzed previously. In agreement with previous results, residual VDAC2 levels after 4h of mitochondrial depolarization revealed an increased amount of S115D-VDAC2 while a decrease in S115A-VDAC2 levels was observed (Figure 4.28A-B). On the other hand, while K120R-, S115A/K120R- and S115D/K120R-VDAC2 levels were not significantly different when compared to WT-VDAC2, an increased amount of S115A/K120R mutant was observed compared to S115A-VDAC2, suggesting delayed turnover of the S115A mutant upon abolishing ubiquitination of K120 (Figure 4.28A-B). Interestingly, the opposite effect was observed for S115D/K120R-VDAC2 (Figure 4.28A-B).

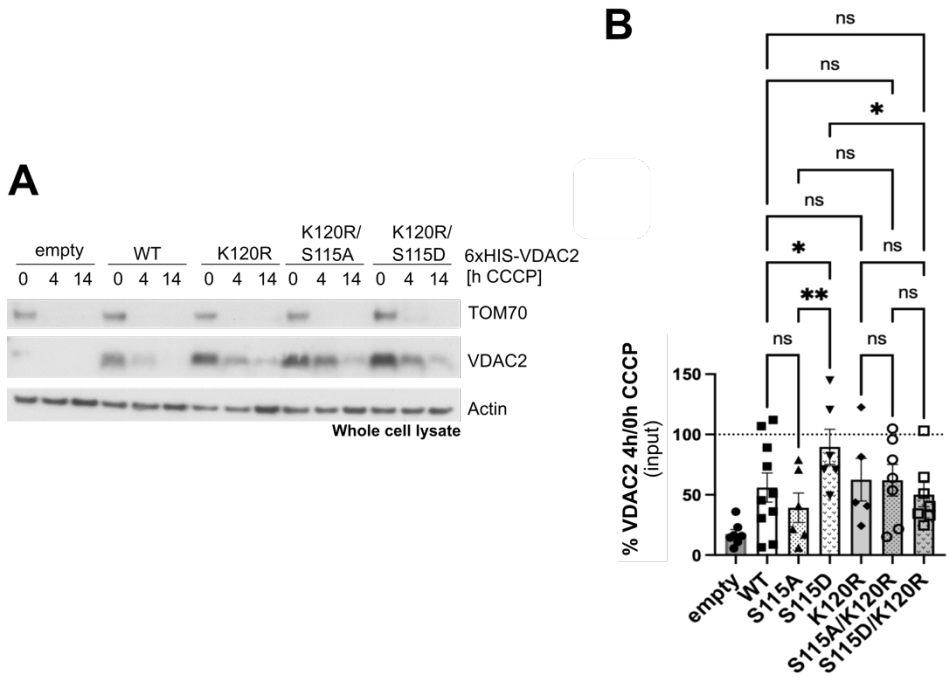


Figure 4.28: Influence of K120R, S115A-120R and S115D-K120R on total VDAC2 turnover. (A-B) Representative Western blots (A) and Western blot quantification (B) showing VDAC2 levels after transfection of WT-, K120R-, S115A/K120R- or S115D/K120R-VDAC2. Normalized VDAC2 levels to non-treated conditions. Bars: mean ± SEM.

Further, to allow for the identification of changes in over-expressed WT- and mutant-VDAC2 turnover, Ni-NTA pulldown was performed for all constructs under CCCP-depolarizing conditions (Figure 4.29). Here, residual VDAC2 levels were normalized to WT-VDAC2 levels of each experiment in order to allow appropriate comparison between experiments. The same procedure was performed for total and K27-specific VDAC2 ubiquitination (Figure 4.29).

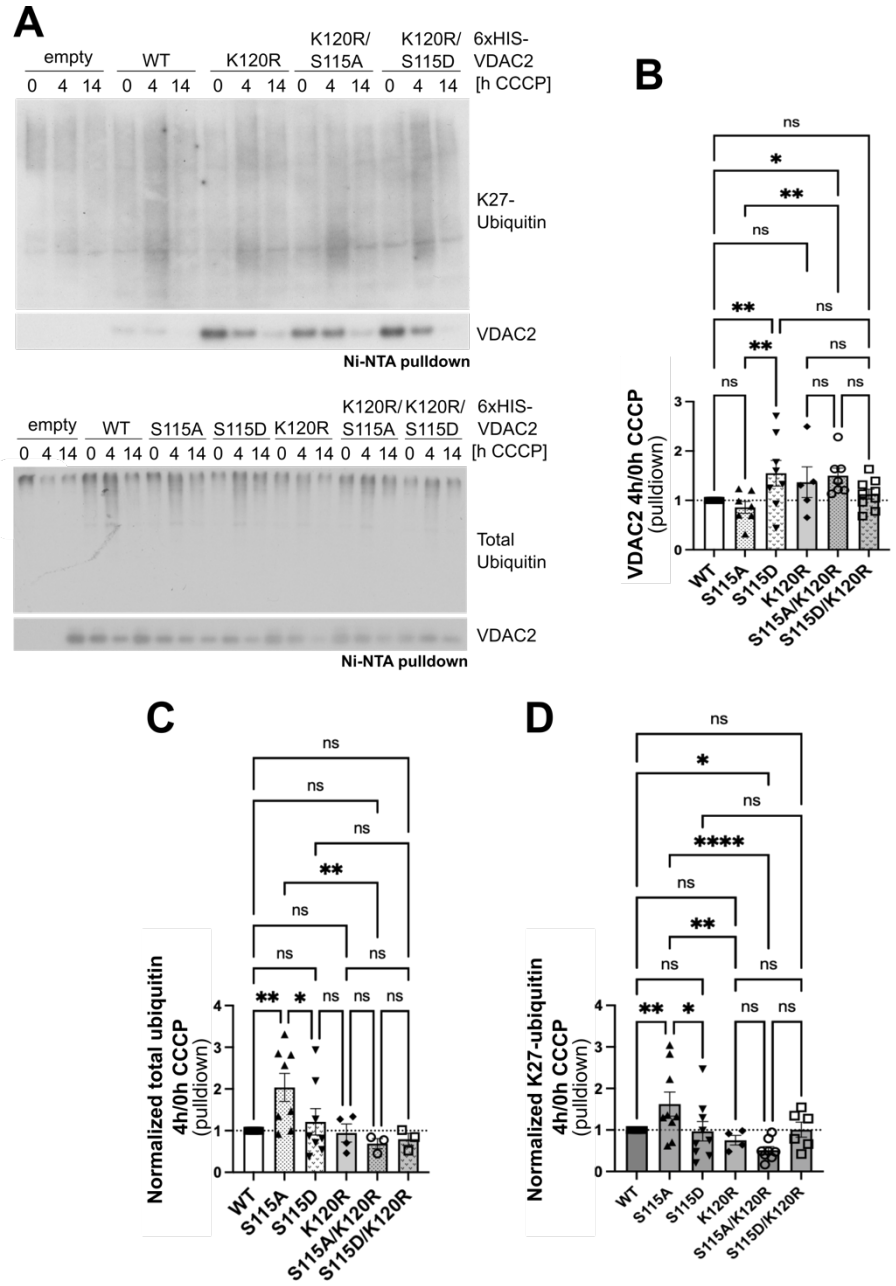


Figure 4.29: Influence of single and double VDAC2 mutants on over-expressed 6HIS-VDAC2 turnover levels. (A-B) Representative Western blots of Ni-NTA pulldown (A) and Western blot quantifications (B) showing VDAC2 levels after transfection of WT-, K120R-, S115A/K120R- or S115D/K120R-VDAC2. Normalized VDAC2 levels to non-treated conditions. **(C-D)** Quantification of (C) total ubiquitin or (D) K27-linked ubiquitin chains upon transfection of WT VDAC2 or mutants. Normalized ubiquitin levels to empty vector and further to VADC2 levels of the same blot. Bars: mean ± SEM.

Similar to what was observed in whole cell lysate samples, an increase in S115D-VDAC2 levels compared to WT-VDAC2 was observed, contrasting to a slight decrease of S115A-VDAC2 after 4h of CCCP treatment (Figure 4.29A-B). Surprisingly, when ubiquitination at K120 was blocked together with a 85econdar-dead mutation in S115, S115A/K120R-VDAC2 levels increased significantly when compared to S115A-VDAC2 (Figure 4.29A-B). On the other hand, while differences between single 85econdar-mimic mutant and double S115D/K120R mutant did not

show to be significant, the turnover rate of S115D/K120R-VDAC2 was similar to the one observed in WT-VDAC2 conditions (Figure 4.29A-B). A similar pattern was observed for the single K120 mutant (Figure 4.29A-B). In addition, changes in total and K27-ubiquitin only seemed to influence the ubiquitination state of S115A/K120R as a significant decrease for total and K27-ubiquitination when compared to S115A-VDAC2 was observed (Figure 4.29A, C and D). In contrast, total or K27-linked ubiquitination levels of either K120R or S115D/K120R did not seem to change when compared to WT-VDAC2, even though a slight decrease in total ubiquitin or K27-linked chains was observed for both mutants (Figure 4.29A, C and D).

In summary, these data suggest that the third cytosolic loop of VDAC2 to be important for VDAC2 turnover. More specifically, S115 de-phosphorylation (S115A) allows the formation of K27-ubiquitin chains on K120, triggering VDAC2 ubiquitin-dependent turnover. Such changes are highly noted when a de-phosphorylation status of S115 is mimicked and ubiquitination at its proximal K120 is abolished, strongly indicating that ubiquitination at K120 is influenced by the phosphorylation status of S115. In addition, given that a high variability in protein turnover as well as ubiquitination pattern is observed when phospho-mimic mutations alone or in combination with ubiquitin-dead mutations are introduced in these particular residues, it is possible that that such individual amino-acid substitutions might compromise protein stability or protein-protein interactions (discussed in chapter 5.6).

4.14. Proteomic ubiquitylome screen reveals TAX1BP1 ubiquitination to take place upon PINK1/parkin induction

At the beginning of this study, only few reports had linked the autophagy adaptor TAX1BP1 with mitophagy and indicated the autophagy receptor to have a 86econdary role in the pathway, as other autophagy receptors (i.e: OPTN) could induce mitophagy in a more efficient manner (61,73,75,175). In this study, mass-spectrometry screen of total ubiquitylome allowed for the identification of ubiquitinated residues in TAX1BP1 (Table 4.3). Most of the ubiquitinated lysines were found in the coiled-coil (CC) region, which lies next to the ubiquitin binding domain (UBA) (Figure 4.30A). Among the detected ubiquitinated lysines, K549 was the only one that revealed a potentially different behavior when comparing WT- to C431A-parkin expressing cells (Figure 4.30B). Ubiquitination dynamics indicated an increase in K549 ubiquitination after early mitochondria depolarization (e.g: 2h CCCP) (Figure 4.30B). Previous examples in the literature indicated PTM of autophagy receptors to act as regulatory mechanism for autophagy receptor activity (61,73,182,183). Thus, we hypothesized that the same could be true for TAX1BP1. Due

to limited reports on TAX1BP1 involvement in mitophagy at the time of this study, validation experiments were initially performed in order to (i) control for true ubiquitination of the autophagy adaptor and (ii) the potential implications of TAX1BP1 ubiquitination (chapters 4.14-15). Further, in order to understand if the observed PTM could have an impact on TAX1BP1 functionality, its involvement in PINK1/parkin mitophagy was characterized (chapters 4.16-4.22).

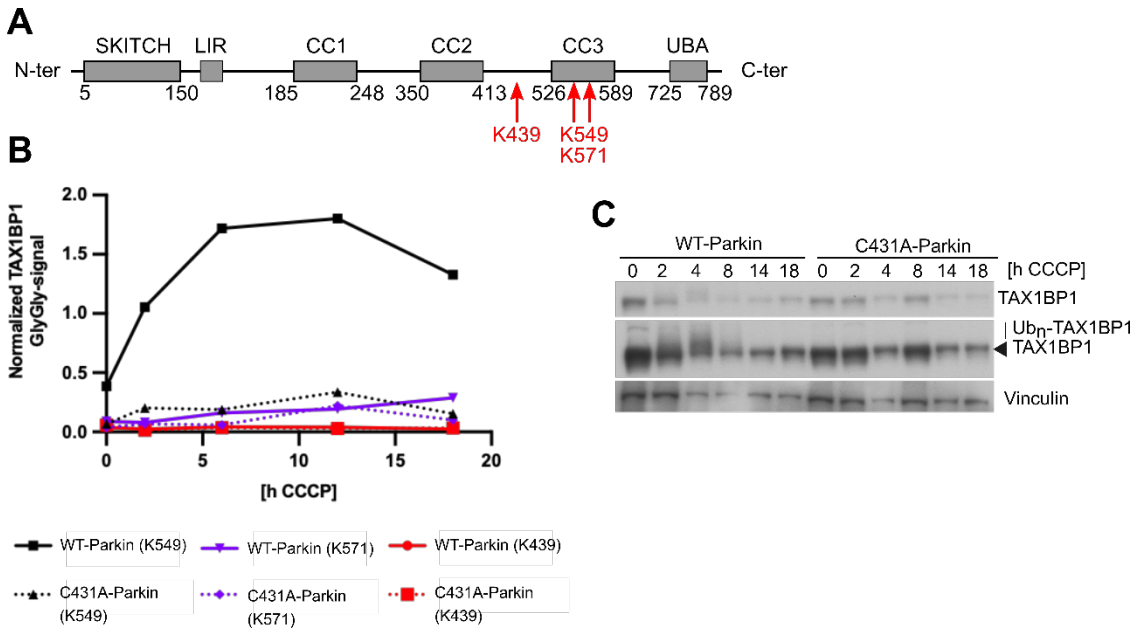


Figure 4.30: **Ubiquitination of TAX1BP1 upon CCCP-induced mitophagy in WT- and C431A-parkin HeLa**. **(A-B)** Ubiquitination of TAX1BP1 during mitophagy. (A) TAX1BP1 domain structure and localization of the identified ubiquitinated lysines in ubiquitylome screen. (B) Normalized Gly-Gly peptide signal of the identified ubiquitinated residues in WT- and C431A-parkin expressing cells during mitophagy time-course. **(C)** Validation of ubiquitinated TAX1BP1 in WT-parkin expressing cells only under mitophagy time-course.

First, ubiquitination of TAX1BP1 protein was validated by means of classic Western blot analysis after inducing mitophagy in WT- and C431A-parkin HeLa at different time-points (Figure 4.30C). Indeed, ubiquitination of TAX1BP1 in WT-parkin cells appeared after 2h and was extended until 8h of mitochondrial depolarization, in accordance with proteomics analysis (Figure 4.30B and C). Similarly, no ubiquitinated species of TAX1BP1 were observed under C431A-parkin expressing cells (Figure 4.30C). Thus, we could confirm an increase in TAX1BP1 ubiquitination after early mitochondrial depolarization.

4.15. Ubiquitination of TAX1BP1 takes place after first UPS OMM degradation step

Ubiquitinated TAX1BP1 species seem to be increased upon mitochondrial depolarization in a parkin-dependent manner (Figure 4.30). Importantly, earlier stages of mitophagy are

characterized by a strong increase in proteasome-targeting ubiquitination's (see chapter 4.7-8). Thus, to discard that TAX1BP1 ubiquitination triggers the protein for UPS-dependent degradation, proteasomal inhibition experiments were performed. For this purpose, N-terminally tagged 6HIS-TAX1BP1 as well as 6HIS-empty vector were transfected to WT-Parkin HeLa. After transfection, cells were treated either with vehicle or the proteasomal inhibitor MG132 prior to mitochondria depolarization with CCCP. Overall, normal mitochondria elimination was observed under depolarizing conditions and the immobilization of ubiquitinated TOM70 could confirm successful proteasome inhibition (Figure 4.31A). In addition, ubiquitination of the transfected TAX1BP1 was prominent after 2h of mitochondrial depolarization while no ubiquitination was observed after pre-UPS inhibition (Figure 4.31A).

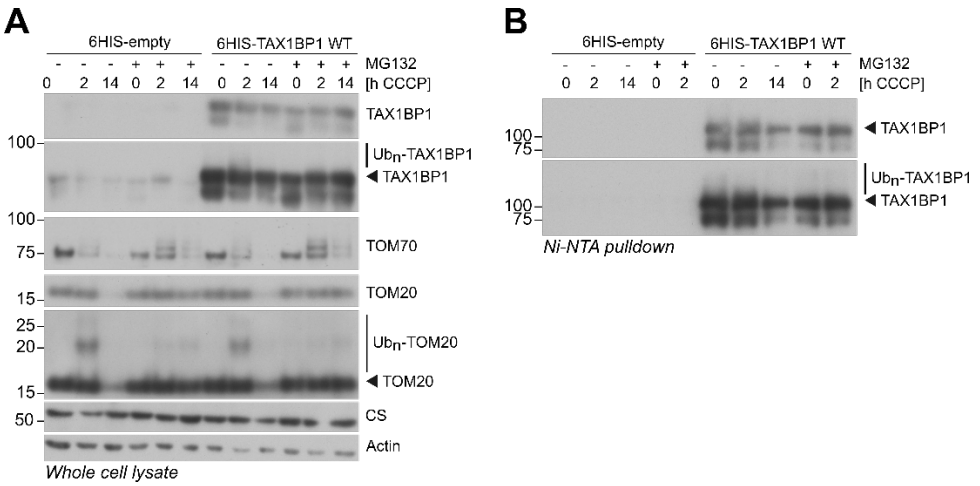


Figure 4.31: Proteasome inhibition influence on TAX1BP1 ubiquitination. (A-B) Representative blots of (A) whole cell lysate samples or (B) Ni-NTA pulldown fractions after transfection of 6HIS-empty of 6HIS-TAX1BP1 upon mitophagy induction combined with vehicle or MG132 pre-treatment.

Ni-NTA pulldown allowed for purification of ubiquitinated 6HIS-TAX1BP1 after 2h of mitochondria depolarization while decreased levels of the protein were observed after 14h of CCCP treatment only (Figure 4.31B). Interestingly, ubiquitinated TAX1BP1 was not detected under conditions of proteasomal inhibition, neither in whole cell lysate or Ni-NTA pulldown samples (Figure 4.31A-B). Thus, these data suggest that ubiquitinated TAX1BP1 is not targeted for proteasomal degradation. Additionally, while it has been demonstrated that proteasomal degradation is a pre-requisite for successful mitophagy (135,136) (see chapter 4.7-8), TAX1BP1 ubiquitination only seems to appear under successful mitophagy conditions, potentially indicating that these ubiquitination events likely take place after early UPS-degradation of OMM proteins.

4.16. TAX1BP1 translocates to mitochondria upon mitochondrial depolarization

After having validated a general ubiquitination pattern of TAX1BP1 after mitochondria depolarization and seeing that these ubiquitination events are linked to PINK1/parkin mitophagy induction, sub-cellular localization of endogenous TAX1BP1 upon mitophagy induction was assessed.

While TAX1BP1 did not seem to co-localize with the ER marker calnexin (Figure 4.32A), it engaged with the lysosomal marker LAMP1 under basal conditions (Figure 4.32B-C, panel i). Interestingly, while basal TAX1BP1 did not co-localize with the mitochondrial network at all, TAX1BP1 engaged with mitochondria after early mitophagy induction (2h CCCP) as well as after extended depolarization times (14h CCCP) (Figure 4.32B-C, panels ii-v), confirming TAX1BP1 as an autophagy adaptor involved in PINK1/parkin mitophagy. In addition, endogenous TAX1BP1 was found to also co-localize with LAMP1-puncta (Figure 4.32C). TAX1BP1 puncta were either in close apposition (open arrowheads) or overlapping (closed arrowheads) with LAMP1 puncta (Figure 4.32C, panels i-v). There data suggested TAX1BP1 to be engaged with lysosomes under basal conditions and further translocate to mitochondria upon stress-induced mitochondria depolarization.

Importantly, under mitochondria depolarization conditions, TAX1BP1 seemed to behave similarly to the well-known autophagy adaptor p62/SQSTM (Figure 4.32D-E). Both autophagy adaptors engaged with fragmented mitochondria at early stages of the pathway (Figure 4.32D, panels ii-iii) as well as with mitochondrial remnants after long depolarization treatments (Figure 4.32D, panels iv-v). Interestingly, the recognition of both autophagy adaptors at late stages of the pathway seemed somewhat redundant (Figure 4.32D): while some of the inner-mitochondrial remnants were found to be recognized by both of the autophagy adaptors (Figure 4.32D, panels i), some SSBP1 aggregates were more enriched with either TAX1BP1 or p62/SQSTM (Figure 4.32D, panels ii-iii). Additionally, situations where none of the autophagy receptors were involved in the recognition of inner mitochondrial aggregates were also observed (Figure 4.32D, panel iv).

Taken together, these data are in agreement with previous studies, where p62/SQSTM as well as TAX1BP1 are considered secondary autophagy receptors and a certain redundancy among all autophagy receptors is acknowledged (75,184,185).

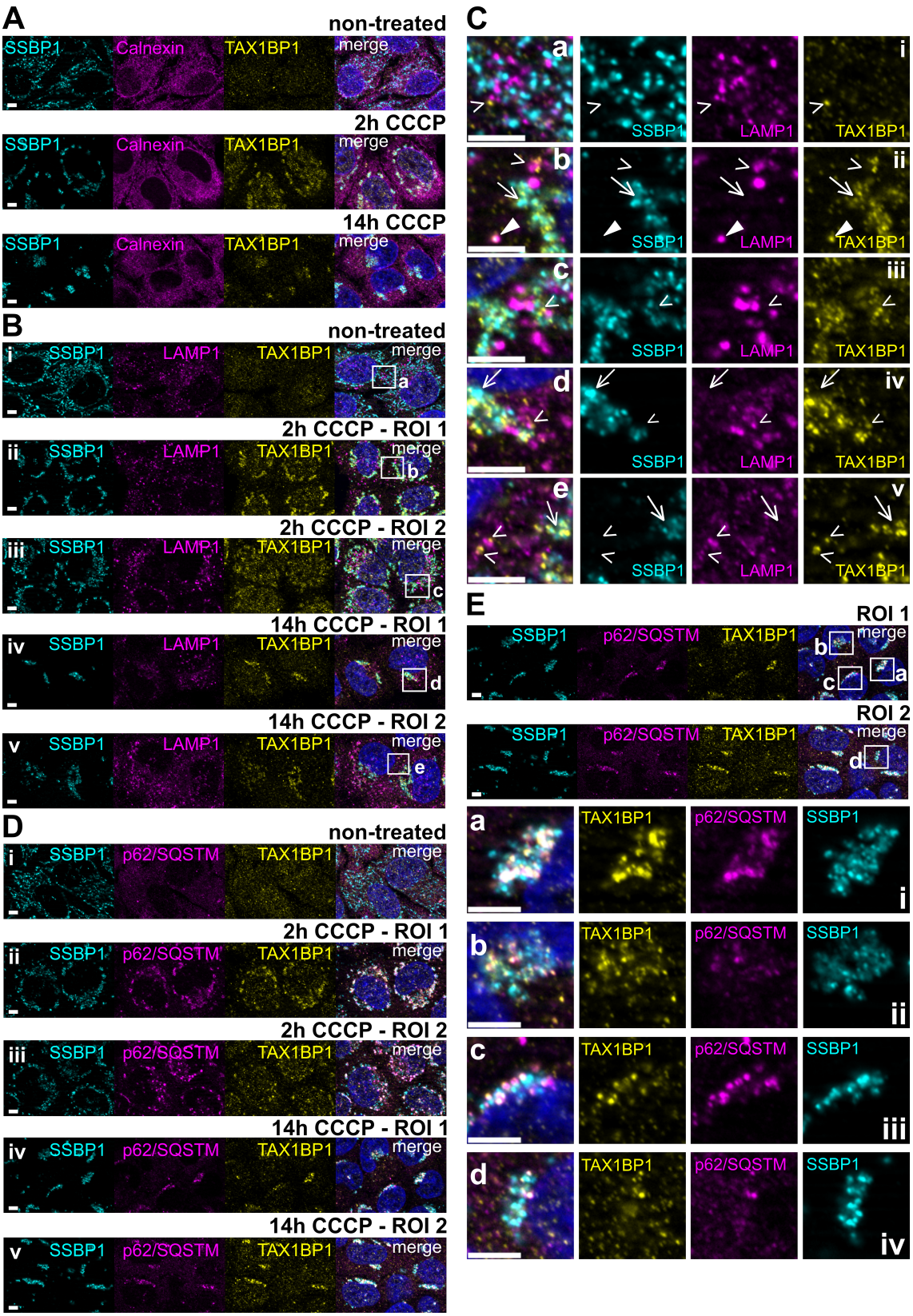


Figure 4.32: Endogenous TAX1BP1 engages with LAMP1 and p62/SQSTM upon mitochondrial depolarization. (A) Representative images showing localization of calnexin (magenta), TAX1BP1 (yellow) and SSBP1 (cyan) at the indicated CCCP treatment time-points. **(B-C)** Representative images showing localization of LAMP (magenta), TAX1BP1 (yellow) and SSBP1 (cyan) at the indicated CCCP treatment time-points. **(C)** Zoomed regions from panel (B) are shown. Closed arrowheads indicate TAX1BP1 puncta overlapping with LAMP1 puncta. Open arrowheads indicate TAX1BP1 in close apposition with LAMP1. Arrows indicate mitochondrial aggregates recognized by TAX1BP1. **(D-E)** Representative images showing localization of p62/SQSTM (magenta), TAX1BP1 (yellow) and SSBP1 (cyan) at the

indicated CCCP treatment time-points. **(E)** Top panels correspond to panels iv-v from panel (D). Zoom panels (a-d) indicate complete (a), partial (b and c) or no recognition (d) of SSBP1 aggregates by p62/SQSTM and TAX1BP1 after 14 h of CCCP treatment. In (B), (D-E) two different ROIs are shown to account for different mitophagy stages within the same cell population: ROI1 represents > 50% while ROI2 represents <50% of cell population. All scale bars: 5μm.

4.17. TAX1BP1 engages with LAMP1 as well as TOM20- and SSBP1-puncta

Because endogenous TAX1BP1 was mostly enriched on fragmented mitochondria and TAX1BP1-puncta were less prominent under these conditions (Figure 4.32B-C), over-expressed TAX1BP1 was used to qualitatively assess the involvement of the autophagy receptor with LAMP1 as well as with TOM20- and SSBP1-puncta (Figure 4.33).

Under basal conditions, 6HIS-TAX1BP1 co-localized with LAMP1, indicating lysosomal localization of the autophagy receptor (Figure 4.33A-B, panel i). Additionally, similar to what was observed for endogenous TAX1BP1, 6HIS-TAX1BP1 translocated to mitochondria upon mitophagy induction (Figure 4.33A, panel ii). However, in cells where mitochondrial fractionation was not yet so prominent, over-expressed TAX1BP1 still co-localized with LAMP1, indicating a potential shift from lysosomes to mitochondria upon depolarization induction (Figure 4.33A, panel iii). After intermediate and extended depolarization times (4-14h CCCP), over-expressed TAX1BP1 co-localized with both depolarized mitochondria as well as LAMP1-puncta in a similar fashion as observed for endogenous TAX1BP1 (Figures 4.33A, panel iv-vii and 4.33B, panels ii-vi). In addition, over-expressed TAX1BP1 showed to co-localize with TOM20-puncta, upon intermediate and late depolarization treatment (4-18h CCCP) (Figure 4.33C-D). Interestingly, TAX1BP1 was also found to recognize SSBP1-puncta devoid of TOM20 (Figure 4.33D, panel c).

Taken together, these data indicate that 6HIS-TAX1BP1 is found at the lysosomal network under basal conditions and translocates to the mitochondria upon mitochondrial depolarization (Figure 4.33A-B). Intringuingly, TAX1BP1 translocation to mitochondria does not seem to involve the totality of the available TAX1BP1 (Figure 4.33A-B), similarly as what was observed under endogenous expressing conditions (Figure 4.32). In addition, in agreement with what was observed for endogenous TAX1BP1, 6HIS-TAX1BP1 seems to be able to recognize both TOM20 as well as SSBP1 (Figure 4.33), indicating no particular specificity for outer- or inner-mitochondrial substrates.

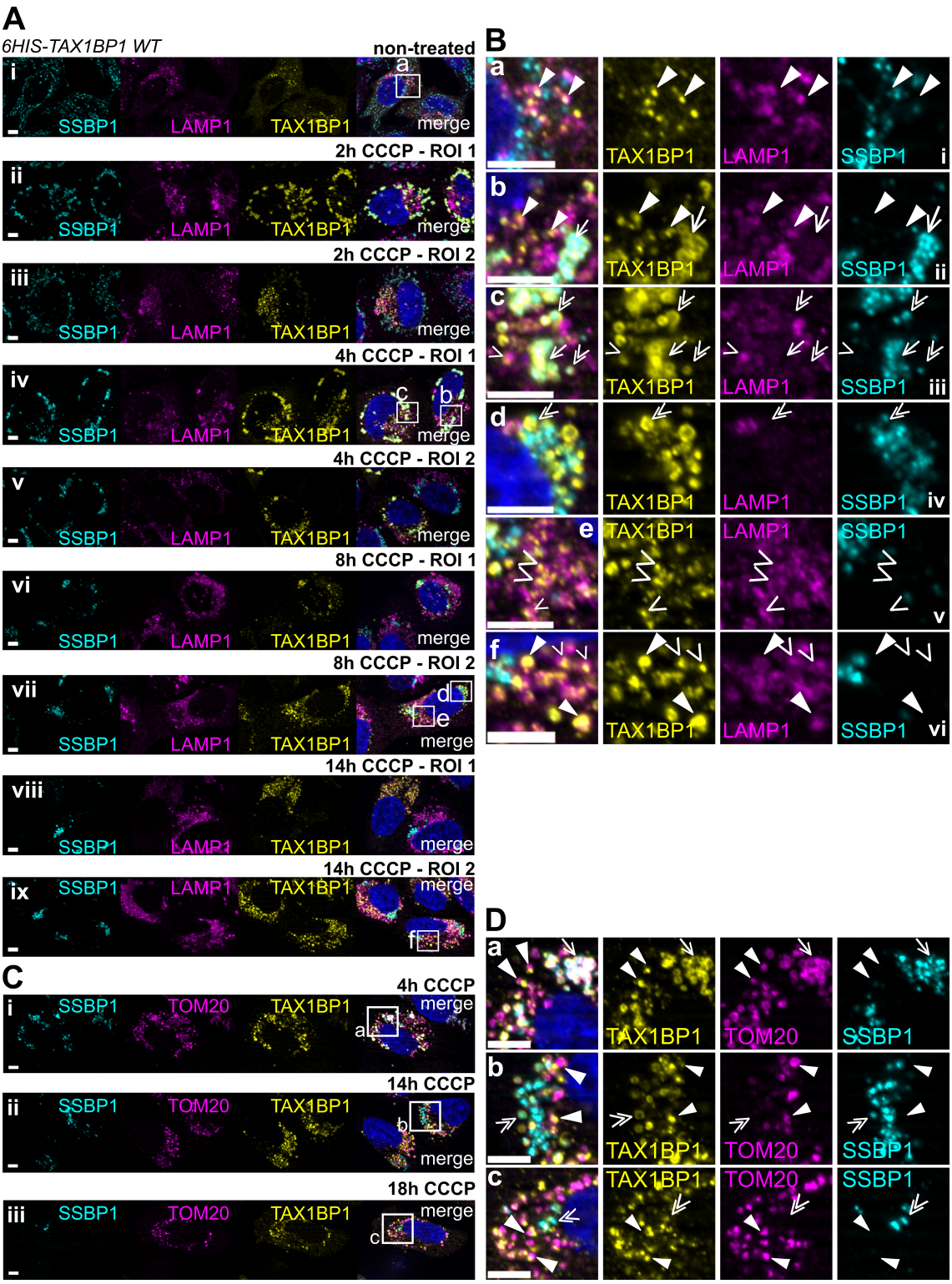


Figure 4.33: Over-expressed TAX1BP1 engages with LAMP1, TOM20 and SSBP1 upon mitochondrial depolarization. **(A-B)** Representative images showing localization of LAMP (magenta), TAX1BP1 (yellow) and SSBP1 (cyan) at the indicated CCCP treatment time-points after transfection with 6HIS-TAX1BP1 WT. **(A)** Two different ROIs are shown to account for different mitophagy stages within the same cell population: ROI1 represents >50% while ROI2 represents <50% of cell population. **(B)** Zoomed regions from panel (B) showing different LAMP1 and TAX1BP1 colocalization. Closed arrowheads indicate TAX1BP1 puncta overlapping with LAMP1 puncta. Open arrowheads indicate TAX1BP1 in close apposition with LAMP1. Arrows indicate mitochondrial aggregates recognized by TAX1BP1. Double open arrowheads indicate SSBP1-puncta recognized by TAX1BP1. **(C-D)** Representative images showing TAX1BP1 (yellow) co-localization with TOM20- (magenta) and SSBP1-puncta (cyan) at the indicated treatment time-points. Regions of interest in (C) are zoomed in panel (D). Closed arrowheads indicate TOM20 puncta recognized by TAX1BP1. Arrows

indicate mitochondrial aggregates recognized by TAX1BP1. Double open arrowheads indicate SSBP1-puncta recognized by TAX1BP1. All scale bars: 5μm.

4.18. Ubiquitinated TAX1BP1 translocates to mitochondria upon depolarization

As previously shown, TAXABP1 is ubiquitinated and translocates to mitochondria upon mitochondrial depolarization conditions (Figure 4.32-33). Thus, in order to be sure that the ubiquitinated form of TAX1BP1 is found on depolarized mitochondria, sub-cellular fractionation experiments were performed: crude mitochondria fractions (CM) were subjected to sucrose gradient purification in order to obtain enriched mitochondrial fractions devoid of ER or lysosomes. Basal as well as early depolarization conditions were analyzed (Figure 4.34).

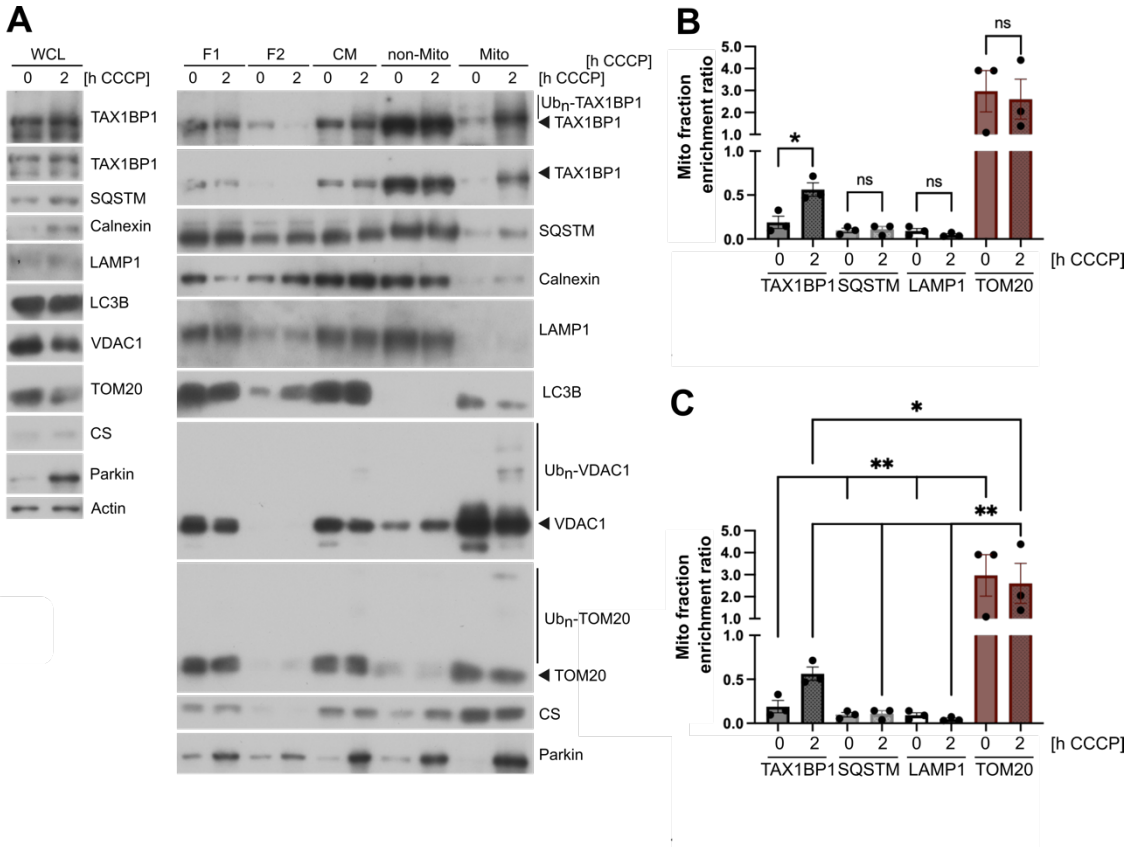


Figure 4.34: TAX1BP1 and p62/SQSTM sub-cellular localization upon mitophagy induction. **(A)** Representative Western blots before (WCL) and after fractionation upon basal or mitophagy induced conditions. **(B-C**) Enrichment ratio of mitochondrial (Mito) fraction before or after mitophagy induction for the indicated proteins. Enrichment ratio changes are either compared (B) within each other after mitochondrial depolarization or (C) to TOM20 enrichment ratios before and after mitochondrial depolarization, respectively. F1: fraction 1, F2: fraction 2, CM: crude mitochondria, non-Mito: non-enriched mitochondria, Mito: enriched mitochondria. Bars: mean ± SEM. **: p<0.005, *: p<0.05, ns: non-significant.

Sucrose fractionation allowed for enrichment of total and ubiquitinated mitochondrial proteins in the enriched mitochondrial fraction (Mito). Additionally, an enrichment of parkin was also observed in the mitochondrial fraction, serving as a control of parkin translocation and

successful mitophagy initiation. The non-mitochondrial fraction (non-Mito) contained great amounts of LAMP1 and calnexin, while mitochondrial proteins were reduced in this fraction (Figure 4.34A). Consistently, TAX1BP1 ubiquitination quickly appeared after mitochondrial depolarization and was observed in whole cell lysate samples (WCL) as well as in CM fractions (Figure 4.34A). Interestingly, while TAX1BP1 ubiquitination appeared in both mitochondrial and non-mitochondrial fractions, ubiquitinated TAX1BP1 seemed to be enriched in the mitochondrial fraction compared to the non-Mito fraction after 2h of CCCP treatment (Figure 4.34A). Total TAX1BP1 was enriched in the Mito fraction after early depolarization (Figure 4.34A-B), however, its protein levels were much lower than the OMM protein TOM20 (Figure 4.34C).

As a comparison, the behavior of p62/SQSTM was also monitored. In this case, p62/SQSTM was not highly enriched in neither crude nor mitochondrial fractions after short depolarization treatment (Figure 4.34A). Actually, p62/SQSTM enrichment ratio in the mitochondrial fraction was lower than TAX1BP1 and did not seem to change upon early mitochondrial depolarization (Figure 4.34B-C). Surprisingly, a great proportion of p62/SQSTM remained in F1 -prior to obtaining crude mitochondrial fraction (Figure 4.34A)-, while a great amount of the protein was found to be enriched in the non-Mito fraction, similarly to what was observed for TAX1BP1 and LAMP1 (Figure 4.34A). While TAX1BP1 translocation fits with immunofluorescence data (see Figures 4.32-33) and further supports the idea of the autophagy receptor being engaged with the lysosomal network, the validation of p62/SQSTM translocation under the same conditions was not successful. As p62/SQSTM involvement with PINK1/parkin mitophagy has been linked in this and other studies (59,62) (Figures 4.11 and 4.32), limitations of the sucrose fractionation technique (e.g: increased p62/SQSTM at F1) might explain the discrepancies observed for p62/SQSTM. On the other hand, one cannot discard that p62/SQSTM translocation to mitochondria is more prominent at a later time-point of the pathway, perhaps suggestive of a more secondary role of p62/SQSTM in comparison to TAX1BP1. Future studies involving other canonical autophagy receptors (i.e: OPTN) in sucrose fractionation analysis might help validate the behavior of TAX1BP1 as a secondary autophagy receptor in the context of parkin-dependent mitophagy. In summary, these data indicate that ubiquitinated TAX1BP1 translocates to mitochondria upon depolarization.

4.19. TAX1BP1 knock-down does not impair overall mitophagy in WT-parkin HeLa

After having characterized TAX1BP1 as an autophagy receptor involved in PINK1/parkin mitophagy (Figure 4.32-33), its relevance in the context of mitochondrial turnover was assessed. For this purpose, knock-down of TAX1BP1 was combined with mitochondrial depolarization treatments in WT-parkin HeLa (Figure 4.35).

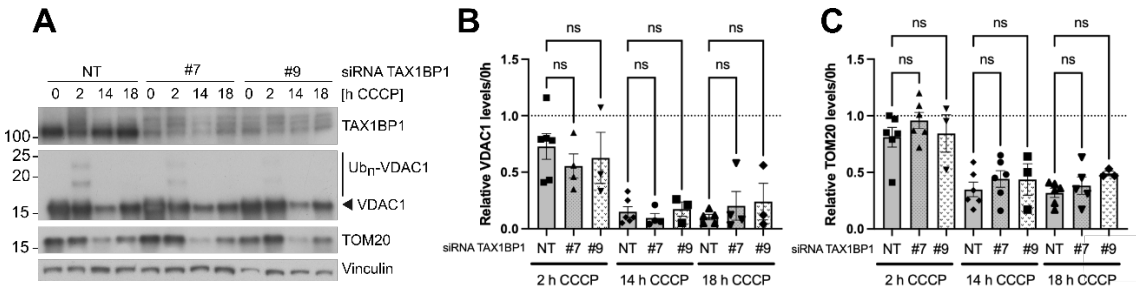


Figure 4.35: TOM20 and VDAC2 turnover is not impaired upon TAX1BP1 knock-down. (A) Representative Western blot showing mitophagy curves for non-targeting and two different siRNA against TAX1BP1. **(B-C)** Quantification analysis for changes in (B) VDAC1 and (C) TOM20. Bars: mean ± SEM. NT: non-targeting, ns: non-significant.

Overall, no significant impairment on VDAC1 and TOM20 turnover was observed after knock-down of TAX1BP1 (Figure 4.35). Because HeLa cells rely on basal expression of other canonical autophagy receptors apart from TAX1BP1 (e.g: OTPN, p62/SQSTM, NDP52 and NBR1) (75), it is not surprising that the single silencing of one of the autophagy receptors impairs the elimination of autophagy-linked mitochondrial proteins. Thus, these data suggest that TAX1BP1 deficiency is compensable by other autophagy adaptors and fit with previous observations in this study, where inner mitochondrial clumps were not recognized by the autophagy adaptor (Figure 4.32E).

4.20. Over-expression of TAX1BP1 enhances mitophagy in WT-parkin HeLa

While knock-down of TAX1BP1 had no negative influence on the overall rate of mitochondrial turnover, we hypothesized that the over-expression of the autophagy receptor could enhance the overall rate of mitochondrial turnover in our cell model. For this purpose, WT 6HIS-TAX1BP1 was transfected in WT-parkin HeLa and the turnover of specific OMM and matrix proteins was assessed. As expected, TAX1BP1 over-expression did not have any effect on MFN1 turnover (Figure 4.36A-B). However, it enhanced the turnover rate of TOM20 after 14h of CCCP treatment (Figure 4.36A-C). In addition, a slight enhancement on CS turnover was observed after 14h of mitochondrial depolarization (Figure 4.36A-D).

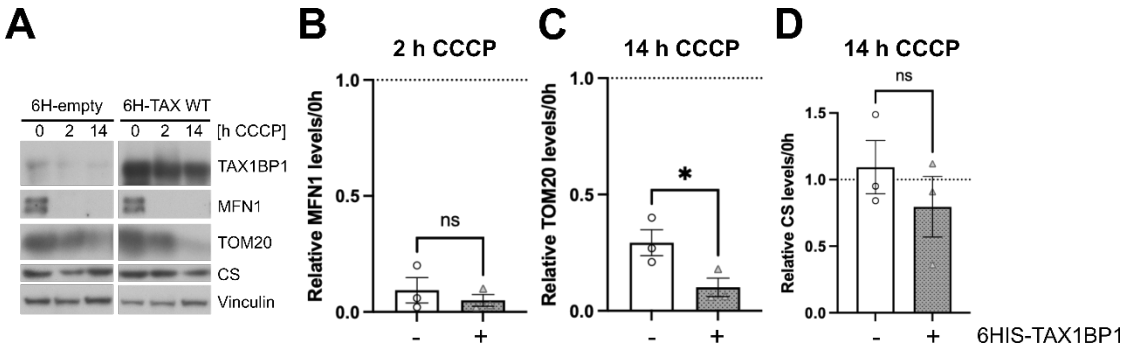


Figure 4.36: Mitochondrial protein degradation effects upon over-expression of 6HIS-TAX1BP1. (A) Representative Western blots showing degradation of the indicated mitochondrial markers after mitochondrial depolarization upon transfection with 6HIS-empty vector or 6HIS-TAX1BP1. **(C-D)** Western blot quantification analysis for changes in (B) MFN2, (C) TOM20 and (D) CS. Bars: mean ± SEM. 6H-TAX: 6HIS-TAX1BP1, *: $p<0.05$, ns: non-significant.

To further gain better significance on the impact of mitochondrial turnover upon TAX1BP1 overexpression, single cell analysis of mitochondrial area –represented by SSBP- after CCCP-induced mitophagy was performed with CellProfiler (Figure 4.37). Upon quantification, mitochondrial area of 6HIS-TAX1BP1 transfected cells was significantly reduced after 4h and 14h of CCCP treatment when compared to empty vector conditions (Figure 4.37A-C). More specifically, a mean of 15% and 31.6% SSBP1 degradation was observed after 4h and 14h of CCCP, respectively (Figure 4.37D), indicating a mild enhancement of mitophagy upon transfection of 6HIS-TAX1BP1 on WT-parkin expressing cells.

Taken together, over-expression of TAX1BP1 seemed to slightly enhance total mitochondrial turnover on WT-parkin expressing cells, both at early and late stages of the pathway (Figures 4.36-37). Thus, these data confirm the ability of TAX1BP1 to target TOM20 as well as matrix proteins (CS and SSBP1) and therefore validate TAX1BP1 as an autophagy adaptor involved in PINK1/parkin mitophagy.

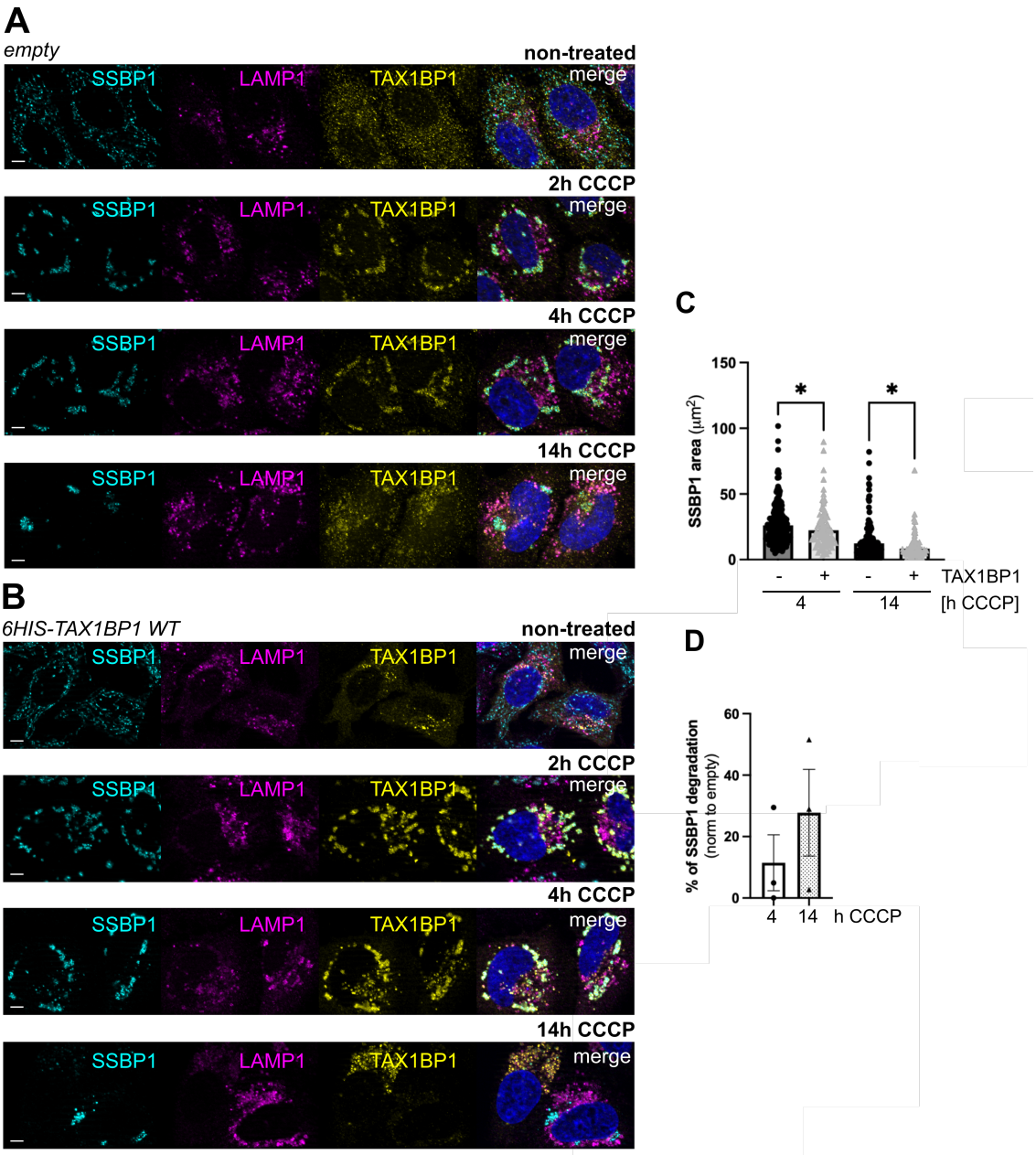


Figure 4.37: Single cell analysis on SSBP1 degradation upon over-expression of 6HIS-TAX1BP1. (A-B) Representative images showing TAX1BP1 (yellow), LAMP1 (magenta) and SSBP1 (cyan) after transfection of (A) empty plasmid or (B) 6HIS-TAX1BP1 WT. **(C)** Single-cell analysis of SSBP1 area in cells expressing 6HIS-empty vector or 6HIS-TAX1BP1 after the indicated time-points of mitochondrial depolarization. Each data point represents a single cell value. **(D)** Percentage of SSBP1 degradation normalized to empty plasmid transfection degradation levels after the indicated treatment time-points. Each data point represents the mean value of an experimental replicate. Bars: mean ± SEM. h: hours, *: $p<0.05$. Scale bars: 5µm.

4.21. Influence of TAX1BP1 on mitophagy progression in a knock-out autophagy adaptor Hela cell line

As previously seen, TAX1BP1 is involved in PINK1/parkin mitophagy and its over-expression is able to mildly enhance mitochondrial turnover when all autophagy receptors are endogenously expressed (see previous chapter). Consistently, TAX1BP1 is not considered one of the essential

autophagy adaptors (75). Indeed, when TAX1BP1 was silenced in WT-parkin HeLa, no significant changes in mitochondrial protein turnover where observed (Figure 4.8.6). Thus, it is not surprising that, when over-expressing the autophagy adaptor, only a mild enhancement mitochondrial turnover is observed (Figure 4.37D). Hence, in order to characterize the effects of TAX1BP1-dependent mitochondrial turnover on PINK1/parkin mitophagy, mitochondrial turnover was assessed in a HeLa cell line (penta-KO HeLa) which lacks expression of all five autophagy receptors reported to be involved in parkin-dependent mitophagy: p62/SQSTM, OTPN, TAX1BP1, NDP52 and NBR1 (75) (Table 2.1). Importantly, because HeLa cells lack endogenous parkin expression (166), all experiments performed with this cell line involved co-transfection of parkin and TAX1BP1 (see below).

4.21.1. Over-expression of wild-type TAX1BP1 rescues defective mitophagy

When penta-KO cells were exposed to mitochondrial depolarization together with parkin over-expression only, a 50% degradation rate of MFN1 was observed after 2h of CCCP treatment which increased to 75-80 % upon extended depolarization treatment (Figure 4.38A-B). Interestingly, a 50% degradation of both OMM and IMM proteins was observed after 8h of mitochondrial depolarization and parkin transfection only (Figure 4.38A-B). However, under these conditions, the elimination of OMM and IMM proteins took place at once and not in a sequential manner as observed in WT-parkin HeLa cells (see chapter 4.2) (Figure 4.38B).

On the other hand, equally to parkin transfection conditions only, an initial 50% degradation of MFN1 was observed which was enhanced upon extended CCCP-treatment and co-expression of parkin and TAX1BP1 (Figure 4.38A-C), indicative of TAX1BP1-independent turnover mechanisms for MFN1 as already reported in this and other studies (49). An increase in the turnover of VDAC1 and TOM20 could be observed both under parkin transfection only or in combination with TAX1BP1 when compared to non-transfecting conditions (Figure 4.38C). However, the addition of TAX1BP1 did not dramatically enhance the turnover of these two OMM proteins (Figure 4.38C). Turnover of IMM and matrix proteins was not affected neither under conditions of parkin transfection only, nor after the addition of WT TAX1BP1 after 8h of CCCP treatment (Figure 4.38A-C). Of note, COX4 and CS protein levels were already reduced at this time-point under non-transfected conditions, potentially due to CCCP-induced depolarization which compromises mitochondrial import and thus, may trigger the degradation of cytosolically translated proteins that cannot be imported (Figure 4.38C).

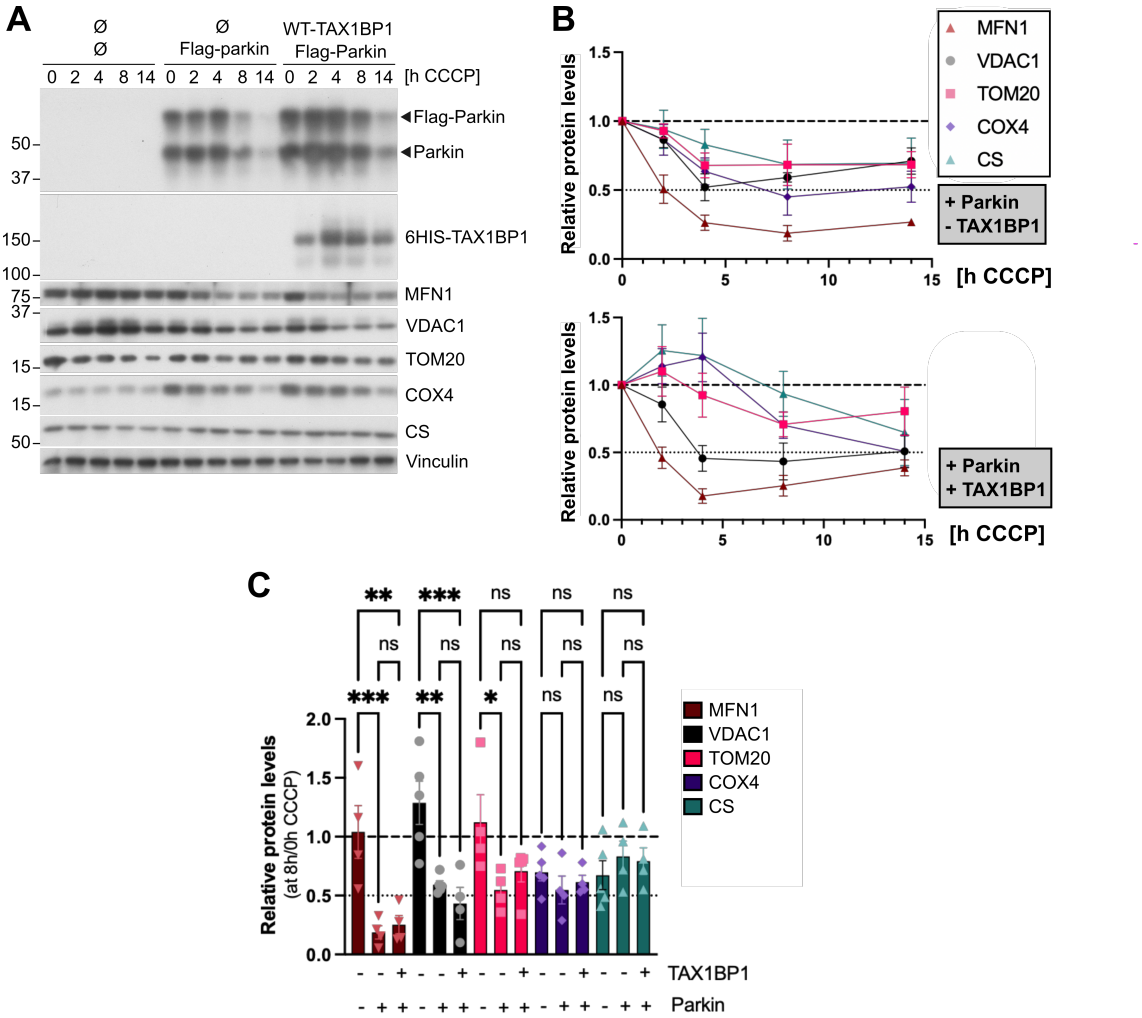


Figure 4.38: Western blot analysis of mitochondrial turnover in penta-KO cells after co-transfection of Flag-parkin and 6HIS-TAX1BP1 WT or Flag-parkin alone. (A) Representative Western blots showing degradation upon CCCP treatment in penta-KO transfected cells with both empty plasmids (∅), empty HIS plasmid combined with Flag-parkin or 6HIS-TAX1BP1 WT combined with Flag-parkin transfection. **(B)** Mitophagy curve of Penta-KO cells only transfected with Flag-parkin or in combination with TAX1BP1. Data points: mean ± SEM. **(C)** Mitochondrial turnover of specific mitochondrial markers after 8h of CCCP treatment upon no transfection, parkin transfection only or in combination with WT TAX1BP1. Bars: mean ± SEM. ***: p<0.0005, ***: p<0.001, *: p<0.05, ns: non-significant. Data published in (173).

Overall, these data suggest different mitochondrial degradation dynamics upon expression of parkin alone or in combination with WT TAX1BP1 (Figure 4.38). Thus, in order to confirm if parkin alone can trigger mitochondrial degradation or if the expression of an autophagy receptor like TAX1BP1 is needed for complete mitochondrial removal, mitochondrial morphology and area were analyzed both in a qualitative and quantitative manner (Figure 4.39). In these experiments, mitochondrial area will be assessed with the matrix marker SSBP1. Given that matrix proteins levels were not affected at a time-point of <8h CCCP (Figure 4.38B-C), the analysis performed with CellProfiler will be used to monitor mitophagy by measuring SSBP1 mitochondrial area as a readout for mitochondrial fragmentation as well as mitophagy progression (see below).

As expected, no apparent mitochondrial fragmentation was observed in non-transfected penta-KO cells, even after 8h of CCCP treatment (Figure 4.39C, panel i). On the other hand, a slight mitochondrial fragmentation effect was observed under non-treated conditions upon transfection of parkin alone or in combination with WT TAX1BP1 (Figure 4.39A, panels ii and iii). Moreover, a strong increase on mitochondrial fragmentation was observed after 4 and 8h of CCCP treatment, upon transfection of parkin alone or in combination with WT TAX1BP1 (Figure 4.39B-C, panel ii and iii). Interestingly, single cell analysis of mitochondrial SSBP1 area revealed a significant decrease upon transfection of parkin and TAX1BP1 after 4h of CCCP in comparison to non-transfected conditions or parkin-transfected conditions only (Figure 4.39D). In addition, a slight decrease on mitochondrial area was also observed on penta-KO cells transfected with parkin only in comparison to non-transfected cells after 4 and 8h CCCP treatment (Figure 4.39D-E), indicating that parkin alone can trigger mitochondrial fractionation and a milder mitochondrial turnover on cells lacking autophagy receptors involved in parkin-dependent mitophagy.

Taken together, these data indicate that TAX1BP1 can rescue defective mitophagy in penta-KO HeLa cells over-expressing parkin (Figures 4.38-39). On the other hand, parkin alone might also induce mitochondrial turnover in a less effective manner (Figure 4.39), perhaps involving ubiquitin-independent autophagy receptors (51).

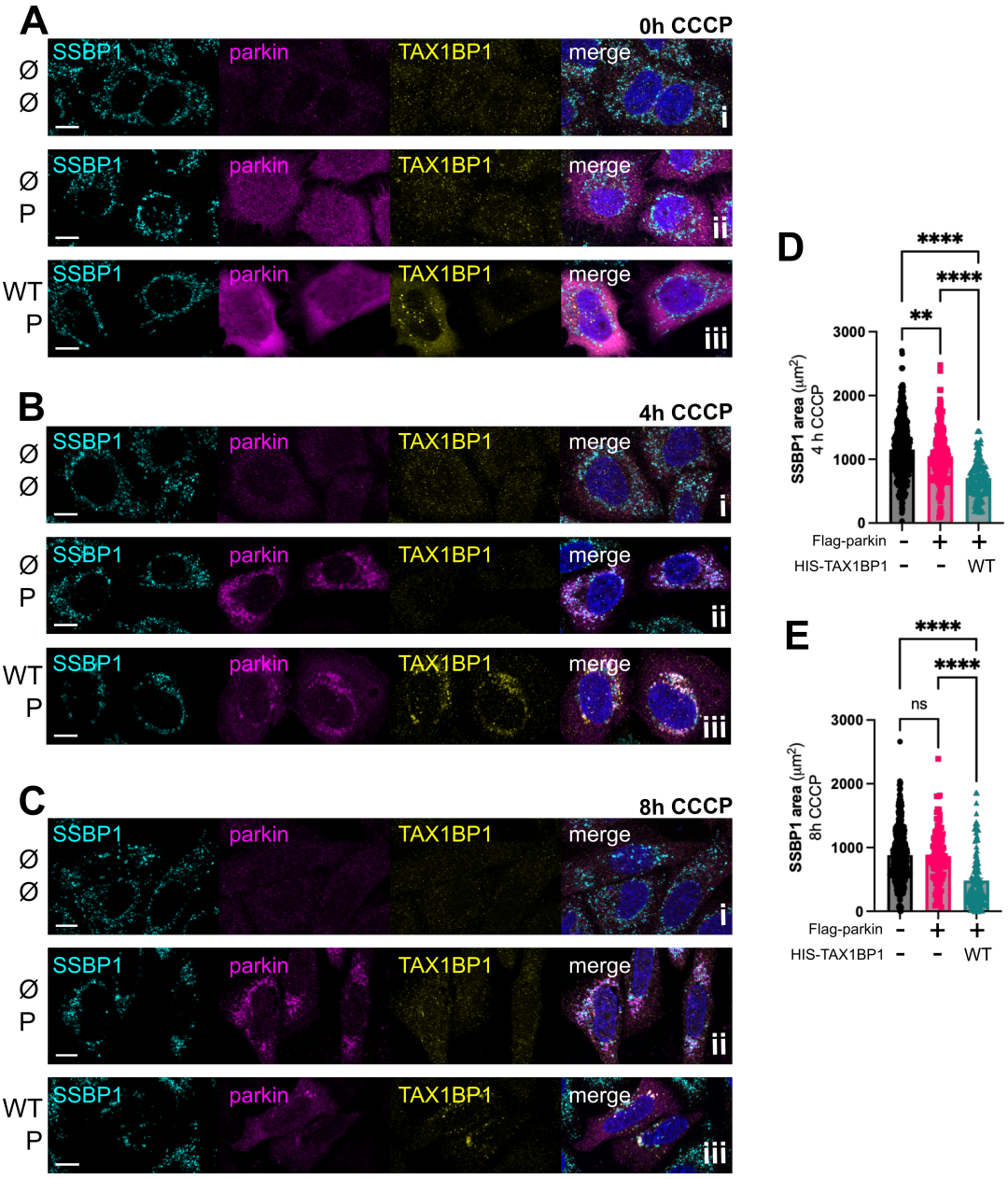


Figure 4.39: Mitochondrial turnover in penta-KO HeLa is rescued after co-transfection of Flag-parkin and 6HIS-TAX1BP1 WT. (A-C) Representative images showing TAX1BP1 (green), Parkin (magenta) and SSBP1 (cyan) after (A) no treatment, (B) 4h or (C) 8h of CCCP treatment. Scale bars = 10 µm. **(D-E)** Single-cell analysis of SSBP1 area upon (D) 4h or (E) 8h of mitochondrial depolarization for transfection conditions of empty plasmid (-,-), flag-parkin transfection only (+,-) or flag-parkin combined with WT 6HIS-TAX1BP1 (+, WT). Each data point represents a single cell value. Scale bars: 5 µm. Bars: mean ± SEM. ∅: empty plasmid, P: flag-parkin, WT: WT 6HIS-TAX1BP1, h: hours, ****: p<0.0001, **: p<0.005, *: p<0.05, ns: non-significant. ∅: empty plasmid, P: flag-parkin, WT: WT 6HIS-TAX1BP1, h: hours

4.21.2. Changes in mitochondrial turnover under K549R- and ΔCC3-TAX1BP1 expression

Proteomics analysis of overall ubiquitination events happening upon mitochondrial depolarization in WT- and C431A-parkin expressing cells revealed a potential parkin-dependent ubiquitination on K549 of TAX1BP1 (Figure 4.30A-B) (132). In addition, as previously shown, the expression of WT TAX1BP1 in combination with parkin has a positive effect on mitochondrial turnover in penta-KO HeLa cells (Figures 4.38-39). Hence, to test if the observed ubiquitination at K549R or the region CC3 had an impact on overall mitophagy, N-terminally 6xHIS-tagged ubiquitin-dead (K549R) as well as ΔCC3-TAX1BP1 mutants were generated (Figure 4.40A). First, TAX1BP1 ubiquitination as well as protein-specific turnover of mitochondrial proteins was analyzed via Western blot (Figure 4.40B).

Interestingly, a reduction on TAX1BP1 ubiquitination was observed upon deletion of CC3 but not when ubiquitination was specifically abolished at K549 (Figure 4.40B), suggesting other TAX1BP1 ubiquitination sites outside CC3. On the other hand, transfection of K549R- or ΔCC3-TAX1BP1 did not seem to compromise overall mitochondrial turnover (Figure 4.40B). Unfortunately, quantitative Western blot-based analysis of changes in specific mitochondrial protein turnover upon expression of WT, K549R- or ΔCC3-TAX1BP1 was inconclusive, as only mild transient non-significant effects on specific OMM protein turnover were observed (data not shown). Thus, to gain a better insight on the influence of K549 and CC3 regions of TAX1BP1 on mitochondrial turnover, mitochondrial area of positively co-transfected cells was analyzed at 4h and 8h of CCCP treatment with CellProfiler. Overall, all TAX1BP1 constructs seemed to behave equally under non-treated conditions: all over-expressed isoforms of TAX1BP1 were found in puncta that did not co-localize with mitochondria but were found at the close vicinity of the mitochondrial network (Figure 4.40C). Importantly, while parkin translocation as well as mitochondria fragmentation were observed under all transfection conditions and mitochondria depolarization (Figure 4.40D), a stronger reduction on mitochondrial network size was seen upon co-expression of parkin and all TAX1BP1 constructs when compared to parkin transfection conditions only (Figure 4.40D-E). Additionally, all TAX1BP1 constructs promoted a strong reduction of mitochondrial size after 4-8h of mitochondrial depolarization when compared to parkin transfection only (Figure 4.40D-E). As previously seen in WT-parkin HeLa, WT-TAX1BP1 translocation to mitochondria did not involve 100% of total TAX1BP1 and the same was observed for both mutants (Figure 4.40D). However, while all TAX1BP1 mutants were able to

translocate to mitochondria upon CCCP treatment, the ΔCC3 mutant seemed to behave slightly different, showing a reduced overlap on fragmented mitochondria in some cases (Figure 4.40D, panel v-vi and zoom panels e-f). After 4-8h of mitochondria depolarization, mitochondria size was reduced in all conditions when compared to parkin transfection conditions only (Figure 4.40F-G). Interestingly, an increase in mitochondrial area was observed for ΔCC3-TAX1BP1 compared to WT-TAX1BP1 after 4h CCCP (Figure 4.40F).

Taken together, these data suggest the region CC3 of TAX1BP1 to have mild effects on TAX1BP1 functionality without affecting overall mitochondrial turnover. In contrast, K549 mutation did not have an impact on neither overall TAX1BP1 ubiquitination or behavior, suggesting additional TAX1BP1 ubiquitination sites on the CC3 region, which may have compensatory effects on overall TAX1BP1 ubiquitination.

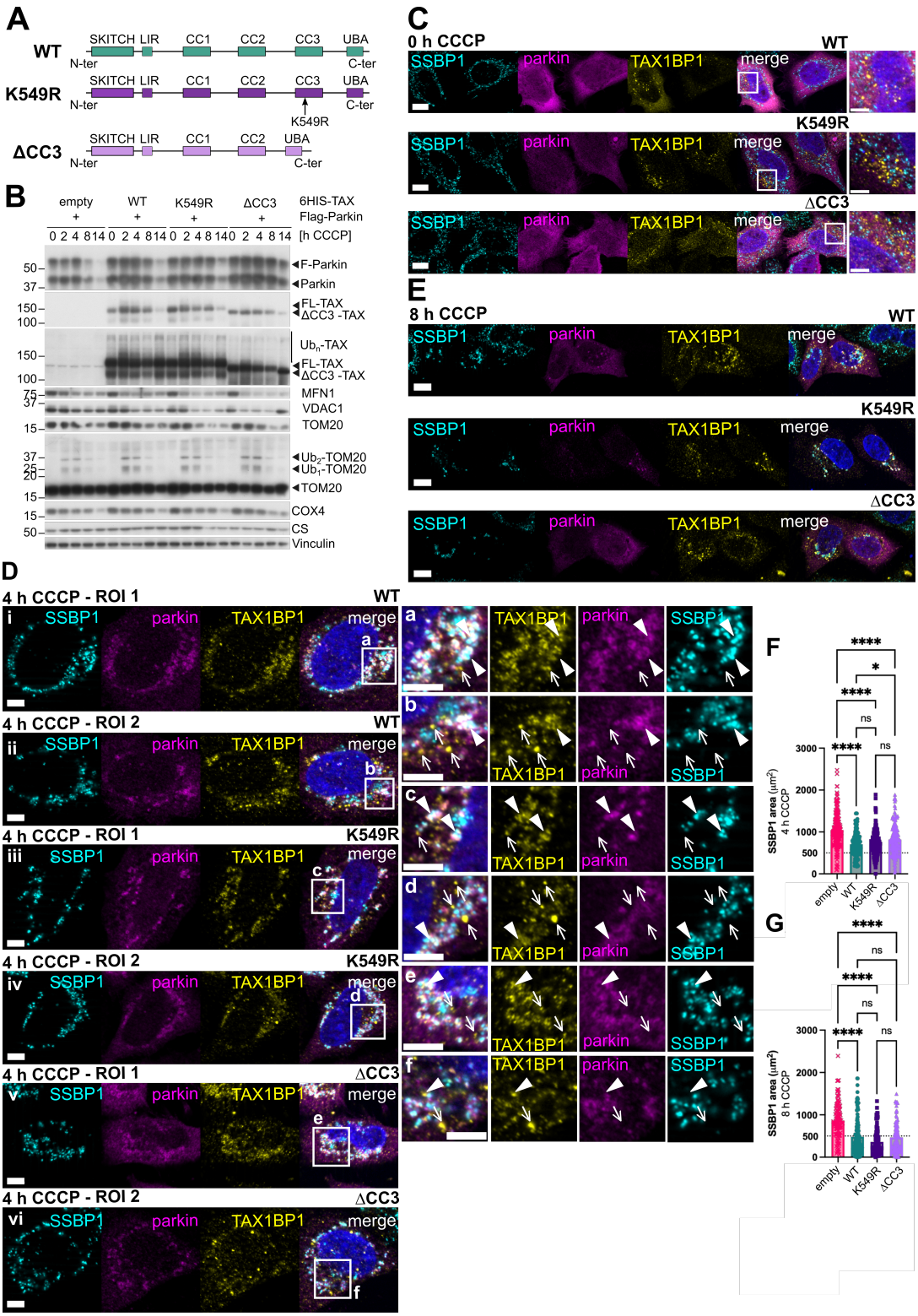


Figure 4.40: Global mitochondrial turnover effects upon over-expression of WT, K549R or ΔCC3 TAX1BP1. (A) Schematic representation of the generated 6HIS-TAX1BP1 constructs. **(B)** Representative Western blots showing mitochondrial protein turnover after the indicated treatments and double-transfection conditions. **(C-E)** Representative immunofluorescence images showing TAX1BP1 localization (C) at basal levels or after (D) 4h or (E) 8h of mitochondrial depolarization. In panel (D) two ROIs are shown according to TAX1BP1-dependent SSBP1 overlap: ROI1 represents > 50% SSBP1 overlap while ROI2 represents < 50 % overlap SSBP1. Regions of interest are zoomed on the right. Arrow heads represent SSBP1 material where parkin and TAX1BP1 are translocated to mitochondria. Arrows indicate TAX1BP1 not engaged with mitochondria. **(F-G)** Single-cell analysis of SSBP1 area upon expression of each TAX1BP1 construct cells expressing each of the TAX1BP1 constructs after (F) 4h or (G) 8h of mitochondrial

depolarization treatment. All conditions include additional Flag-parkin transfection. Each data point represents a single cell value. Scale bars: 10 μm. Bars: mean ± SEM. h: hours, ****: p<0.0001, *: p<0.05, ns: non-significant.

4.21.3. Changes in K549R- and ΔCC3-TAX1BP1 translocation to mitochondria

Early mitochondrial depolarization time-points induced the translocation of both TAX1BP1 mutants (Figure 4.40D-E). However, mitochondrial translocation of ΔCC3-TAX1BP1 seemed to be milder in comparison to WT-TAX1BP1 (Figure 4.40D, panel vi). Thus, in order to confirm if the mutations induced in TAX1BP1 had any effect on the translocation of the autophagy adaptor to mitochondria, CellProfiler quantification of mitochondrial area overlapped by TAX1BP1 was performed (Figure 4.41A-B). Because mitochondrial material will be assessed with the matrix marker SSBP1, the analysis was performed using an early time-point in which matrix material is not targeted for degradation. Importantly, previous data from this work has shown that CS is not degraded at 4h of CCCP while mitochondria still contained >50% of TOM20 and were highly fragmented (Figure 4.38B, 4.40B and 4.40D). Thus, the time-point of 4h CCCP was chosen to analyze TAX1BP1 translocation on fragmented mitochondria, here represented with the matrix marker SSBP1 (Figures 4.41-43). In addition, to allow for optimized recognition of TAX1BP1 staining, only cells with TAX1BP1 intensities over 10 arbitrary intensity units (aiu) were considered (see section 3.6.4 for more details).

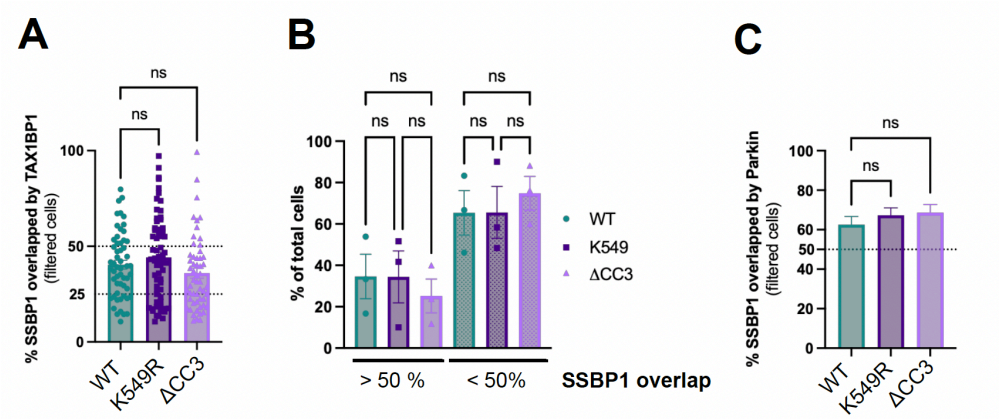


Figure 4.41: Single cell analysis of SSBP1 area covered by WT, K549R- and ΔCC3-TAX1BP after 4h of CCCP-depolarization. (A) Percentage of overlapped SSBP1 regions for each TAX1BP1 construct after filtering out low TAX1BP1 intensity cells. Each data point represents a single cell. **(B)** Proportion of total cells with ≥ 50 % (left) or ≤ 50 % (right) of SSBP1 area overlapped by TAX1BP1. Each data point represents the average percentage of one experimental replicate. **(C)** Percentage of overlapped SSBP1 by parkin under WT, K549R and ΔCC3-TAX1BP1 expression conditions. All conditions include additional Flag-parkin transfection. Only cells above 10 aiu of TAX1BP1 were considered for this analysis Bars: mean ± SEM.

Overall, K549R and ΔCC3 mutations did not seem to strongly affect the proportion of overlapped SSBP1 (Figure 4.41A). However, slight differences on the mean percentage of SSBP1 covered by

both K549R- and ΔCC3-TAX1BP1 mutants were observed. While all constructs had overlapping percentages ranging from 10 to 50 %, an increased number of cells with >50% overlap expressing K549R-TAX1BP1 was observed when compared to WT-TAX1BP1 (Figure 4.41A). On the other hand, the opposite effect was seen for ΔCC3-TAX1BP1 expressing conditions: while a slightly reduced number of cells was able to cover >50% of SSBP1, a greater number of cells showed overlapping percentages below 50% when compared to WT-TAX1BP1 expressing conditions (Figure 4.41A). This effect was mildly seen when computing percentages of cells below and above this threshold for all experimental replicates (Figure 4.41B). As the recognition of ubiquitinated proteins via autophagy receptors is downstream of parkin translocation, it could be that the differences observed on TAX1BP1-overlap were due to differences on parkin translocation to mitochondria. As seen previously, parkin was found on mitochondria upon 4h of mitochondrial depolarization under all TAX1BP1 expressing conditions (Figure 4.40D-E), thus it is not surprising that no differences were observed on parkin-dependent overlap of SSBP1 material upon expression of any of TAX1BP1 mutants (Figure 4.41C). These data may indicate that the small differences observed on K549R- and ΔCC3-TAX1BP1 translocation to mitochondria could be due to a dysregulation on the recognition of ubiquitinated cargo and not because of an indirect reduction of mitochondrial parkin translocation. Alternatively, given that ΔCC3-TAX1BP1 expression triggered a transient impairment on mitochondrial degradation at 4h of CCCP treatment (Figure 4.40F), one cannot discard the possibility of ΔCC3 to have an impact on the interaction of the LIR domain of the autophagy receptor with ATG proteins, perhaps leading to a transient delay on the recruitment of the autophagosome elongation machinery on mitochondria at a specific time point of the pathway.

As previously seen, TAX1BP1 translocation upon mitochondria depolarization rarely involves 100% of the total TAX1BP1 (Figures 4.33C-D and 4.40D). Thus, we hypothesized that CC3 ubiquitination of TAX1BP1 could also modulate TAX1BP1 translocation to mitochondria. However, the overall percentage of TAX1BP1 involved on the overlap of SSBP1 did not significantly change among TAX1BP1 mutants (Figure 4.42), suggesting that ubiquitination of CC3 does not influence TAX1BP1 translocation.

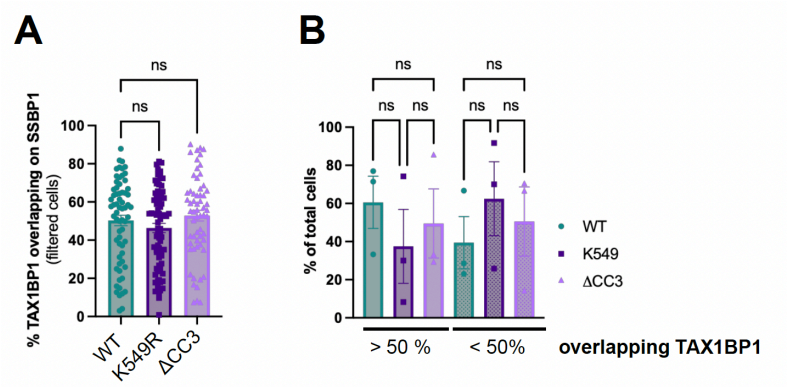


Figure 4.42: Filtered single cell analysis of WT, K549R- and ΔCC3-TAX1BP translocation after CCCP-induced depolarization. (A) Percentage of overlapping TAX1BP1 for each TAX1BP1 construct after 4 h CCCP. Each data point represents a single cell. **(B)** Proportion of total cells with ≥ 50 % (left) or ≤ 50 % (right) of overlapping TAX1BP1 on SSBP1 after 4h CCCP. Each data point represents the average percentage of one experimental replicate. All conditions include additional Flag-parkin transfection. Only cells above 10 aiu of TAX1BP1 were considered for this analysis. Bars: mean ± SEM. ns: non-significant.

Because there was an increased variability in both the percentage of overlapped SSBP1 as well as the proportion of translocated TAX1BP1 upon expression of all TAX1BP1 constructs (Figures 4.41A-B and 4.42A-B), we wondered if this variability could be explained by correlation. For example, in case of a positive correlation relationship between these two variables, one would expect that increased recognition of SSBP1 aggregates (overlapped SSBP1) would be related to an increased proportion of TAX1BP1 involved in the recognition (overlapping TAX1BP1).

Correlation analysis of the proportion of overlapping TAX1BP1 (y) with overlapped SSBP1 (x) percentage showed to be strongly significant for WT TAX1BP1 and less significant for both TAX1BP1 mutants (Table 4.7). Interestingly, when plotting for the XY relationship of WT-TAX1BP1, data seemed to follow an increasing tendency of active TAX1BP1 (y) being able to overlap increasing proportions of SSBP1 (x) (Figure 4.43A). However, this relationship was not linear, but followed a model of decay after a maximum of SSBP1 region was covered (Figure 4.43A). For this reason, a suitable non-linear regression model was used to explain WT TAX1BP1 binding behavior (Figure 4.43A and Table 4.7). Interestingly, while correlation analysis was significant for all three TAX1BP1 constructs, when trying to apply the same model for K549R- and ΔCC3-TAX1BP1, a decrease in correlation significance was observed in both cases (Figure 4.43B-C and Table 4.7), suggesting differential binding behaviors of the ones observed for WT-TAX1BP1.

Table 4.7: **Correlation and regression analysis of percentage of SSBP1 area covered by WT- or TAX1BP1 mutants.** Percentage of SSBP1 area covered by TAX1BP1 (X) is related to the proportion of total TAX1BP1 involved in mitochondrial translocation (Y). Person's test was implemented to test for correlation between the two variables. Non-linear regression analysis with a polynomial curve fit was used as a model curve for all TAX1BP1 constructs. Statistical significance was established for p<0.05.

	WT	***K549R***	***ΔCC3***
Pearson test			
r	0.52	0.40	0.36
R^2	0.27	0.16	0.13
p-value	<0.0001	<0.001	<0.05
Non-linear regression			
Equation	$y = 8.14 + 2.64x - 0.03x^2$	$y = 6.76 + 1.49x - 0.88x^2$	$y = 18.25 + 1.99x - 0.21x^2$
R^2	0.625	0.303	0.243

Next, to discard if the observed loss of correlation between translocating TAX1BP1 and the overlapped SSBP1 area in K549R and ΔCC3-TAX1BP1 could be due to an upstream lack of parkin translocation on mitochondria, percentage of the total parkin translocation and area of SSBP1 covered by parkin on the same individual cells was analyzed for all three TAX1BP1 expressing conditions (Figure 4.43D-F). As previously seen, no drastic differences were observed for parkin translocation in all conditions, with approximately >80% of SSBP1 material being recognized by parkin upon expression of all three TAX1BP1 constructs (Figure 4.44D-F). Hence, suggesting that the previous differences observed in TAX1BP1 mitochondria translocation might be due to events taking place downstream of parkin translocation, likely involving the interaction of TAX1BP1 with ubiquitin chains or lapidated ATGs.

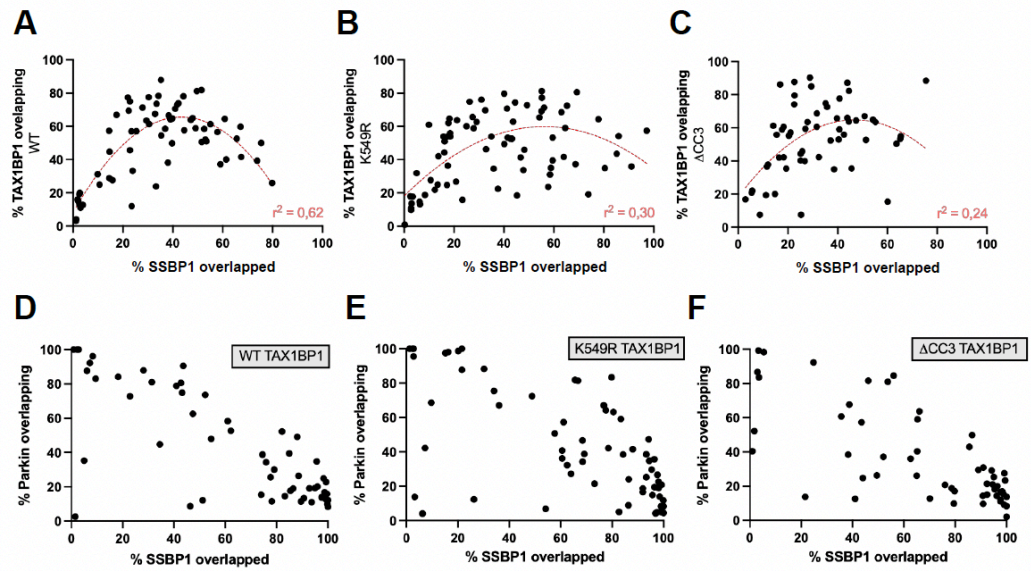


Figure 4.43: Single cell correlation analysis of the percentage of overlapping WT, K549R- and ΔCC3-TAX1BP and percentage of overlapped SSBP1 area after 4h of CCCP-induced depolarization. (A-C) Correlation of percentage of SSBP1 area covered (X) by (A) WT-TAX1BP1 (B) K549R-TAX1BP1 or (C) ΔCC3-TAX1BP1 related to the proportion of total TAX1BP1 involved in mitochondrial translocation (Y) after 4h CCCP. **(D-F)** Correlation of percentage of SSBP1 area (X) and the total percentage of parkin involved in the recognition (Y) in the same single-cell population of (A-B)

after expression of (D) WT-TAX1BP1, (E) K549R-TAX1BP1 or (F) ΔCC3-TAX1BP1. Each data point represents a single cell. Non-linear regression curve model (red). Only cells above 10 aiu of TAX1BP1 were considered for this analysis.

Taken together, while the data-set used for this analysis is rather small and thus it is difficult to extract solid conclusions, these preliminary data suggest the region CC3 of TAX1BP1 to have an impact on TAX1BP1 translocation to mitochondria and transiently delay mitochondria degradation, perhaps influencing the interactions at the LIR or UBD domains of the autophagy receptor or altering its dimerization. Future studies will be needed to decipher the contribution of ubiquitinated CC3 on TAX1BP1 functionality regulation.

5. Discussion

Research on Parkinson's disease has been ongoing for more than 200 years, with the first links of mitochondrial health and parkinsonian-like phenotypes being reported during late 1970s and early 1980s. However, it was not until much later that a clear relationship between patient PD mutations on PINK1 and PARKIN genes could be related to defective mitochondrial turnover (186). From that point on until the present day, research on PINK1/parkin mitophagy expanded and has helped unravel the specific mechanisms leading to pathway activation and recognition of damaged mitochondria which trigger the subsequent autophagic removal of the organelle (97,187). Importantly, while the events triggering the activation and expansion of PINK1/parkin mitophagy are now well characterized, the later stages of the pathway leading to complete mitochondria elimination remain understudied. Despite of this, mitophagy is conceived as a process that requires the autophagic engulfment of the entire organelle for complete mitochondria elimination via a process termed *wholesale mitophagy* (44,59).

In this study, we demonstrate that PINK1/parkin dependent mitophagy occurs in a piecemeal manner, involving the sequential degradation of mitochondrial sub-compartment proteins. Importantly, both early and late stages of the pathway depend on UPS and autophagy degradation systems. In addition, the behaviour of TAX1BP1 during PINK1/parkin piecemeal mitophagy is characterized as well as the implication of site-specific novel parkin-dependent ubiquitination of the autophagy adaptor detected in this study. Lastly, a regulatory mechanism of VDAC2 turnover depending on residue-specific phosphorylation and parkin-dependent ubiquitination is described.

5.1. Can PINK1/parkin degradation occur in a piecemeal manner?

5.1.1. Evidence for PINK1/parkin mitophagy

PINK1/parkin mitophagy activation is characterized by an increase in pS65-ubiquitin, triggering parkin-dependent ubiquitination of many OMM proteins which are later rapidly degraded through UPS or recognized by autophagy receptors (49,51,62). In turn, it is widely accepted that the autophagic targeting of damaged mitochondria triggers the degradation of the whole organelle via a process termed wholesale mitophagy (44,59,116), even though piecemeal parkin-dependent mitophagy has been occasionally reported (98,135,172,188,189). In this study, the combined proteomics, protein biochemical-based and image-based analysis helped

confirm the activation of PINK1/parkin autophagy by revealing an upregulation of pS65-ubiquitin (Figure 4.1C) which was followed by a general OMM parkin-dependent ubiquitination (Figures 4.9B-C and 4.10A-B). Importantly, many of the identified ubiquitinated OMM proteins are in agreement with other proteomic studies revealing extensive OMM ubiquitination under parkin-expressing conditions (68,129,174). Among those, we could validate the proteasomal-dependent degradation of MFN1 as well as ubiquitinations of the TOM import complex and VDACs (Figure 4.17, 4.20 and Table 4.2). In addition, subsequent autophagy receptor recognition of ubiquitinated mitochondria was confirmed via immunofluorescence analysis (Figures 4.11A and 4.32-33) while TEM allowed for the confirmation of autophagosome formation and engulfment of damaged mitochondria (Figure 4.14), consistent with previous reports (62,73,75,135,176,190). Overall, these data confirmed PINK1/parkin initiation and execution steps that promote mitochondrial turnover.

5.1.2. Differential degradation of mitochondrial proteins

Interestingly, while early steps of the pathway were in agreement with previous studies, the later events culminating with the removal of the whole organelle did not fit in with the premise of wholesale mitophagy. Here, combined proteomics, Western blot analysis and immunofluorescence experiments indicated that parkin-dependent mitophagy involved sequential sub-organelle degradation, where OMM and inner- mitochondrial protein turnover occurred in two distinct temporal windows. More specifically, protein analysis revealed that while OMM degradation was taking place after 2-8h of CCCP-induced depolarization, IMM and matrix protein degradation did not occur until later stages (8-18h CCCP) (Figures 4.2-5). Importantly, endogenous parkin expression conditions revealed similar but much delayed kinetic differences on mitochondrial sub-compartment degradation (Figures 4.7-8), suggesting the observed sub-organelle turnover differences to account for a generalized phenomenon in mammalian cells. Additionally, the kinetic turnover differences of sub-compartment protein degradation could be linked to differential ubiquitination of mitochondrial sub-compartments, as evidenced by ubiquitylome and Western blot analysis (Figure 4.9B-C).

PINK1/parkin mitophagy has been a focus of research since only sixteen years ago and thus it can be considered a relatively new emerging field. Moreover, the strong dynamics of the pathway allow for two differential focuses: degradation of mitochondrial proteins and/or coupling of the autophagic machinery. Hence, the combination of these two aspects complicates a consensual approach on how to systematically study selective mitochondrial degradation.

Indeed, most of the studies targeting parkin-dependent mitophagy rely on OMM markers or mitochondrial dyes to assess mitochondrial degradation and/or mostly investigate mitochondrial degradation under short depolarization time-points only, being limited the studies that rely on extended depolarization time-points (62,129,177) or multiple mitochondrial markers (129,131,135,136). Furthermore, there are even fewer studies that rely on a combined approach assessing (i) the involvement of the autophagy machinery and (ii) mitochondrial degradation by using several sub-organelle markers (68,75,135). However, despite the limited number of studies, some authors indicated degradation kinetic differences of mitochondrial sub-compartment proteins (68,75,136). In addition, parkin-dependent ubiquitination of inner mitochondrial proteins occurring under both endogenous and over-expressed parkin conditions has been additionally reported in the recent years (68,131) (see Table 5.1).

Thus, it is possible that mitochondrial sub-compartment degradation occurs sequentially under both endogenous and over-expressed parkin conditions but might have been overlooked due to a systematic focus on OMM protein degradation and the use of early depolarization time points. Interestingly, while the examples are limited, there are few reports indicating that piecemeal mitochondrial turnover can occur both in a parkin-dependent and independent manner. For example, Yang and Yang have reported that after localized mitochondria depolarization using a stress-induced light-activation approach, localized ubiquitinated mitochondrial regions were subsequently targeted by autophagosomes in a parkin-dependent manner (98,189). More recently, Ordureau and colleagues revealed that over-expressed COX4 (mito-GFP) and matrix material (mito-mCherry) in induced neurons (iNeurons) was differentially degraded after extended depolarization, with matrix material resembling the SSBP1- and CS-aggregates found in this study (68). In WT-parkin HeLa, while inner mitochondrial aggregates did not directly co-localize with lysotracker after 14h of CCCP, inner mitochondrial markers like COX4 or CS engaged into puncta additionally overlapped with lysotracker (Figure 13B-C). In contrast, inner mitochondrial aggregates in iNeurons partially co-localized with lysosomes after extended depolarization (68). Discrepancies between the study of Ordureau *et al.* and this present work might be due to differences rising from the use of different cellular models. As their name indicates, iNeurons are mature neurons and thus are far away from a mitotic cell line such as WT-parkin HeLa cells, the present cellular model used in this study.

Furthermore, an interesting parkin-dependent non-canonical mechanism for the degradation of TOM20 was reported under the name of mitochondrial derived vesicles (MDVs), directly delivered to the lysosomal network without intermediate autophagosomal targeting

(171,172,188). In addition, Le Guerroué and colleagues reported the degradation of MTX1 and MIC60 to occur differentially from TOM20 and PDH in a parkin-independent manner involving LC3C-autophagosome formation (191), while a recent study from Abudu *et al.* identifies basal parkin-independent piecemeal degradation of SAM50 and MICOs complex to occur in a p62/SQSTM-dependent manner (192). Thus, data from this work strengthens the idea of piecemeal mitophagy occurring in a parkin-dependent manner, specifically and sequentially targeting sub-organelle degradation after the induction of acute mitochondrial depolarization.

5.1.3. Are later stages of PINK1/parkin mitophagy characterized by the formation of mitoplasts?

Immunofluorescence data from this study revealed different morphologies of OMM and inner mitochondrial proteins at later stages of PINK1/parkin mitophagy (Figure 4.5). While IMM and matrix proteins were engaged in aggregate-shaped structures that were not directly delivered to the lysosomal network, OMM proteins were engaged in puncta-like structures which were directly targeted by lysosomes (Figures 4.12-13). As previously mentioned, TOM20 material can be directly engaged in lysosomes without the need of autophagosome targeting via MDV formation. Thus, to discard if those events would account for the observed piecemeal mitophagy phenomenon observed, autophagy targeting of TOM20 puncta-like material was analyzed. Importantly, immunofluorescence data revealed p62/SQSTM recognition of mitochondrial material engaged in puncta-like shapes (Figure 4.11A), while EGFP-LC3B transfection experiments indicated that most of mitochondrial puncta were engaged in autophagosomes (Figure 4.11B-E). Hence, suggesting that MDVs would not account for the major degradation pathway targeting mitochondrial turnover in our model. Interestingly, inner mitochondrial aggregates were not (yet) directly targeted by the lysosomal machinery and only limited autophagosome targeting was observed after intermediate CCCP-depolarization (Figure 4.11C, ROI 1). However, in cells where mitophagy was more advanced, matrix material became eventually engaged in autophagosomes and lysosomes (Figure 4.11C, ROI 2), suggesting delayed autophagic targeting of inner mitochondrial proteins. Interestingly, Hsieh and Yang have recently suggested that mitochondrial aggregates formed upon induction of PINK1/parkin need to be disassembled in smaller aggregates in order to be targeted by autophagosomes (189). Similarly, Ordureau and colleagues recently showed that matrix aggregates are reduced in size and targeted by lysosomes in iNeurons (68). Even though no OMM marker was included in these later experiments, these data may suggest the degradation of inner mitochondrial aggregates eventually relies on autophagosome targeting. Thus, while the observed delayed targeting of

inner mitochondrial aggregates is in accordance with the mitochondrial structures observed by Hsieh and Yang, the specific events involved in mitochondrial sub-compartment specific autophagic targeting remain to be elucidated (see chapter 5.1.4).

On the other hand, the presence of inner mitochondrial aggregates together with autophagosomal targeting of outer mitochondrial proteins occurring on a similar time window, suggested the formation of mitochondrial aggregates devoid of OMM, otherwise termed as mitoplasts. Strikingly, similar structures have been characterized in a recent study in which over-expression of the E3 ligase GP78 alone or in combination with mitochondrial depolarization induced dual degradation of both ER and mitochondria and the formation of mitoplasts (146). In order to assess this point, TEM experiments were performed (Figure 4.14). Given that the identification of true double mitochondrial membrane structures is strictly related to appropriate sample preparation and their distinction was sometimes unclear at basal conditions (data not shown), TEM experiments could not confirm the presence of mitoplasts at late stages of mitophagy. Interestingly, while most of the mitochondria observed had long membrane regions containing both OMM and IMM (Figure 4.14C), data from previous experiments indicated complete OMM protein degradation at a similar time-point (Figures 4.3-4.5 and 4.11). Thus, it is possible that OMM degradation observed in this study can only account for OMM protein degradation and not for complete OMM removal (including lipids). On the other hand, when focusing on mitochondrial structures engaged in an additional autophagosomal membrane, events of ruptured OMM were identified (Figure 4.14C). This is in agreement with other studies reporting OMM rupture during mitophagy and further supports the sequential sub-organelle degradation model presented in this study (76,135). Nevertheless, we cannot discard that the OMM defects observed might occur after autophagosomal targeting and thus, future experiments allowing targeted identification of mitochondrial sub-compartment markers combined with TEM could help clarify this point (i.e: immunogold TEM).

5.1.4. Autophagic targeting of ubiquitinated mitochondria and mitochondrial sub-compartments

Immunofluorescence data from this study suggested both p62/SQSTM and TAX1BP1 autophagy receptors to be involved in the recognition of ubiquitinated inner- mitochondrial material (Figure 4.32D-E). Early studies on p62/SQSTM have indicated the autophagy adaptor to be essential (62) but also dispensable (185) for parkin-dependent mitochondrial turnover, strongly suggesting the possibility of other autophagy receptors of being able to compensate for its

function. Similarly, while TAX1BP1 has been also described to be able to recognize ubiquitinated mitochondria and interact with building autophagosomes (73,176,190), its ability to rescue defective mitophagy in a pentaKO cells has been proven to be milder than other autophagy receptors (i.e: OPTN or NDP52) (75). Again, suggesting a certain redundancy on autophagy receptor functions. Hence, given that the extended analysis on the involvement of all ubiquitin-dependent autophagy receptors in PINK1/parkin mitophagy is perhaps not thorough enough in this study, we cannot discard that other autophagy receptors like OPTN or NDP52 could be involved in the specific recognition of inner mitochondrial aggregates. Along these lines, Hoshino *et al.* recently indicated that the specific knock down of autophagy-related proteins had a strong effect on IMM and matrix protein turnover while OMM protein degradation was less affected (190). Thus, while it is clear that final stages of PINK1/parkin mitophagy require proper functionality of all complexes involved in basal autophagy, it is possible that the degradation of inner mitochondrial aggregates requires the presence of specific autophagy receptors. Future experiments focused on the investigation of the interactome of inner mitochondrial aggregates would help clarify this issue.

The current model of PINK1/parkin mitophagy posits that different ubiquitin chain linkages on OMM proteins trigger different degradation fates; for example, K48-linked chains promote proteasomal degradation while K63-linked ubiquitin chains trigger the recognition of autophagy receptors (59). Importantly, parkin is known to synthesize K6, K11, K27, K48 and K63-liked ubiquitin chains (68,131). Moreover, it has been reported that specific DUBs may have a preference on certain ubiquitin-linkage types. For example, recent studies have reported USP30 to systematically act on K6-linked chains of OMM substrates (67,68) while its activity diminishes on phosphorylated K6-linked ubiquitin chains (67,137). Similarly, USP15 has been reported to act on both K48- and K63-linked chains (193). Hence, it is possible that the initiation, progression and autophagic targeting phases of PINK1/parkin mitophagy involves a specific ubiquitin-linkage code as other authors have already suggested (59,194). Based on this, it remains speculative if specific chain linkage types could be a signature of ubiquitinated inner- mitochondrial proteins and if those could drive the specific recognition of major or minor autophagy receptors. Future studies combining powerful proteomic tools allowing specific identification of ubiquitin-chain linkage on specific mitochondrial substrates may help elucidate this extensively pursued question in the field of mitophagy.

Another possibility for a potential specific autophagic targeting of inner mitochondrial material would be the direct interaction of IMM proteins with the autophagic machinery. A recent work

from Wei and colleagues suggests the IMM protein prohibitin 2 (PBH2) as an internal mitochondrial protein which directly interacts with LC3B after parkin-dependent mitophagy initiation and OMM rupture (76). In this case, autophagosome coupling to PHB2 could occur through the exposure of IMM regions occurring after previous OMM rupture, a phenomenon already reported to occur in parkin-dependent mitophagy in this and other studies (76,135) (Figure 4.14C). Alternatively, mitochondrial lipids like cardiolipin (CL) have been reported to be able to bind to LC3B or beclin-1 in situations of mitochondrial depolarization (153,154). While those events have been described to occur only in a parkin-independent manner, it is speculative if remaining CL at the IMM after extended depolarization and partial OMM removal could directly interact with LC3B and promote autophagosome formation in a parkin-dependent manner. Future studies regarding this point are needed to clarify this issue.

In summary, it is likely that parkin-dependent mitochondrial turnover promotes the degradation of mitochondria by sequentially targeting its sub-compartments for degradation. This phenomenon might have been overlooked in the past due to a lack of focus on the later time points of the pathway combined with an under investigation of multiple mitochondrial sub-compartment proteins. Further, it remains to be elucidated if specific recognition by major autophagy adaptors might influence the specific targeting of ubiquitinated OMM or inner mitochondrial material, perhaps through recognition of a specific ubiquitin-linkages. Future studies are needed to understand if early and later stages of the pathway rely on selective autophagy receptor recognition of specific cargo or ubiquitin-linkage chains.

Table 5.1: Summary of PINK1/parkin-dependent mitophagy studies with a focus on mitochondria elimination or autophagic targeting of mitochondria. Description of study according to *in vivo* model used, parkin expression and treatments are specified. Approach on pathway dynamics is described as follows: use of (1) individual time-points (early, 1-6h), (2) individual time-points (extended, 1-24h) or (3) live cell imaging (extended). Mitochondrial identification approach is described as follows: use of mitochondrial dyes (MitoTracker or TMRE), over-expression of fluorescently labelled mt-targeted proteins or mt-KR, direct detection of mitochondrial proteins and/or TEM. AA: Antimycin A, AO: Antimycin/Oligomycin, AOF: antioxidant deprivation, LIS: light-induced-stress, BafA: BafilomycinA, Lac: Lactacystin, Epox: Epoxomycin, mt: mitochondria, agg.: aggregate, AP: autophagosome, NF: not focused in study, N/A: not applicable, E: endogenous, OE: overexpressed

Study, Reference	Model	Cell type	Parkin	Dynamics	Mitochondria identification	Treatment	Mitochondria elimination	Autophagy machinery targeting
(170)	Neurons	Mature neurons	E	3	Mitochondrial dyes OE of KillerRed or mt-targeted proteins	AA	NF	Localized complete: LC3B and lysosomal colocalization
(195)	Nuerons	Mature neurons	E	1	Mitochondrial dyes OE mt-targeted proteins	AA and AOF	NF	Localized complete: mt colocalization with OPTN and LC3B
(168)	Liver tissue	Hepatocytes	E	1	TEM	None	NF	Localized complete: AP engulfment of mitochondria
(169)	Hepatocytes	Hepatocytes	E	3	Mitochondrial dyes	Starvation	NF	Localized complete: LC3B and lysosomal colocalization of mitochondria
(172)	HeLa Parkin^{+}	Epithelial immortalized	OE	1	OMM, IMM and matrix proteins	AA	Incomplete: MDV formation; OMM degradation only	NF
(98)	COS7	Fibroblast immortalized	OE	3	Mitochondrial dyes KillerRed OE	LIS	NF	Localized complete: time-dependent local colocalization of mitochondria with parkin- and LC3B-positive structures
(189)	HeLa Parkin+	Epithelial immortalized	OE	3	Mitochondrial dyes OE mt-targeted proteins	LIS	NF	Localized complete: time-dependent colocalization of mitochondria with parkin, LC3B and omegasome; mitochondria agg. formation
(75)	HeLa Parkin^{+}	Epithelial immortalized	OE	2	OMM, IMM proteins mtDNA	AO	Piecemeal: sequential degradation of mt proteins (late)	Localized complete: LC3B and AR co-localization with TOM20 (early)

Table 5.1: (continued)

Study	Model	Cell type	Parkin	Dynamics	Mitochondria identification	Treatment	Mitochondria elimination	Autophagy machinery targeting
(135)	Parkin+ MEFs	Embryonic fibroblasts	OE	2	OMM, IMM, matrix proteins TEM	CCCP	Complete: more OMM vs. matrix degradation; OMM rupture; mitochondria in AP	NF
						CCCP + BafA	Incomplete: OMM and COXIII agg.	
						CCCP + Lac	Incomplete: TOM20 agg. And mitochondria in AP	
	FIP200-/- MEFs					CCCP	Incomplete: OMM removal only, no AP	
						CCCP + BafA	Incomplete: OMM removal only, few AP	
						CCCP + Lac	Incomplete: limited OMM removal, no AP	
	ATG5-/- MEFS					CCCP	Incomplete: OMM removal only	
						CCCP + BafA	Incomplete: OMM removal only	
						CCCP + Lac	Defective	
(196)	Parkin+ MEFs	Embryonic fibroblasts	OE	1	Mitochondrial dyes TEM	CCCP	NF	Localized complete: LC3B, ULK1, WIPI1, ATG16L, ATG14 and WIPI co-localization with mt and AP engulfment of mt
	FIP200-/- MEFs					CCCP	NF	Defective: no ULK1, LC3B, ATG16L, WIPI co-localization with mt and no AP engulfment of mt
	ATG3-/- MEFs				Mitochondrial dyes	CCCP	NF	Defective: no LC3B, ATG16L, WIPI co-localization with mt
(68)	iNeurons	Mature neurons	E	2	mt-targeted proteins	AO	Incomplete: matrix-targeted proteins form aggregates after extended treatment (16-24h) which are not positive for COX4	Localized complete: Lysotracker co-localization with matrix-targeted protein after extended treatment (16-24h)

Table 5.1: (continued)

Study	Model	Cell type	Parkin	Dynamics	Mitochondria identification	Treatment	Mitochondria elimination	Autophagy machinery targeting
(73)	HeLa Parkin+	Epithelial immortalized	OE	1	OMM proteins	CCCP	NF	Complete: OPTN, SQSTM, TAX1BP1 and NDP52 co-localization with TOM20
(136)	HeLa Parkin+	Epithelial immortalized	OE	2	OMM, IMM and matrix proteins	CCCP	Incomplete: differential degradation of OMM, IMM and matrix proteins	NF
						CCCP	Defective	
						CCCP + Epo	Defective	
	ATG3-/- MEFs	Embrionic fibroblasts				CCCP	Incomplete: differential degradation of OMM, IMM and matrix proteins	
(61)	HeLa Parkin+	Epithelial immortalized	OE	1	Mitochondrial dyes mt-mKemia OE	CCCP	NF	Complete: TBK1 co-localization with mt
(177)	N2a/FRT	Neuroblasts	OE	2	OMM and matrix proteins	CCCP	NF	Co-localization of p62/SQSTM, LC3B andf LAMP1 structures with HSP60 and TOM20
This work	HeLa Parkin^{+}	Epithelial immortalized	OE	2	OMM, IMM, matrix proteins TEM	CCCP	Complete (see text)	Complete (see text)
						CCCP + MG132	Defective	NF
	HEK293	Kidney immortalized	E		OMM and matrix proteins	CCCP	Incomplete	
					OMM, IMM and matrix proteins	CCCP + MG132	Defective	
	NPCs	Neuronal precursors			OMM and matrix proteins	AO + ApoI	Incomplete	

5.2. Is parkin accountable for ubiquitination of all mitochondrial material?

Mitochondria depolarization triggers an increase in PINK1-dependent phosphorylated ubiquitin at the OMM which promotes the activation of parkin though parkin UBL phosphorylation at S65, triggering parkin translocation to mitochondria (124,125,134). Once at the mitochondria, parkin ubiquitinates numerous mitochondrial proteins which are later targeted for degradation (126,129).

Proteomic as well as Western blot data confirmed a global increase in ubiquitinated OMM proteins after early mitochondrial depolarization (Table 4.2, cluster 5). Moreover, in agreement with other proteomic studies (126,129), many known parkin substrates were identified to be ubiquitinated upon early CCCP-depolarization under WT-parkin expression conditions only (i.e: MFN1, VDAC1/2 and TOM20) (Figure 4.9B-C). In addition, immunofluorescence data provided evidence of clear parkin translocation upon early mitochondrial depolarization (Figures 4.1B, 4.15A and 4.19A). Overall, confirming parkin-dependent ubiquitination of OMM at early stages of mitophagy. However, while ubiquitination of known OMM substrates could be clearly linked to parkin-dependent activity, the involvement of parkin at later stages of mitophagy was less clear. On one hand, proteomics as well as Western blot data indicated that parkin protein levels were reduced after long depolarization treatments (Figure 4.15D-E). On the other hand, immunofluorescence analysis of parkin translocation indicated the E3 ligase was rarely engaged with inner mitochondrial aggregates (Figure 4.15B-C). Moreover, a reduction on inner mitochondrial aggregates ubiquitination was observed after extended depolarization treatment (Figure 4.10). Overall, these data suggested several scenarios: (i) parkin degradation could occur at later stages of mitophagy, (ii) ubiquitination of inner mitochondrial material might not directly be parkin-dependent and (iii) late stages of mitophagy might additionally involve DUBs activity.

Examples of decreased parkin levels after extended mitochondria depolarization have also been reported (68,133). Interestingly, in a recent study by Shiiba *et al.* it is suggested that parkin can be targeted to the proteasome upon MITOL-dependent ubiquitination at K220 during late stages of mitophagy (142). In our case, proteomics data indicated parkin to be increasingly ubiquitinated at K48 (parkin UBL), while no ubiquitination of K220 was found (Figure 4.16 and Table 4.4). Along these lines, early reports have indicated that parkin is initially autoinhibited via the UBL domain, sterically hindering interactions with E2 ubiquitin enzymes on its catalytic site (124,127) (Figure 2.8). In addition, after PINK1-mediated activation of parkin through UBL phosphorylation, the E3 ligase is reported to undergo self-ubiquitination at several residues of

its UBL domain, including K27 and K48 (125–127). Moreover, while it has been previously suggested that direct parkin autoubiquitination may involve K48-linked ubiquitin chains -known to trigger proteasomal degradation of the targeted proteins (59,197), a later study identified K6-linked ubiquitin chains to be predominantly built on K48 residue of parkin UBL (66). Interestingly, early mitochondrial depolarization experiments with ubiquitin dead parkin mutants at K27/48 residues did not promote the intrinsic translocation of parkin, contrary to what was observed for parkin mutants lacking the UBL domain (126). Similarly, other studies have demonstrated that mutations in K48 of parkin do not render the protein inactive (134,198). In addition, it has been previously reported that the K48 residue of parkin is a critical point of interaction during parkin autoinhibited state (127). Overall, these suggests that ubiquitination of parkin UBL may occur upon parkin full activation. In addition, while early events triggering the progression of PINK1/parkin mitophagy are directly dependent on parkin ubiquitination of OMM proteins, it is likely that after extended OMM ubiquitination and induction of autophagic targeting of OMM, the remaining active parkin engaged at the OMM is together degraded with OMM material. This degradation could take place in an unspecific manner, with parkin being degraded along with OMM material or could alternatively involve PTMs of parkin triggering its specific degradation, perhaps via the ubiquitination of K220 as suggested by Shiiba *et al.* or through direct UBL ubiquitination (66,125–127). Future studies combining stable expression of ΔUBL, K48R and K27R-parkin, biochemical enrichment of the protein and mass-spectrometry analysis of parkin ubiquitination would certainly help elucidate this point.

On the other hand, while ubiquitination of inner mitochondrial proteins has been recently observed under endogenous and parkin over-expressing conditions (68,126,129), similar results have been observed upon enzymatically inactive parkin conditions (68). Hence, while these later events might not be representative for parkin-dependent mitophagy, they suggest the presence of other E3 ligases capable of ubiquitinating mitochondrial material upon induced depolarization. Recent studies have suggested a regulatory interaction of parkin with the mitochondrial E3-ligase MITOL, indicating that initial parkin activity is dependent on previous OMM ubiquitination by MITOL (133) and that late stages of mitophagy induce MITOL translocation to peroxisomes and ER (142,199). Hence, given that one of the proposed sources for autophagosome formation are ER-mitochondria contact sites (44,200,201) and that late stages of mitophagy are likely to involve rupture or degradation of OMM (76,135), it is possible that MITOL could be involved in the ubiquitination of IMM and matrix proteins at late stages of the pathway. In addition, other E3 ligases, like MUL1, GP78 and HUWE1, previously reported to interact with one of the parkin subtrates (i.e: MFN), could also be involved in this process (143–

145,148). Alternatively, there are two scenarios that would help explain the presence of inner mitochondrial ubiquitination at later stages of mitophagy: (i) late parkin ubiquitination of available IMM proteins after OMM rupture occurs right before parkin degradation and/or (ii) there is an increase in DUB activation right after the degradation of active parkin. Future studies allowing inducible E3 ligase silencing at later stages of mitophagy combined with targeted mass-spectrometry of ubiquitinated proteins might help clarify this point.

5.3. Influence of the proteasome at early stages PINK1/parkin mitophagy

5.3.1. Is proteasomal degradation a pre-requisite for mitophagy progression?

PINK1/parkin mitophagy triggers proteasome-dependent degradation of specific OMM proteins (6). For example, MFN1/2 are rapidly targeted by the proteasome and their degradation promotes mitochondrial fragmentation (49,50). On the other hand, the mitochondrial fusion factor DRP1 has also been reported to be specifically targeted by the proteasome after early mitochondrial depolarization (181). Considering the need of mitochondrial fragmentation to occur in order to allow successful mitophagy, the degradation of a fission factor like DRP1 in the context of mitophagy might be counter intuitive. In this context, some authors have indicated that early steps of PINK1/parkin mitophagy drive the recruitment of DRP1 and subsequent mitochondrial fission (202,203). Moreover, it has additionally been suggested that initial UPS degradation is essential for subsequent mitochondria turnover (49,136). While this later aspect is perhaps not considered a consistent finding as other authors have reached opposite conclusions (135), a recent study has nicely shown that autophagy receptor silencing, completely impaired the degradation of inner mitochondrial proteins while the degradation of OMM proteins was partly unaffected (190). Thus, supporting the idea that OMM degradation not only involves autophagic targeting but also that additional degradation pathways (e.g: UPS degradation) might be involved.

In this study, pre-inhibition of the UPS extensively impaired mitochondrial turnover, affecting proteins from all sub-compartments (Figures 4.17 and 4.19B). Moreover, proteasome-dependent mitochondrial turnover was observed both under over-expressing and endogenous parkin conditions and could be validated through mass-spectrometry analysis (Figures 4.17, 4.18 and 4.21). Additionally, consistent with previous studies, an increase in ubiquitinated MFN1 was observed after pre-UPS inhibition (Figures 4.17A, 4.20 and 4.21) (49,50). Importantly, mitochondria were found in perinuclear aggregates containing parkin as well as proteins from

all sub-compartments (Figures 4.17B and 4.19), suggestive of parkin activity being maintained after extended proteasome inhibition and mitochondrial depolarization conditions. Thus, in agreement with previous studies, data from this work confirms that parkin-dependent mitophagy induces proteasomal degradation, specifically influencing MFN1 levels at early stages of the pathway (49,50,136). Additionally, considering that mitochondrial turnover was severely attenuated upon pre-UPS treatment conditions and that parkin was found on mitochondria, it is likely that an initial proteasome-dependent degradation of OMM proteins is needed for subsequent parkin-dependent mitophagy progression. While this is in agreement with previous studies (49,136,190), it contradicts the conclusions reached by Yoshii S. and colleagues. Discrepancies with the later might arise from differential experimental systems as suggested by the authors (135).

5.3.2. Does UPS degradation influence the turnover of distinct OMM proteins?

In addition to kinetic turnover differences affecting sub-organelle proteins, data from this work has indicated that OMM proteins are differentially targeted for degradation upon acute mitochondrial depolarization (Figures 4.3-4.4 and 4.5A). For example, while MFN1 and TOM70 appeared to be almost degraded after 2h of CCCP, TOM20 and VDAC remained ubiquitinated after 2-4h of mitochondrial depolarization (Figure 4.3). Consistent with other studies, proteasomal degradation of MFN1 seemed to occur after early mitochondrial depolarization (1-2h CCCP) (49,136,203). On the other hand, the recognition of ubiquitinated mitochondria by the autophagy receptors assayed in this study was initiated after 2h but was mostly prominent after 4h of CCCP (Figure 4.32B and D), consistent with other studies (62,75). Thus, would it be possible that parkin-dependent ubiquitinations differently trigger the degradation of proteasomal and autophagy dependent OMM proteins?

Surprisingly, pre-UPS inhibition combined with CCCP treatment triggered a decrease in TOM20 and VDAC ubiquitination (Figure 4.17A). Importantly, data from this work has demonstrated that TOM20 is directly targeted by autophagy receptors and autophagosomes (Figures 4.11A-E and 4.33C-D), in agreement with previous studies reporting direct autophagy receptor, LC3B or lysosomal engagement with OMM regions during parkin-dependent mitophagy (62,73,75,204). Similarly, VDAC1 has been characterized to also interact with p62/SQSTM and changes in VDAC1 poly- and mono-ubiquitination have been suggested to serve as a cell survival switch, promoting mitophagy and inhibiting apoptosis, respectively (62,205). Hence, while ubiquitination of both TOM20 and VDAC induce their autophagic turnover, it is possible that the specific ubiquitination

events of TOM20 and VDAC leading to autophagy receptor recognition occur after an initial UPS-dependent degradation step of specific OMM proteins. Alternatively, if we consider the amount of increased OMM ubiquitination 124ccurring at early stages of mitophagy and the presumably unspecific E3 ligase activity of parkin (133,134), one cannot discard that the observed differences in ubiquitination of early (i.e: MFN1) and late (i.e: VDAC, TOM20) OMM substrates are a consequence of reduced spatial availability of parkin late substrates at early stage of the pathway (<2h CCCP).

Next, in order to try to answer how proteasome degradation could differentially influence distinct OMM proteins at early stages of the pathway, combined delayed proteasomal inhibition experiments and proteomic analysis were performed (Figure 4.21A and D). In addition to confirm MFN1 as a proteasomal-dependent substrate, a milder proteasome influence on TOM70 and RHOT2 was observed at <2h CCCP, with both proteins having lower significance levels in comparison to MFN1 (Figure 4.21D). Interestingly, their degradation rate was stronger than the one observed for TOM20 and VDAC2/3, which showed no influence for the proteasome after 2h of mitochondrial depolarization (Figure 4.21D). Hence, potentially indicating that MFN1, TOM70 and RHOT2 degradation occurs during 0-2h of CCCP, while complete turnover of TOM20 and VDAC1 may take place at a later time point. While previous studies have suggested that both RHOT1/2 have similar degradation kinetics (206), only RHOT1 degradation has been reported to occur in a UPS-dependent manner (206,207). Similarly as for DRP1, ubiquitination of RHOT1/2 are suggested to not trigger a proteasomal-dependent degradation of the protein but to contribute in parkin recruitment at the OMM (208). Lastly, data from this work together with other studies have indicated both TOM70 and RHOT2 to be ubiquitinated in a parkin-dependent manner (Table 4.2) (68,174).

Taken together, these results confirm MFN1 to be a UPS target and suggest RHOT2 and TOM70 to be additional UPS targets. Additionally, proteasomal inhibition induced a reduced accumulation of ubiquitinated TOM20 and VDAC1, indicating that complete turnover of TOM20 and VDAC2 is indirectly influenced by the proteasome. This events allow for the speculation of the autophagic targeting of TOM20 and VDAC2 to occur downstream of a first proteasome-dependent degradation wave on specific OMM proteins, potentially occurring at a time-window of <2h CCCP. Future studies will be needed to understand in more detail the temporal implications of UPS targeting and autophagic targeting of individual OMM proteins.

5.4. Influence of the proteasome at late stages of PINK1/parkin mitophagy

Late stages of PINK1/parkin mitophagy (8-14h CCCP) induced the formation of inner mitochondrial aggregates that were limitedly targeted by autophagosomes and lysosomes (Figures 4.11B, C, F and G and 4.12-13). However, after extended depolarization treatment (14-18h CCCP), matrix proteins were no longer engaged in aggregates but localized in autophagosomes and lysosomes (Figure 4.11C and 4.13C), suggesting intermediate degradation steps for the final turnover of inner mitochondrial aggregates. Hence, could late stages of mitophagy be influenced by the proteasome in a similar manner as it occurs at earlier stages? Delayed proteasome experiments indicated an impairment on the degradation of inner mitochondrial proteins (Figure 4.22B-C) and an increase in mitochondrial aggregates (Figure 4.22D-F), which could be additionally validated through LC-MS/MS analysis (Figure 4.23A-B). These data suggested matrix protein turnover to be more susceptible of an additional proteasome degradation step. Given that parkin-dependent mitophagy has been reported to induce OMM breaking in previous studies (76,135) and in this work (Figure 4.14C), it is likely that UPS targeting of inner mitochondrial material could be dependent on that step. Along these lines, a recent report has described that upon OMM breaking, inner mitochondrial proteins like PHB2 would be available for direct autophagosome targeting (76). In our model, recognition of inner mitochondrial material was mediated by the autophagy receptors p62/SQSTM and TAX1BP1, however its direct targeting was sometimes limited (Figure 4.32E), suggesting the involvement of other autophagy receptors. Alternatively, inner mitochondrial aggregates could be directly targeted to autophagosomes via CL (expanded in chapter 5.1.4).

Single protein analysis allowed for the identification of the cluster of matrix ribosomal proteins (MRPL) to be significantly upregulated upon delayed proteasome inhibition conditions (Figure 4.23C and Table 4.5). Interestingly, accumulated targets also included the OMM and IMM proteins, metaxin-2 (MTX2) and metalloprotease YME1L1, both related to mitochondria architecture via cristae remodeling and mitochondrial fusion regulation (5,209). While MTX2 is reported to interact with SAM50 and the MICOS complex, and thus provides a link to cristae architecture (210,211), YME1L1 has been suggested to regulate OPA1 cleavage (26). Importantly, OPA1 is also known to be implicated in both cristae architecture and mitochondrial fusion (27,28). TEM data allowed us to identify events of broken OMM in autophagosome-engulfed mitochondria already after 4h of CCCP (Figure 4.14C). In addition, most of the mitochondria observed had a dysregulated cristae structure at that time point (Figure 4.14C) and after extended CCCP treatment (data not shown). Both MTX2 and YME1L1 belonged to two

of the clusters which were significantly downregulated at late stages of mitophagy (14-18h CCCP) (Table 4.5 and 4.2) and were additionally found ubiquitinated at that time point (132). Thus, given that both MTX2 and YME1L1 are both involved in cristae architecture and TEM images indicated dysregulated cristae upon long mitochondrial depolarization treatment, it is possible that MTX2 and YME1L1 are long-lived proteins responsible of cristae remodeling at late stages of the pathway. Along these lines, previous reports have indicated a relationship between cristae morphology homeostasis and PINK1/parkin mitophagy, where SAM50 silencing induced parkin-dependent mitochondrial turnover in a similar piecemeal manner as described by this work (212). In addition, others have indicated that OPA1 cleavage is enhanced upon CCCP treatment (26), which would inevitably argue for implications of mitochondrial fusion and perhaps also cristae remodeling during late stages of PINK1/parkin mitophagy. Nevertheless, given that both cristae remodeling and late stages of parkin-dependent mitophagy can be still considered emerging fields of research (5), future studies are needed to understand the relationship of these factors in the context of PINK1/parkin mitophagy.

On the other hand, we cannot discard that the accumulation of inner mitochondrial proteins observed is due to the accumulation of cytosolically translated mitochondrial proteins that cannot be imported into the organelle. Ordureau *et al.* reported ubiquitination of MTX2 and YME1L1 under earlier depolarization conditions in the absence of USP30 (68). Interestingly, recent studies have suggested USP30 to regulate ubiquitination of inner mitochondrial proteins for their successful import (213,214). Consequently, while the results presented in this work may point to directed UPS degradation of specific OMM and IMM substrates for the successful degradation of inner mitochondrial aggregates and thus, the identified substrates should be treated as potential candidates, validation studies will be needed to prove their relevance at later stages of PINK1/parkin mitophagy.

5.5. TAX1BP1 involvement in PINK1/parkin mitophagy

5.5.1. Defining TAX1BP1 role in the process: non-essential autophagy adaptor?

Extensive research focused on the selective removal of mitochondria allowed for the identification of at least five ubiquitin-dependent autophagy receptors to be involved in parkin-dependent mitophagy: OPTN, NDP51, TAX1BP1, p62/SQSTM and NBR1 (44,51,59). At the start of this study, the role of TAX1BP1 in mitophagy was not extensively investigated, with only few reports linking the autophagy adaptor with parkin-dependent mitophagy (73,75). Previous

reports have indicated TAX1BP1 activity to not be essential for mitochondrial elimination, as other autophagy receptors (e.g: OPTN) can induce mitophagy in a more effective manner than TAX1BP1 (75). In contrast, a recent proteomics study combining several mitophagy screen readouts, indicated that the specific downregulation of TAX1BP1 strongly compromises parkin-dependent mitochondrial degradation in muscle cells (190). On the other hand, TAX1BP1 has been recently linked with aggrephagy (92,215) and lysophagy (85). Additionally, differences in the interaction of TAX1BP1 and other autophagy receptors with ATG8 proteins have been identified, with TAX1BP1 being able to interact with both LC3B and LC3C (89). Overall, indicating that TAX1BP1 might be a highly versatile autophagy receptor involved in many autophagic degradation pathways and not exclusively in mitophagy.

In agreement with previous studies, data from this work indicated that TAX1BP1 translocated to mitochondria and was able to recognize both OMM and inner mitochondrial material upon mitochondria depolarization (Figures 4.32-33) (61,73,75,92,175,190). On the other hand, its translocation was not complete given that a considerable amount of TAX1BP1 remained partially engaged with the lysosomal marker LAMP1 at early and late stages of the pathway (Figures 4.33B, D and 4.34). In addition, TAX1BP1 silencing did not impair overall degradation of OMM proteins and its engagement with inner mitochondrial aggregates was limited (Figure 4.35). However, over-expression of TAX1BP1 in a ubiquitin-binding autophagy receptor deficient model (pentaKO HeLa) was able to rescue defective mitophagy (Figure 4.38-41) Additionally, the single transfection of the autophagy adaptor in WT-parkin HeLa cells mildly enhanced mitochondria turnover (Figure 4.36-37). Hence, we can confirm TAX1BP1 as an autophagy receptor capable of promoting mitophagy when the expression of other parkin-dependent mitophagy-related autophagy receptors is compromised (e.g: pentaKO HeLa). However, in situations where other autophagy receptors are expressed (e.g: p62/SQSTM), TAX1BP1 may adopt accessory roles which allow for an improvement in mitochondrial turnover. Overall, these data are in agreement with previous reports suggesting TAX1BP1 to function as a non-essential autophagy receptor in the context of parkin-dependent mitophagy (75).

5.5.2. Trying to understand the behavior of ubiquitin-dead TAX1BP1 mutants

Mass spectrometry analysis of the general ubiquitination events taking place after induction of PINK1/parkin mitophagy revealed ubiquitination of TAX1BP1 after early mitochondrial depolarization (Table 4.3 and Figure 4.30). Interestingly, a similar TAX1BP1 ubiquitination pattern than the one observed in this study was previously reported after milder mitochondrial

stress induction (73) (Figures 4.30C and 4.31), however the specific implications of this PTM on the context of parkin-dependent mitophagy were not further pursued in that study.

In order to identify the relevance of the identified TAX1BP1 ubiquitination's, ubiquitination-dead site-specific and domain deletion TAX1BP1 mutants were generated, directly affecting the ubiquitinated regions found upon PINK1/parkin induction on WT-parkin cells (Figure 4.40A). Remarkably, deletion of the CC3 region drastically reduced the overall TAX1BP1 ubiquitination while the single K549 ubiquitin-dead mutant had no effect (Figure 4.40B). These data indicate that most of the ubiquitinated lysines responsible for overall TAX1BP1 ubiquitination might be localized at the CC3 domain but are not exclusive of this region, as total TAX1BP1 ubiquitination was not completely abolished in the ΔCC3 mutant (Figure 4.40B). On the other hand, none of the mutations had any effect on overall TAX1BP1 autophagy adaptor functions as defective mitochondrial turnover could be rescued after transfection all TAX1BP1 mutants (Figures 4.40B-G). However, a potential decrease in the detection of ubiquitinated TOM20 for ΔCC3 mutant was observed (Figure 4.40B). Together, these experiments are indicative of a potential role of the region CC3 in TAX1BP1 functions occurring downstream of parkin ubiquitination.

Ubiquitination of other autophagy adaptors has been reported to regulate their affinity for ubiquitinated cargo. For example, ubiquitination or de-ubiquitination of the UBA domain of p62/SQSTM is known to modulate the autophagy receptor affinity to ubiquitinated cargo through regulation of its oligomerization status (182,183,216). On the other hand, OPTN ubiquitination has been reported to allow oligomerization with p62/SQSTM and enhance the overall autophagic flux (217). Additionally, it has been shown in *in vitro* membrane models that TAX1BP1 interacts with FIP200 during aggrephagy (215), while others have shown that the UBA domain of the autophagy adaptor can interact with both K63 and K48 ubiquitin chains (89). Hence, the overall results presented in this study allow for the speculation of the CC3 region of TAX1BP1 to have an influence on TAX1BP1 functionality at different levels. First, given that there was an increased amount of ubiquitinated TOM20 under expression conditions of ΔCC3, it is possible that CC3 is involved in the interaction of the UBA domain with ubiquitin chains. Secondly, similarly as it is observed for OPTN-p62/SQSTM oligomerization, it is plausible that ubiquitination of CC3 triggers TAX1BP1 oligomerization which could have a direct impact on the percentage of TAX1BP1 covering mitochondrial aggregates, matching the results obtained in this work (Figures 4.41A and 4.43A-C). Additionally, given that ΔCC3-TAX1BP1 expression promoted a transient delay on mitochondrial degradation, we cannot discard that CC3 is also involved in the recruitment or interaction of autophagic proteins (i.e: FIP200). Future experiments will be

needed to fully understand the importance of CC3 in TAX1BP1 functionality and decipher its potential interaction with ubiquitin chains or autophagic proteins. In addition, the generation of stable pentaKO cell lines would certainly improve the investigation of the ubiquitin-dead mutations on TAX1BP1 and how it may specifically recognize OMM, IMM and matrix cargo. On the other hand, immunoprecipitation experiments might help unravel differences in TAX1BP1 oligomerization or autophagy-related protein interaction upon expression of the different TAX1BP1 mutants.

5.6. An example of PTM crosstalk in mitophagy: VDAC1/2

VDAC proteins represent one of the most abundant proteins at the OMM (14) and are known to be parkin-dependent targets during mitophagy (131,176) (Table 4.2 and Figures 4.1C, 4.3 and 4.4). Mass spectrometry analysis of phosphorylation and ubiquitination events during parkin-dependent mitophagy revealed the third cytosolic loop of both VDAC1 and VDAC2 to be phosphorylated and ubiquitinated during mitophagy induction (Figure 4.24). Mitophagy experiments combining the over-expression of phospho-dead and phospho-mimic VDAC2 mutants indicated that, while the overall mitochondrial turnover was not affected upon expression of any of the mutants (Figure 4.27D-E), the specific turnover of VDAC2 was influenced by mimicking phosphorylation and dephosphorylation alone on S115 or in combination with ubiquitin-dead mutation on K120 (Figures 4.26 and 4.28-29). More specifically, turnover of VDAC2 was enhanced when dephosphorylation of S115 was mimicked, potentially due to an increase in total and K27-linked ubiquitin chains (Figures 4.26). Importantly, those effects were reverted when ubiquitination on K120 was prevented with a ubiquitin-dead mutation in that residue alone, together with a phospho-dead mutation at S115 or in combination with a phospho-mimic mutation at S115 (Figures 4.28 and 4.29). Overall, strongly suggesting that ubiquitination of VDAC2 at K120 is downstream of S115 dephosphorylation upon CCCP-induction of parkin-dependent mitophagy (Figure 5.1).

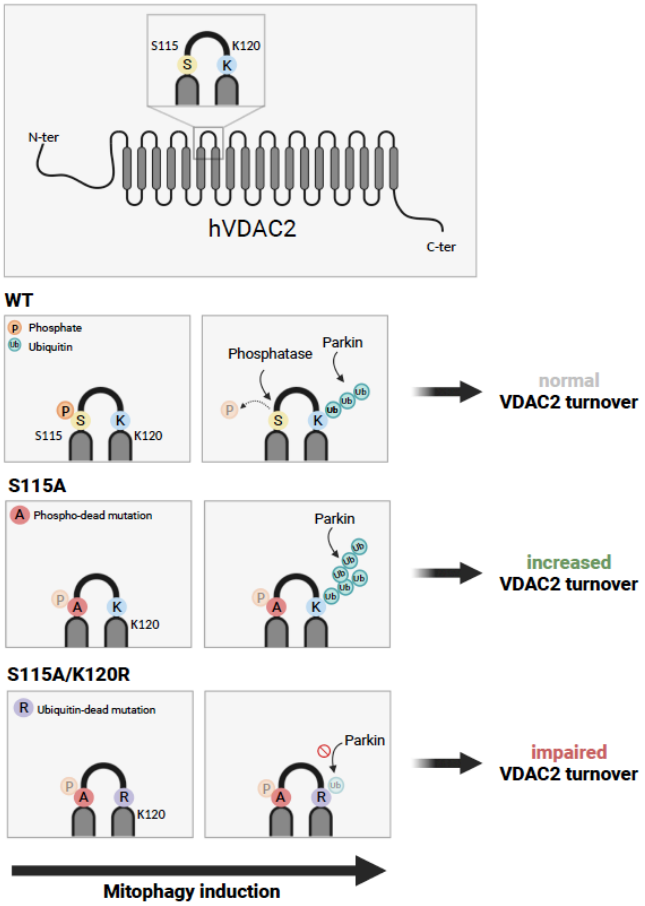


Figure 5.1: Schematic representation of phosphorylation and ubiquitination cross-talk in VDAC2. Under normal conditions, VDAC2 is phosphorylated at S115. Upon mitophagy induction, S115 is dephosphorylated and later, K120 is ubiquitinated in a parkin-dependent manner, normally triggering WT-VDAC2 turnover. When a phosphor-dead situation is mimicked (S115A), ubiquitination of K120 is increased and so is VDAC2 turnover. However, if ubiquitination at K120 is prevented (e.g: ubiquitin dead mutation, K120R), VDAC2 turnover is impaired. Created with Biorender. Adapted from Zittlau and Lechado-Terradas *et al.*, 2022 (132).

Recent parkin-dependent ubiquitylome studies have been able to decipher the specific lysines targeted for parkin-dependent mitophagy, mostly indicating that OMM protein turnover involves ubiquitination at several lysine residues (68,126,129,131). Importantly, VDAC1/2 parkin-dependent ubiquitination were detected in both K104 and K120 residues among others, confirming ubiquitination of VDAC2 to occur in the identified residues of this present study (Table 4.2). Interestingly, residues of the identified loop are highly conserved among several vertebrate species and VDAC isoforms (218). Importantly, VDACs have been suggested to play a pivotal role in cell fate decision with recent studies reporting that parkin-dependent mono- or poly-ubiquitination of VDAC1 can strongly prevent the induction of apoptosis (205). In addition, several studies have reported specific interaction of VDAC1 with the anti- and pro-apoptotic proteins (37–42). However, while there is no evidence so far for VDAC2 interactors, it is possible that relevant protein-protein interactions may also apply (219,220). Indeed, a recent study reported differential structural behavior of VDAC2 in comparison to VDAC1 isoforms and suggested a predominant role in apoptosis regulation for VDAC2 (221). Moreover, a recent

report has identified a relationship between S104 phosphorylation mediated by the serine/threonine-protein kinase SGK1, which influences total VDAC1 ubiquitination in the context of apoptosis regulation through mPTP formation (222). In this case, Zhou *et al.* indicate that VDAC1 dephosphorylation at S104 would prevent global VDAC1 ubiquitination and trigger apoptosis through cytochrome c release in a parkin-independent manner. In addition, a previous report indicated parkin-dependent K27-ubiquitin chains on VDAC1 triggered the recognition of p62/SQSTM (62). Hence, while the study from Zhou *et al.* strongly differs from the results obtained in this study and only accounts for VDAC1, it is tempting to speculate that the third cytosolic loop of both VDAC1 and VDAC2 may potentially play a role in cellular fate decision, as it has previously been suggested (218). A possible model on the regulation of cellular fate decision could involve three systems: (i) parkin-dependent ubiquitination, (ii) phosphatase targeting of mitochondrial proteins and (iii) VDAC proteins as a substrate potentially regulated via PTM through the specific E3 ligase parkin as well as phosphatases, potentially influencing the mitophagy activation or mPTP formation under similar stressing conditions (Figure 5.2).

In short, data from this work provides supporting evidence for a potential crosstalk of phosphorylation and ubiquitination on VDAC proteins, ultimately having an impact on their autophagic turnover via K27-linked ubiquitin chains. Moreover, despite not having identified the responsible phosphatases for the dephosphorylation of S115 of VDAC2, this study enhances the suggested role of phosphatases and kinases being involved in mitochondrial homeostasis (223). Future studies on this topic will be needed to validate: (a) if the observed regulatory mechanisms of VDAC2 turnover also apply for VDAC1, (b) if both VDACs are similarly implicated on cellular fate decision and (c) which phosphatase might be the responsible for the observed dephosphorylations on VDAC2.

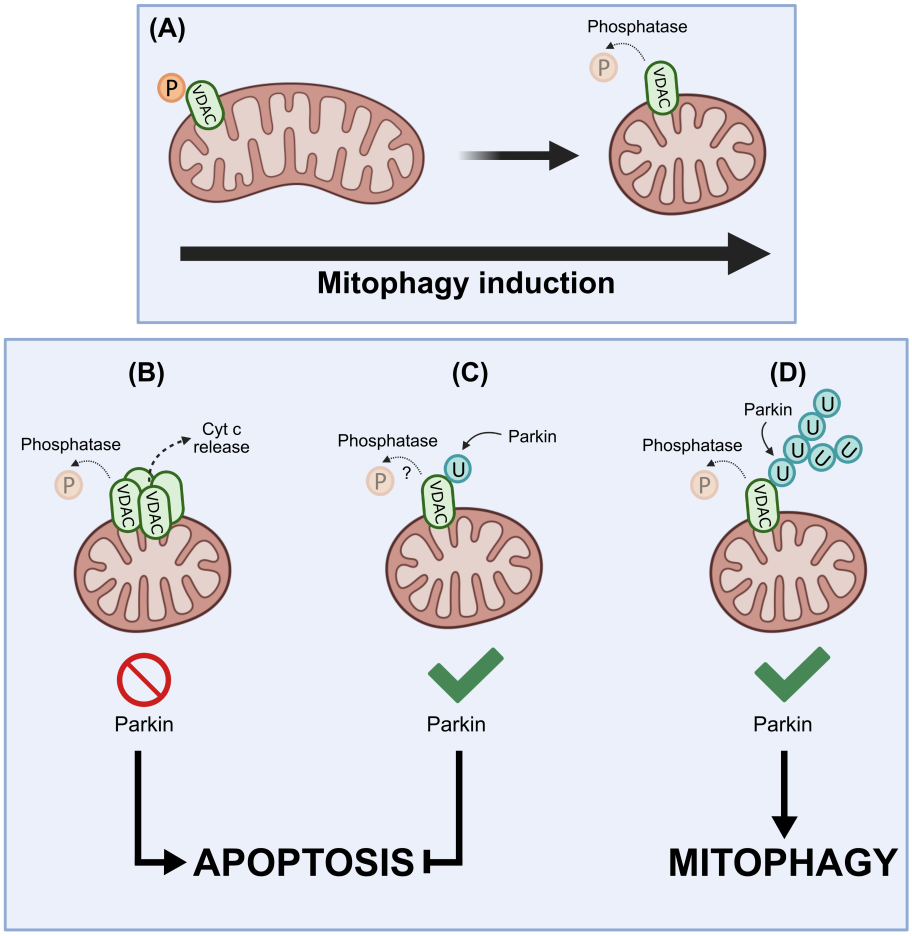


Figure 5.2: PTMs of VDAC influence cell fate decisions: between apoptosis and mitophagy. (A) VDAC is phosphorylated at basal conditions but undergoes dephosphorylation upon mitophagy induction (i.e: CCCP). **(B)** Dephosphorylation of parkin may induce mPTP formation if parkin is not present. **(C)** However, if parkin is present and VDAC undergoes parkin-dependent mono-ubiquitination, apoptosis is prevented. It is not clear if dephosphorylation of VDAC applies in this case. **(D)** On the other hand, if VDAC2 undergoes parkin-depednent poly-ubiquitination, parkin-dependent mitophagy cell viability is promoted via mitophagy activation. Created with Biorender.

5.7. An updated model of PINK1/parkin mitophagy

The mechanisms underlaying PINK1/parkin mitophagy have been a focus of ongoing research since the early 2000. Since then and until the present day, many efforts have contributed in understanding the regulatory key steps needed for PINK1/parkin pathway activation and progression, mainly characterized by the increased parkin-dependent ubiquitination's on numerous OMM substrates and subsequent recognition by autophagy receptors (59). In addition, the general mechanisms leading to final mitochondrial turnover have mostly been accounted for wholesale mitophagy, assuming a complete engulfment of the organelle that leads to final mitochondria elimination (44). This present work contradicts this general assumption as it gathers evidence for an alternative piecemeal mitochondrial degradation model which has already been suggested by others (68,75,98,135,136,172,189) (see Table 5.1).

Moreover, this study reveals additional proteasomal-dependent regulatory steps for final mitochondria elimination during late stages of the pathway (see chapters 4.7-10). Hence, an updated model of PINK1/parkin dependent mitochondrial turnover will be described based on the presently discussed results (Figure 5.3).

The multiple ways of inducing PINK1/mitophagy all converge on the strong ablation of mitochondrial homeostasis, leading to an impairment of mitochondrial import machinery and subsequent accumulation of PINK1 at the OMM (Figure 5.3.1). PINK1 accumulation triggers PINK1-dependent phosphorylation of ubiquitin molecules which promotes parkin activation and its translocation to the OMM (Figure 5.3.1). Once engaged with mitochondria, parkin recognizes phosphorylated ubiquitin and mediates the attachment of additional ubiquitin molecules, leading to the formation of ubiquitin chains on OMM substrates (Figure 5.3.2). While parkin is able to build several types of ubiquitin chain linkages, K63- and K48-linked ubiquitin chains are two of the most prominent on mitochondria (129,131). Importantly, different ubiquitin targeting triggers distinct degradation pathways: K48-linked chains induce UPS mediated degradation while K63-linked chains promote the recognition of autophagy adaptors (52,57). Initial ubiquitination events promote the UPS-mediated degradation of several substrates (i.e: MFN1, RHOT1 and DRP1) which in turn trigger the fragmentation of the whole mitochondrial network (Figure 5.3.3). In addition to proteasome-targeted ubiquitin chains, parkin also mediates the addition of other chain types which are later recognized by autophagy receptors (Figure 5.3.4). Consecutively, autophagy receptor recognition engages the OMM cargo with building autophagosomes. At this point, parkin degradation might take place in a proteasome or autophagy-dependent manner (Figure 5.3.5). At this stage, the autophagosomes -mostly carrying OMM material- are later fused with lysosomes, leading to complete cargo degradation and completing a first autophagosomal wave of the process (Figure 5.3.6). After OMM protein removal, inner mitochondrial aggregates with damaged OMM are available for subsequent ubiquitination and further autophagy receptor recognition (Figure 5.3.7-8). Ubiquitination of inner mitochondria aggregates might be mediated through parkin-independent mechanisms (Figure 5.3.7). In a similar way as during early stages of the pathway, ubiquitination of inner mitochondrial proteins drives the targeting of autophagy receptors (Figure 5.3.8). Additionally, prior to inner mitochondrial engulfment to autophagosomes, a potential novel UPS-dependent degradation step is required to further allow complete degradation of the remaining aggregates (Figure 5.3.8). Later steps of the pathway leading to complete mitochondrial turnover are mediated through autophagosome engulfment and fusion to lysosomes, similarly as observed for OMM removal (Figure 5.3.9-11).

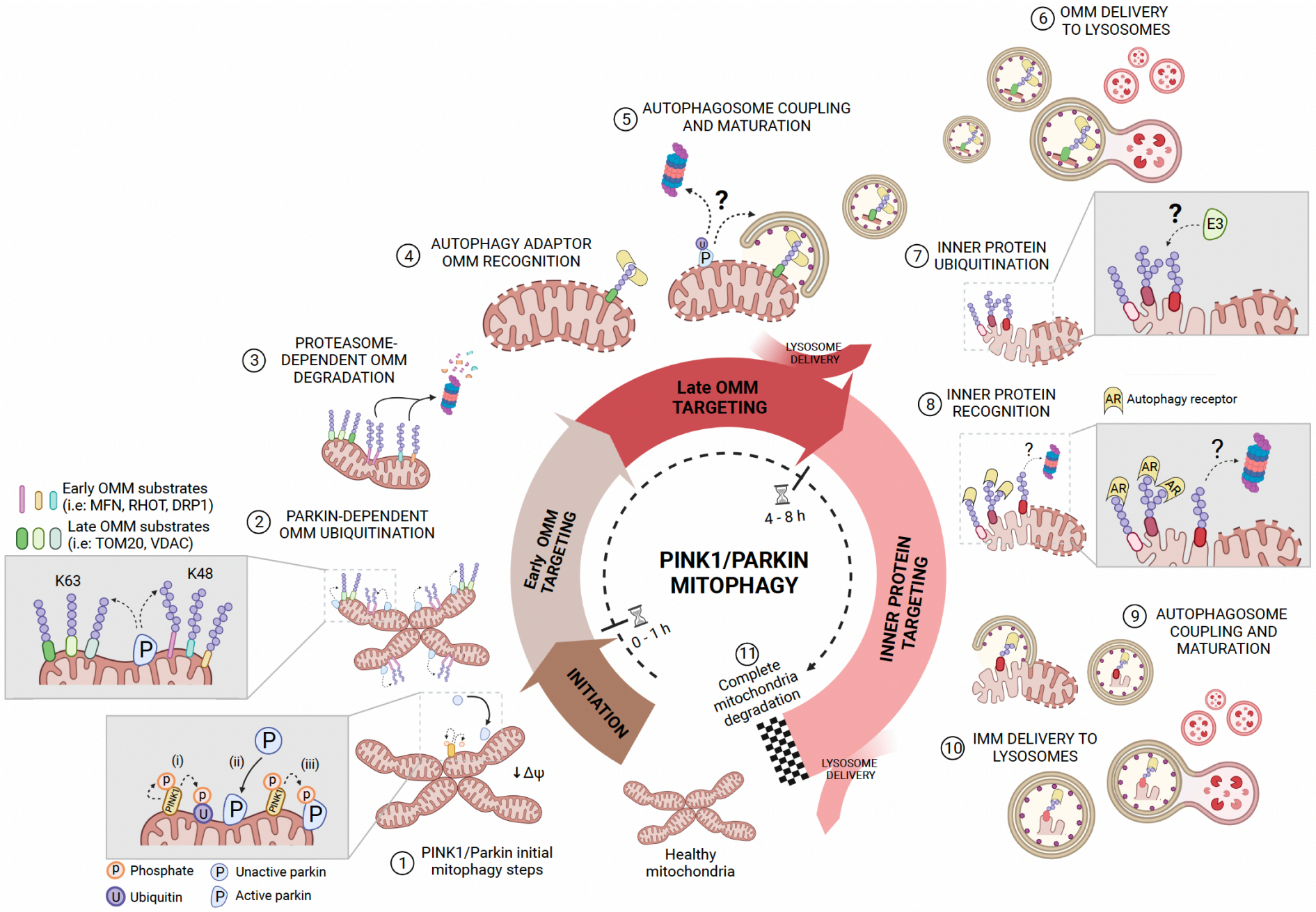

6 OMM DELIVERY TO LYSOSOMES
5 AUTOPHAGOSOME COUPLING AND MATURATION
4 AUTOPHAGY ADAPTOR OMM RECOGNITION
7 INNER PROTEIN UBIQUITINATION
E3
3 PROTEASOME-DEPENDENT OMM DEGRADATION
LYSOSOME DELIVERY
Late OMM TARGETING
8 INNER PROTEIN RECOGNITION
AR Autophagy receptor
Early OMM substrates (i.e: MFN, RHOT, DRP1)
Late OMM substrates (i.e: TOM20, VDAC)
2 PARKIN-DEPENDENT OMM UBIQUITINATION
K63
K48
4 - 8 h
PINK1/PARKIN MITOPHAGY
Early OMM TARGETING
INNER PROTEIN TARGETING
0 - 1 h
INITIATION
11 Complete mitochondria degradation
LYSOSOME DELIVERY
9 AUTOPHAGOSOME COUPLING AND MATURATION
10 IMM DELIVERY TO LYSOSOMES
↓Δψ
1 PINK1/Parkin initial mitophagy steps
Healthy mitochondria
Phosphate
Unactive parkin
Ubiquitin
Active parkin

Figure 5.3: Dynamics of PINK1/parkin mitophagy: early and late stages. Once the health of basal mitochondria is compromised via depolarizing agents (i.e: CCCP), PINK1 accumulates at the OMM (1). This triggers PINK1 activation via auto-phosphorylation, further phosphorylating existing ubiquitin molecules at the OMM which promote parkin recruitment to mitochondria. Once parkin is close to the OMM, PINK1 is able to phosphorylate the E3 ligase, rending parkin to a fully active state. (2-3) Once at the OMM, parkin builds different ubiquitin-chain linkages on several OMM proteins, triggering different protein fates. While K48 ubiquitin chains trigger the rapid degradation via the UPS, K63 ubiquitin chains promote the recognition of autophagy receptors. Thus, OMM proteins targeted with K48 linked chains can be considered early OMM substrates while proteins targeted with K63 linked chains are referred as late OMM substrates. On the other hand, (4) K63-linked ubiquitin chains promote the recognition of autophagy receptors (here as; adaptors) which later engage with building autophagosomes (5). At this stage, it is possible that parkin is degraded via the proteasome or along with mitochondrial cargo. (6) The autophagosomes containing mostly OMM material further reach the stage of closure and are eventualy fused with lysosomes, promoting the complete degradation of OMM material. (7) After most of OMM proteins are removed, inner mitochondrial aggreagtes are available for subsequent ubiquitination, likely via E3 ligases other than parkin. (8) Ubiquitination of inner mitochondrial aggregates triggers the recognition of autophagy adaptors, similarly as observed in early stages (see 4). Additionally, inner mitochondrial aggregates are targeted by the proteasome. (9) Similar as in earlier stages, autophagy receptor recognition of ubiquitinated inner mitochondrial proteins triggers the coupling of building autophagosomes which will (10) later fuse with lysosomes, (11) leading to the complete elimination of mitochondrial material. Created with Biorender. Adapted from Lechado-Terradas *et al.*, 2022 (173) with BioRender.com (2022).

5.8. Wholesale or piecemeal PINK1/parkin mitophagy?

PINK1/parkin dependent mitophagy triggers the degradation of mitochondria in a ubiquitin-dependent manner and it is widely accepted that mitochondrial turnover involves the engulfment of the whole organelle (59,177). There might be some studies which could be examples of wholesale mitophagy and those may show (i) complete localization of mitochondrial material with the autophagy machinery, (ii) autophagosome structures engulfing mitochondria or may have a (iii) strong focus on mitochondrial protein degradation. However, most of these studies rely on mitochondria dyes or targeted mitochondrial proteins as reporters and do not account for a broad temporal window of the pathway but rather rely on individual or limited time points (61,73,195,196). Importantly, other studies have reported alternative PINK1/parkin mitophagy involving piecemeal mitochondrial degradation; either characterized by (i) a sequential degradation of mitochondrial proteins, (ii) targeting of the autophagic machinery on localized mitochondrial stressed regions or (iii) the formation of MDVs in response to mild stress (68,98,135,136,172,189). Thus, in order to have a better understanding of the relevance of the PINK1/parkin model described in the work, the most relevant PINK1/parkin-dependent mitophagy studies that globally reported piecemeal mitochondrial degradation in addition to studies in which the autophagy involvement was assessed, are summarized in Table 5.1.

Importantly, of all the studies presented here (Table 5.1), only two of them rely on the autophagic targeting of OMM and matrix proteins in a neuron-like cellular model (68,177). The rest of the studies either include the use of mitochondrial dyes, mitochondrially targeted over-expressed proteins, identification of TOM20 alone and/or account for a limited time-window of the pathway, mostly including early time-points only (Table 5.1). While other authors have already indicated the importance on the use of several OMM, IMM and matrix proteins for the study of mitophagy (135), the importance of assessing complete mitochondria degradation should also be taken into account (75,134,189). Interestingly, one of the reported studies using neuronal models identified inner mitochondrial structures resembling the CS- and SSBP1-aggregates in WT-parkin HeLa described in this present work (Figure 4.5) (68). On the other hand, autophagic targeting of mitochondrial material reported by Ordureau *et al.* and Matsumoto *et al.* does not completely match the observations made for WT-parkin HeLa in this study (68,177). In addition, while Ordureau and colleagues reported a delayed mitophagy kinetics in iNeurons and these findings are in agreement with the mitophagy kinetics observed for NPCs in this work (Figure 4.8), mitophagy kinetics reported by Matsumoto and colleagues

seem to be enhanced when using neuronal cell lines with parkin over-expression. Thus, provided that differences in mitophagy progression have been observed between different cell lines in this and other studies, it is likely that parkin-dependent mitophagy kinetics is subject to parkin expression levels (Table 5.1) (224). Similarly, differences in the expression of autophagy-related genes could also influence the rate of autophagic targeting and building of autophagosomes. In addition, it is possible that different kinds of mitochondrial stress inducers promote distinct forms of mitochondrial turnover as observed by McLelland and colleagues, with mild stressors like Antimycin A -but not CCCP- promoting the formation of MDVs in cells over-expressing parkin (172).

After all, parkin-dependent mitophagy is a process that relies on three distinct dynamic signaling systems: (i) parkin-dependent ubiquitination, (ii) autophagy machinery activation and (iii) autophagosome maturation and thus, the kinetics of each of the individual system could have an impact on the overall mitophagy rate. Thus, parkin-dependent mitophagy might not be as simple as it might have been expected in the early days, as it was largely assumed that mitochondria would be degraded via the engulfment of the whole organelle. However, this and other studies indicate that this might not be a holistic mechanism and that for example, mitophagy rate as well as its turnover mechanism can vary in response to different parkin expression levels and type of mitochondrial stress induction, respectively. In this sense, future studies accounting for the distinction of wholesale and piecemeal PINK1/parkin mitophagy in combination with the appropriate use of relevant *in vivo* models, will certainly shed light on the importance of the two existing turnover models and reveal their importance in tissue-specific cell populations.

5.9. Outlook

Since the discovery of the first implications of PINK1 and PARKIN genes on the specific removal of mitochondria ten years ago, a lot of efforts have converged into deciphering the activating and progression mechanisms that link ubiquitinated mitochondria with the autophagy machinery (225). However, limited investigation of late stages of the pathway and thorough analysis of several mitochondrial sub-compartment proteins throughout the process, has perhaps led to a not accurate definition of PINK1/parkin mitophagy, which is mostly linked to the assumption of mitochondria elimination occurring via the engulfment of the complete organelle (51,59,116,225–227). This present work sheds some light on the overall dynamic process of PINK1/parkin mitophagy, with a particular focus on the late stages of the pathway

that allow for complete mitochondria turnover. Overall, an updated model of the pathway in which turnover occurs in a piecemeal manner is presented. Interestingly, PINK1/parkin mitophagy requires both autophagy and proteasomal degrading systems at early and late stages of the pathway. Later stages of PINK1/parkin mitophagy may depend on parkin-independent ubiquitination of IMM and matrix proteins that initially trigger their degradation via the UPS and subsequent activation of the autophagy machinery, similarly as what is observed for early stages. Further delivery of the ubiquitinated IMM and matrix proteins could be mediated by ubiquitin-dependent or independent autophagy receptors.

One of the first steps to further understand the relevance of this proposed model would be to assess if phenotypical similarities are observed under milder stress-induced conditions. For example, an increase in ROS production using mt-KR could be implemented to further elucidate this point. Next, to further elucidate the potential disease relevance of the novel steps described in the new model of PINK1/parkin mitophagy proposed in this study (e.g: late UPS involvement), it would be important to further validate the proposed model in a more disease-relevant system for neurodegeneration, such as NPCs or the SH-SY5Y cell line. Further validation steps could include the use of patient derived iPSC to test for mitophagy progression defects and rescue of the phenotype observed at later stages upon transfection of PINK1 or parkin WT isoforms. Additionally, an important issue that lacks elucidation and clear understanding in the field of ubiquitin-dependent mitophagy is the proof of concept for a ubiquitin code, which is suggested to be important for ubiquitin-dependent autophagy receptor recognition of ubiquitinated substrates (59,176,194). Importantly, it would also be necessary to elucidate if different E3 ligases could expand this code and if the combination of other PTMs (i.e: phosphorylation, SUMOylation, glycosylation) on pre-existing ubiquitin chains could add another layer of regulation in the whole process (51,223).

One of the main features of the PINK1/parkin model described in this work is a differential targeting of mitochondria sub-compartment proteins. TEM experiments allowed the identification of ruptured OMM regions and were overall in agreement with the model presented. However, to validate differential OMM protein degradation and confirm if complete OMM protein degradation cannot account for total OMM turnover (see chapter 4.2-4.4), a targeted TEM approach specifically targeting TOM20 or other OMM proteins could be employed.

In addition, the implication of later UPS-dependent steps at late stages of the pathway is an important aspect of the novel model of parkin-dependent mitophagy proposed in this study.

Validation experiment on this point should firstly be focused on discarding UPS-dependent degradation of cytosolically translated mitochondrial proteins that cannot be properly imported after extended mitochondrial depolarization treatment. Experiments focusing on the sub-cellular localization of the identified targets could shed initial hints on the relevance of this novel regulation step, either by the use of imaging or sub-cellular fractionating techniques with additional internal controls that would account for mitochondrial or cytosolic localization. Alternatively, matrix-translated mitochondrial proteins could be deliberately chosen and their loss or gain of ubiquitination upon delayed UPS inhibition during mitophagy could be initially validated via mass-spectrometry using a similar ubiquitylome approach as the one used in this study (132).

Mass-spectrometry analysis of the mitochondrial proteome under conditions of delayed UPS-inhibition suggested the existence of long lived OMM and IMM proteins that might have an important role at late stages of PINK1/parkin mitophagy. First validation steps in this direction should be aimed to confirm a potential relationship between the target proteins with the UPS. Here, a rather simple biochemical approach could be applied, combining the use of immunoprecipitation or pulldown experiments to analyze the ubiquitination patterns of the protein upon normal mitophagy conditions and delayed UPS-inhibition during mitophagy.

Proteasomal degradation at early stages of the pathway was suggested to differentially influence OMM proteins. Initial validation experiments should include delayed proteasome inhibition conditions at multiple time-points during early stages of the pathway. Further, experiments combining enrichment of mitochondrial material together with mass-spectrometry identification of the major ubiquitin chain linkage at multiple time-points during early stages of the pathway with and without delayed proteasomal inhibition could help clarify, if different ubiquitin chain linkages on OMM substrates can directly influence proteasomal or autophagy-dependent degradation during early stages.

Later ubiquitination events observed on IMM and matrix proteins were suggested to not involve parkin activity as the E3 ligase was observed to undergo degradation. Validation experiments should include mitophagy curve experiments including basal or inhibitory conditions at several time-points. Given that the mechanisms of parkin degradation are yet unclear and they might involve both the UPS and autophagy machinery, appropriate inhibitory conditions should be used to target both systems (e.g: BafA and MG132 combined). First experiments could involve the quantification of relative parkin levels in WT-parkin HeLa cells without the need of protein immunoprecipitation or pulldown, provided that no endogenous parkin is expressed in HeLa cells. Additionally, overall parkin ubiquitination could be further assessed using a simple biochemical approach combining pulldown purification of the protein

and further parkin ubiquitination analysis either via Western blot or ubiquitination-targeted mass-spectrometry.

The lack of parkin enrichment on inner mitochondrial aggregates suggested additional E3 ligases other than parkin to potentially be responsible for IMM and matrix ubiquitination (142–146,148,199,228). Validation experiments of potential novel E3 ligases would require the generation of parkin stable cell lines combined with inducible silencing of the potential E3 ligase targets. Further functional validation could involve simple immunofluorescence mitophagy readouts as the ones employed in this study or more sophisticated assays involving over expression of fluorescent mitochondrial proteins, further allowing live image analysis (98,189) or cell sorting (190). In addition, inner mitochondrial aggregate ubiquitination was significantly limited in comparison to parkin-dependent degradation at early stages of the pathway. Based on this, an increase in DUB activity at late stages of the pathway is additionally suggested to be involved at later stages of the PINK1/parkin mitophagy. Here, an initial proof-of-concept experiment should be applied. For this purpose, iRNA libraries targeting DUBs could be implemented in combination with high throughput mitophagy readouts (190).

Furthermore, ubiquitin-dependent and independent autophagy receptors have also been suggested in this study to be involved in specific recognition of distinct mitochondrial sub-compartments. Ubiquitin-dependent autophagy receptors could be differentially selective according to the specific recognition of individual ubiquitin-linkage chains (i.e: ubiquitin code), which might differ from early to late stages, provided that there might be novel E3 ligases involved at later stages of the pathway (see above). Experiments focused on validating this point would require powerful proteomic tools similar to the ones employed by other authors in the field (68,131), further allowing the identification of distinct ubiquitin chain-linkages at early and late stages of the pathway. Together, combined with delayed proteasomal experiments that would further allow the enrichment of inner mitochondrial aggregates, could provide a technical approach for studying the significance of the suggested ubiquitin code and specifically identify potential differences on major ubiquitin chain linkage types during early and late stages of mitophagy. On the other hand, ubiquitin-independent autophagy receptors are additionally suggested to play a role in linking inner mitochondrial aggregates to the autophagy machinery. Validation of the interaction could be assessed via the use of protein pulldowns allowing for in-between comparisons of control conditions and delayed UPS inhibition and extended mitophagy.

Finally, a deeper look into the implications of PTM on OMM substrates, indicated an existing crosstalk between phosphorylation and ubiquitination PTMs of VDAC2 which directly had an influence on its turnover. It is further suggested in this study, that similar regulations might exist for VDAC1, perhaps directly influencing cellular fate, in agreement with other authors (218,229). First, it would be needed to validate if VDAC1 is similarly regulated by such PTM crosstalk at the same cytosolic loop. Later, if the previous hypothesis turns to be true, a subsequent validation on the implications of this PTM crosstalk on cell survival should be performed. For this purpose, one could employ interactome assays of WT and phospho- dead and mimic mutations alone or in combination with ubiquitin-dead mutations of both VDAC1/2. Interaction readouts would include increased or decreased detection of Bcl-2 family members for each mutant, which could be then indicative of pro- or anti-apoptotic implications of the combined PTM regulation suggested in this study.

Future studies involving combined approaches including high throughput readout assays, powerful proteomic tools for the identification of ubiquitin specific linkage chains on OMM substrates and inducible silencing mechanisms (i.e: E3 ligases or new targets) will certainly shed some light on the regulatory mechanisms of mitophagy, potentially involving novel ubiquitin effectors, modulators or adaptors capable of interacting along the multiple complex layers of PINK1/parkin mitophagy.

References

1. Allen CA, Van Der Giezen M, Allen JF. Chapter 3: Origin, function, and transmission of mitochondria. In: Origin of Mitochondria and Hydrogenosomes. Springer Berlin Heidelberg; 2007. p. 39–56.
2. Richard Altmann. Die Elementarorganismen und ihre beziehungen zu den zellen. Leipzig: Veit & Comp; 1890.
3. Ernster L, Schatz G. Mitochondria: A Historical Review. J Cell Biol. 1981;91(3):227–55.
4. Nass MMK, Nass S. Intramitochondrial Fibers With Dna Characteristics. I. Fixation and Electron Staining Reactions. J Cell Biol. 1963;19:593–611.
5. Giacomello M, Pyakurel A, Glytsou C, Scorrano L. The cell biology of mitochondrial membrane dynamics. Nat Rev Mol Cell Biol. 2020;21(4):204–24.
6. Pickles S, Vigié P, Youle RJ. Mitophagy and Quality Control Mechanisms in Mitochondrial Maintenance. Curr Biol. 2018;28(4):R170–85.
7. Picca A, Mankowski RT, Burman JL, Donisi L, Kim JS, Marzetti E, et al. Mitochondrial quality control mechanisms as molecular targets in cardiac ageing. Nat Rev Cardiol. 2018;15(9):543–54.
8. Kitada T, Aakawa S, Hattori N, Matsumine H, Yokochi M, Mizuno Y, et al. Mutations in the parkin gene causeautosomal recessive juvenile parkinsonism. Nat Lett. 1998;169(1993):166–9.
9. Valente EM, Abou-Sleiman PM, Caputo V, Muqit MMK, Harvey K, Gispert S, et al. Hereditary early-onset Parkinson's disease caused by mutations in PINK1. Science (80-). 2004;304(5674):1158–60.
10. Poewe W, Seppi K, Tanner CM, Halliday GM, Brundin P, Volkmann J, et al. Parkinson disease. Nat Rev Dis Prim. 2017;3:1–21.
11. Doblado L, Lueck C, Rey C, Samhan-arias AK, Prieto I, Stacchiotti A, et al. Mitophagy in human diseases. Int J Mol Sci. 2021;22(8):1–51.
12. Benda C. Die Histiogenese der Spermien. In: Ueber die Spermatogenese der Vertebraten und höherer Evertebraten, II. 1898. p. 393–8.
13. Spinelli JB, Haigis MC. The multifaceted contributions of mitochondria to cellular metabolism. Nat Cell Biol. 2018;20(7):745–54.
14. Shoshan-Barmatz V, De Pinto V, Zweckstetter M, Raviv Z, Keinan N, Arbel N. VDAC, a multi-functional mitochondrial protein regulating cell life and death. Mol Aspects Med. 2010;31(3):227–85.
15. Tamura Y, Kawano S, Endo T, Endo T. Lipid homeostasis in mitochondria. Biol Chem. 2020;401(6–7):821–33.
16. Nolfi-Donegan D, Braganza A, Shiva S. Mitochondrial electron transport chain: Oxidative phosphorylation, oxidant production, and methods of measurement. Redox Biol. 2020;37:101674.
17. Evans CS, Holzbaur ELF. Quality Control in Neurons: Mitophagy and Other Selective Autophagy Mechanisms. J Mol Biol. 2020;432(1):240–60.

18. Mishra P, Chan DC. Metabolic regulation of mitochondrial dynamics. J Cell Biol. 2016;212(4):379–87.
19. Pagliuso A, Cossart P, Stavru F. The ever-growing complexity of the mitochondrial fission machinery. Cell Mol Life Sci. 2018;75(3):355–74.
20. Friedman JR, Webster BM, Mastronarde DN, Verhey KJ, Voeltz GK. ER sliding dynamics and ER-mitochondrial contacts occur on acetylated microtubules. J Cell Biol. 2010;190(3):363–75.
21. Manor U, Bartholomew S, Golani G, Christenson E, Kozlov M, Higgs H, et al. A mitochondria-anchored isoform of the actin-nucleating spire protein regulates mitochondrial division. Elife. 2015;4:1–27.
22. Korodova F, Ramabhadran V, Higgs H. An actin-dependent step in mitochondrial fission mediated by the ER-Associated formin INF2. Science (80-). 2013;339:464–8.
23. Tilokani L, Nagashima S, Paupe V, Prudent J. Mitochondrial dynamics: Overview of molecular mechanisms. Essays Biochem. 2018;62(3):341–60.
24. Brandt T, Cavellini L, Kühlbrandt W, Cohen MM. A mitofusin-dependent docking ring complex triggers mitochondrial fusion in vitro. Elife. 2016;5:1–23.
25. Ban T, Ishihara T, Kohno H, Saita S, Ichimura A, Maenaka K, et al. Molecular basis of selective mitochondrial fusion by heterotypic action between OPA1 and cardiolipin. Nat Cell Biol. 2017;19(7):856–63.
26. Song Z, Chen H, Fiket M, Alexander C, Chan DC. OPA1 processing controls mitochondrial fusion and is regulated by mRNA splicing, membrane potential, and Yme1L. J Cell Biol. 2007;178(5):749–55.
27. Hu C, Shu L, Huang X, Yu J, Li liuju, Gong L, et al. OPA1 and MICOS Regulate mitochondrial crista dynamics and formation. Cell Death Dis. 2020;11(10).
28. Frezza C, Cipolat S, Martins de Brito O, Micaroni M, Beznoussenko G V., Rudka T, et al. OPA1 Controls Apoptotic Cristae Remodeling Independently from Mitochondrial Fusion. Cell. 2006;126(1):177–89.
29. Devine MJ, Kittler JT. Mitochondria at the neuronal presynapse in health and disease. Nat Rev Neurosci. 2018;19(2):63–80.
30. Wu Z, Ho WS, Lu R. Targeting Mitochondrial Oxidative Phosphorylation in Glioblastoma Therapy. NeuroMolecular Med. 2022;24(1):18–22.
31. Haworth RA, Hunter DR. The Ca2+-induced membrane transition in mitochondria. II. Nature of the Ca2+ trigger site. Arch Biochem Biophys. 1979;195(2):460–7.
32. Massari S, Azzone GF. The equivalent pore radius of intact and damaged mitochondria and the mechanism of active shrinkage. BBA - Bioenerg. 1972;283(1):23–9.
33. Kwong JQ, Molkentin JD. Physiological and Pathological Roles of the Mitochondrial Permeability Transition Pore in the Heart. Cell Metab. 2015;21(2):206–14.
34. Peña-Blanco A, García-Sáez AJ. Bax, Bak and beyond — mitochondrial performance in apoptosis. FEBS J. 2018;285(3):416–31.
35. Keinan N, Tyomkin D, Shoshan-Barmatz V. Oligomerization of the Mitochondrial Protein Voltage-

Dependent Anion Channel Is Coupled to the Induction of Apoptosis. Mol Cell Biol. 2010;30(24):5698–709.

36. Gonçalves RP, Buzhynskyy N, Prima V, Sturgis JN, Scheuring S. Supramolecular Assembly of VDAC in Native Mitochondrial Outer Membranes. J Mol Biol. 2007;369(2):413–8.
37. Malia TJ, Gerhard W. NMR Structural Investigation of the Mitochondrial Outer Membrane Protein VDAC and its Interaction with Anti-apoptotic Bcl-xL. Biochemistry. 2007;46(2):514–525.
38. Hiller S, Garces R. Solution structure of VDAC-1 in detergent micelles. Biol Chem. 2009;321(5893):1206–10.
39. Shimizu S, Narita M, Tsujimoto Y. BcL-2 family proteins regulate the release of apoptogenic cytochrome c by the mitochondrial channel VDAC. Nature. 1999;399:484–7.
40. Shimizu S, Tsujimoto Y. Proapoptotic BH3-only Bcl-2 family members induce cytochrome c release, but not mitochondrial membrane potential loss, and do not directly modulate voltage-dependent anion channel activity. Proc Natl Acad Sci U S A. 2000;97(2):577–82.
41. Abu-Hamad S, Zaid H, Israelson A, Nahon E, Shoshan-Barmatz V. Hexokinase-I protection against apoptotic cell death is mediated via interaction with the voltage-dependent anion channel-1: Mapping the site of binding. J Biol Chem. 2008;283(19):13482–90.
42. Maiuri MC, Le Toumelin G, Criollo A, Rain JC, Gautier F, Juin P, et al. Functional and physical interaction between Bcl-XL and a BH3-like domain in Beclin-1. EMBO J. 2007;26(10):2527–39.
43. Breda CN de S, Davanzo GG, Basso PJ, Saraiva Câmara NO, Moraes-Vieira PMM. Mitochondria as central hub of the immune system. Redox Biol. 2019;26(June):101255.
44. Dikic I, Elazar Z. Mechanism and medical implications of mammalian autophagy. Nat Rev Mol Cell Biol. 2018;19(6):349–64.
45. Kocaturk NM, Gozuacik D. Crosstalk between mammalian autophagy and the ubiquitin-proteasome system. Front Cell Dev Biol. 2018;6(OCT):1–27.
46. Nath D, Shadan S. The ubiquitin system. Nature. 2009;458(7237):421.
47. Nandi D, Tahiliani P, Kumar A, Chandu D. The ubiquitin-proteasome system. J Biosci. 2006;31(1):137–55.
48. Heinemeyer W, Ramos PC, Dohmen RJ. Ubiquitin-proteasome system. Cell Mol Life Sci. 2004;61(13):1562–78.
49. Tanaka A, Cleland MM, Xu S, Narendra DP, Suen DF, Karbowski M, et al. Proteasome and p97 mediate mitophagy and degradation of mitofusins induced by Parkin. J Cell Biol. 2010;191(7):1367–80.
50. Gegg ME, Cooper JM, Chau KY, Rojo M, Schapira AHV, Taanman JW. Mitofusin 1 and mitofusin 2 are ubiquitinated in a PINK1/parkin-dependent manner upon induction of mitophagy. Hum Mol Genet. 2010;19(24):4861–70.
51. Lechado-Terradas A, Zittlau KI, Macek B, Fraiberg M, Elazar Z, Kahle PJ. Regulation of mitochondrial cargo-selective autophagy by posttranslational modifications. J Biol Chem. 2021;297(5):101339.
52. Herhaus L, Dikic I. Expanding the ubiquitin code through post-translational modification. EMBO

Rep. 2015;16(9):1071–83.

53. Akutsu M, Dikic I, Bremm A. Ubiquitin chain diversity at a glance. J Cell Sci. 2016;129(5):875–80.
54. Mendes ML, Fougeras MR, Dittmar G. Analysis of ubiquitin signaling and chain topology cross-talk. J Proteomics. 2020;215(January):103634.
55. Dikic I, Wakatsuki S, Walters KJ. Ubiquitin-binding domains from structures to functions. Nat Rev Mol Cell Biol. 2009;10(10):659–71.
56. Clague MJ, Urbé S, Komander D. Breaking the chains: deubiquitylating enzyme specificity begets function. Nat Rev Mol Cell Biol. 2019;20(6):338–52.
57. Komander D, Rape M. The ubiquitin code. Annu Rev Biochem. 2012;81(March):203–29.
58. Kwon YT, Ciechanover A. The Ubiquitin Code in the Ubiquitin-Proteasome System and Autophagy. Trends Biochem Sci. 2017;42(11):873–86.
59. Wade Harper J, Ordureau A, Heo JM. Building and decoding ubiquitin hains for mitophagy. Nat Rev Mol Cell Biol. 2018;19(2):93–108.
60. Komander D, Clague MJ, Urbé S. Breaking the chains: Structure and function of the deubiquitinases. Nat Rev Mol Cell Biol. 2009;10(8):550–63.
61. Richter B, Sliter DA, Herhaus L, Stolz A, Wang C, Beli P, et al. Phosphorylation of OPTN by TBK1 enhances its binding to Ub chains and promotes selective autophagy of damaged mitochondria. Proc Natl Acad Sci U S A. 2016;113(15):4039–44.
62. Geisler S, Holmström KM, Skujat D, Fiesel FC, Rothfuss OC, Kahle PJ, et al. PINK1/Parkin-mediated mitophagy is dependent on VDAC1 and p62/SQSTM1. Nat Cell Biol. 2010;12(2):119–31.
63. Cunningham CN, Baughman JM, Phu L, Tea JS, Yu C, Coons M, et al. USP30 and parkin homeostatically regulate atypical ubiquitin chains on mitochondria. Nat Cell Biol. 2015;17(2):160–9.
64. Ordureau A, Heo JM, Duda DM, Paulo JA, Olszewski JL, Yanishevski D, et al. Defining roles of PARKIN and ubiquitin phosphorylation by PINK1 in mitochondrial quality control using a ubiquitin replacement strategy. Proc Natl Acad Sci U S A. 2015;112(21):6637–42.
65. MacDonald BT, Tamai K, He X. Wnt/β-Catenin Signaling: Components, Mechanisms, and Diseases. Dev Cell. 2009;17(1):9–26.
66. Durcan TM, Tang MY, Pérusse JR, Dashti EA, Aguileta MA, McLelland G, et al. USP 8 regulates mitophagy by removing K 6-linked ubiquitin conjugates from parkin . EMBO J. 2014;33(21):2473–91.
67. Gersch M, Gladkova C, Schubert AF, Michel MA, Maslen S, Komander D. Mechanism and regulation of the Lys6-selective deubiquitinase USP30. Nat Struct Mol Biol. 2017;24(11):920–30.
68. Ordureau A, Paulo JA, Zhang J, An H, Swatek KN, Cannon JR, et al. Global Landscape and Dynamics of Parkin and USP30-Dependent Ubiquitylomes in iNeurons during Mitophagic Signaling. Mol Cell. 2020;77(5):1124-1142.e10.
69. De Duve C, Pressman BC, Gianetto R, Wattaux R, Applemans F. Tissue fractionation studies. 6. Intracellular distribution patterns of enzymes in rat-liver tissue. Biochem J. 1955;60(4):604–17.

70. De Duve C. The Lysosome Concept. Lysosomes. 1963;1–35.
71. Tsukada M, Ohsumi Y. Isofation and characterization of autophagy-defective mutants of Saccharomyces cerevisiae. FEBS J. 1993;333(1):169–74.
72. Stolz A, Ernst A, Dikic I. Cargo recognition and trafficking in selective autophagy. Nat Cell Biol. 2014;16(6):495–501.
73. Heo JM, Ordureau A, Paulo JA, Rinehart J, Harper JW. The PINK1-PARKIN Mitochondrial Ubiquitylation Pathway Drives a Program of OPTN/NDP52 Recruitment and TBK1 Activation to Promote Mitophagy. Mol Cell. 2015;60(1):7–20.
74. Wong YC, Holzbaur ELF. Temporal dynamics of PARK2/parkin and OPTN/optineurin recruitment during the mitophagy of damaged mitochondria. Autophagy. 2015;11(2):422–4.
75. Lazarou M, Sliter DA, Kane LA, Sarraf SA, Wang C, Burman JL, et al. The ubiquitin kinase PINK1 recruits autophagy receptors to induce mitophagy. Nature. 2015;524(7565):309–14.
76. Wei Y, Chiang WC, Sumpter RJ, Mishra P, Levine B. Prohibitin 2 Is an Inner Mitochondrial Membrane Mitophagy Receptor. Cell. 2018;176(5):139–48.
77. Hanna RA, Quinsay MN, Orogo AM, Giang K, Rikka S, Gustafsson ÅB. Microtubule-associated protein 1 light chain 3 (LC3) interacts with Bnip3 protein to selectively remove endoplasmic reticulum and mitochondria via autophagy. J Biol Chem. 2012;287(23):19094–104.
78. van Humbeeck C, Cornelissen T, Hofkens H, Mandemakers W, Gevaert K, de Strooper B, et al. Parkin interacts with ambra1 to induce mitophagy. J Neurosci. 2011;31(28):10249–61.
79. Strappazzon F, Nazio F, Corrado M, Cianfanelli V, Romagnoli A, Fimia GM, et al. AMBRA1 is able to induce mitophagy via LC3 binding, regardless of PARKIN and p62/SQSTM1. Cell Death Differ. 2015;22(3):419–32.
80. Liu L, Feng D, Chen G, Chen M, Zheng Q, Song P, et al. Mitochondrial outer-membrane protein FUNDC1 mediates hypoxia-induced mitophagy in mammalian cells. Nat Cell Biol. 2012;14(2):177–85.
81. Rogov V V., Suzuki H, Marinković M, Lang V, Kato R, Kawasaki M, et al. Phosphorylation of the mitochondrial autophagy receptor Nix enhances its interaction with LC3 proteins. Sci Rep. 2017;7(1):1–12.
82. Sentelle RD, Senkal CE, Jiang W, Ponnusamy S, Gencer S, Panneer Selvam S, et al. Ceramide targets autophagosomes to mitochondria and induces lethal mitophagy. Nat Chem Biol. 2012;8(10):831–8.
83. Bhujabal Z, Birgisdottir ÅB, Sjøttem E, Brenne HB, Øvervatn A, Habisov S, et al. FKBP8 recruits LC3A to mediate Parkin-independent mitophagy. EMBO Rep. 2017;18(6):947–61.
84. Murakawa T, Yamaguchi O, Hashimoto A, Hikoso S, Takeda T, Oka T, et al. Bcl-2-like protein 13 is a mammalian Atg32 homologue that mediates mitophagy and mitochondrial fragmentation. Nat Commun. 2015;6(May).
85. Eapen V V., Swarup S, Hoyer MJ, Paulo JA, Harper JW. Quantitative proteomics reveals the selectivity of ubiquitin-binding autophagy receptors in the turnover of damaged lysosomes by lysophagy. Elife. 2021;10:1–36.

86. Chauhan S, Kumar S, Jain A, Ponpuak M, Mudd MH, Kimura T, et al. TRIMs and Galectins Globally Cooperate and TRIM16 and Galectin-3 Co-direct Autophagy in Endomembrane Damage Homeostasis. Dev Cell. 2016;39(1):13–27.

87. Koerver L, Papadopoulos C, Liu B, Kravic B, Rota G, Brecht L, et al. The ubiquitin-conjugating enzyme UBE 2 QL 1 coordinates lysophagy in response to endolysosomal damage . EMBO Rep. 2019;20(10).

88. Wild P, Farhan H, McEwan DG, Wagner S, Rogov V V., Brady NR, et al. Phosphorylation of the autophagy receptor optineurin restricts Salmonella growth. Science (80-). 2011;333(6039):228–33.

89. Tumbarello DA, Manna PT, Allen M, Bycroft M, Arden SD, Kendrick-Jones J, et al. The Autophagy Receptor TAX1BP1 and the Molecular Motor Myosin VI Are Required for Clearance of Salmonella Typhimurium by Autophagy. PLoS Pathog. 2015;11(10):1–26.

90. Thurston TLM, Wandel MP, Von Muhlinen N, Foeglein Á, Randow F. Galectin 8 targets damaged vesicles for autophagy to defend cells against bacterial invasion. Nature. 2012;482(7385):414–8.

91. Zheng YT, Shahnazari S, Brech A, Lamark T, Johansen T, Brumell JH. The Adaptor Protein p62/SQSTM1 Targets Invading Bacteria to the Autophagy Pathway. J Immunol. 2009;183(9):5909–16.

92. Sarraf SA, Shah H V., Kanfer G, Pickrell AM, Holtzclaw LA, Ward ME, et al. Loss of TAX1BP1-Directed Autophagy Results in Protein Aggregate Accumulation in the Brain. Mol Cell. 2020;80(5):779-795.e10.

93. Kirkin V, Lamark T, Sou YS, Bjørkøy G, Nunn JL, Bruun JA, et al. A Role for NBR1 in Autophagosomal Degradation of Ubiquitinated Substrates. Mol Cell. 2009;33(4):505–16.

94. Pankiv S, Clausen TH, Lamark T, Brech A, Bruun JA, Outzen H, et al. p62/SQSTM1 binds directly to Atg8/LC3 to facilitate degradation of ubiquitinated protein aggregates by autophagy*[S]. J Biol Chem. 2007;282(33):24131–45.

95. Korac J, Schaeffer V, Kovacevic I, Clement AM, Jungblut B, Behl C, et al. Ubiquitin-independent function of optineurin in autophagic clearance of protein aggregates. J Cell Sci. 2013;126(2):580–92.

96. Bjørkøy G, Lamark T, Brech A, Outzen H, Perander M, Øvervatn A, et al. p62/SQSTM1 forms protein aggregates degraded by autophagy and has a protective effect on huntingtin-induced cell death. J Cell Biol. 2005;171(4):603–14.

97. Ohsumi Y. Historical landmarks of autophagy research. Cell Res. 2014;24(1):9–23.

98. Yang JY, Yang WY. Bit-by-bit autophagic removal of parkin-labelled mitochondria. Nat Commun. 2013;4.

99. Kim J, Kundu M, Viollet B, Guan KL. AMPK and mTOR regulate autophagy through direct phosphorylation of Ulk1. Nat Cell Biol. 2011;13(2):132–41.

100. Zachari M, Ganley IG. The mammalian ULK1 complex and autophagy initiation. Essays Biochem. 2017;61(6):585–96.

101. Collier JJ, Suomi F, Oláhová M, McWilliams TG, Taylor RW. Emerging roles of ATG7 in human

health and disease. EMBO Mol Med. 2021;13(12):1–20.

102. Johansen T, Lamark T. Selective Autophagy: ATG8 Family Proteins, LIR Motifs and Cargo Receptors. J Mol Biol. 2020;432(1):80–103.

103. Terešak P, Lapao A, Subic N, Boya P, Elazar Z, Simonsen A. Regulation of PRKN-independent mitophagy. Autophagy. 2022;18(1):24–39.

104. Klionsky DJ, Abdelmohsen K, Abe A, Abedin MJ, Abeliovich H, Arozena AA, et al. Guidelines for the use and interpretation of assays for monitoring autophagy (3rd edition). Autophagy. 2016;12(1):1–222.

105. Georgakopoulos ND, Wells G, Campanella M. The pharmacological regulation of cellular mitophagy. Nat Chem Biol. 2017;13(2):136–46.

106. Langston JW, Ballard P, Tetrud JW, Irwin I. Chronic Parkinsonism in Humans Due to a Product of Meperidine~Analog Synthesis. 1977;1738(1975):8–10.

107. Yang JY, Yang WY. Spatiotemporally controlled initiation of Parkin-mediated mitophagy within single cells. Autophagy. 2011;7(10):1230–8.

108. Wang Y, Nartiss Y, Steipe B, McQuibban GA, Kim PK. ROS-induced mitochondrial depolarization initiates PARK2/PARKIN-dependent mitochondrial degradation by autophagy. Autophagy. 2012;8(10):1462–76.

109. Jin SM, Lazarou M, Wang C, Kane LA, Narendra DP, Youle RJ. Mitochondrial membrane potential regulates PINK1 import and proteolytic destabilization by PARL. J Cell Biol. 2010;191(5):933–42.

110. Greene AW, Grenier K, Aguileta MA, Muise S, Farazifard R, Haque ME, et al. Mitochondrial processing peptidase regulates PINK1 processing, import and Parkin recruitment. EMBO Rep. 2012;13(4):378–85.

111. Yamano K, Youle RJ. PINK1 is degraded through the N-end rule pathway. Autophagy. 2013;9(11):1758–69.

112. Matsuda N, Sato S, Shiba K, Okatsu K, Saisho K, Gautier CA, et al. PINK1 stabilized by mitochondrial depolarization recruits Parkin to damaged mitochondria and activates latent Parkin for mitophagy. J Cell Biol. 2010;189(2):211–21.

113. Narendra DP, Jin SM, Tanaka A, Suen DF, Gautier CA, Shen J, et al. PINK1 is selectively stabilized on impaired mitochondria to activate Parkin. PLoS Biol. 2010;8(1).

114. Sekine S. PINK1 import regulation at a crossroad of mitochondrial fate: The molecular mechanisms of PINK1 import. J Biochem. 2020;167(3):217–24.

115. Okatsu K, Oka T, Iguchi M, Imamura K, Kosako H, Tani N, et al. PINK1 autophosphorylation upon membrane potential dissipation is essential for Parkin recruitment to damaged mitochondria. Nat Commun. 2012;3:1–7.

116. Onishi M, Yamano K, Sato M, Matsuda N, Okamoto K. Molecular mechanisms and physiological functions of mitophagy. EMBO J. 2021;40(3):1–27.

117. Trempe JF, Sauvé V, Grenier K, Seirafi M, Tang MY, Meńade M, et al. Structure of parkin reveals mechanisms for ubiquitin ligase activation. Science (80-). 2013;340(6139):1451–5.

118. Riley BE, Lougheed JC, Callaway K, Velasquez M, Brecht E, Nguyen L, et al. Structure and function

of Parkin E3 ubiquitin ligase reveals aspects of RING and HECT ligases. Nat Commun. 2013;4(May):1–9.

119. Wauer T, Komander D. Structure of the human Parkin ligase domain in an autoinhibited state. EMBO J. 2013;32(15):2099–112.
120. Kumar A, Aguirre JD, Condos TE, Martinez-Torres RJ, Chaugule VK, Toth R, et al. Disruption of the autoinhibited state primes the E3 ligase parkin for activation and catalysis. EMBO J. 2015;34(20):2506–21.
121. Wauer T, Simicek M, Schubert A, Komander D. Mechanism of phospho-ubiquitin-induced PARKIN activation. Nature. 2015;524(7565):370–4.
122. Kazlauskaite A, Martínez-Torres RJ, Wilkie S, Kumar A, Peltier J, Gonzalez A, et al. Binding to serine 65-phosphorylated ubiquitin primes Parkin for optimal PINK 1-dependent phosphorylation and activation . EMBO Rep. 2015;16(8):939–54.
123. Sauvé V, Lilov A, Seirafi M, Vranas M, Rasool S, Kozlov G, et al. A Ubl/ubiquitin switch in the activation of Parkin. EMBO J. 2015;34(20):2492–505.
124. Gladkova C, Maslen SL, Skehel JM, Komander D. Mechanism of parkin activation by PINK1. Nature. 2018;559(7714):410–4.
125. Sauvé V, Sung G, Soya N, Kozlov G, Blaimschein N, Miotto LS, et al. Mechanism of parkin activation by phosphorylation. Nat Struct Mol Biol. 2018;25(7):623–30.
126. Sarraf SA, Raman M, Guarani-Pereira V, Sowa ME, Huttlin EL, Gygi SP, et al. Landscape of the PARKIN-dependent ubiquitylome in response to mitochondrial depolarization. Nature. 2013;496(7445):372–6.
127. Chaugule VK, Burchell L, Barber KR, Sidhu A, Leslie SJ, Shaw GS, et al. Autoregulation of Parkin activity through its ubiquitin-like domain. EMBO J. 2011;30(14):2853–67.
128. Rakovic A, Shurkewitsch K, Seibler P, Grünewald A, Zanon A, Hagenah J, et al. Phosphatase and tensin homolog (PTEN)-induced Putative Kinase 1 (PINK1)-dependent ubiquitination of endogenous parkin attenuates mitophagy: Study in human primary fibroblasts and induced pluripotent stem cell-derived neurons. J Biol Chem. 2013;288(4):2223–37.
129. Ordureau A, Paulo JA, Zhang W, Ahfeldt T, Zhang J, Cohn EF, et al. Dynamics of PARKIN-Dependent Mitochondrial Ubiquitylation in Induced Neurons and Model Systems Revealed by Digital Snapshot Proteomics. Mol Cell. 2018;70(2):211-227.e8.
130. Okatsu K, Koyano F, Kimura M, Kosako H, Saeki Y, Tanaka K, et al. Phosphorylated ubiquitin chain is the genuine Parkin receptor. J Cell Biol. 2015;209(1):111–28.
131. Antico O, Ordureau A, Stevens M, Singh F, Nirujogi RS, Gierlinski M, et al. Global ubiquitylation analysis of mitochondria in primary neurons identifies endogenous Parkin targets following activation of PINK1. Sci Adv. 2021;7(46):1–22.
132. Zittlau KI, Lechado-Terradas A, Nalpas N, Geisler S, Kahle PJ, MacEk B. Temporal Analysis of Protein Ubiquitylation and Phosphorylation During Parkin-Dependent Mitophagy. Mol Cell Proteomics. 2022;21(2):100191.
133. Koyano F, Yamano K, Kosako H, Tanaka K, Matsuda N. Parkin recruitment to impaired

mitochondria for nonselective ubiquitylation is facilitated by MITOL. J Biol Chem. 2019;294(26):10300–14.

134. Ordureau A, Sarraf SA, Duda DM, Heo JM, Jedrychowski MP, Sviderskiy VO, et al. Quantitative proteomics reveal a feedforward mechanism for mitochondrial PARKIN translocation and ubiquitin chain synthesis. Mol Cell. 2014;56(3):360–75.
135. Yoshii SR, Kishi C, Ishihara N, Mizushima N. Parkin mediates proteasome-dependent protein degradation and rupture of the outer mitochondrial membrane. J Biol Chem. 2011;286(22):19630–40.
136. Chan NC, Salazar AM, Pham AH, Sweredoski MJ, Kolawa NJ, Graham RLJ, et al. Broad activation of the ubiquitin-proteasome system by Parkin is critical for mitophagy. Hum Mol Genet. 2011;20(9):1726–37.
137. Sato Y, Okatsu K, Saeki Y, Yamano K, Matsuda N, Kaiho A, et al. Structural basis for specific cleavage of Lys6-linked polyubiquitin chains by USP30. Nat Struct Mol Biol. 2017;24(11):911–9.
138. Wang Y, Serricchio M, Jauregui M, Shanbhag R, Stoltz T, Di Paolo CT, et al. Deubiquitinating enzymes regulate PARK2-mediated mitophagy. Autophagy. 2015;11(4):595–606.
139. Simicek M, Lievens S, Laga M, Guzenko D, Aushev VN, Kalev P, et al. The deubiquitylase USP33 discriminates between RALB functions in autophagy and innate immune response. Nat Cell Biol. 2013;15(10):1220–30.
140. Geisler S, Jäger L, Golombek S, Nakanishi E, Hans F, Casadei N, et al. Ubiquitin-specific protease USP36 knockdown impairs Parkin-dependent mitophagy via downregulation of Beclin-1-associated autophagy-related ATG14L. Exp Cell Res. 2019;384(2):111641.
141. Niu K, Fang H, Chen Z, Zhu Y, Tan Q, Wei D, et al. USP33 deubiquitinates PRKN/parkin and antagonizes its role in mitophagy. Autophagy. 2020;16(4):724–34.
142. Shiiba I, Takeda K, Nagashima S, Ito N, Tokuyama T, Yamashita S, et al. MITOL promotes cell survival by degrading Parkin during mitophagy. EMBO Rep. 2021;22(3):1–16.
143. Yun J, Puri R, Yang H, Lizzio MA, Wu C, Sheng ZH, et al. MUL1 acts in parallel to the PINK1/parkin pathway in regulating mitofusin and compensates for loss of PINK1/parkin. Elife. 2014;3:1–26.
144. Puri R, Cheng XT, Lin MY, Huang N, Sheng ZH. Mul1 restrains Parkin-mediated mitophagy in mature neurons by maintaining ER-mitochondrial contacts. Nat Commun. 2019;10(1):1–19.
145. Fu M, St-Pierre P, Shankar J, Wang PTC, Joshi B, Nabi IR. Regulation of mitophagy by the Gp78 E3 ubiquitin ligase. Mol Biol Cell. 2013;24(8):1153–62.
146. Mookherjee D, Das S, Mukherjee R, Bera M, Jana SC, Chakrabarti S, et al. RETREG1/FAM134B mediated autophagosomal degradation of AMFR/GP78 and OPA1 —a dual organellar turnover mechanism. Autophagy. 2020;17(7):1–24.
147. Guardia-Laguarta C, Liu Y, Lauritzen KH, Erdjument-Bromage H, Martin B, Swayne TC, et al. PINK1 content in mitochondria is regulated by ER-associated degradation. J Neurosci. 2019;39(36):7074–85.
148. Di Rita A, Peschiaroli A, D'Acunzo P, Strobbe D, Hu Z, Gruber J, et al. HUWE1 E3 ligase promotes PINK1/PARKIN-independent mitophagy by regulating AMBRA1 activation via IKKα. Nat Commun.

2018;9(1).

149. Villa E, Proïcs E, Rubio-Patiño C, Obba S, Zunino B, Bossowski JP, et al. Parkin-Independent Mitophagy Controls Chemotherapeutic Response in Cancer Cells. Cell Rep. 2017;20(12):2846–59.
150. Shirane M, Nakayama KI. Inherent calcineurin inhibitor FKBP38 targets Bcl-2 to mitochondria and inhibits apoptosis. Nat Cell Biol. 2003;5(1):28–37.
151. Merkwirth C, Martinelli P, Korwitz A, Morbin M, Brönneke HS, Jordan SD, et al. Loss of Prohibitin Membrane Scaffolds Impairs Mitochondrial Architecture and Leads to Tau Hyperphosphorylation and Neurodegeneration. PLoS Genet. 2012;8(11).
152. Thuaud F, Ribeiro N, Nebigil CG, Désaubry L. Prohibitin ligands in cell death and survival: Mode of action and therapeutic potential. Chem Biol. 2013;20(3):316–31.
153. Chu CT, Ji J, Dagda RK, Jiang JF, Tyurina YY, Kapralov AA, et al. Cardiolipin externalization to the outer mitochondrial membrane acts as an elimination signal for mitophagy in neuronal cells. Nat Cell Biol. 2013;15(10):1197–205.
154. Li XX, Tsoi B, Li YF, Kurihara H, He RR. Cardiolipin and Its Different Properties in Mitophagy and Apoptosis. J Histochem Cytochem. 2015;63(5):301–11.
155. Pacelli C, Giguère N, Bourque MJ, Lévesque M, Slack RS, Trudeau LÉ. Elevated Mitochondrial Bioenergetics and Axonal Arborization Size Are Key Contributors to the Vulnerability of Dopamine Neurons. Curr Biol. 2015;25(18):2349–60.
156. Burbulla LF, Song P, Mazzulli JR, Zampese E, Wong YC, Jeon S, et al. Dopamine oxidation mediates mitochondrial and lysosomal dysfunction in Parkinson's disease. Science (80-). 2017;357(6357):1255–61.
157. Geisler S, Holmström KM, Treis A, Skujat D, Weber SS, Fiesel FC, et al. The PINK1/Parkin-mediated mitophagy is compromised by PD-associated mutations. Autophagy. 2010;6(7):871–8.
158. Cha GH, Kim S, Park J, Lee E, Kim M, Lee SB, et al. Parkin negatively regulates JNK pathway in the dopaminergic neurons of Drosophila. Proc Natl Acad Sci U S A. 2005;102(29):10345–50.
159. Park J, Lee SB, Lee S, Kim Y, Song S, Kim S, et al. Mitochondrial dysfunction in Drosophila PINK1 mutants is complemented by parkin. Nature. 2006;441(7097):1157–61.
160. Geisler S, Vollmer S, Golombek S, Kahle PJ. The ubiquitin-conjugating enzymes UBE2N, UBE2L3 and UBE2D2/3 are essential for Parkin-dependent mitophagy. J Cell Sci. 2014;127(15):3280–93.
161. Krebiehl G, Ruckerbauer S, Burbulla LF, Kieper N, Maurer B, Waak J, et al. Reduced basal autophagy and impaired mitochondrial dynamics due to loss of Parkinson's disease-associated protein DJ-1. PLoS One. 2010;5(2).
162. Reinhardt P, Glatza M, Hemmer K, Tsytsyura Y, Thiel CS, Höing S, et al. Derivation and Expansion Using Only Small Molecules of Human Neural Progenitors for Neurodegenerative Disease Modeling. PLoS One. 2013;8(3).
163. Schwarz L, Casadei N, Fitzgerald JC. Generation of R272Q, S156A and K572R RHOT1/Miro1 point mutations in iPSCs from a healthy individual using FACS-assisted CRISPR/Cas9 genome editing. Stem Cell Res. 2021;55:102469.

164. Tyanova S, Temu T, Sinitcyn P, Carlson A, Hein MY, Geiger T, et al. The Perseus computational platform for comprehensive analysis of (prote)omics data. Nat Methods. 2016;13(9):731–40.

165. Rath S, Sharma R, Gupta R, Ast T, Chan C, Durham TJ, et al. MitoCarta3.0: An updated mitochondrial proteome now with sub-organelle localization and pathway annotations. Nucleic Acids Res. 2021;49(D1):D1541–7.

166. Denison SR, Wang F, Becker NA, Schüle B, Kock N, Phillips LA, et al. Alterations in the common fragile site gene Parkin in ovarian and other cancers. Oncogene. 2003;22(51):8370–8.

167. Iguchi M, Kujuro Y, Okatsu K, Koyano F, Kosako H, Kimura M, et al. Parkin-catalyzed ubiquitin-ester transfer is triggered by PINK1-dependent phosphorylation. J Biol Chem. 2013;288(30):22019–32.

168. Ylä-Anttila P, Vihinen H, Jokitalo E, Eskelinen EL. Chapter 10 Monitoring Autophagy by Electron Microscopy in Mammalian Cells. Methods Enzymol. 2009;451(C):143–64.

169. Kim I, Lemasters JJ. Mitochondrial degradation by autophagy (mitophagy) in GFP-LC3 transgenic hepatocytes during nutrient deprivation. Am J Physiol - Cell Physiol. 2011;300(2):308–17.

170. Ashrafi G, Schlehe JS, LaVoie MJ, Schwarz TL. Mitophagy of damaged mitochondria occurs locally in distal neuronal axons and requires PINK1 and Parkin. J Cell Biol. 2014;206(5):655–70.

171. Neuspiel M, Schauss AC, Braschi E, Zunino R, Rippstein P, Rachubinski RA, et al. Cargo-Selected Transport from the Mitochondria to Peroxisomes Is Mediated by Vesicular Carriers. Curr Biol. 2008;18(2):102–8.

172. McLelland GL, Soubannier V, Chen CX, McBride HM, Fon EA. Parkin and PINK1 function in a vesicular trafficking pathway regulating mitochondrial quality control. EMBO J. 2014;33(4):282–95.

173. Lechado-Terradas A, Schepers S, Zittlau KI, Sharma K, Ok O, Fitzgerald JC, et al. Parkin-dependent mitophagy occurs via proteasome-dependent steps sequentially targeting separate mitochondrial sub-compartments for autophagy. Autophagy Reports. 2022;1(1):576–602.

174. Sarraf SA, Sideris DP, Giagtzoglou N, Ni L, Kankel MW, Sen A, et al. PINK1/Parkin Influences Cell Cycle by Sequestering TBK1 at Damaged Mitochondria, Inhibiting Mitosis. Cell Rep. 2019;29(1):225-235.e5.

175. Rose CM, Isasa M, Ordureau A, Prado MA, Beausoleil SA, Jedrychowski MP, et al. Highly Multiplexed Quantitative Mass Spectrometry Analysis of Ubiquitylomes. Cell Syst. 2016;3(4):395-403.e4.

176. Heo JM, Harper NJ, Paulo JA, Li M, Xu Q, Coughlin M, et al. Integrated proteogenetic analysis reveals the landscape of a mitochondrial-autophagosome synapse during PARK2-dependent mitophagy. Sci Adv. 2019;5(11).

177. Matsumoto G, Shimogori T, Hattori N, Nukina N. TBK1 controls autophagosomal engulfment of polyubiquitinated mitochondria through p62/SQSTM1 phosphorylation. Hum Mol Genet. 2015;24(15):4429–42.

178. Ivankovic D, Chau KY, Schapira AHV, Gegg ME. Mitochondrial and lysosomal biogenesis are activated following PINK1/parkin-mediated mitophagy. J Neurochem. 2016;136(2):388–402.

179. Mindell JA. Lysosomal acidification mechanisms. Annu Rev Physiol. 2012;74:69–86.

180. Zhou J, Tan SH, Nicolas V, Bauvy C, Yang N Di, Zhang J, et al. Activation of lysosomal function in the course of autophagy via mTORC1 suppression and autophagosome-lysosome fusion. Cell Res. 2013;23(4):508–23.

181. Wang H, Song P, Du L, Tian W, Yue W, Liu M, et al. Parkin ubiquitinates Drp1 for proteasome-dependent degradation: Implication of dysregulated mitochondrial dynamics in Parkinson disease. J Biol Chem. 2011;286(13):11649–58.

182. Peng H, Yang F, Hu Q, Sun J, Peng C, Zhao Y, et al. The ubiquitin-specific protease USP8 directly deubiquitinates SQSTM1/p62 to suppress its autophagic activity. Autophagy. 2020;16(4):698–708.

183. Lee YJ, Chou TF, Pittman SK, Keith AL, Razani B, Weihl CC. Keap1/Cullin3 Modulates p62/SQSTM1 Activity via UBA Domain Ubiquitination. Cell Rep. 2017;19(1):188–202.

184. Shi J, Fung G, Deng H, Zhang J, Fiesel F, Springer W, et al. NBR1 is dispensable for PARK2-mediated mitophagy regardless of the presence or absence of SQSTM1. Cell Death Dis. 2015;6(10):1–9.

185. Narendra DP, Kane LA, Hauser DN, Fearnley IM, Youle RJ. p62/SQSTM1 is required for Parkin-induced mitochondrial clustering but not mitophagy; VDAC1 is dispensable for both. Autophagy. 2010;6(8):1090–106.

186. Przedborski S. The two-century journey of Parkinson disease research. Nat Rev Neurosci. 2017;18(4):251–9.

187. Kirkin V. History of the Selective Autophagy Research: How Did It Begin and Where Does It Stand Today? J Mol Biol. 2020;432(1):3–27.

188. Soubannier V, McLelland GL, Zunino R, Braschi E, Rippstein P, Fon EA, et al. A vesicular transport pathway shuttles cargo from mitochondria to lysosomes. Curr Biol. 2012;22(2):135–41.

189. Hsieh CW, Yang WY. Omegasome-proximal PtdIns(4,5)P 2 couples F-actin mediated mitoaggregate disassembly with autophagosome formation during mitophagy. Nat Commun. 2019;10(1):1–12.

190. Hoshino A, Wang W jia, Wada S, McDermott-Roe C, Evans CS, Gosis B, et al. The ADP/ATP translocase drives mitophagy independent of nucleotide exchange. Nature. 2019;575(7782):375–9.

191. Le Guerroué F, Eck F, Jung J, Starzetz T, Mittelbronn M, Kaulich M, et al. Autophagosomal Content Profiling Reveals an LC3C-Dependent Piecemeal Mitophagy Pathway. Mol Cell. 2017;68(4):786-796.e6.

192. Abudu YP, Shrestha BK, Zhang W, Palara A, Brenne HB, Larsen KB, et al. Samm50 acts with p62 in piecemeal basal- and oxphos-induced mitophagy of sam and micos components. J Cell Biol. 2021;220(8).

193. Cornelissen T, Haddad D, Wauters F, Van Humbeeck C, Mandemakers W, Koentjoro B, et al. The deubiquitinase USP15 antagonizes Parkin-mediated mitochondrial ubiquitination and mitophagy. Hum Mol Genet. 2014;23(19):5227–42.

194. Nguyen TN, Padman BS, Lazarou M. Deciphering the Molecular Signals of PINK1/Parkin Mitophagy. Trends Cell Biol. 2016;26(10):733–44.

195. Evans CS, Holzbaur ELF. Degradation of engulfed mitochondria is rate-limiting in optineurin-mediated mitophagy in neurons. Elife. 2020;9:1–30.

196. Itakura E, Kishi-Itakura C, Koyama-Honda I, Mizushima N. Structures containing Atg9A and the ULK1 complex independently target depolarized mitochondria at initial stages of Parkin-mediated mitophagy. J Cell Sci. 2012;125(6):1488–99.

197. Imai Y, Soda M, Takahashi R. Parkin suppresses unfolded protein stress-induced cell death through its E3 ubiquitin-protein ligase activity. J Biol Chem. 2000;275(46):35661–4.

198. Liu JY, Inoshita T, Shiba-Fukushima K, Yoshida S, Ogata K, Ishihama Y, et al. Ubiquitination at the lysine 27 residue of the Parkin ubiquitin-like domain is suggestive of a new mechanism of Parkin activation. Hum Mol Genet. 2022;31(15):2623–38.

199. Koyano F, Yamano K, Kosako H, Kimura Y, Kimura M, Fujiki Y, et al. Parkin-mediated ubiquitylation redistributes MITOL/March5 from mitochondria to peroxisomes. EMBO Rep. 2019;20(12):1–29.

200. Hamasaki M, Furuta N, Matsuda A, Nezu A, Yamamoto A, Fujita N, et al. Autophagosomes form at ER-mitochondria contact sites. Nature. 2013;495(7441):389–93.

201. Böckler S, Westermann B. Mitochondrial ER contacts are crucial for mitophagy in yeast. Dev Cell. 2014;28(4):450–8.

202. Buhlman L, Damiano M, Bertolin G, Ferrando-Miguel R, Lombès A, Brice A, et al. Functional interplay between Parkin and Drp1 in mitochondrial fission and clearance. Biochim Biophys Acta - Mol Cell Res. 2014;1843(9):2012–26.

203. Pryde KR, Smith HL, Chau KY, Schapira AHV. PINK1 disables the anti-fission machinery to segregate damaged mitochondria for mitophagy. J Cell Biol. 2016;213(2):163–71.

204. Wong YC, Ysselstein D, Krainc D. Mitochondria-lysosome contacts regulate mitochondrial fission via RAB7 GTP hydrolysis. Nature. 2018;554(7692):382–6.

205. Ham SJ, Lee D, Yoo H, Jun K, Shin H, Chung J. Decision between mitophagy and apoptosis by Parkin via VDAC1 ubiquitination. Proc Natl Acad Sci U S A. 2020;117(8):4281–91.

206. Birsa N, Norkett R, Wauer T, Mevissen TET, Wu HC, Foltynie T, et al. Lysine 27 ubiquitination of the mitochondrial transport protein miro is dependent on serine 65 of the parkin ubiquitin ligase. J Biol Chem. 2014;289(21):14569–82.

207. Wang X, Winter D, Ashrafi G, Schlehe J, Wong YL, Selkoe D, et al. PINK1 and Parkin target miro for phosphorylation and degradation to arrest mitochondrial motility. Cell. 2011;147(4):893–906.

208. Safiulina D, Kuum M, Choubey V, Gogichaishvili N, Liiv J, Hickey MA, et al. Miro proteins prime mitochondria for Parkin translocation and mitophagy. EMBO J. 2019;38(2):1–18.

209. Eramo MJ, Lisnyak V, Formosa LE, Ryan MT. The “mitochondrial contact site and cristae organising system” (MICOS) in health and human disease. J Biochem. 2020;167(3):243–55.

210. Xie J, Marusich MF, Souda P, Whitelegge J, Capaldi RA. The mitochondrial inner membrane

protein Mitofilin exists as a complex with SAM50, metaxins 1 and 2, coiled-coil-helix coiled-coil-helix domain-containing protein 3 and 6 and DnaJC11. FEBS Lett. 2007;581(18):3545–9.

211. Ott C, Ross K, Straub S, Thiede B, Götz M, Goosmann C, et al. Sam50 Functions in Mitochondrial Intermembrane Space Bridging and Biogenesis of Respiratory Complexes. Mol Cell Biol. 2012;32(6):1173–88.
212. Jian F, Chen D, Chen L, Yan C, Lu B, Zhu Y, et al. Sam50 Regulates PINK1-Parkin-Mediated Mitophagy by Controlling PINK1 Stability and Mitochondrial Morphology. Cell Rep. 2018;23(10):2989–3005.
213. Phu L, Rose CM, Tea JS, Wall CE, Verschueren E, Cheung TK, et al. Dynamic Regulation of Mitochondrial Import by the Ubiquitin System. Mol Cell. 2020;77(5):1107-1123.e10.
214. Jacoupy M, Hamon-Keromen E, Ordureau A, Erpapazoglou Z, Coge F, Corvol JC, et al. The PINK1 kinase-driven ubiquitin ligase Parkin promotes mitochondrial protein import through the presequence pathway in living cells. Sci Rep. 2019;9(1):1–15.
215. Turco E, Savova A, Gere F, Ferrari L, Romanov J, Schuschnig M, et al. Reconstitution defines the roles of p62, NBR1 and TAX1BP1 in ubiquitin condensate formation and autophagy initiation. Nat Commun. 2021;12(1):1–16.
216. Peng H, Yang J, Li G, You Q, Han W, Li T, et al. Ubiquitylation of p62/sequestosome1 activates its autophagy receptor function and controls selective autophagy upon ubiquitin stress. Cell Res. 2017;27(5):657–74.
217. Liu Z, Chen P, Gao H, Gu Y, Yang J, Peng H, et al. Ubiquitylation of Autophagy Receptor Optineurin by HACE1 Activates Selective Autophagy for Tumor Suppression. Cancer Cell. 2014;26(1):106–20.
218. De Pinto V. Renaissance of vdac: New insights on a protein family at the interface between mitochondria and cytosol. Biomolecules. 2021;11(1):1–12.
219. Colombini M. VDAC: The channel at the interface between mitochondria and the cytosol. Mol Cell Biochem. 2004;256–257(1–2):107–15.
220. Naghdi S, Hajnóczky G. VDAC2-specific cellular functions and the underlying structure. Biochim Biophys Acta - Mol Cell Res. 2016;1863(10):2503–14.
221. Manzo G, Serra I, Magrí A, Casu M, De Pinto V, Ceccarelli M, et al. Folded Structure and Membrane Affinity of the N-Terminal Domain of the Three Human Isoforms of the Mitochondrial Voltage-Dependent Anion-Selective Channel. ACS Omega. 2018;3(9):11415–25.
222. Zhou B, Kreuzer J, Kumsta C, Wu L, Kamer KJ, Cedillo L, et al. Mitochondrial Permeability Uncouples Elevated Autophagy and Lifespan Extension. Cell. 2019;177(2):299-314.e16.
223. Wang L, Qi H, Tang Y, Shen HM. Post-translational Modifications of Key Machinery in the Control of Mitophagy. Trends Biochem Sci. 2020;45(1):58–75.
224. Grenier K, McLelland GL, Fon EA. Parkin- and PINK1-dependent mitophagy in neurons: Will the real pathway please stand up? Front Neurol. 2013;4 JUL(July):1–8.
225. Montava-Garriga L, Ganley IG. Outstanding Questions in Mitophagy: What We Do and Do Not Know. J Mol Biol. 2020;432(1):206–30.

226. Goiran T, Eldeeb MA, Zorca CE, Fon EA. Hallmarks and Molecular Tools for the Study of Mitophagy in Parkinson's Disease. Cells. 2022;11(13).

227. Quinn PMJ, Moreira PI, Ambrósio AF, Alves CH. PINK1/PARKIN signalling in neurodegeneration and neuroinflammation. Acta Neuropathol Commun. 2020;8(1):189.

228. Wang HJ, Guay G, Pogan L, Sauvé R, Nabia IR. Calcium regulates the association between mitochondria and a smooth subdomain of the endoplasmic reticulum. J Cell Biol. 2000;150(6):1489–97.

229. Risiglione P, Zinghirino F, Di Rosa MC, Magrì A, Messina A. Alpha-synuclein and mitochondrial dysfunction in parkinson's disease: The emerging role of vdac. Biomolecules. 2021;11(5).

7.Apendix

7.1. Abbreviations

aiu	Arbitrary intensity units
APS	Ammonium persulfate
AR	Autophagy receptor
ARIH1	E3 ubiquitin ligase ARIH1
ATP	Adenosine triphosphate
BSA	Bovines Serumalbumin
CCCP	Carbonyl cyanide m-chlorophenyl hydrazone
CL	Cardiolipin
COX4	Citrochrome c oxidase subunit iv
DNA	Deoxyribonucleic acid
DTT	1,4-Dithiothreitol (DTT)
DUB	Deubiquitinating enzyme
EM	Enriched mitochondria (fraction)
ETC	Electron transport chain
FBS	Fetal bovine serum
FKBP18	Peptidyl-prolyl cis-trans isomerase FKBP18
GABARAP	Gamma-aminobutyric acid receptor-associated protein
GP78	E3 ubiquitin-protein ligase AMFR
GTP	Guanosine-5'-triphosphate
HPA	Human protein atlas
HRP	Horseadish peroxidase
HUWE1	E3 ubiquitin-protein ligase HUWE1
IBR	In-between ring region (Parkin)
IMM	Inner mitocondrial membrane
IMS	Inter mitochondrial space
LC3	Microtubule-associated proteins 1A/1B light chain 3
LIR	LC3 interacting region
MDV	Mitochondria derived vesicles
MFN1/2	Mitofusin-1/2
MG132	N-Benzyloxycarbonyl-L-leucyl-L-leucyl-L-leucinal (proteasome inhibitor)
MITOL	E3 ubiquitin-protein ligase MARCHF5
MTS	Mitochondrial targeting sequence
MTX	Metaxin
MUL1	Mitochondrial ubiquitin ligase activator of NFKB 1
NDP52	Calcium-binding and coiled-coil domain-containing protein 2 (CALCOCO2)
NEM	Non-enriched mitochondria (fraction)

NGS	Normal goat serum
Ni-NTA	Nickel coupled to nitrilotriacetic acid
NPC	Neural precursor cells
OMM	Outer mitocondrial membrane
OPA-1	Dynamin-like 120 kDa protein
p62/SQSTM	Sequestosome-1
PBH2	Prohibitin-2
PBS	Phosphate buffered saline
PD	Parkinson's disease
PDVF	Polyvinylidene difluoride
pentaKO	HeLa cells lacking OPTN, p62/SQSTM, TAX1BP1, NBR1 and NDP52
PINK1	Serine/threonine-protein kinase PINK1
pS65-ubiquitin	Phosphorylated ubiquitin at S65
PTM	Post-translational modification
RBR	Ring-between ring
RHOT1/2	Mitochondrial Rho GTPase 1/2
RNA	Ribonucleic acid
ROI	Region of interest
ROS	Reactive oxygen species
SAP	Shrimp Alkaline Phosphatase
SDS	Sodium dodecyl sulphate
SEM	Standard error of the mean
SSBP1	Single-stranded DNA-binding protein
TAX1BP1	Tax1-binding protein 1
TBS	Tris buffered saline
TEM	Transmission electron microscopy
TMT	Tandem mass tag
TOM	Translocase of the outer membrane
TOM20	Mitochondrial import receptor subunit TOM20 homolog
TOM70	Mitochondrial import receptor subunit TOM70
UBD	Ubiquitin binding domain
UBL	Ubiquitin-like domain
UPS	Ubiquitin proteasome system
VDAC	Voltage-dependnet anion channel
WCL	Whole cell lysate
WT	Wild-type
YME1L1	ATP-dependent zinc metalloprotease YME1L1

7.2. List of Figures

Figure 2.1: Sub-organelle organization of mitochondria 6
Figure 2.2: Mitochondrial dynamics 6
Figure 2.3: Oxidative phosphorylation and ATP production of mitochondria 8
Figure 2.4: Ubiquitin conjugating system and UPS-mediated degradation 10
Figure 2.5: Cellular consequences of distinct ubiquitin chain-linkages 11
Figure 2.6: Selective autophagic degradation pathway 14
Figure 2.7: Dynamics of PINK1/parkin mitophagy 17
Figure 2.8: Structural organization of active Parkin 19
Figure 4.1: General mitophagy on stable WT- and C431A-parkin HeLa cells 43
Figure 4.2: Proteomic analysis of mitochondrial sub-compartment turnover kinetics 45
Figure 4.3: Western blot analysis of mitochondrial sub-compartment turnover kinetics 46
Figure 4.4: Turnover of MFN1 and TOM70 is upstream of TOM20 degradation 47
Figure 4.5: Morphological differences of OMM and inner- mitochondrial markers upon mitochondrial turnover 59
Figure 4.6: Relative parkin expression levels in HEK293, wild-type NPC (wtNPC) and WT-parkin HeLa cell lines 50
Figure 4.7: CCCP-induced mitophagy in HEK293 cell line 51
Figure 4.8: Induced mitophagy in wild-type NPC cell lines 52
Figure 4.9: Mitochondrial sub-compartment ubiquitination kinetics 53
Figure 4.10: Fragmented mitochondria and inner- mitochondrial aggregates are ubiquitinated upon mitochondrial depolarization 55
Figure 4.11: p62/SQSTM and LC3B engagement on mitochondrial cargo after mitochondrial depolarization 59
Figure 4.12: Mitochondrial sub-compartment cargo is differentially engaged with LAMP1 61
Figure 4.13: Mitochondrial sub-compartment cargo is differentially engaged with active lysosomes 62
Figure 4.14: Figure 4.14: Transmission electron microscopy images of mitochondria in WT-parkin HeLa cells 63
Figure 4.15: Parkin sub-cellular localization and expression levels over the course of mitophagy 65
Figure 4.16: Parkin ubiquitination during mitophagy 66
Figure 4.17: Mitophagy impairment upon pre-proteasomal inhibition in WT-parkin HeLa 68
Figure 4.18: Mitophagy impairment upon pre-proteasomal inhibition in HEK293 69
Figure 4.19: Parkin remains on mitochondria upon pre-proteasomal inhibition 70
Figure 4.20: Reduction of VDAC and TOM20 ubiquitination after pre-UPS inhibition 71
Figure 4.21: Proteomic analysis of the influence of UPS on OMM protein degradation 73
Figure 4.22: Turnover of inner- mitochondrial proteins is influenced by UPS 75

Figure 4.23: Proteomics analysis of the influence of UPS on inner- mitochondrial protein degradation 77
Figure 4.24: Phosphorylation and ubiquitin dynamics of VDAC1/2 over the course of mitophagy 79
Figure 4.25: Influence of phospho-mimic S115 on total VDAC2 turnover 80
Figure 4.26: Influence of phospho-mimic S115 on 6HIS-VDAC2 turnover 81
Figure 4.27: Mitochondrial morphology upon WT-, S115A- and S115D-VDAC2 transfection 83
Figure 4.28: Influence of K120R, S115A-120R and S115D-K120R on total VDAC2 turnover 84
Figure 4.29: Influence of single and double VDAC2 mutants on over-expressed 6HIS-VDAC2 turnover levels 85
Figure 4.30: Ubiquitination of TAX1BP1 upon CCCP-induced mitophagy in WT- and C431A-parkin HeLa 87
Figure 4.31: Proteasome inhibition influence on TAX1BP1 ubiquitination 88
Figure 4.32: Endogenous TAX1BP1 engages with LAMP1 and p62/SQSTM upon mitochondrial depolarization 90
Figure 4.33: : Over-expressed TAX1BP1 engages with LAMP1, TOM20 and SSBP1 upon mitochondrial depolarization 92
Figure 4.34: TAX1BP1 and p62/SQSTM sub-cellular localization upon mitophagy induction 93
Figure 4.35: TOM20 and VDAC2 turnover is not impaired upon TAX1BP1 knock-down 95
Figure 4.36: Mitochondrial protein degradation effects upon over-expression of 6HIS-TAX1BP1 96
Figure 4.37: Single cell analysis on SSBP1 degradation upon over-expression of 6HIS-TAX1BP1 97
Figure 4.38: Western blot analysis of mitochondrial turnover in penta-KO cells after co-transfection of Flag-parkin and 6HIS-TAX1BP1 WT or Flag-parkin alone. 99
Figure 4.39: Mitochondrial turnover in penta-KO HeLa is rescued after co-transfection of Flag-parkin and 6HIS-TAX1BP1 WT 101
Figure 4.40: Global mitochondrial turnover effects upon over-expression of WT, K549R or ΔCC3 TAX1BP1 104
Figure 4.41: Single cell analysis of SSBP1 area covered by WT, K549R- and ΔCC3-TAX1BP CCCP-depolarization 105
Figure 4.42: Filtered single cell analysis of WT, K549R- and ΔCC3-TAX1BP translocation after CCCP-induced depolarization 107
Figure 4.43: Single cell correlation analysis of percentage of overlapping WT, K549R- and ΔCC3-TAX1BP and percentage of overlapped SSBP1 area after 4 h of CCCP-induced depolarization 108
Figure 5.1: Schematic representation of phosphorylation and ubiquitination cross-talk in VDAC2 130
Figure 5.2: PTMs of VDAC influence cell fate decisions: between apoptosis and mitophagy 132
Figure 5.3: Dynamics of PINK1/parkin mitophagy: early and late stages 134-135

7.3. List of Tables

Table 2.1: Autophagy receptors involved in mammalian selective autophagy. 13
Table 3.1: List of chemicals used in this study 25
Table 3.2: List of buffers and solutions used in this study 27
Table 3.3: List of constructs used in this study. 29
Table 3.4: List of mutagenesis and cloning primers used in this study 29
Table 3.5: List of sequencing primers used in this study 30
Table 3.7: List of cell lines used in this study. 32
Table 3.8: Specific sequences of siRNA used for TAX1BP1 knock-down experiments. 33
Table 3.9: List of primary antibodies used in this work. 36-37
Table 3.10: List of secondary antibodies used in this work. 37
Table 4.1: Phosphoproteome and ubiquitylome labeling schemes for each treatment conditions and parkin-expressing HeLa cell line 44
Table 4.2: List of ubiquitination sites on OMM, IMM and matrix proteins 54
Table 4.3: List of autophagy adaptors detected in LC-MS/MS analysis upon mitophagy induction in WT-parkin HeLa 57
Table 4.4: List of ubiquitination sites found on Parkin 67
Table 4.5: List of OMM, IMM and matrix proteins highly upregulated upon delayed UPS inhibition and extended CCCP treatment 78
Table 4.6: List of proteins that undergo phosphorylation and ubiquitination on close by residues upon PINK1/parkin mitophagy induction 78
Table 4.7: Correlation and regression analysis of percentage of SSBP1 area covered by WT- or TAX1BP1 mutants. 108
Table 5.1: Summary of PINK1/parkin-dependent mitophagy studies and their potential relevance for wholesale or piecemeal mitochondrial turnover. 117-119

Acknowledgements

Most of all, I would like to thank Prof. Dr. Philipp J. Kahle for providing me the opotunity to become a PhD student in his research group, where I not only had the change to grow as a scientist but also as a person. I would like to personally thank him for the guidance, the motivation and the mentoring though out this journey. Thanks, Philipp.

Secondly, I would like to thank Prof. Dr. Jennifer Ewald from the University of Tübingen for accepting to be one of the official reviewers; for reading and giving a second opinion on this present work. Additionally, special thanks to Prof. Dr. Boris Maceck from the Interfaculty Institut of Cell Biology of the University of Tübingen, for the strong collaboration during these years and his valuable feedback and input on the project. I would also like to thank Prof. Zvulun Elazar from the Faculty of Biology of the Weizmann Institut of Sciences in Israel, for being part of the thesis advisory committee and providing valuable feedback during these years. Additional thanks to Prof. Dr. Steffan Geimer and Prof. Dr. Benedikt Westermann from the Faculty of Biology of the University of Bayreuth, for the valuable collaboration in the last year, for allowing us to visualize high resolution mitochondria and providing valuable input on TEM image analysis and mitochondria structure. Further, I would like to also thanks Dr. Julia Fitzgerald from the Faculty of Medicine of the University of Tübingen, for the strong collaboration during this last year and for providing valuable feedback all along.

My appreciation also goes to all the past and present colleagues from the Functional neurogenetics group. Special thanks to Dr. Sven Geisler, for the patience, the guidance and the mentoring throughout my first years of my PhD. Additionally, special thanks to Dr. Jorge García Morato and Bernadette Dahl, for sharing techno sessions during lab peak hours and making me feel a little bit more at home in this little bubble that Tübingen is. I would also like to thank Sandra Schepers, for the brainstorming sessions and valuable discussions at dusk. Additional speciall thanks to all my MOMbrane peers for the shred companionship along the way. Particularly, the warmest thanks to Katharina Zittlau, for never getting tired of endlessly explaining the intricalities of MS data analysis and having the energy to brainstorm and discuss new experiments all along.

Per últim, m'agradaria donar les gràcies als meus pares. Per què sense ells això no hauria estat posible. Per tot el suport rebut durant tot el camí desde la distància, que hi és, però cal saber fer que es noti menys. De la mateixa manera m'agradaria donar les gràcies a tots els amics que sempre hi son, als vells i als nous, als que viuen lluny i als que que no. Només per ser-hi, que ja és molt. Gracias, a todos. Danke an allen.

Publications

Lechado-Terradas A, Schepers S, Zittlau KI, Sharma K, Ok O, Fitzgerald JC, Geimer S, Westermann B, Macek B, Kahle PJ. Parkin-dependent mitophagy occurs via proteasome-dependent steps sequentially targeting separate mitochondrial sub-compartments for autophagy, Autophagy Reports **2022**, 1:1, 576-602.

Zittlau KI*, **Lechado-Terradas A***, Nalpas N, Geisler S, Kahle PJ, Macek B. Temporal Analysis of Protein Ubiquitylation and Phosphorylation During Parkin-Dependent Mitophagy. Mol Cell Proteomics **2022**; 21(2):100191. *co-authorship

Lechado-Terradas A, Zittlau KI, Macek B, Fraiberg M, Elazar Z, Kahle PJ. Regulation of mitochondrial cargo-selective autophagy by posttranslational modifications. J Biol Chem **2021**; 297(5):101339.

Geisler S, Jäger L, Golombek S, Nakanishi E, Hans F, Casedei N, **Lechado-Terradas A**, Linnemann C, Kahle PJ. Ubiquitin-specific protease UPS36 knockdown impairs Parkin-dependent mitophagy via downregulation of Beclin-1-associated autophagy-related ATG14L. Exp Cell Res **2019**; 384(2):111641.

Collaborations

Data that did not directly emerge from the author is directly indicated in the text and figures legends. Additionally, the following table summarizes the collaborations surrounding this work in deeper detail (see below).

Topic: **Study of proteome, ubiquitylome and phosphoproteome during early and late stages of PINK1/parkin mitophagy.**	
Relevant chapters	4.2-4.5, 4.11, 4.14
Publication	Zittlau KI*, **Lechado-Terradas A***, Nalpas N, Geisler S, Kahle PJ, Macek B. Temporal Analysis of Protein Ubiquitylation and Phosphorylation During Parkin-Dependent Mitophagy. Mol Cell Proteomics 2022; 21(2):100191. Pubmed: PMID 34974192 *co-authorship
Contributors	
Katharina Zittlau	Sub-cellular fractionation of cellular extracts, sample preparation for LC-MS/MS, proteomic data analysis
Nicolas Nalpas	Proteomic data analysis and interpretation
Sven Geisler	Assistance in data interpretation
Anna Lechado-Terradas	Mitophagy induction in WT- and C431A-parkin cells, obtention of cellular extracts, validation of sequential sub-cellular protein degradation and ubiquitination of OMM proteins, phosphorylation and ubiquitination cross-talk analysis in VDAC2
Topic: **Electron microscopy of mitophagy induced WT-parkin HeLa cells**	
Relevant chapters	4.3.3
Publication	**Lechado-Terradas A**, Schepers S, Zittlau KI, Sharma K, Ok O, Fitzgerald JC, Geimer S, Westermann B, Macek B, Kahle PJ. Parkin-dependent mitophagy occurs via proteasome-dependent steps sequentially targeting separate mitochondria sub-compartments for autophagy. (Accepted for publication, Oct. 2022)
Contributors	
Stefan Geimer	Sample processing and image acquisition, assistance in image interpretation
Benedikt Westermann	Assistance in image interpretation
Orkun Ok	Fixation of cells
Anna Lechado-Terradas	Mitophagy induction in WT-parkin cells, fixation of cells

Topic: **Impact of proteasome degradation at late stages of PINK1/parkin mitophagy**	
Relevant chapters	4.9
Publication	**Lechado-Terradas A**, Schepers S, Zittlau KI, Sharma K, Ok O, Fitzgerald JC, Geimer S, Westermann B, Macek B, Kahle PJ. Parkin-dependent mitophagy occurs via proteasome-dependent steps sequentially targeting separate mitochondrial sub-compartments for autophagy, Autophagy Reports **2022**, 1:1, 576-602.
Contributors	
Sandra Schepers	Mitophagy induction and inhibition treatments, sample processing and data analysis. Part of student's master thesis (University of Tübingen)
Anna Lechado	Experimental design
Topic: **Proteomic analysis of proteasome-dependent degradation of mitochondrial proteins**	
Relevant chapters	4.8 and 4.10
Publication	**Lechado-Terradas A**, Schepers S, Zittlau KI, Sharma K, Ok O, Fitzgerald JC, Geimer S, Westermann B, Macek B, Kahle PJ. Parkin-dependent mitophagy occurs via proteasome-dependent steps sequentially targeting separate mitochondrial sub-compartments for autophagy, Autophagy Reports **2022**, 1:1, 576-602.
Contributors	
Katharina Zittlau	Sample preparation for LC-MS analysis. Proteomic data analysis (Figures 4.21A-C and 4.23A-B) and assessment
Anna Lechado	Partial proteomic data analysis using Perseus software with the help from K. Zittlau (Figures 4.21D and 4.23C).